Convention on Long-range Transboundary Air Pollution

emep

Co-operative programme for monitoring and evaluation of the long-range transmission of air pollutants in Europe

STATUS REPORT
2/2021 July 2021

Heavy metals and POPs: Pollution assessment of toxic substances on regional and global scales

Status Report 2/2021

msc-e & ccc & ceip & ioś-pib

Cover Photo: Michael Gauss

EMEP Status Report 2/2021

July 2021

Heavy metals and POPs: Pollution assessment of toxic substances on regional and global scales

METEOROLOGICAL SYNTHESIZING CENTRE - EAST

Ilia Ilyin, Nadezhda Batrakova, Aleksey Gusev, Mikhail Kleimenov, Olga Rozovskaya, Victor Shatalov, Irina Strizhkina, Oleg Travnikov

CHEMICAL CO-ORDINATING CENTRE

Knut Breivik, Helene Lunde Halvorsen, Pernilla Bohlin Nizzetto, Katrine Aspmo Pfaffuffer, Wenche Aas

CEIP/Umweltbundesamt Austria

Katarina Mareckova, Stephan Poupa, Robert Wankmueller, Bernhard Ullrich

Institute of Environmental Protection- National Research Institute/IOŚ-PIB, Poland

Anna Degórska

MCS-E

Meteorological Synthesizing Centre - East

2nd Roshchinsky proezd, 8/5
115419 Moscow
Russia
Phone.: +7 926 292 00 18
E-mail: msce@msceast.org
Internet: www.msceast.org

CCC

Norwegian Institute for Air Research (NILU)

P.O. Box 100NO-2027 Kjeller
Norway
Phone: +47 63 89 80 00
Fax: +47 63 89 80 50
E-mail: kjetil.torseth@nilu.no
Internet: www.nilu.no

CEIP

Umweltbundesamt GmbH

Spittelauer Lände 5
1090 Vienna
Austria
Phone:+43-(0)1-313 04
Fax: +43-(0)1-313 04/5400
E-mail: emep.emissions@umweltbundesamt.at
www.umweltbundesamt.at

IOŚ-PIB

Institute of Environmental Protection - National Research Institute

ul. Krucza 5/11d
00-548 Warsaw
Poland
Phone: +48 22 3750650
E-mail: anna.degorska@ios.edu.pl
http://www.etv.ios.edu.pl/

EXECUTIVE SUMMARY

Heavy metals and persistent organic pollutants (POPs) are toxic substances known for their harmful effects on human health and biota. The priority heavy metals and POPs addressed by the Convention on Long-range Transboundary Air Pollution (CLRTAP) include lead (Pb), cadmium (Cd), mercury (Hg), polychlorinated biphenyls (PCBs), polychlorinated dibenzo(p)dioxins and dibenzofurans (PCDD/Fs), hexachlorobenzene (HCB), and polyaromatic hydrocarbons (PAHs). The priority PAHs are benzo(a)pyrene (B(a)P), benzo(b)fluoranthene (B(b)F), benzo(k)fluoranthene (B(k)F), and indeno(1,2,3-cd)pyrene (IcdP). Co-operative Programme for Monitoring and Evaluation of Long-range Transmission of Air Pollutants in Europe (EMEP, www.emep.int) performs scientific support of implementation of the Protocols. Centre on Emission Inventories and Projections (CEIP) is responsible for coordinating the emission related work of EMEP. Methodological guidance on monitoring activity in the EMEP region is carried out by Chemical Coordinating Centre (CCC). Information on results of atmospheric transboundary transport modelling is provided by Meteorological Synthesizing Centre – East (MSC-E).

Main activities of the EMEP centres in the field of heavy metals and POPs, carried out in accordance with the bi-annual workplan of the Convention for 2020-2021 [ECE/EB.AIR/144/Add.2], are overviewed in this Status report. The report includes information on the current status of emissions, monitoring, model assessment of pollution levels in the EMEP region, research and model development as well as cooperation with subsidiary bodies to the Convention, national and international organizations. More detailed information is also available in technical reports [*Travnikov et al.*, 2021, *Gusev et al.,* 2021; *Aas et al.*, 2021; *Pinterits et al.,* 2021; *Schindlbacher et al.,* 2021] and Supplementary Data Reports on heavy metals [*Strizhkina et al.*, 2021a] and POPs [*Strizhkina et al.*, 2021b] as well as on the websites (www.msceast.org, https://projects.nilu.no/ccc/reports.html, https://www.ceip.at/).

Emissions

Completeness and consistency of submitted emission data have improved significantly since EMEP has been collecting information on emissions. In 2021 44 parties reported data on emissions of priority heavy metals, and 45 countries – on POPs. However, uncertainty of the reported data is considered relatively high. Time series of the reported data for 2000-2019 are analysed separately for the western and eastern parts of the EMEP domain. In the western part the reduction of emissions make up 16% for PAHs, about 60% for PCDD/Fs, 65% for PCB, and 95% for HCB. For heavy metals the reductions are around 40% for Cd, 50% for Hg and 70% for Pb. In the eastern part of the EMEP region time series are inconsistent exhibiting large variations explained by incomplete reporting in particular countries. Emission data for 2018 reported in 2021 were compared with 2018 emissions reported in 2020. For 26 countries, data changed by more than ±15 % for one or several pollutants. In contrast, for six countries the changes due to recalculations are below 1%.

Main emission sectors in the EMEP region are *Industry production*, *Public electricity and heat production*, and *Other stationary combustion* (*Residential combustion*). *Industry production* is the main emission sector for Cd, Pb, Hg and PCB. Most of PAHs are emitted by *Other stationary combustion* sector. Besides, this and *Industry production* sectors are almost equally important for PCDD/Fs. For HCB the main sector is *Public electricity and heat production*.

Sectoral gridded heavy metal and POP emissions were reported by 33 countries. For the remaining areas missing emissions are gap-filled and spatially distributed by expert estimates. Final emissions maps for modelling were generated by MSC-E based on the reported emissions data collected and gap-filled by CEIP and supplemented by additional information on vertical distribution, seasonal variation and chemical speciation of emissions. Global emission maps were also prepared based on data derived from research projects and expert estimates.

Monitoring

Monitoring activity for EMEP is coordinated by CCC. In 2019, there were 37 sites measuring heavy metals in both aerosols and precipitation, and altogether there were 65 measurement sites. 24 sites were measuring mercury in either air or precipitation, 14 of these with concurrent measurements in air and precipitation. The highest concentrations in air and precipitation of the first (Pb, Cd) and second (As, Ni, Cu, Cr) priority metals are in general seen in Eastern Europe. However, there are hotspots for some elements in other parts of Europe (around the English Channel, Cyprus, Italy). The highest Hg concentrations in air take place in Poland followed by sites in Germany and UK, while in precipitation the highest concentrations are seen in the Czechia and in Finland.

Quality of heavy metal measurements is evaluated via EMEP laboratory intercomparisons carried out annually. The majority of EMEP laboratories participating in the intercomparisons report results of good quality, however a few laboratories would benefit from the quality improving. In particular, for the results related to 2019, only 3 laboratories do not satisfy the accepted data quality objective for As and Cu, 2 for Zn and 1 for Pb, whereas all laboratories passed for Cd, Cr and Ni. In order to assess and improve quality of Hg measurements it is recommended to perform a field intercomparison or to include Hg into regular EMEP laboratory intercomparison studies.

In total there are 39 sites reporting 2019 data on POPs whereof 27 sites with measurements in both air and precipitation. Along with active air sampling method, recommended within EMEP, passive air sampling is widely used as a complementary approach. For instance, involving data from comprehensive passive air sampling campaign carried out across European countries in 2016 together with the GLEMOS model simulations allowed establishing the prevailing role of long-range atmospheric transport of a number of POPs in Norway.

The new strategic plan for 2020-2029 includes recommendation for monitoring of POPs other than those listed for Level 2 stations as well as organic contaminants of emerging concern (CECs), for example, polybrominated diphenyl ethers (PBDEs), per- and polyfluorinated alkyl substances (PFAS) and short-chain chlorinated paraffins (SCCPs). In general, the concentrations of PBDEs and PFAS are

low at the EMEP sites but analysis of the spatial pattern for these new POPs is hampered by limited number of stations, lack of laboratory intercomparisons and high uncertainty of data. Concentrations of CECs are higher than those of PAHs and other legacy POPs. This fact shows the importance of including CECs in monitoring programmes.

Status of heavy metal and POP pollution in 2019

Pollution levels of Pb, Cd, Hg, PAHs, PCDD/Fs, HCB and PCB-153 in 2019 are analyzed for the EMEP region. Overall pollution load is the highest in Central Europe where the most significant average deposition fluxes of Pb, Cd, Hg and PAHs take place. The lowest levels of pollution occur in Northern Europe as well as in Caucasus and Central Asia. At the same time, the highest PCB-153, HCB and PCDD/Fs deposition fluxes take place in Western, Eastern and Southern Europe, respectively.

In order to evaluate changes caused by inter-annual meteorological variability between the current (2019) and previous (2018) years, the pollution patterns for these years based on the same emission data were compared. Pollution levels of all considered contaminants declined in Southern Europe, and almost all – in Western Europe. In Central and Northern Europe the changes were insignificant (within ±10%). In Eastern Europe and Caucasus and Central Asia deposition of most pollutants increased. The exception is the changes of Cd and Pb. The levels of Pb and Cd significantly declined in most of sub-regions. Especially large decline (around 30%) is noted for Central Asia due to decrease of contribution of wind re-suspension in 2019.

Verification of the modelling results was carried out by comparing modelled concentrations in air and wet deposition fluxes with the corresponding values measured at stations of the EMEP monitoring network. Reasonably good agreement between modelled and observed concentrations is noted for Pb and Cd. Mean relative bias for Pb and Cd air concentrations is 4% and 23%, respectively, and for majority of stations the deviations between modelled and observed values lie within a factor of two. However, the model tends to underestimate the observed wet deposition fluxes by 30% for Pb and 35% for Cd. Modelling results are in agreement with measured background Hg^0 concentrations, with relative bias ranging from -10% to 20%. Although the model tends to overestimate the observed Hg deposition fluxes, the deviation between modelled and observed values is within a factor of two for most of stations.

Evaluation of modelling results for PAHs against the EMEP measurements showed almost no bias for B(a)P and IcdP, while for B(b)F and B(k)F some overestimation of observed air concentrations was obtained (about 60% and 23%, respectively). For most of selected monitoring sites, the difference between the modelling results and measured concentrations is within a factor of two. For PCB-153, HCB and PCDD/Fs the model predictions are within a factor of 2 compared to measured concentrations.

The deposition fluxes of heavy metals within the EMEP region are formed by EMEP anthropogenic emissions, secondary emissions (wind re-suspension of dust particles containing Pb and Cd, natural/legacy emissions of Hg), and emissions from sources located outside the EMEP region (non-

EMEP sources). For Pb the contributions of the EMEP anthropogenic and secondary emissions are comparable, whereas for Cd the role of EMEP anthropogenic emissions is prevalent. The contribution of non-EMEP sources of Pb and Cd is relatively low for the EMEP countries as a whole, varying from 5% to 25% in Europe and reaching 30-35% in Central Asia and Caucasus. In case of Hg, the main contributor to deposition in the EMEP region is non-EMEP sources followed by EMEP anthropogenic sources. The contribution of secondary emissions within the EMEP region is minor.

The contribution of the EMEP anthropogenic sources to total deposition of PAHs ranges from about 70% in the Caucasus and Central Asia to 80% and higher in Central Europe. The relative contribution of secondary sources and non-EMEP anthropogenic sources is much lower. For other POPs the contribution of the EMEP anthropogenic sources to total deposition in the considered sub-regions is 20-50% for PCDD/Fs, 15-40% for PCB-153, and 1-3% for HCB. The contribution of secondary emissions in the EMEP countries is approximately 60% for PCDD/Fs, 70% for PCB-153 and 75% for HCB.

Deposition fluxes of Pb, Cd and Hg to different types of land cover within the EMEP domain were also calculated to support the Working Group on Effects (WGE) in assessing adverse effects of heavy metals on ecosystems and human health. However, it would be important to update the existing evaluation of the adverse effects on human health and biota.

Model assessment and monitoring data for 2019 indicated high level of annual mean B(a)P air concentrations, exceeding the EU target value, in some of EMEP countries (e.g. Poland, Croatia, Slovakia, Czechia, Hungary, and some EECCA countries). Thus, considerable part of total population of the EMEP countries was exposed to B(a)P air concentrations higher than the air quality guidelines (7% for the EU target level and 63% for the WHO reference level). Besides, importance to consider wider list of toxic PAHs in the assessment of population exposure was highlighted. In particular, model estimates of B(a)P-equivalent air concentrations of 4 PAHs showed higher fractions of population living in the areas of concentrations above the EU target value (15%) and of WHO reference level (more than 70%).

In addition to the pollution assessment for the EMEP countries, atmospheric loads of heavy metals and POPs to remote regions such as the Arctic and the marginal seas (the Baltic, Black, Caspian, Mediterranean and North Seas) is evaluated and discussed in the report. Besides, the regional assessment within the EMEP domain is supported by global-scale simulations to take into account effect of long-range transport of the pollutants from emission sources located in other regions and continents. It is particular relevant for Hg and some POPs (HCB, PCDD/Fs), which are characterized by long residence time in the atmosphere. However, improvement of the global-scale assessment requires additional efforts for development of global emissions inventories for heavy metals and POPs in co-operation with other international bodies (UN Environment, Stockholm Convention, Minamata Convention).

Research and development

Analysis of the factors responsible for temporal changes of Hg and PAH pollution in different regions of the globe was initiated by MSC-E in cooperation with Task Force on Hemispheric Transport of Air Pollution (TF HTAP). Along with anthropogenic emissions, these factors include meteorological conditions, chemical properties of the atmosphere, surface characteristics, etc. Results of the pilot model simulations for the 1990-2018 period indicate gradual decrease in atmospheric concentrations of the considered pollutants in the European region. The long-term dynamics of all three pollutants in Europe is primarily determined by changes in anthropogenic emissions both inside and outside the region. Source apportionment has shown that contribution of regional sources to PAH pollution levels in Europe remain predominant over the whole period. For Hg, prevailing contribution of regional sources decreases over the period and is replaced by increasing contribution of East Asian sources. Other factors additionally contribute to temporal variability of the pollutants. Thus, the proposed approach can be applicable for understanding of long-term pollution dynamics. However, the results are sensitive to uncertainties of the key input parameters

MSC-E continued research activities to improve assessment of PAH pollution levels in the EMEP region and to contribute to the analysis of the effectiveness of measures to reduce unintentional releases of PAHs. In particular, analysis of long-term changes of the observed and modelled PAH concentrations, exemplified by B(a)P, demonstrates that most significant decrease takes place in Western, Central, and Northern Europe (by 65%, 60%, and 40%, respectively). However, the levels in Caucasus and Central Asia increased by 65%. The major contributor to B(a)P concentrations in the EMEP countries is *Residential Combustion* emission sector. Noticeable contribution was also made by the *Industry sector* in the beginning of the 1990s in Northern, Western and Southern Europe. However, later on its share decreased significantly. Besides, countries of Southern Europe are characterized by considerable contribution of the *Agriculture sector*.

In more detail, PAH pollution on a national scale was assessed as a part of a case study for Poland. Current stage of the study is focused on the model assessment of B(a)P pollution in the country. using three different emission data sets, based on national inventories and emission scenarios. The model simulations with the scenario emissions allow improving agreement between the model and measurements and indicate possible underestimation of national B(a)P emissions in Poland. Further steps of the study can include multi-model simulations, application of more detailed temporal and spatial disaggregation of B(a)P emissions, and co-operation with national experts in monitoring, modelling, and emissions.

Gaseous exchange of POPs and Hg between the atmosphere and vegetation is an important process that affects their distribution in the environment. A new model parameterization of the air-vegetation exchange processes for GLEMOS has been developed. The effect of the implementation of updated air-surface gaseous exchange parameterization was evaluated using a one-year simulation of PCB-153. The application of the updated scheme resulted in considerable changes of simulated PCB concentrations in vegetation and soils in different parts of the EMEP region. The modelling results obtained with the new model parameterization need to be further evaluated against available measurements in the vegetation and soil compartments..

Information on land cover is essential for estimation of ecosystem-dependent deposition fluxes. Long-term changes in the surface conditions are considered as one of the important factors which can possibly affect changes of heavy metal and POP levels in the EMEP and other regions. To study the impact of time variable land cover on the GLEMOS model simulations a new data set based on MODIS satellite observations was analyzed and compared with the currently used dataset. The main differences between the considered datasets are related to fractions of urban and cropland types of land cover. It is important to stress that currently there is still no agreed land cover data to be used within EMEP and the Working Group on Effects (WGE). A harmonized dataset is crucial for assessment of ecosystem-dependent deposition fluxes and evaluation of ecosystem critical loads exceedances.

Both the model parameterisations and input data require periodical revisions and updates to keep the model in line with new findings of the scientific community. This year updates of the GLEMOS modelling system for Hg include utilizing a new Hg global emission data set used for generation of boundary concentrations for the EMEP domain, and new data on atmospheric concentrations of reactants involved into the Hg atmospheric chemistry. The updated version of the model demonstrates better performance than the previous one in terms of comparison with observations. Besides, it should be noted that the Centre continues research activities focused on the study of Hg chemical mechanisms in the atmosphere in collaboration with other scientific groups. The ultimate aim of the research is improvement of the model estimates of Hg pollution levels in the EMEP countries.

Pollution by microplastics is recognized as a global problem affecting all environmental compartments. Once released into the atmosphere, microplastics can be transported over long distances and can affect human health and biota. The adverse health effects of microplastics can be attributed to the presence of toxic constituents. Besides, microplastics can absorb and accumulate other pollutants, including heavy metals and POPs. The main source of microplastic releases to the atmosphere is secondary emission from the land and the ocean. Currently, data on the quantitative characteristics of the emission of microplastics into the atmosphere, as well as information on the processes that determine their atmospheric transport, are limited, and further research is required.

Cooperation

An overview of MSC-E activities in the field of assessment of heavy metal and POP pollution in the EMEP region and on a global scale was presented at the recent virtual TFMM meeting. Much attention was paid to the analysis of long-term changes of heavy metal and POP pollution levels. In particular, the changes of Hg and PAH levels in Europe and other regions of the globe were studied. Besides, the pollution changes were examined in the framework of cooperation with the regional marine conventions (HELCOM and OSPAR). Along with this, main results of a country-specific case study of PAH pollution in Poland were presented. Finally, directions of future research activities in the field of heavy metals and POPs relevant to TFMM work were discussed during the special sub-session of the meeting devoted to heavy metals, POPs, chemicals of emerging concern, and microplastics.

MSC-E continues collaboration with the Task Force on Hemispheric Transport of Air Pollution (TF HTAP) on Hg and POP pollution assessment. In particular, the Centre and TF HTAP jointly hosted two workshops to identify near-term opportunities and longer-term research needs to improve the scientific basis for assessment of Hg and POP pollution and trends. The workshops examined current work and efforts throughout the international science community aimed at addressing Hg and POP pollution problem on global and regional scales. A program of multi-model assessment and attribution of long-term Hg and POP pollution trends in the EMEP and other regions was proposed by MSC-E. Pilot results of a model assessment of Hg and POP pollution trends and their attribution to various factors (changes in anthropogenic emissions, meteorological conditions, atmospheric chemistry, land cover etc.) were presented to illustrate possible outcome of the study and input data required.

MSC-E took part in the twenty-fourth meeting organized by Task Force on Health. The assessment of PAHs pollution levels in the EMEP region, analysis of the key sources and trends were presented. The assessment was prepared to contribute to the analysis of effectiveness of the Protocol on POPs) in co-operation with Task Force on Techno-economic Issues (TFTEI) and Task Force on Health. The Task Force was informed about the changes of PAH emissions, modelled and observed concentrations over the recent 20 years in the EMEP region, population exposure to B(a)P concentrations exceeding threshold levels, and model experiments on evaluation of joint toxicity of the group of sixteen PAHs.

MSC-E continued cooperation with international organizations such as the Arctic Monitoring and Assessment Programme (AMAP), Minamata Convention, Stockholm Convention, European Commission, HELCOM and OSPAR . Recently, MSC-E participated in the AMAP Assessment of the Arctic pollution by Hg (AMAP Mercury Assessment 2021). The Centre also took part in the Minamata Online Session “Multimedia modelling of global mercury movement” aimed to bridge the scientific community and international policy to better understand abilities of the multimedia mercury modelling for assessing the state of the environment and effectiveness of pollution control measures. In the framework of cooperation with HELCOM, atmospheric deposition of selected heavy metals and POPs to the Baltic Sea were estimated for the period 1990-2018. Finally, the work on assessment of Pb, Cd and Hg deposition to the sub-regions of the OSPAR maritime area was initiated.

Future activities

Future research activities of the EMEP Centre’s will be aimed at improvement of heavy metal and POP pollution assessment in the EMEP region. CEIP will continue to review and improve reported emission inventories, further elaborate the gap-filling procedures and analyze sectoral composition of emissions. Detailed assessment of PAH pollution levels will be continued with focus on the analysis of population exposure to PAH and atmospheric aerosol from combustion sources. In particular, the MSC-E will contribute to a multi-model analysis of B(a)P pollution levels as a part of the TFMM/EuroDelta-Carb intercomparison exercise. Activities aimed at improvement of the modelling approaches for assessment of Hg and POP long-term trends, source-receptor relationships, and future projections will be initiated in collaboration with TF HTAP. They will include a multi-model

study of Hg dispersion and cycling on a global scale with focus on air-surface exchange and secondary/natural emissions, global/regional multi-model evaluation of source-receptor relationships for combustion-related POPs, as well as contribution to the TF THAP exploratory workshops on wildfires, chemicals of emerging concern (CEC) and microplastics. The country-scale assessment of heavy metal and POP pollution in a form of case studies will be continued aiming at detailed analysis of pollution levels in selected countries and refinement of the EMEP operational modelling. Ecosystem-related analysis of heavy metal pollution will be performed in co-operation with WGE. Besides, the assessment of atmospheric pollution of the marine environment with heavy metals and POPs will be carried out in collaboration with HELCOM and OSPAR. Finally, the Centre will continue co-operation with Stockholm and Minamata Conventions and other international bodies in relation to assessment of POP and Hg pollution.

ACKNOWLEDGEMENTS

The operational and research activities described in this report have been funded by the EMEP Trust Fund. Besides, the modelling activity on evaluation of marine pollution was funded by HELCOM and OSPAR.

CONTENTS

INTRODUCTION

Heavy metals and persistent organic pollutants (POPs) are toxic substances known for their harmful effects on human health and biota. A number of international organizations, including the UNECE Convention on Long-range Transboundary Air Pollution (hereafter, CLRTAP or the Convention), pay significant attention to mitigation of the environmental problems caused by heavy metal and POP pollution. The priority heavy metals and POPs addressed by the Convention include lead (Pb), cadmium (Cd), mercury (Hg), polychlorinated biphenyls (PCBs), polychlorinated dibenzo(p)dioxins and dibenzofurans (PCDD/Fs), hexachlorobenzene (HCB) and polyaromatic hydrocarbons (PAHs). The priority PAHs are benzo(a)pyrene (B(a)P), benzo(b)fluoranthene (B(b)F), benzo(k)fluoranthene (B(k)F), and indeno(1,2,3-cd)pyrene (IcdP).

Within the Convention the Protocols on Heavy Metals and POPs were adopted in 1998 and amended in 2012 and 2009, respectively. Co-operative Programme for Monitoring and Evaluation of Long-range Transmission of Air Pollutants in Europe (EMEP, www.emep.int) performs scientific support of implementation of the Protocols. Centre on Emission Inventories and Projections (CEIP) is responsible for coordinating the emission related work of EMEP. Methodological guidance on monitoring activity in the EMEP region is carried out by Chemical Coordinating Centre (CCC). Model assessment of atmospheric transboundary pollution by heavy metals and POPs is provided by Meteorological Synthesizing Centre – East (MSC-E). Aspects related to ecosystems and human health exposure to heavy metal and POP pollution are addressed by the Working Group on Effects (WGE).

Main activities of the EMEP Centres in the field of heavy metals and POPs pollution assessment and overview of the pollution state in 2019 are summarized in this Status Report. The activities were carried out in accordance with bi-annual workplan of the Convention for 2020-2021 [ECE/EB.AIR/144/Add.2]. Information on heavy metal and POP emissions in the EMEP region is summarized in Chapter 1. Chapter 2 describes the results of the pollution measurements in the EMEP monitoring network in 2019 as well as supplementary measurement data. The status of transboundary pollution in 2019 is discussed in Chapter 3. The results presented in the chapter are based on emission data related to the previous (2018) year and characterise pollution changes caused by interannual meteorological variability. The updated results based on emissions of 2019 are described in Annex B. MSC-E research and model developments are overviewed in Chapter 4. Chapter 5 summarises EMEP cooperation on heavy metals and POPs with Subsidiary Bodies of the Convention and other international organizations. And finally, main challenges and plans for future activities are formulated.

More detailed information on MSC-E research is available in supplementary and technical reports of the Centre. In particular, additional information on transboundary pollution modelling and evaluation of the modelling results is presented in Supplementary Data Reports on heavy metals [*Strizhkina et al.*, 2021a] and POPs [*Strizhkina et al.*, 2021b]. Pilot results on attribution of long-term changes of Hg and POP pollution to regional and extra-regional sources performed in co-operation with the Task Force on Hemispheric Transport of Air Pollution (TF HTAP) are discussed in [*Travnikov et al*. 2021]. Progress in assessment of PAH pollution levels and their trends are described in [*Gusev et al.*, 2021]. Besides, description of the current stable version of the Global EMEP Multi-media Modelling System (GLEMOS) as well as information on heavy metal and POP pollution in the EMEP region and individual EMEP countries are presented at the MSC-E website (www.msceast.org).

Chapter 1. EMISSIONS OF HEAVY METALS AND POPs

1.1. Official emission data for 2019

The EMEP Reporting guidelines [*UNECE*, 2014] request all Parties to the *LRTAP Convention* to report annually emissions and activity data of air pollutants (SO_x, NO_x, NMVOCs, NH_3, CO, heavy metals, POPs, particulate matter (PM) and voluntary black carbon (BC). Information on large point sources (LPS), projection data and gridded data should be reported every four years.

1.1.1. Reporting of emission inventories in 2021

Completeness and consistency of submitted data have improved significantly since EMEP has been collecting information on emissions (Fig. 1.1). 48 (94%) Parties submitted data to CEIP in 2021[1], 44 Parties reported data on priority heavy metals (Cd, Hg, Pb), from which 40 Parties provided time series, three Parties reported only 2018 data, 40 Parties reported data on five additional heavy metals (Arsenic (As), chromium (Cr), copper (Cu), nickel (Ni), selenium (Se), zinc (Zn) and their compounds) (Fig. 1.2). 45 Parties reported data on POPs (total PAHs, PCDD/Fs, HCB, PCBs), out of which 44 also reported data on additional PAHs (B(a)P, B(b)F, B(k)F, IcdP).

The quality of submitted data across countries differs quite significantly. When compiling the inventories, countries have to use the newest available version of the EMEP/EEA air pollutant emission inventory guidebook, which is the version of 2019 [*EMEP/EEA Guidebook*, 2019]. However, many countries still use the Guidebook 2016 [*EMEP/EEA Guidebook*, 2016] or older versions. Uncertainty of reported data (national totals, sectoral data) is considered to be relatively high (CEIP/ Uncertainties 2021). The completeness of reported data is not satisfactory for all pollutants and sectors either. Detailed information on recalculations, completeness and key categories, plus additional review findings, can be found in the annual CEIP technical inventory review reports and its Annexes[2].

[1] *The original submissions from the Parties can be accessed via the CEIP homepage on* https://www.ceip.at/status-of-reporting-and-review-results/2021-submission

[2] https://www.ceip.at/review-of-emission-inventories/technical-review-reports

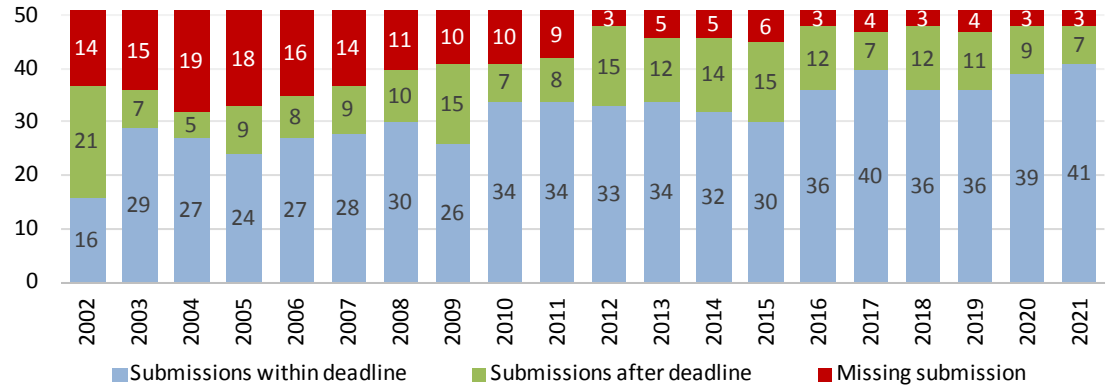

Fig. 1.1. *Number of parties reporting emission data to EMEP since 2002, as of 1 June 2021.*

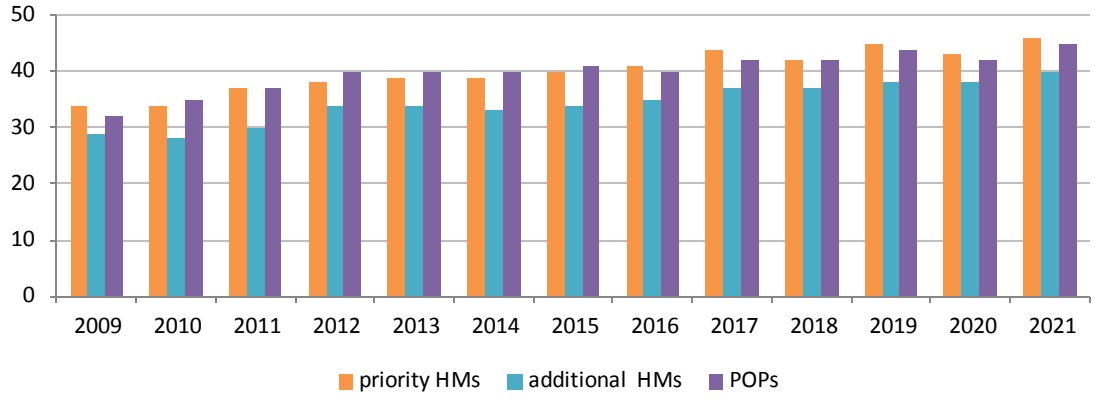

Fig. 1.2. *Number of parties reporting of heavy metals and POPs to EMEP since 2009, as of 1 June 2021.*

1.1.2. Emission trends in the EMEP area – reported data

For priority heavy metals and POPs the emission trends and completeness of reported data show different pictures for the EMEP-East and EMEP-West regions. The EMEP-West region includes the EU27 countries, Monaco, Albania, Bosnia&Herzegovina, North Macedonia, Montenegro, Serbia, Iceland, Liechtenstein, Norway, Switzerland and the United Kingdom. The EECCA countries and Turkey are summarized in the EMEP-East region[3].

EMEP West area – POPs

The strong fluctuations in emission trends of POPs for the EMEP-West region (Fig. 1.3) are mostly due to the reporting of single countries. The high reductions of HCB from 2001 to 2002 are due to the strong decrease in emissions reported by Germany. Liechtenstein does not report PCB. Bosnia & Herzegovina does not report any data.

[3] https://www.ceip.at/review-of-emission-inventories/review-process

Main revisions in reporting

- The strong peak in HCB emissions 2009 from Albania is removed.
- The peak in 2013 B(k)F emissions from Spain is removed and the national total has been revised by -85 % for the whole time series.
- Austria started to report the four PAH compounds B(a)P, B(b)F, B(k)F and IcdP.

Emission trends of POPs 2000 to 2019 (excluding Serbia) Table 1.1 and Fig. 1.3 show reported data and trends for POPs 2000 to 2019 in the EMEP WEST area without Serbia.

Table 1.1. *POPs 2000-2019 in the EMEP West area without Serbia (reported data)*

	B(a)P, t	B(b)F, t	B(k)F, t	IcdP, t	PAHs, t	PCDD/F, g TEQ	HCB,kg	PCBs,kg
2000	262	285	137	142	929	4 500	3 998	6 980
2001	266	289	140	143	940	3 787	4 092	6 476
2002	262	286	137	139	925	3 683	768	5 966
2003	269	292	140	144	947	3 197	572	5 504
2004	269	291	139	143	944	3 252	435	5 027
2005	278	300	143	146	966	3 078	422	4 787
2006	287	308	146	150	992	2 686	310	4 577
2007	276	322	140	148	989	2 562	303	4 284
2008	288	309	146	155	990	2 553	279	4 089
2009	280	297	138	152	930	2 295	241	3 622
2010	297	314	146	162	994	2 406	221	3 606
2011	269	282	133	146	906	2 265	236	3 401
2012	280	296	138	155	943	2 277	234	3 241
2013	273	290	136	152	919	2 196	292	3 027
2014	245	260	122	137	833	2 073	315	2 899
2015	247	263	124	139	842	2 093	194	2 803
2016	254	269	127	141	861	2 060	246	2 707
2017	251	267	125	140	854	2 064	264	2 667
2018	240	257	121	135	824	1 992	224	2 706
2019	228	244	114	129	782	1 942	219	2 462
Trend 2000 to 2019	-13%	-14%	-17%	-9%	-16%	-57%	-95%	-65%
Change 2000 to 2019	-34	-41	-23	-12	-148	-2 558	-3 780	-4 518

From 2000 to 2019, **PCDD/F** emissions have been reduced by 57% (-2558 g TEQ) with major reductions between 2000 and 2009 (-49%). Major reductions are reported by France (-451 g TEQ), Slovakia (- 843 g TEQ) and Portugal (-296 g TEQ). All countries except Albania (+32%), Liechtenstein (+21%) and Malta (+2150%) reported decreasing emissions since the year 2000.

The strongest PCDD/F emissions reductions occurred in GNFR-sectors *A_PublicPower* (-1171 g TEQ), *J_Waste* (-757 g TEQ) and *B_Industry* (-401 g TEQ). PCDD/F emissions from *C_OtherStationaryComb* have the highest share (42%) in 2019 but have been reduced by only -136 g TEQ since 2000.

From 2000 to 2019, **HCB** emissions have been reduced by 95% (-3780 kg) with major reductions between 2000 and 2002 (-81%, -3230 kg) which is mainly due to the reporting of Germany for G-NFR sector *B_Industry* (-2860 kg). All countries except Estonia, Lichtenstein, Latvia, Montenegro and Malta reported decreasing emissions since the year 2000. Between 2002 and 2019 emissions decreased by 72% (- 550 kg) with the largest decreases reported by Spain (-170 kg), Hungary (-117 kg) and Portugal (-100 kg). HCB emissions from *L_AgriOther* have the highest share (35%, 77 kg) in 2019 but have been reduced by only -33 kg since 2000. HCB emissions from *J_Waste* decreased by -88 % (-49 kg) since the year 2000.

From 2000 to 2019, **PCB** emissions have been reduced by 65% (-4518 kg) with major reductions in sector *B_industry* (-3165 kg) and *J_Waste* (-917 kg). All countries except Albania, Austria, Greece, Lithuania, Luxembourgh, Malta and Norway reported decreasing emissions since the year 2000. The decrease in 2018 to 2019 emissions is mainly due to lower emissions from *B_Industry*.

From 2000 to 2019, **PAH** emissions have been reduced by 16% (-148 t) with major reductions in sector *B_Industry* (-79 t) and *C_OtherStationaryComb* (-43 t). The decreasing trend 2017 to 2019 (-73 t) is dominated by Poland (-37 t) and Italy (-9 t) in sector *C_OtherStationaryComb*.

Fig. 1.3 shows the indexed trend (year 2000 = 100%) for POPs in the EMEP-WEST area without Serbia, because it dominates the trend for most of the pollutants.

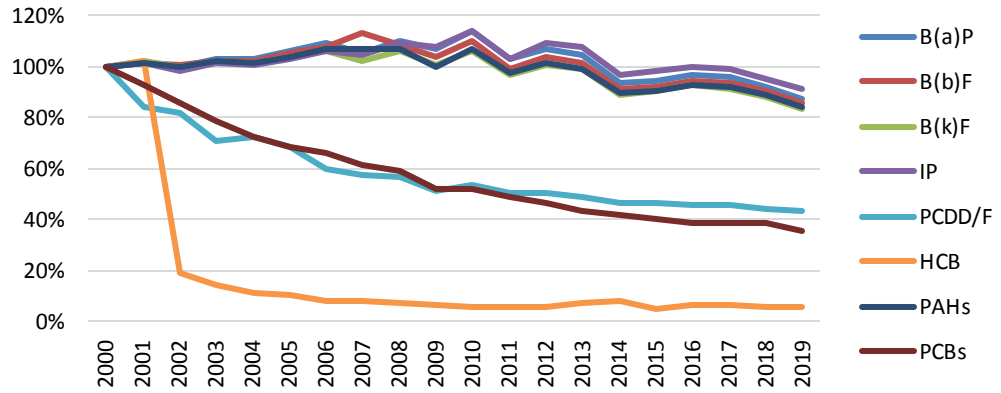

Fig. 1.3. *Emission trends of POPs 2000-2019 in the EMEP West area without Serbia (reported data)*

EMEP East area – POPs

Reporting of POPs in the EMEP East region is quite incomplete and shows high peaks and inconsistent time series. The Russian Federation reported some POPs for the year 2000 only, and Turkey did not report any POPs at all. Belarus did not report data for the year 2000 and incomplete data for 2001. Ukraine reported very high levels of POPs for 2010 to 2013 (constant values) and data from 2017 to

2019. Azerbaijan reported data for the years 2000-2017 but unreasonable high levels of PCDD/F for 2007 to 2014. Georgia reported complete time series but unreasonable high levels of HCB for 2013 to 2017 and unreasonable high levels of PCBs for 2000-2019. Kazakhstan reported complete time series but unreasonable high levels of PCBs for 2000-2017 and 2019 and unreasonable high levels of PAH and PCB for 2019. Kyrgyzstan reported incomplete data for 2010-2012 and complete data for 2016 and 2017. Armenia reported incomplete data for 2007 and 2014 and complete data for 2017 to 2019.

Figure 1.4 shows POPs emissions trends from 2002 to 2018 for EMEP East without Ukraine, Kazakhstan, PCDD/F of Azerbaijan and HCBs, PCBs from Georgia.

The increase of HCB emissions in 2009 is mainly due to the reporting of Azerbaijan and Kazakhstan and the trend from 2016 to 2019 is dominated by Belarus. The drop in POPs emissions in 2018 is mainly due to missing data of Kyrgyzstan. The peaks of PCB emissions in 2007 and 2014 are due to reporting of Armenia. The peak in 2016 PAH emissions is mainly due to reporting of Kyrgyzstan, which reported values for 2016 and 2017 only.

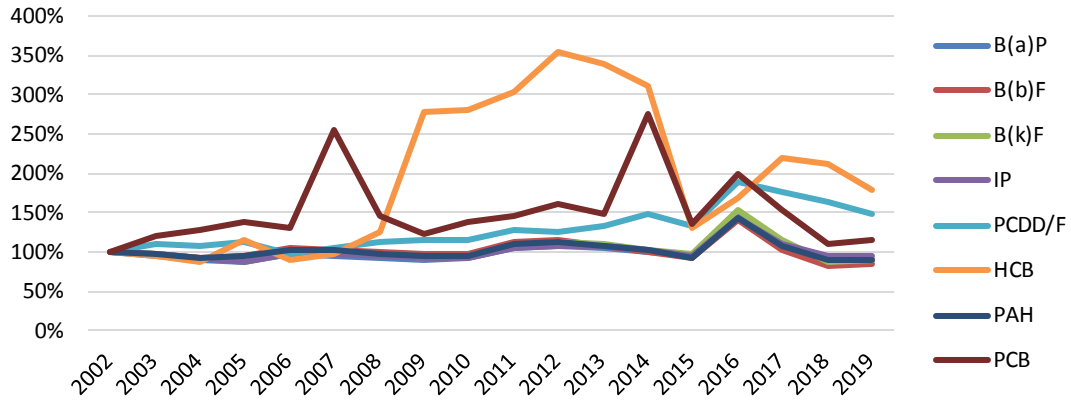

Fig. 1.4. *Emission trends of POPs 2002-2019 in the EMEP East area (reported data) without Ukraine, Kazakhstan, PCDD/F of Azerbaijan and HCBs, PCBs of Georgia.*

EMEP West area – priority heavy metals

Priority heavy metals of the EMEP West area show a rather smooth downtrend and a dip in the year 2009, which reflects the economic recession leading to lower industrial production in that year (Fig. 1.5). The strong decrease of Pb emissions from 2000 to 2002 is mainly due to lower emissions in the transport sector in Italy and Spain. The decrease in 2019 Hg emissions is mainly due to lower emissions reported by Germany (-13%), Spain (-27%), Poland (-9%) and Italy (-7%). The decrease in 2019 Pb emissions is mainly due to lower emissions reported by Bulgaria (-86%), Estonia (-66%) and Poland (-7%). The decrease in 2019 Cd emissions is mainly due to lower emissions reported by Germany (-9%), Bulgaria (-23%) and Poland (-4%).

Table 1.2 and Fig. 1.5 show reported data and trends for priority heavy metals 2000 to 2019 in the EMEP West area.

Table 1.2. *Priority heavy metals 2000-2019 in the EMEP West area.*

	Cd, t	Hg, t	Pb, t
2000	117	105	4 663
2001	112	99	3 512
2002	108	97	2 796
2003	102	95	2 705
2004	99	91	2 484
2005	94	87	2 311
2006	92	85	2 241
2007	88	81	2 192
2008	86	76	2 133
2009	77	66	1 681
2010	78	68	1 745
2011	77	67	1 471
2012	73	65	1 426
2013	72	62	1 390
2014	72	60	1 395
2015	70	57	1 355
2016	71	55	1 320
2017	70	55	1 364
2018	69	54	1 339
2019	66	49	1 212
Trend 2000 to 2019	-43%	-54%	-74%
Change 2000 to 2019	-50	-56	-3 451

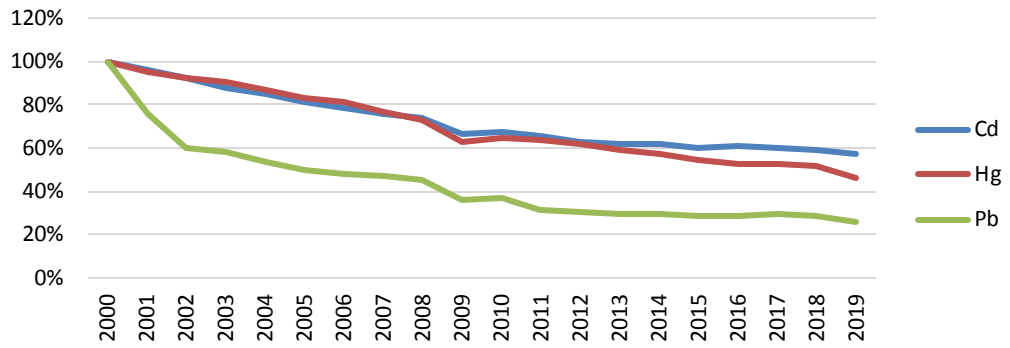

Fig. 1.5. *Emission trends of priority heavy metals 2000-2019 in the EMEP West area (reported data)*

The continuous decrease of Hg emissions since the year 2010 is mainly due to decreases reported by France, Germany, Italy and the United Kingdom.

EMEP East area – priority heavy metals

Unlike EMEP West, *priority heavy metals of the EMEP East area show an unstable trend from 2000 to 2007*, which is mainly due to incomplete reporting (Fig. 1.6). The dip in 2001 Pb and Cd emissions is mainly due to a gap in reporting of the Russian Federation, which reported for 2000, 2002-2006 and 2009 (jump in Cd emissions) only. The Ukraine and Belarus did not report heavy metals for 2000. Azerbaijan and Kyrgyzstan did not report data for 2018 and 2019. Georgia, Kazakhstan, Moldova and Turkey are the only countries, which reported complete time series for all three heavy metals since the year 2000.

The strong increase in Hg emissions from 2017 to 2019 is due unreasonable high emissions reported by Armenia for 2018 (GNFR sector "E_Solvents", the value is about 400 times higher than for 2017 and 2019) and due to unreasonable high emissions reported by Kazakhstan and the Ukraine for 2019 (both a factor of 10 higher than for previous years). The increase in Pb emissions 2019 is due to unreasonable high emissions reported by Kazakhstan (factor of 8 higher than for previous years).

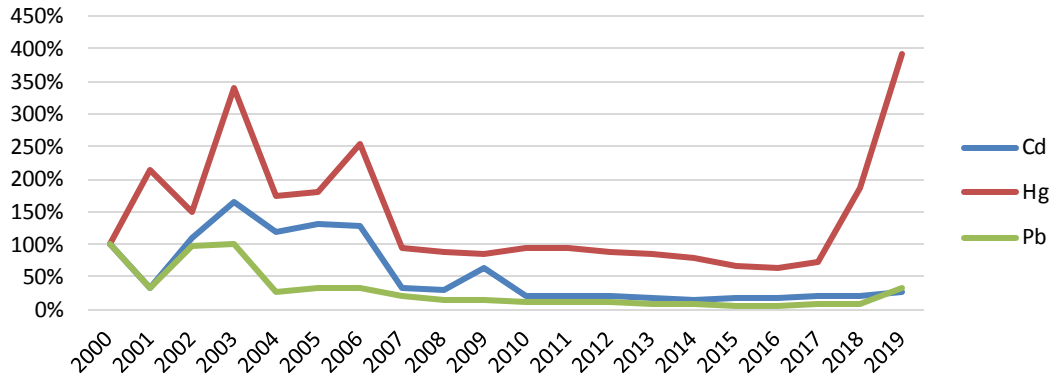

Fig.1.6. *Emission trends of priority heavy metals 2000-2019 in the EMEP East area (reported data).*

1.1.3. Comparison of 2018 data reported in 2020 and in 2021

Emission data for 2018 reported in 2021, were compared with 2018 emissions reported in 2020. For 26 countries, data changed by more than ±15 % for one or several pollutants (see Fig.1.7 and Annex A.2). For six countries, 2018 data is unchanged or nearly unchanged (< 1 %).

Albania, Georgia, Liechtenstein, North Macedonia, Moldova and the Russian Federation reported data in 2021 but did not submit data in the year 2020 or did not submit data on time.

Several countries reported **significant recalculations** for some of the pollutants (see right part of Fig. 1.7, which is displayed in logarithmic scale). Analysis shows that some of the 2018 values reported in the 2020 submissions were comparably low (e.g. Germany: B(b)F, B(k)F, IcdP) or high (Greece: PAHs

and its compounds). Finland revised the four PAH compounds by a factor of +28, mainly due to inconsistencies of PAH data within the 2020 submission. Serbia revised PAH emissions by a factor of +19 which is not very reasonable.

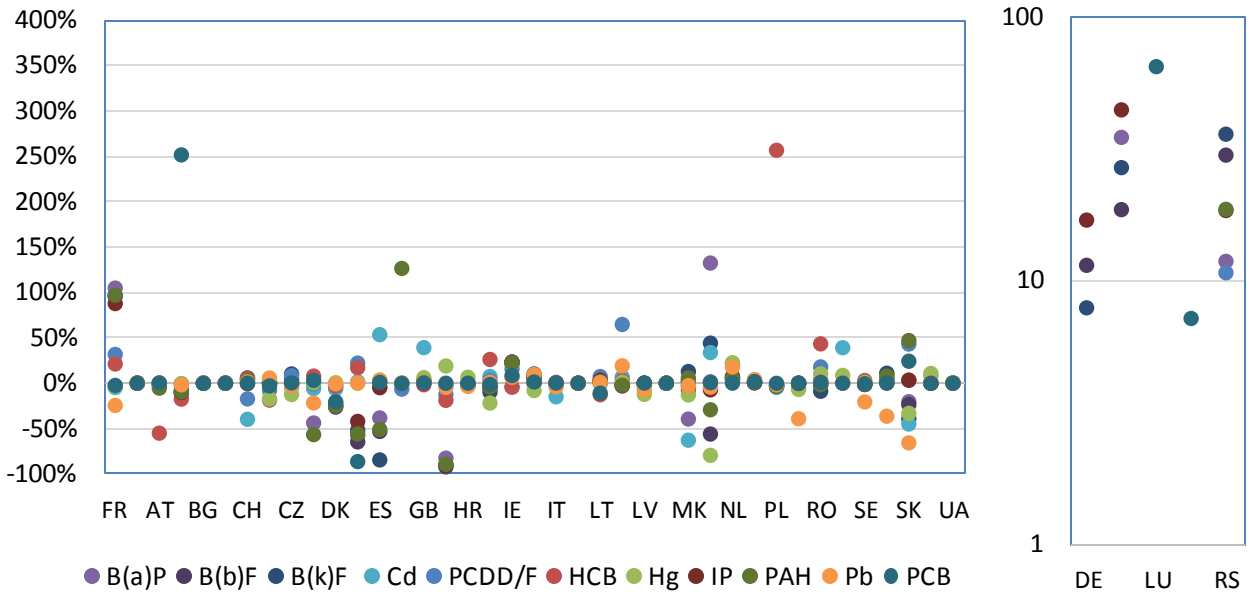

Fig. 1.7. *Recalculations between the 2021 and 2020 submission for 2018 values (reported data). The separate chart on the right shows countries and pollutants with recalculations > 400%, expressed as factors in logarithmic scale.*

1.1.4. Data sets for modellers in 2021

Data used by CEIP were reported by the Parties to the LRTAP Convention as sectoral emissions (NFR14) and National Total emissions according to the UNECE guidelines for reporting emissions and projections data under the LRTAP Convention, Annex I [*UNECE*, 2014].

Reported (NFR[4]) sector data were aggregated to 13 GNFR sectors. In several cases, no data were submitted by the countries, or the reporting is not complete or contains errors. Before modellers can use such emission data, missing or erroneous information has to be filled in or replaced by expert estimates. To gap-fill missing/erroneous data, CEIP typically applies different methods. The gap-filling procedure is fully documented every year in the technical reports which can be downloaded from the CEIP website[5]. After the gap-filling, sector emissions are used for spatial distribution (mapping) to the EMEP grids.

The Parties for which reported data were (partly) replaced in 2021 are Bulgaria, Germany, Finland, Greece, Italy, North Macedonia, Poland, Portugal, Romania, Serbia, Slovakia, Turkey and Ukraine (see Annex A.3).

[4] NFR – Nomenclature for Reporting

[5] https://www.ceip.at/ceip-reports

Contribution of individual sectors to total EMEP heavy metals and POPs emissions

Figure 1.8 shows the *contribution of each GNFR sector to the total emissions of individual air pollutants* (Cd, Hg, Pb, B(a)P, B(b)F, B(k)F, IcdP, PAHs, PCDD/F, HCB, PCB). To provide as complete a picture as possible of the share of the individual sectors in total EMEP emissions, data as used for EMEP models (i.e. gap-filled data) were used for the calculations. The analysis does not include sea regions.

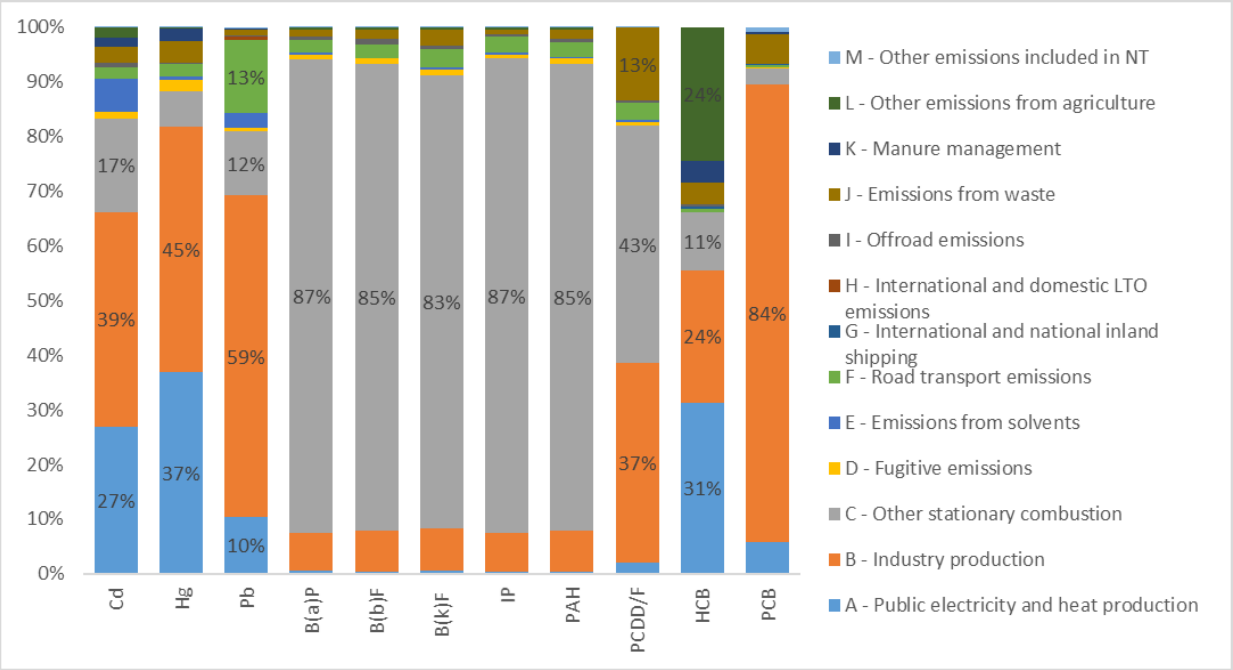

Fig. 1.8. *GNFR sector contribution to national total emissions in 2019, EMEP area without sea regions (only percentages above 10% are labelled).*

It is evident that the combustion of fossil fuels and processing of raw materials is responsible for a significant part of heavy metals and POPs emissions.

Industry production emits about 39 % of **Cd** emissions, followed by 27% from public power and heat plants.

The industry production sector emit about 45% of total **Hg** emissions, followed by energy industries, which released 37% of total emissions, mainly from coal power plants.

About 59% of **Pb** emissions are released by the industry production sector, while each of the other sectors contributes to a maximum of about 13%. Road transport (leaded gasoline) only contributes 13%.

The largest source of **PAHs** and its compounds (B(a)P, B(b)F, B(k)F, IcdP) is the 'other stationary combustion' sector, which contributes 85% of total PAH emissions. The main source of PAH

emissions are coal and wood stoves/boilers in households. About 7% of PAH emissions are related to the industry production sector.

With 43% of total emissions, the 'other stationary combustion' sector contributes most to **PCDD/F** emissions. The main source of PCDD/F emissions are coal and wood stoves/boilers in households. Industry production plants (metal industries) contribute 37% of total PCDD/F emissions and the waste sector (mainly waste incineration) contributes about 13%.

With 31% of total emissions, public electricity and heat production sector is responsible for a large share of **HCB** emissions, followed by industry production with a share of 24% and 'other emissions from agriculture' with a share of 24%. 'Other stationary combustion' only contributes to 11% of total HCB emissions. France contributes to 21% of HCB emissions from 'other emissions from agriculture', Spain to 11%, Poland to 12% and the UK to 13%, which is due to application of **pesticides** (NFR 3Df). Ukraine contributes to 26% of HCB emissions from agriculture (NFR 3Dc Farm-level agricultural operations including storage, handling and transport of agricultural products) which probably also includes pesticide application.

The dominating sector for **PCB** emissions is the industrial sector, which contributes 84% to total emissions.

Figure 1.9 illustrates the sector contribution for the EMEP West region and the EMEP East region. North Africa is included in the EMEP East region. The comparison of both graphs highlights some significant differences between West and East.

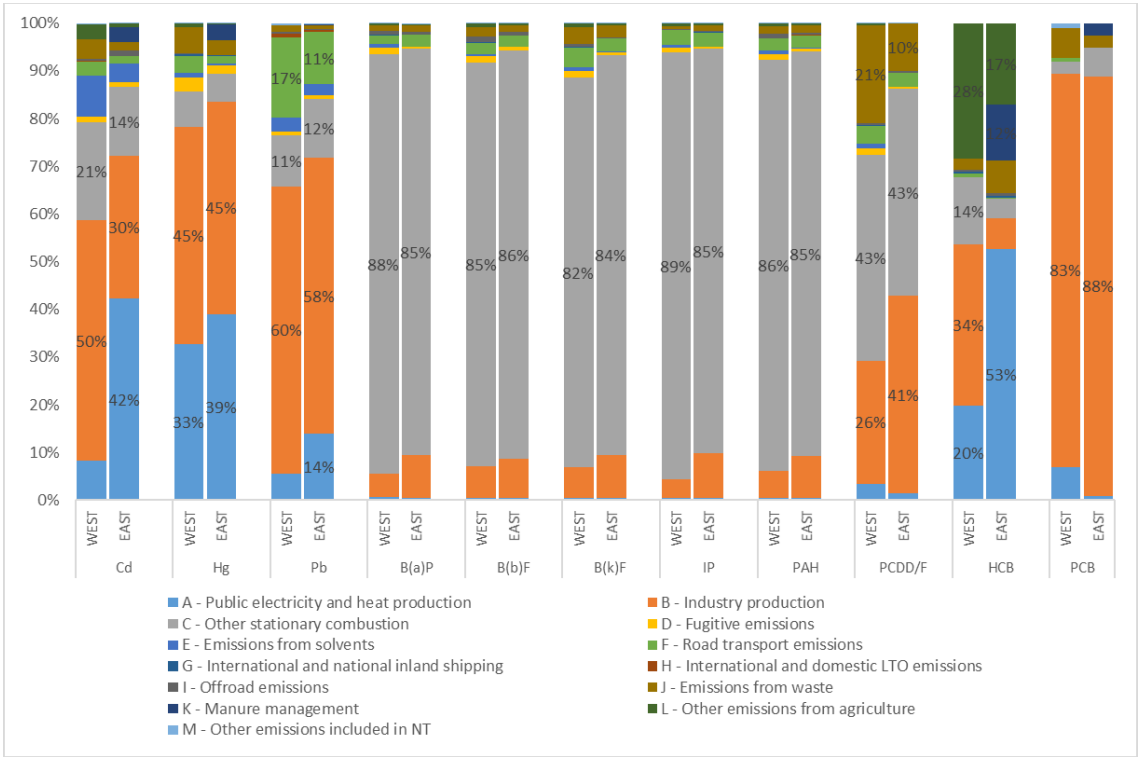

Fig. 1.9. *GNFR sector contribution to national total emissions in 2019 for the EMEP West and EMEP East areas (Only percentages above 10% are labelled. 'Remaining Asian Areas' are included in the EMEP East region and North Africa is included in the EMEP West region).*

The continuous revision of inventory data for many countries shows that POPs emissions have the highest uncertainties of all pollutant groups. In addition, data for EMEP East region is subject to incomplete reporting or delays in reporting. Especially for POPs, one should therefore draw conclusions carefully when comparing the shares between EMEP East and EMEP West regions.

Reporting of gridded data

After the first round of submissions in 2017, 2021 was the second year for which EMEP countries were obliged to report gridded emissions in the grid resolution of 0.1°x0.1° (long/lat). 33 of the 48 countries which are considered as a part of the EMEP area reported sectoral gridded heavy metal and POP emissions in the new resolution until June 2021.

The majority of gridded sectoral emissions in 0.1°x0.1° (long/lat) resolution have been reported for the year 2015 (32 countries). For 2019 gridded sectoral emissions have been reported by 28 countries, for 2016 and 2017 by five countries and for 2018 by four countries. Compared to the 2017 reporting, gridded data are available for 10 additional countries in 2021.

Fifteen countries reported gridded emissions additionally for previous years (one country for the whole time series from 1980 to 2019; one country for the whole time series from 1990 to 2019; seven countries for the years 1990, 1995, 2000, 2005 and 2010; one country for the years 1990, 2000, 2005 and 2010; one country for the years 2000, 2005 and 2010; one country for the year 2005; one country for the year 2010; and two countries for the year 2014).

Reported gridded sectoral data in 0.1°x0.1° (long/lat) resolution, which can be used for the preparation of gridded emissions for modellers, covers less than 20 % of the cells within the geographic EMEP area. For the remaining areas missing emissions are gap-filled and spatially distributed using expert estimates. Reported grid data can be downloaded from the CEIP website[6]. An overview of gridded data in 0.1°x0.1° (long/lat) resolution reported in 2017, 2020 and 2021 is provided in Table 1.3.

[6] https://www.ceip.at/status-of-reporting-and-review-results/2021-submission

Table 1.3. *Gridded emissions reported until 2017, 2020 and 2021*

Country	2017	2020	2021	Comments
	Gridded data available for the years…	Gridded data available for the years…	Gridded data available for the years…	
Austria	2015	2015	2000, 2005, 2010, 2015, 2019	
Belgium	2015	2015	2015, 2019	
Bulgaria	2015	2015	2015, 2019	
Croatia	1990, 1995, 2000, 2005, 2010, 2015	1990, 1995, 2000, 2005, 2010, 2015	1990, 1995, 2000, 2005, 2010, 2015, 2019	
Cyprus			1990, 1995, 2000, 2005, 2010, 2015, 2019	
Czechia	2015	2015	2015, 2019	
Denmark	2015	2015	2015, 2019	
Estonia		1990, 1995, 2000, 2005, 2010, 2015	1990, 1995, 2000, 2005, 2010, 2015, 2019	
Finland	2014, 2015	2014[a], 2015[a], 2016, 2017, 2018[a]	1990, 1995, 2000, 2005, 2010, 2015, 2016, 2017, 2019	[a] Gridded data for 2014, 2015 and 2018 could not be used for the preparation of spatial distributed emission data in 2020
France		2015	2015, 2019	
North Macedonia		2015	2015, 2019[b]	[b] The submission of gridded emissions was too late to be considered for the preparation of gridded data for modelers in 2021
Georgia		2015	2015	
Germany			1990, 1995, 2000, 2005, 2010, 2015, 2019	
Greece		2015	2015, 2019	
Hungary	2015[c]	2015	2015	[c] The submission of gridded emissions was too late to be considered for the preparation of gridded data for modelers in 2017
Ireland	2015	2015	2015, 2019[d]	[d] The submission of gridded emissions was too late to be considered for the preparation of gridded data for modelers in 2021
Italy		2015[e]	2015[e]	[e] Reported gridded data was replaced by CAMS and EDGAR proxies
Latvia	2015	2015	2015, 2019	

Lithuania	2015[f]	2015	2015, 2019[g]	[f] Reported gridded emissions only on national total level, which could not be used for the gridding, which is done on sectoral level [g] The submission of gridded emissions was too late to be considered for the preparation of gridded data for modelers in 2021
Luxembourg	2015	2015	2015, 2019	
Malta		2016	2016	Grid reporting not in the defined 0.1°x0.1° coordinates
Monaco	2014, 2015	2014-2016	2014-2019	
Netherlands		1990, 1995, 2000, 2005, 2010, 2015	1990, 1995, 2000, 2005, 2010, 2015, 2019	
Norway	1990, 1995, 2000, 2005, 2010, 2015	1990, 1995, 2000, 2005, 2010, 2015	1990, 1995, 2000, 2005, 2010, 2015, 2019	
Poland	2014, 2015	2014, 2015, 2018	2014, 2015, 2018, 2019	
Portugal	2015	2015	2015, 2019	The spatial disaggregation of sector 'F – Road Transport' was replaced by CAMS proxies
Romania	2005	2005, 2015	2005, 2015	
Slovakia	2015	2015	2015, 2019	
Slovenia	2015	2015	2015, 2019	
Spain	1990-2015	1990-2018	1990-2019	The spatial disaggregation of sector 'F – Road Transport' was replaced by CAMS proxies
Sweden		1990, 2000, 2005, 2010, 2015	1990, 2000, 2005, 2010, 2015, 2019	
Switzerland	1980-2015	1980-2018	1980-2019	
United Kingdom	2010, 2015	2010, 2015	2010, 2015, 2019	

Gridded data of 2019 in resolution 0.1° x 0.1° (long/lat)

For this year, it was agreed with the modellers to perform gap-filling and gridding for the year 2019 in 0.1° x 0.1° longitude/latitude resolution on GNFR sector level.

The 0.1° x 0.1° GNFR grids of heavy metals (Cd, Hg, Pb) and POPs (B(a)P, B(b)F, B(k)F, IcdP, PCDD/Fs, HCB) were spatially distributed based on the gridding system developed by CEIP. A map of total Pb emissions in 2019 is shown in Fig. 1.10 as an example. The system is module based and uses as a first step reported gridded emission data for each country and sector where it is available and usable. If

no reported gridded data in the 0.1° x 0.1° (long/lat) resolution is available, reported gridded PM data is used as a proxy for spatial disaggregation. If reported PM data is not available either, PM data from the Copernicus Atmospheric Monitoring Service (CAMS-81, CAMS-REG-AP) and the Emission Database for Global Atmospheric Research (EDGAR) is used as a proxy [*JRC*, 2019; *Crippa*, 2019].

Reported gridded data in 0.1° x 0.1° (long/lat) resolution was used from Austria, Belgium, Bulgaria, Croatia, Cyprus, Czechia, Denmark, Estonia, Finland, France, Georgia, Germany, Greece, Hungary, Ireland, Latvia, Luxembourg, Malta, Monaco, Netherlands, North Macedonia, Norway, Poland, Portugal, Romania, Slovakia, Slovenia, Spain, Sweden, Switzerland and the United Kingdom.

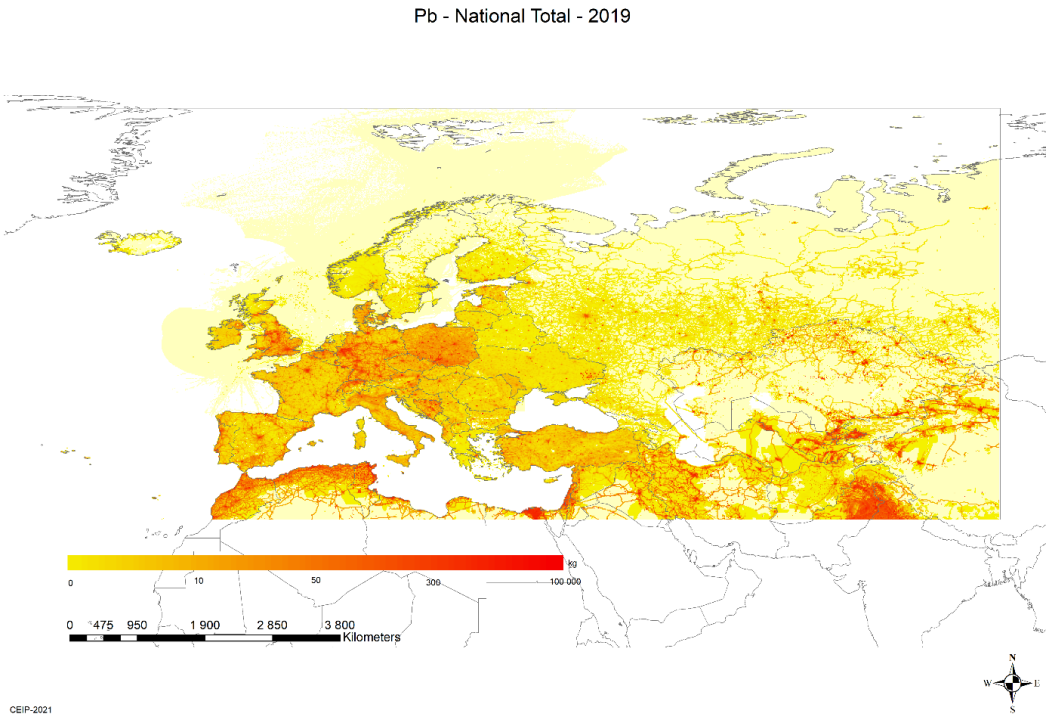

Fig. 1.10. *Visualized gap-filled and gridded Pb emissions in 0.1°x0.1° long-lat resolution.*

1.2. Emission data for modelling

Regional emissions

Model assessment of heavy metal and POP pollution in the EMEP domain was made on the basis of gridded emission data with spatial resolution 0.1°x0.1° provided by CEIP (*http://www.ceip.at*). Pollution levels of heavy metals and POPs in 2019 (Chapter 3) were evaluated using emission data, reported for the previous year 2018. Update of the modelling results based on the new emission data for 2019 is available in Annex B and at the MSC-E web site: https://en.msceast.org/index.php/pollution-assessment/emep-domain-menu. Detailed description of estimated heavy metal and POP emissions in the EMEP countries, gap-filling methods, and expert

estimates used for preparation of the emission inventory, can be found in the CEIP Technical reports [*Poupa and Wankmueller*, 2020; *Poupa et al.,* 2020].

Model simulations for Pb, Cd, Hg and PAHs were based on the officially reported emission data. For PCBs, PCDD/Fs and HCB a combination of official emission data and expert estimates was applied for modelling. In particular, for the assessment of PCB pollution officially reported inventories were combined with available expert estimates of emissions. Currently reported PCB emissions provide only total amount of PCBs without specifying particular congeners emissions. However, modelling of PCBs requires definition of emissions of particular PCB congeners. Therefore, to evaluate transport and fate of individual PCB congeners, the congener specific emission inventory by *K.Breivik et al*. [2007] was used for modelling. The indicator congener PCB-153 was selected to characterize transboundary transport and pollution by PCBs. Spatial distribution of PCB-153 emissions was constructed on the base of gridded PCB emissions officially provided by 28 EMEP countries (namely, Austria, Belgium, Bulgaria, Croatia, the Czechia, Denmark, Finland, France, Georgia, Greece, Hungary, Ireland, Italy, Latvia, Lithuania, Luxembourg, North Macedonia, Monaco, Norway, Poland, Portugal, Romania, Slovakia, Slovenia, Spain, Sweden, Switzerland and the UK). For other EMEP countries, which did not report gridded emission data, gridded population density was used for spatial allocation of emissions.

Estimates of PCDD/F emissions, officially reported by the EMEP countries, may incorporate considerable uncertainties due to incomplete coverage of all potential sources [*Breivik et al.*, 2004; *Fiedler*, 2007; *Pulles et al.*, 2005; *Pulles et al.*, 2006] that might lead to underestimation of releases to the atmosphere. For this reason, a scenario, representing maximum level of PCDD/F emissions, was used in the model simulations. The maximum emission scenario was prepared on the basis of the uncertainty range reported by 15 EMEP countries in their inventory information reports (namely, Austria, Belarus, Belgium, Croatia, Cyprus, Denmark, Estonia, Finland, France, Latvia, Poland, Republic of Moldova, Sweden, Switzerland, and the UK). Difference between the maximum and average estimates of PCDD/F emissions in these countries varied from a factor of 1.3 for France up to a factor of 5.2 for Denmark. For other EMEP countries, which did not report uncertainty range in their inventories, the maximum level of national PCDD/F emissions was assumed to be 3-fold higher compared to the officially reported emissions in accordance with the expert estimates [*Pulles et al.*, 2006; *Bogdal et al.*, 2014]. Thus, total PCDD/F emission in the EMEP countries according to the maximum emission scenario exceeded reported data in the inventories by a factor of 3.5 on average. This approach has already been applied in the model assessment [*Gusev et al*., 2018].

Similarly, a scenario representing maximum level of emissions to the atmosphere was prepared and applied for HCB model simulations. The scenario was based on the data on the uncertainty range of HCB emissions reported by 14 EMEP countries in their inventory information reports (namely, Austria, Belarus, Belgium, Croatia, Cyprus, Denmark, Estonia, Finland, France, Latvia, Poland, Republic of Moldova, Switzerland, and the United Kingdom). Difference between the maximum and average estimates of HCB emissions in these countries varied from a factor of 1.08 for Cyprus up to a factor of 5.8 for Denmark. For other EMEP countries, which did not report uncertainty range in their inventories, difference between the maximum and average emissions was set to a factor 2.2 (average difference based on the data for above-mentioned countries). The total HCB emissions in

the EMEP countries according to the maximum emission scenario were higher than reported data in the inventories by a factor of 2.8 on average.

Maps illustrating spatial distributions of the pollutants, namely, Pb, Cd, Hg, B(a)P, sum of 4 PAHs, PCDD/Fs, HCB and PCB-153 emission fluxes from anthropogenic sources in the EMEP region, used in the model simulations for 2019, are presented in Fig. 1.11.

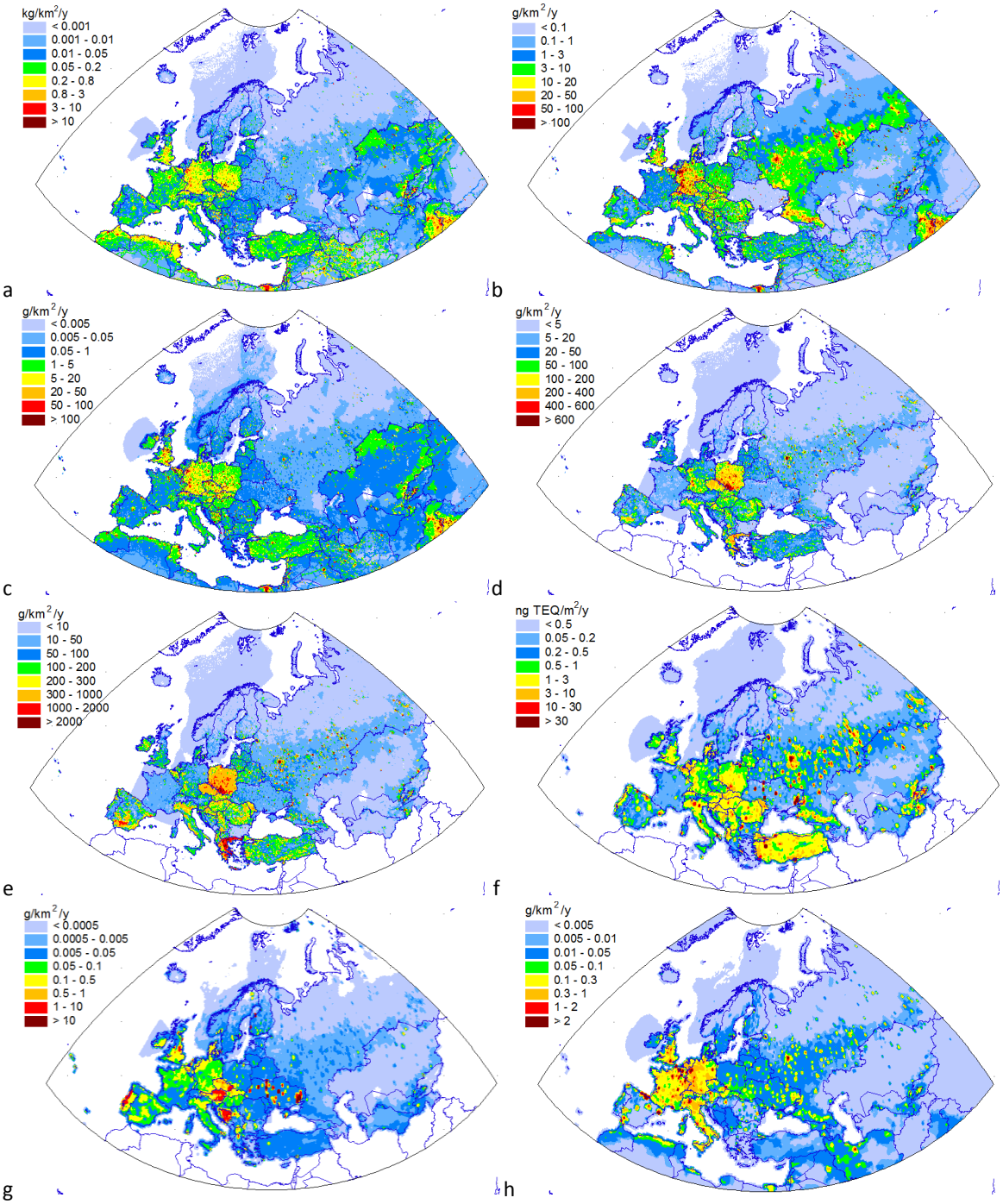

Fig. 1.11. *Spatial distribution of Pb (a), Cd (b), Hg (c), B(a)P (d), sum of 4 PAHs (e), PCDD/Fs (f), HCB (g) and PCB-153 (h) emissions in the EMEP region used in model simulations for 2019.*

Along with gridded emission data, the GLEMOS modelling system requires additional information on heavy metal and POP emissions, namely, intra-annual variations, distribution of emissions with height and chemical speciation of Hg emissions. Necessary vertical and temporal disaggregation of the emissions was generated using the emission pre-processing tool, developed in MSC-E for the GLEMOS modelling system. More detailed information on the emission pre-processing procedure is presented in the heavy metal Status Report [*Ilyin et al.*, 2018].

Global emissions

A number of pollutants, such as mercury and some POPs, are known for their ability to disperse in the atmosphere over the global scale. In order to take into account contribution of intercontinental transport to pollution levels in the EMEP countries and to evaluate boundary and initial conditions required for the regional EMEP modelling, global-scale model simulations are carried out.

Mercury

A new global inventory of mercury anthropogenic emissions for 2015 has been produced as a part of the Global Mercury Assessment 2018. A new improved methodology has been developed for the inventory that allows better characterization of differences between countries in terms of fuels and raw materials used as well as technologies and practices applied. The global mercury emission inventory in 2015 is estimated at 2220 tonnes (range 2000-2820 tonnes) and comprises emissions from the 17 major anthropogenic source sectors, such as artisanal and small-scale gold mining (ASGM), combustion of fossil fuels (mainly coal) in power plants, industrial and residential boilers, metal production (ferrous and non-ferrous), cement production, product use, and cremation. There are three new sectors not previously quantified, namely biomass combustion (for energy production), secondary steel production and Hg emitted during the production of vinyl chloride monomer (VCM), a raw material for plastics including polymer polyvinyl chloride (PVC) [*AMAP/UN Environment*, 2019]. The largest emissions of mercury to the global atmosphere in 2015 are associated with the ASGM (838 tonnes) and stationary combustion of coal (474 tonnes). Other major emission sectors include cement production (233 tonnes) and non-ferrous metal production (228 tonnes).

Figure 1.12 presents the global distribution of anthropogenic emissions of mercury in 2015 in accordance with the new inventory. The map illustrates areas with elevated mercury emissions in Asia (especially, South, East and South-east Asia) associated with energy production and industry, and, in some countries, with ASGM. It also shows the significant contribution of South America, Central America and the

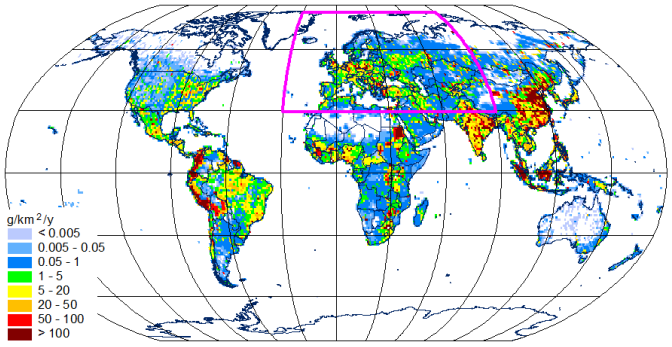

Fig. 1.12. *Global distribution of anthropogenic emissions of mercury in 2015. Pink line depicts boundary of the EMEP region.*

Caribbean, and Sub-Saharan Africa to emissions linked with the ASGM activities. Emissions related with energy production and industrial sources predominate in the industrialized regions of Europe and North America [*AMAP/UN Environment*, 2019].

Contribution of different regions to total mercury emissions on a global scale in 2015 is shown in Fig. 1.13. The majority of the global emission of mercury occurring in Asia (49%, of which 27% is in East Asia) followed by Africa (17%) and South America (13%) [*AMAP/UN Environment*, 2019].

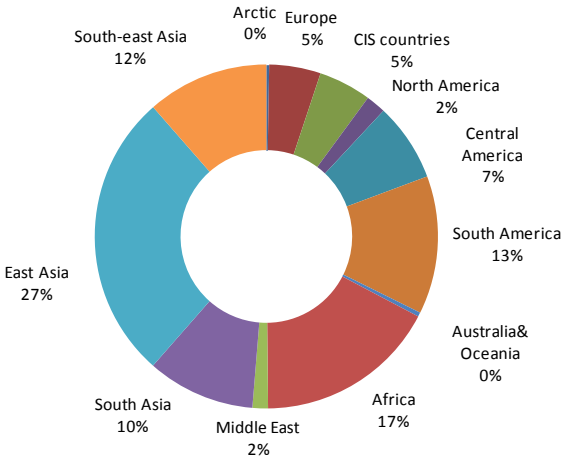

Fig. 1.13. *Contribution of different regions to the global anthropogenic mercury emissions in 2015.*

POPs

Intercontinental transport of PAHs is simulated based on the inventory, developed by the research group of Peking University [*Shen et al.*, 2013]. Global PAH emission inventories with 0.1°x0.1° spatial resolution were elaborated using a bottom-up approach for the period from 1960 to 2014. For the evaluation of global-scale transport and fate of PCDD/Fs, HCB, and PCBs expert estimates of global emissions were utilized. In particular, global gridded emissions of PCDD/Fs to the atmosphere and soil were prepared using the national emission inventories reported by countries to the Stockholm Convention [*Gusev et al.*, 2014; *Shatalov et al.*, 2014]. Model simulations of HCB global-scale transport were carried out on the basis of experimental emission scenario of historical HCB releases during the period covering several recent decades [*Shatalov et al.*, 2010]. For PCB-153 modelling, data on global emissions were derived from the inventory of *Breivik et al.* [2007]. Spatial distributions of B(a)P and PCB-153 emissions, used in the global-scale model simulations for 2019, are shown in Fig. 1.14.

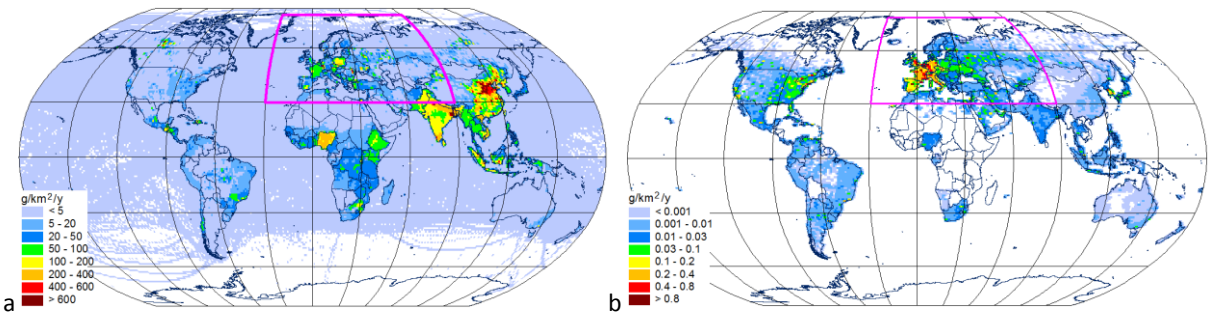

Fig. 1.14. *Spatial distribution of global annual emissions of B(a)P (a) and PCB-153 (b) with spatial resolution 1°x1°, used in the model simulations for 2019. Pink line depicts boundary of the EMEP region.*

Chapter 2. MEASUREMENTS OF HEAVY METALS AND POPs

2.1. Monitoring of heavy metals and POPs in 2019

Heavy metals (HMs) and persistent organic pollutants (POPs) were included in EMEP's monitoring program in 1999. However, earlier data have been reported and are available. The EMEP database, especially for heavy metals, thus also includes older data, even back to 1976 for a few sites. A number of countries have been reporting information on heavy metals and POPs within the EMEP area in connection with different national and international programmes such as HELCOM, AMAP and OSPAR.

The EMEP monitoring strategy [*UNECE*, 2019] defines the monitoring obligations for the Parties. For POPs, polycyclic aromatic hydrocarbons (PAHs), polychlorinated biphenyls (PCBs), hexachlorobenzene (HCB), chlordanes (CHLs), lindane/γ-hexachlorohexane (γ-HCH), α-HCH, and DDT/DDE are part of the compulsory monitoring programme. For heavy metals, Hg, Cd and Pb are the first priority elements while Cu, Zn, As, Cr, Ni are the second priority. In addition to these compounds several Parties report other POPs and trace elements. In addition to regulated POPs, it is recommended to increase the attention on organic contaminants of emerging concern (CECs). A specific chapter is devoted to this topic.

All the data are available from the EBAS database (http://ebas.nilu.no/), and more detailed information about the sites and the measurement methods, these are found in EMEP/CCC's data report on heavy metals and POPs [*Aas et al.*, 2021].

2.1.1. Monitoring of heavy metals in 2019

In 2019, there were 37 sites measuring heavy metals in both aerosols and precipitation, and altogether there were 65 measurement sites. 24 sites were measuring mercury in either air or precipitation, 14 of these with concurrent measurements in air and precipitation. In total, 20 Parties to the Convention reports heavy metal data to EMEP.

Annual averages of As, Cd, Cr, Cu, Ni and Pb concentrations in aerosols and precipitation in 2019 are presented in Fig. 2.1 to Fig. 2.2, and Hg in Fig. 2.3. The spatial distribution of aerosol is better than in precipitation having more sites with observations in precipitation. The highest concentrations are in general seen in Eastern Europe but there are hotspots for some elements in other parts of Europe, i.e., for As, Pb and Cr it is relatively high levels around the English Channel. Cr has in addition to anthropogenic sources high concentrations in crustal material and that can be the reason for relatively high concentration of Cr in Cyprus and Italy.

For mercury in air, the highest concentration is seen in Poland followed by sites in Germany and the United Kingdom, while in precipitation the highest concentrations are seen in the Czech Republic and in Finland. Generally, the observed concentrations in air harmonize very well with regions of Hg emission and modelled concentrations apart from the site in Spain showing extremely low concentrations (0.57 ng/m^3) indicating problems with the measurements. Observed concentrations

of Hg in precipitation in 2019 are similar to 2018, apart from the two sites in southern Sweden showing considerably lower concentrations compared to the anomalous year 2018. Poland continues to report suspiciously low concentrations in precipitation.

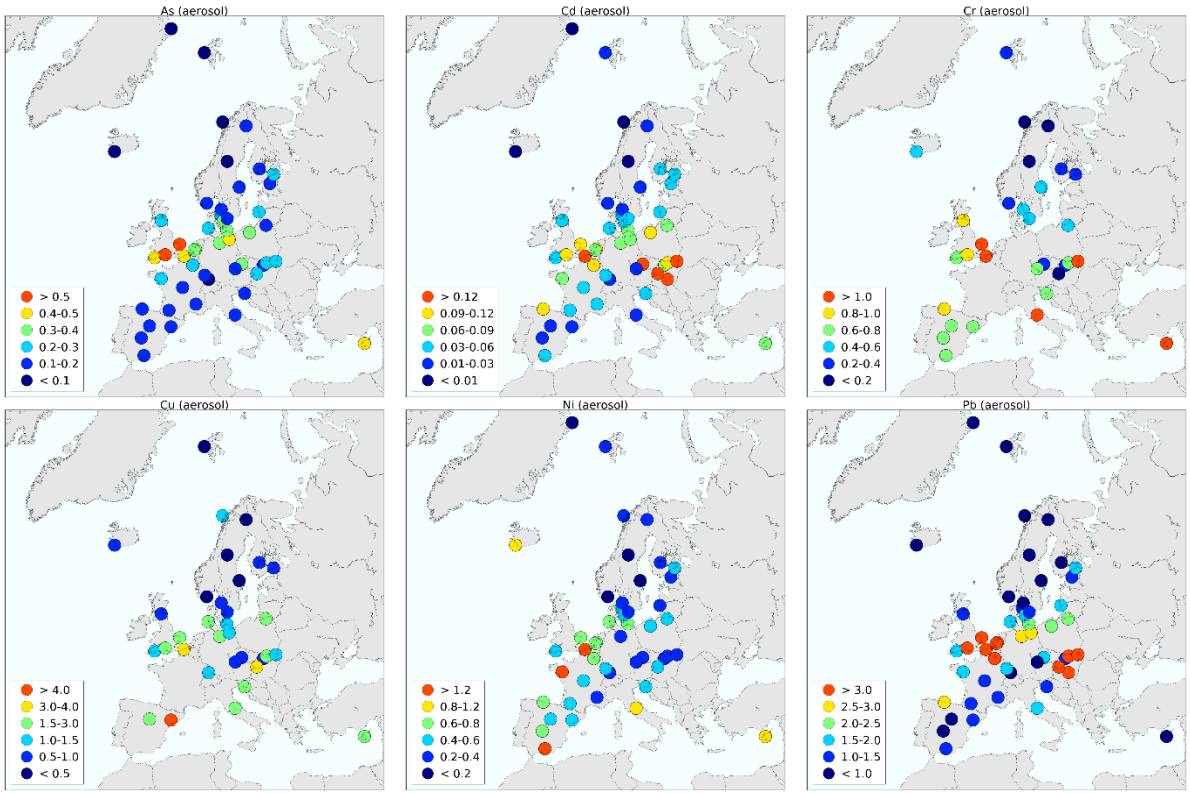

Fig. 2.1. *Annual mean concentrations of As, Cd, Cr, Cu, Ni and Pb in aerosols (ng/m^3) in 2019.*

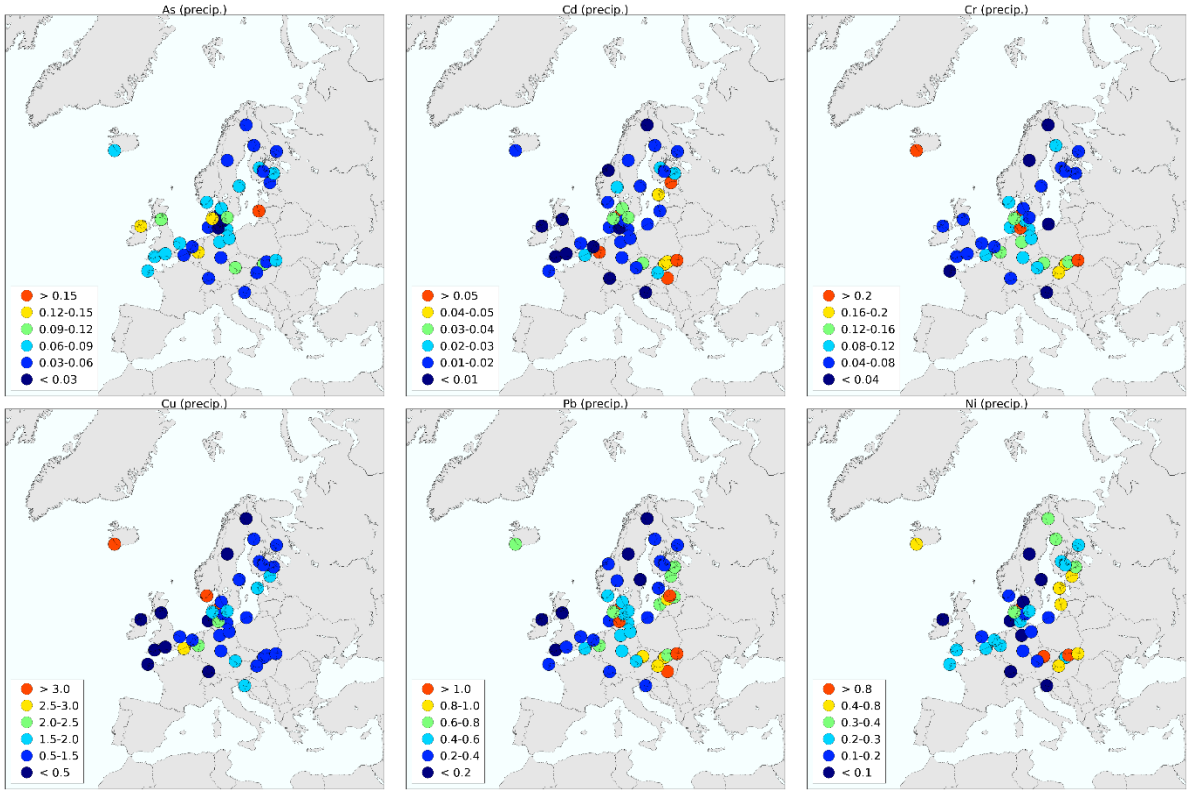

Fig. 2.2. *Annual mean concentrations of As, Cd, Cr, Cu, Ni and Pb in precipitation (µg/L) in 2019.*

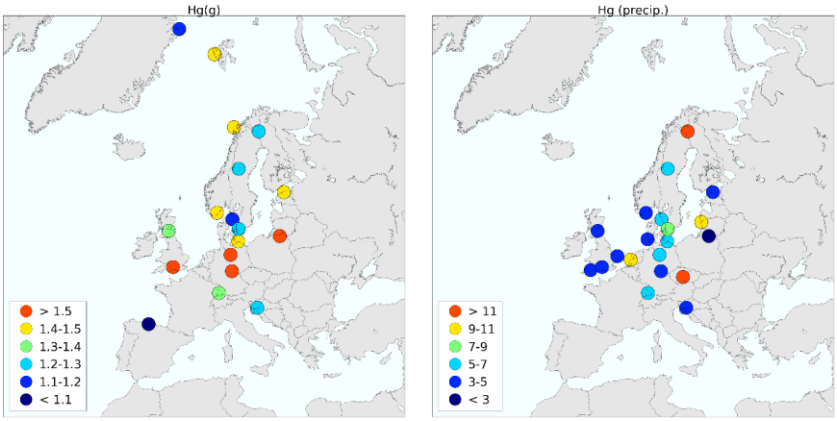

Fig. 2.3. *Annual mean concentrations of mercury in air (ng/m^3) and precipitation (ng/L) in 2019.*

Quality of HM measurements within EMEP

Laboratory intercomparisons have been conducted within EMEP almost since the start of the program, and it has been an important tool to assess and improve the quality of the measurements. All EMEP laboratories are obligated to participate, however in order to ensure comparability between measurements networks, the comparison is also open to other laboratories in relevant programs such as EANET, ICP-Forest etc. Heavy metals were included in the EMEP monitoring program in 1999, and concurrently HMs in precipitation was included in the intercomparison on an annual basis. Based on results from the intercomparison, so-called QA measures are calculated. QA measure is a general term for different procedures involved in the quality assurance (QA) of the measurements. Since 2016, results from these intercomparisons have been available and Parties should link QA measures to the measurement results submitted to EBAS.

QA measures are used to quantify the quality of the measurements. QA metadata are split into QA variability (random errors) and QA bias (systematic errors). The QA variability can be linked to the data quality objectives (DQO) to determine whether the laboratory has passed or not passed the QA measure, and for HM's the criteria is set to 25%. The QA bias is signed with systematic if more than 75% (3 of 4 samples) of the samples in the comparison are systematically negative or positive, giving a possibility for the data user to correct the data if wanted. Results from calculations of QA measures can be found on the EMEP laboratory intercomparison website: https://projects.nilu.no/ccc/intercomparison/index.html

The majority of EMEP laboratories participating in the EMEP laboratory intercomparison report results of good quality, however a few laboratories would benefit from improving their quality. Considering QA bias, representing systematic errors, many laboratories perform well with QA bias better than 10% for most elements, throughout the course of intercomparison rounds (Fig. 2.4). The variability in QA bias between different rounds is rather large for all elements, and the laboratories performance seem rather unchanged, with no general improvement nor exacerbation.

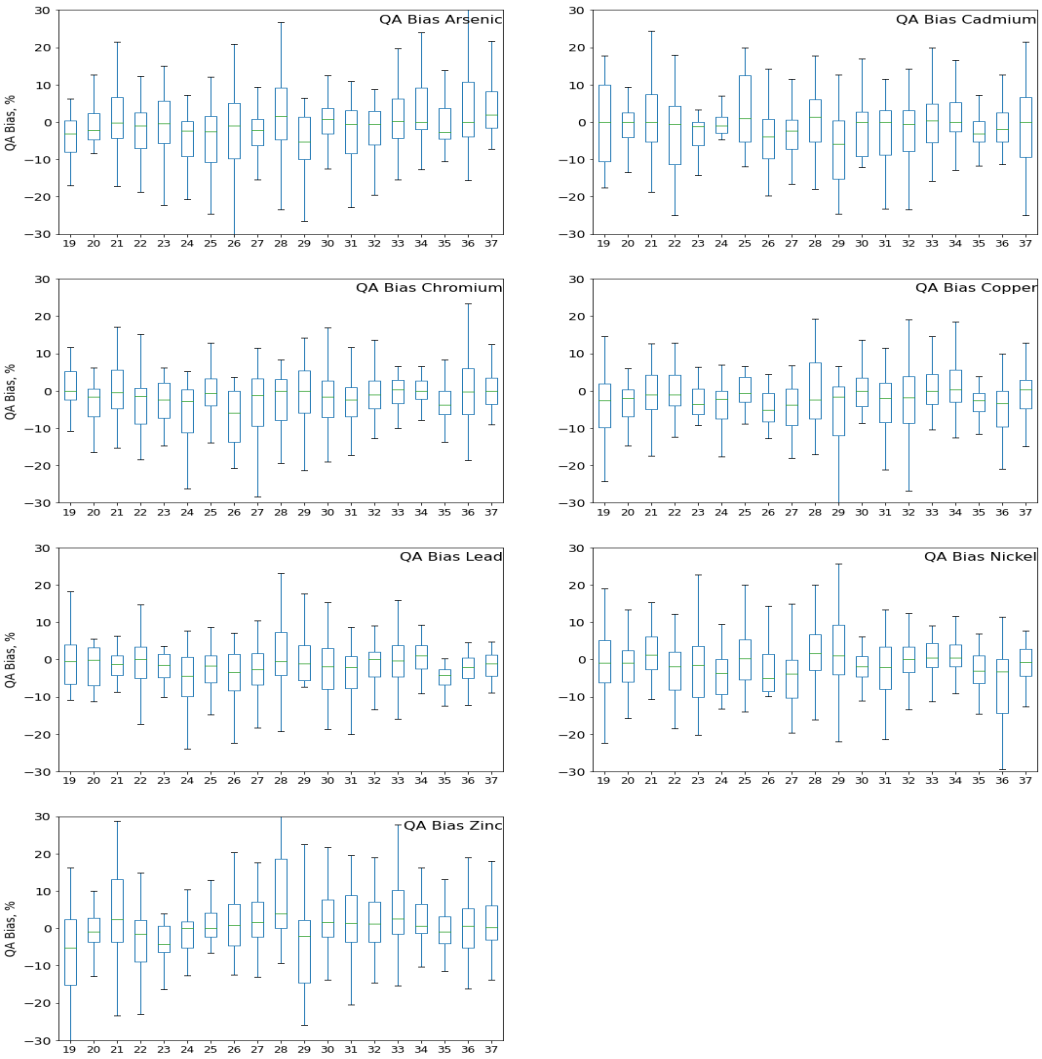

Fig. 2.4. *Box and whisker plots showing the trend in QA bias (systematic errors) for heavy metals in precipitation. The numbers indicate the round of intercomparison from 19 (2001) to 37 (2019) and the box plots are calculated for all the participating laboratories in the different rounds. The green line inside the box represents the median, the lower and upper border of the box represent the 25th and 75th percentile, and the whiskers represent the 10th and 90th percentile.*

Most labs meet the criteria of QA variability set to 25% (Fig. 2.5). Generally, random errors have improved throughout the course of intercomparison rounds, and 75% of the participating laboratories have QA variability within 10%. In particular for round 37 (2019) the results were very good, with only 3 laboratories exceeding the criteria of 25% for As and Cu, 2 for Zn and 1 for Pb, whereas all laboratories passed for Cd, Cr and Ni. It must be noted that when assessing a laboratory's performance in the intercomparison, both QA bias and variability should be considered.

Samples for Hg in precipitation is not provided within the EMEP laboratory intercomparison. The last QA measure taken was in 2005 when UBA (Umweltbundesamt, Germany) arranged a field intercomparison for mercury measurements in air and precipitation within EMEP. We suggest that either a new field intercomparison for Hg would be a good investment to improve quality of Hg measurements in air and precipitation, or to introduce samples for Hg in precipitation to the EMEP laboratory intercomparison.

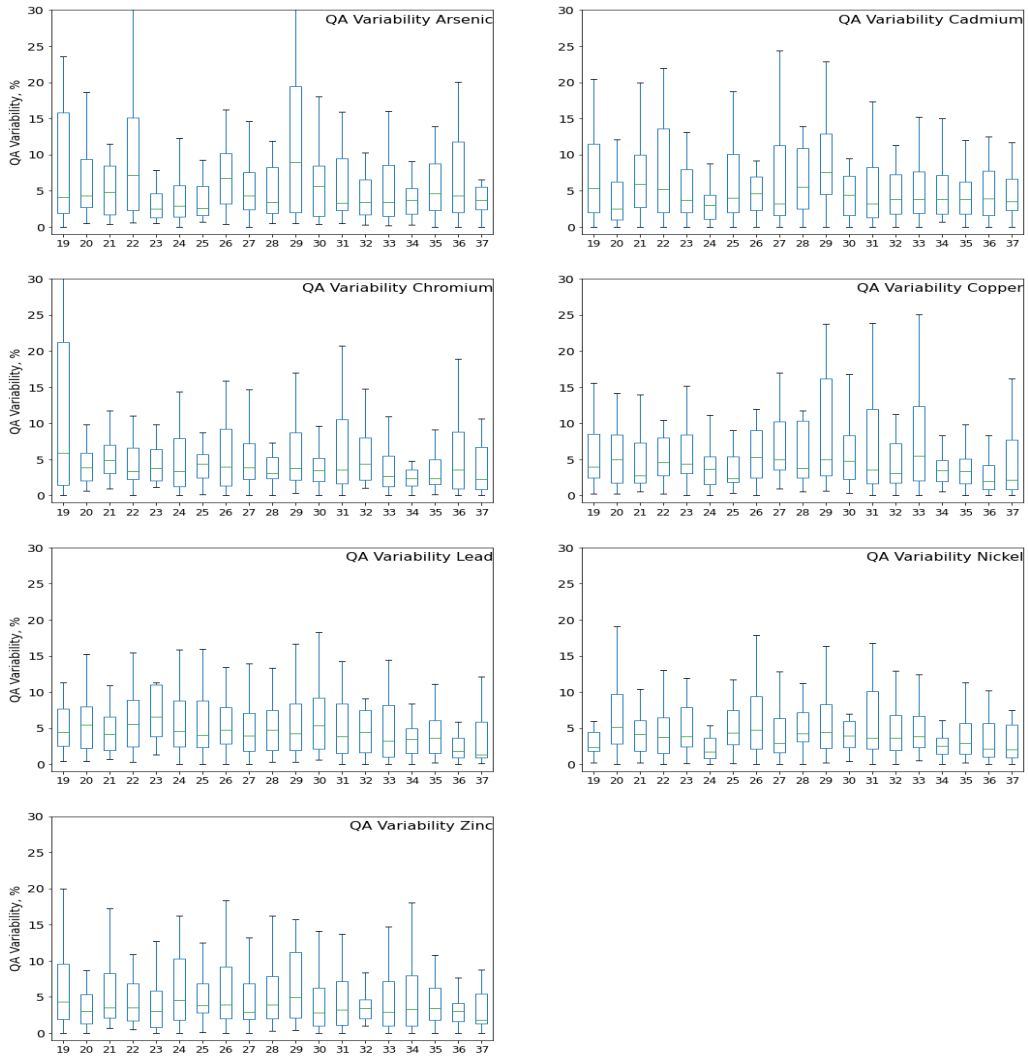

Fig. 2.5. *Box and whisker plots showing the trends in QA variability (random errors) for heavy metals in precipitation. The numbers indicate the round of intercomparison from 19 (2001) to 37 (2019) and the box plots are calculated for all the participating laboratories in the different rounds. The green line inside the box represents the median, the lower and upper border of the box represent the 25th and 75th percentile, and the whiskers represent the 10th and 90th percentile.*

2.1.2. Monitoring of POPs in 2019

The spatial coverage of POP monitoring in Europe is depending on which components in question. Concentration maps of selected POPs are shown in Fig. 2.6. In total there are 39 sites reporting 2019 data on POPs whereof 27 sites with measurements in both air and precipitation. Data are available from 17 Parties. One should further notice that several of the Parties only measure PAHs (i.e. 9 Parties and 26 sites). For precipitation measurements, it is a challenge to compare the observations since the measurements are done using several different methods. There are four different matrices defined for precipitation, i.e. total deposition (precip+dry_dep: 8 sites + 5 Spanish sites with campaign data), concentration in precipitation (precip: 12 sites); concentration in precipitation + POPs deposited in the funnel (precip_tot: 5 sites) and wet deposition (wet dep: 2 sites).

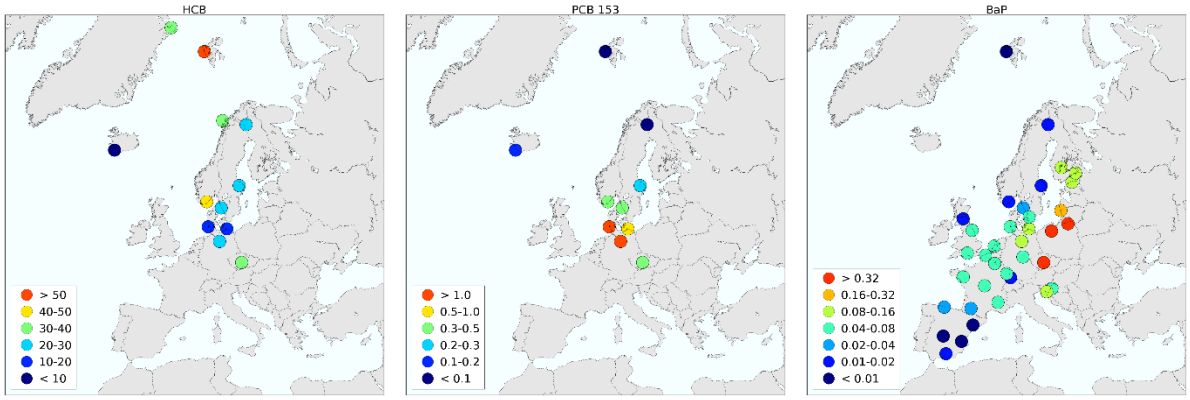

Fig. 2.6. *Annual mean concentrations of HCB, PCB-153, pg/m^3 and benzo[a]pyrene, ng/m^3 in air and aerosols in 2019.*

Passive air sampling in background air

Active air sampling (AAS) of POPs remains as the recommended sampling methods within EMEP [*EMEP*, 2014]. These data are invaluable for measuring concentrations in air and for the evaluation of numerical models within EMEP and beyond. A cost-efficient complementary approach to AAS is passive air sampling (PAS), which have been utilized in several EMEP countries [*Kalina et al.*, 2018 and 2019; *Munoz-Arnanz et al.*, 2016] and many other studies [*Jaward et al.*, 2004; *Pozo et al.*, 2006; *Schuster et al.*, 2011].

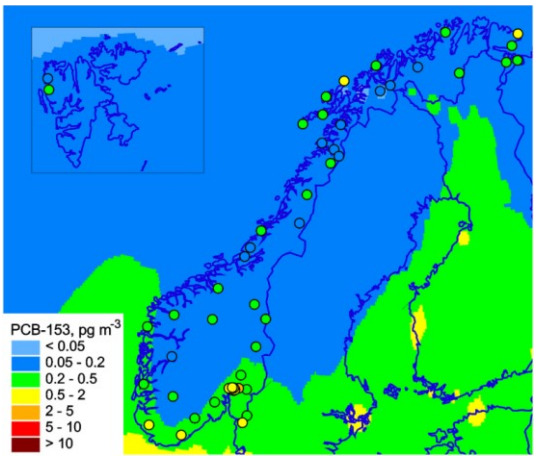

Fig. 2.7. *Observed and predicted spatial patterns of PCB-153 in air during summer 2016 [Halvorsen et al., 2021].*

A comprehensive passive air sampling campaign was carried out across 32 European countries during summer 2016 [*Halvorsen et al.*, 2021]. This campaign covered many EMEP sites and was carried out ten years after a similar campaign in 2006 [*Halse et al.*, 2011]. A key goal was to combine the measurements from the more recent PAS campaign with predictions from the Global EMEP Multi-media Modeling System (GLEMOS). The number of sites was particularly high in Norway, covering 45 background sites on the Norwegian mainland and 2 sites on Svalbard. By using GLEMOS in concert with the PAS data, a specific objective was to assess the relative importance of long-range atmospheric transport and primary and secondary emissions in controlling observed concentrations in Norwegian background air [*Halvorsen et al.*, 2021]. Figure 2.7 shows a comparison of the observed and predicted spatial pattern in air for PCB-153. A general finding was that the GLEMOS model largely reproduces observed concentration in air within a factor of 3. Observed concentrations of PCB-153 in air were furthermore fairly homogenous across Norwegian background sites. This provides strong indications that atmospheric burdens of PCB-153 in background air across Norway are mainly controlled by long-range atmospheric transport. Similar inferences were made for a wide range of

organochlorine pesticides as most POPs showed a limited spatial variability. However, for some POPs for which wet deposition may be an important removal mechanism from the atmosphere, a south-to-north gradient was observed (e.g. γ-HCH and Endosulfan I).

Taken together, the study illustrates the utility of using mechanistic models such as GLEMOS to help interpret monitoring data based on PAS as well as AAS. The applied methodology may furthermore be used to inform background monitoring strategies within EMEP, as well as further refined to address chemicals other than PCB-153.

Observations of POPs other than those listed in Level 2 and organic contaminants of emerging concern (CEC)

Long-term plans of the EMEP strategy on persistent organic pollutants (POPs) recommends monitoring on of polycyclic aromatic hydrocarbons (PAHs), polychlorinated biphenyls (PCBs), hexachlorobenzene (HCB), chlordane, lindane (γ-HCH), α-HCH and DDT/DDE (Level 2). The new strategic plan for 2020-2029 also includes recommendation for monitoring of POPs other than those listed for Level 2 as well as organic contaminants of emerging concern (CECs) (Level 3). Examples of POPs other than those listed in Level 2 are polybrominated diphenyl ethers (PBDEs), per- and polyfluorinated alkyl substances (PFAS) and short-chain chlorinated paraffins (SCCPs). These POPs are included in the 2009 amendment of the Aarhus protocol on POPs.

The rationale for expanding the list of POPs is that new organic chemicals are continuously entering the market, either as substitutes to replace the regulated POPs or to fulfill new demands. These chemicals are often designed to be less persistent, more polar and less hydrophobic than regulated chemicals. Despite that, some may have similar impacts on ecosystems as the legacy POPs while some may fulfill persistence and mobility criteria but do not necessarily bioaccumulate [*Brown*, 2008; *Howard*, 2010]. Therefore, also such chemicals need to be put on equivalent level of concern as traditional POPs. POP-like chemicals of emerging concern (CECs) is an ever-growing list and various studies have identified CECs in remote locations, such as the Arctic [*Carlsson*, 2018; *Krogseth*, 2013; *Möller*, 2010; *Röhler*, 2020; *Wong*, 2018]. Examples of CECs are medium-chain chlorinated paraffins (MCCPs), volatile PFAS, cyclic volatile methyl siloxanes (cVMS), new brominated flame retardants (nBFRs), organophosphorous flame retardants (OPFRs), phthalates, and dechloranes.

Data on POPs other than those listed in Level 2 have been reported from eight sites in the EMEP network (Table 2.1). Data is available from 2006 at Zeppelin, Spitsbergen (NO0042G) and from 2008 at Storhofdi (IS0091R), Birkenes (NO0002R) and Andøya (NO0090R).

Table 2.1. *Monitoring of POPs other than those listed in Level 2 in the EMEP network.*

Station code	Station name	PBDEs	PFAS
DK0010G	Villum R.S. North Greenland	2014	
FI0036R	Pallas/Matorova	2013	2017
IS0091R	Storhofdi	2008	
NO0002R	Birkenes	2008	2006
NO0042G	Zeppelin, Spitsbergen	2006	2006
NO0090R	Andøya	2008-2016	2009
SE0014R	Råö	2013	2013
SE0022R	Norunda Stenen	2018	

In general, the concentrations of PBDEs and PFAS are low at the EMEP sites but analysis of the spatial pattern for these new POPs is hampered by limited number of stations (Figs. 2.8 and 2.9). Another factor hampering the comparison of data on new POPs are lack of intercomparison between laboratories and a bigger uncertainty of data. There is a need to improve data comparability and a stimulation of including also other POPs at a larger number of EMEP sites. Sampling campaigns with alternative sampling and/or analytical strategies, such as passive sampling or active sampling with analysis in a small number of laboratories, can be a complementary strategy to obtain further insight to spatial pattern at a European level.

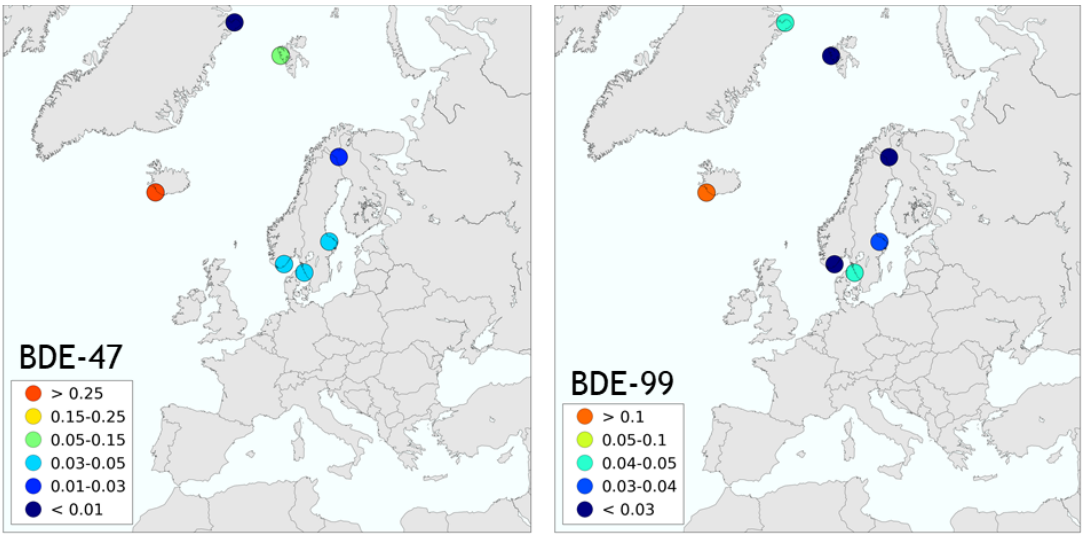

Fig. 2.8. *Spatial coverage and annual mean concentrations of two PBDE congeners in air in 2019, BDE-47 and BDE-99, pg/m^3.*

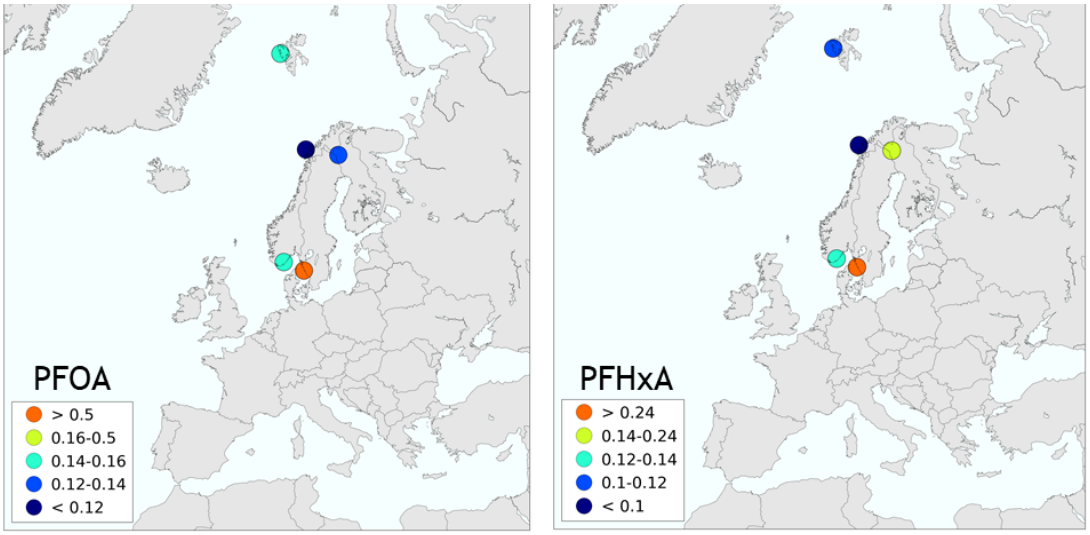

Fig. 2.9. *Spatial coverage and annual mean concentrations of two PFAS substances in air in 2019, PFOA and PFHxA, pg/m^3.*

Temporal trends for the individual sites can be assessed as the same sampling and analytical methodologies have been constant. The trends for PBDEs (BDE-47 and -99) and PFAS (PFOA and PFHxa) show that concentrations have declined at most sites over the individual monitoring periods, shown in Fig. 2.10 and 2.11 respectively.

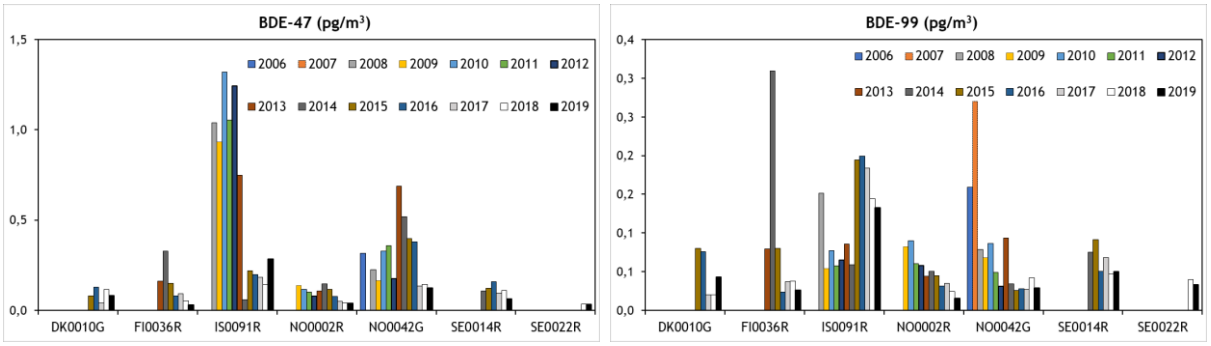

Fig. 2.10. *Annual mean concentrations of two PBDE congeners in air, pg/m^3.*

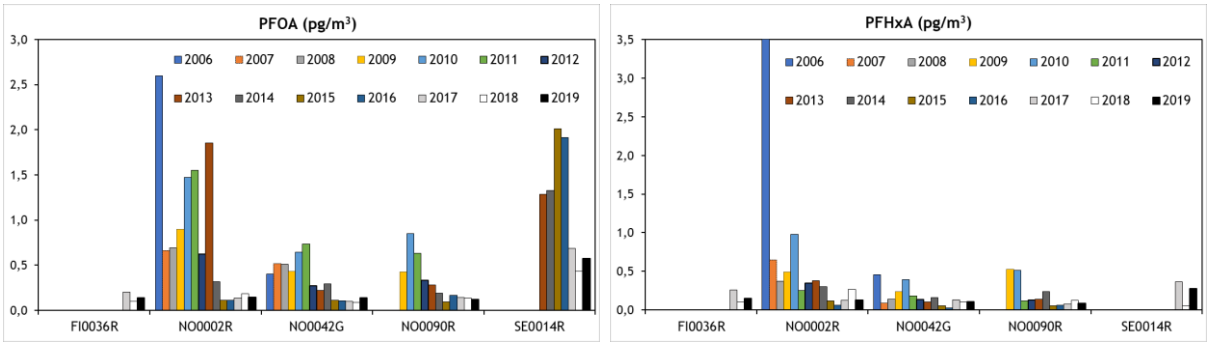

Fig. 2.11. *Annual mean concentrations of two PFAS substances in air, pg/m^3.*

Monitoring of CECs has been initiated by national efforts to gather proofs for persistence, long-range transport, and effects of new chemicals to support and improve regulatory actions. For example, the Norwegian monitoring programme for atmospheric contaminants has included several CECs in the monitoring programme; cVMS and S/MCCPs since 2013, as well as phthalates, novel brominated flame retardants, organophosphorous flame retardants and dechloranes since 2017. The results at Spitsbergen (NO0042) shows that these CECs are detected at concentrations higher than polycyclic aromatic hydrocarbons (PAHs), one-two orders of magnitude higher than other legacy POPs (Fig. 2.12).

The high concentrations of the monitored CECs show their relevance and the importance of including CECs in monitoring programmes. Monitoring at other sites in the EMEP network would give a better understanding of possible long-range atmospheric transport into the Arctic. The challenges related to sampling and analysis mentioned for other POPs above is even more relevant for the CECs as they are still in use. Their ubiquitous presence increases the risk for contamination during sampling and analysis, occasionally making inferences about long-range atmospheric transport challenging. Also sampling methodologies applied for legacy POPs might not be suitable for CECs. Alternative sampling methodologies therefore need to be tested and methods shared within the EMEP monitoring community.

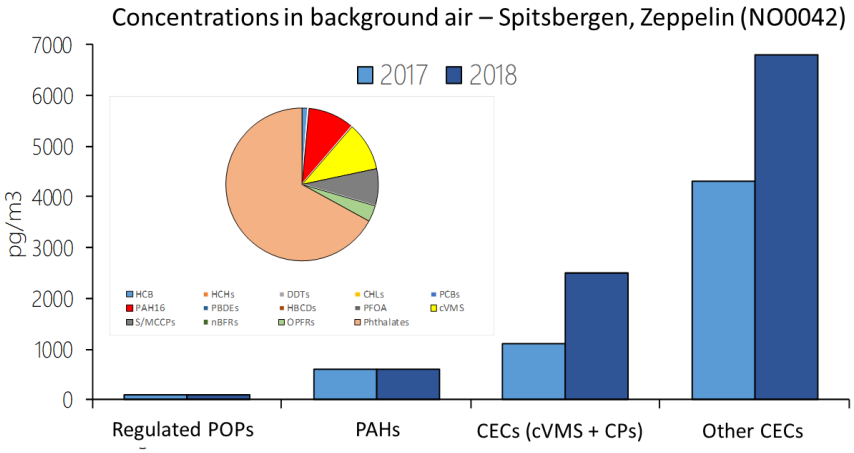

Fig. 2.12. *Annual mean concentrations of POPs (legacy POPs grouped together), PAHs and two groups of CECs. The group "other CECs" include nBFRs, OPFRs and phthalates.*

2.2. Supplementary measurements

EMEP monitoring network is designed to characterize pollution levels in the remote regions not affected by major anthropogenic emission sources. Besides, EMEP stations are located mostly in the northern, western, south-western and central parts of Europe, while in the eastern and south-eastern parts spatial coverage by the EMEP stations is scarce. In order to extent area of analysis of pollution levels and verification of the modelling results via comparison with measurement data, the data from the EMEP network can be complemented with measurement data from other monitoring activities, e.g., by measurements regularly carried out in the EU countries and reported to European Environmental Agency (EEA) [*EEA*, 2020]. The EEA air quality database (AQ e-Reporting) provides the monitoring data on various pollutants including heavy metals (Pb, Cd, Hg as well as second priority metals) and selected POPs (e.g. PAHs).

The EU national monitoring networks are designed to characterize pollution levels for different types of areas, including rural, suburban, urban, industrial, and traffic areas. Therefore, the EEA measurements are useful for evaluation of heavy metal and POP levels in more polluted and densely populated regions compared to the EMEP monitoring data. Besides, the EEA data can be applied in the evaluation of modelling results simulated with fine spatial resolution, e.g., in the framework of country-specific case studies.

In this report available EEA data on measured B(a)P air concentrations in 2019 were used for the analysis of pollution levels. For 2019 the data on B(a)P concentrations in air were available from more than 700 stations (Fig. 2.13). Spatial density of EEA stations is higher compared to that of EMEP in a number of countries, e.g., in Germany, Poland, Italy, the United Kingdom, Spain and France. It is also seen that the levels observed at the EU network are substantially higher than those provided by the EMEP monitoring data.

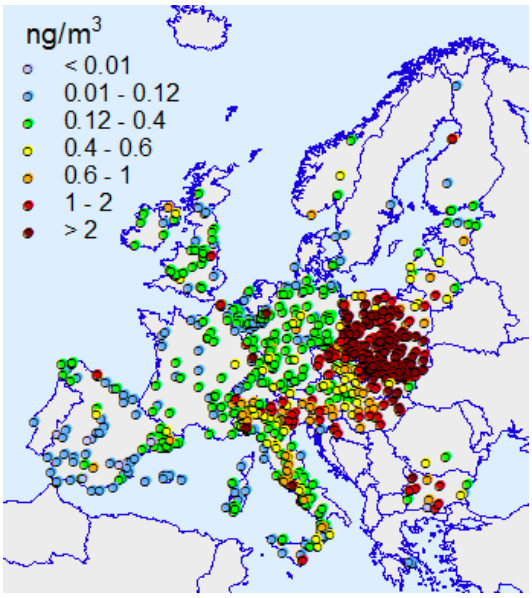

Fig. 2.13. *Concentrations of B(a)P in air observed in 2019 (a) in the EMEP region from EEA AQ e-Reporting database.*

Chapter 3. STATUS OF HEAVY METAL AND POP POLLUTION IN 2019

This chapter is focused on the results of the assessment of heavy metal and POP pollution level in the EMEP countries in 2019. This work is performed according to the mandate of EMEP [ECE/EB.AIR/2019/8] and bi-annual work-plan [ECE/EB.AIR/144/Add.2]. Spatial distribution of air concentrations, total deposition fluxes and results of transboundary transport modelling are discussed. Modelling results described in the chapter are based on the emission data for 2018. The presented changes between the results of current (2019) and previous (2018) year are explained by inter-annual meteorological variability. The effect of changes of emission data is overviewed in Annex B. Besides, information relevant to the assessment of pollution effect on human health and biota is presented. Finally, information on atmospheric contamination of marginal seas, the Arctic region and global-scale pollution is demonstrated.

3.1. Meteorological conditions of 2019

Meteorological conditions have an important effect on the atmospheric pollution levels of heavy metals and POPs. Dispersion of the pollutants over the EMEP region is governed by wind flows in the troposphere and lower stratosphere and by atmospheric stability. Atmospheric precipitation is a crucial parameter for modelling of wet scavenging. Wind suspension of dust particles is affected by wind velocity and soil wetness, which, in turn depends on precipitation. Rates of chemical transformations of POPs and mercury are influenced by air temperature. Finally, exchange of mercury between air and water surface in high latitudes strongly depends on temporal variability of sea ice cover.

Meteorological conditions of a particular year may differ from those in other years. It is explained by relatively short-term inter-annual variability and by long-term climatic changes. Therefore, meteorological conditions in 2019 are compared with current climate and with the conditions that took place in previous (2018) year. Comparison of meteorological conditions of the current and previous years is important for interpretation of changes between pollution levels simulated for these years.

Comparison of the current year with climate is carried out through the analysis of anomalies of air temperature and precipitation. Anomaly is a difference between the value in the current year and climatic norm. Positive value of the anomaly means that temperature or precipitation sum in this year is higher than the climatic norm, and vice versa. Climatic norm is assumed as the average for the period from 1981 to 2010 [*Blunden and Amdt*, 2020].

The year 2019 is considered as the second-warmest in Europe since 1950 [*Blunden and Amdt*, 2020]. Annual mean land near-surface air temperature is 1.1°C, which is very close to previous (2018) year. Positive anomaly of the temperature is noted for most part of Europe varying from 0 - 1°C in Scandinavia, Spain, Ireland and the United Kingdom to 2-3°C in the central and eastern parts of Europe (Poland, Ukraine, Belarus, Lithuania, Romania) (Fig. 3.1a). Significant anomalies (up to 3°C)

have also been recorded for the northern part of Russia and the Arctic. In meteorological winter of 2019 (December, 2018 – February, 2019) positive anomalies take place over most of Europe except for the Mediterranean region. Spring is characterized by positive anomalies in the eastern part of Europe, while in the western part the temperature is close or slightly below the norm. In summer strong positive anomaly occurs over western and central Europe, and strong negative anomaly – over the European part of Russia. The highest anomalies in autumn are recorded over the eastern and south-eastern parts of Europe, while in the northern part (the British Isles and Scandinavia) negative anomalies are observed.

Mean precipitation sum in Europe in 2019 was close to the normal value. However, spatial distribution of the anomaly across Europe is not uniform. Values close to the norm (from -20% to +25%) are observed over the most part of Europe (Fig. 3.1b). Deficit of precipitation takes place in the Baltic region (Estonia, Latvia), Iceland, south-western Spain and some regions in the south-eastern part of Europe. Northern Russia, Middle East, some regions of the Balkan Peninsula, Italy, Spain and Norway experience precipitation higher than normal. Strong deficit of precipitation in winter occurs in Estonia, Hungary as well as in the southern (Italy, Spain, Portugal) and the western (the United Kingdom, France) parts of Europe. In Central, south-eastern Europe and Turkey the winter is wetter than normal. In spring Iberian Peninsula and France remained drier than normal. In central Europe and Scandinavia precipitation exceeds the dimatic mean value. Summer is characterized by deficit of precipitation over major part of Europe. The exceptions are the British Isles, the European part of Russia and Turkey. In autumn an excess of precipitation is observed over the most part of western, central and northern Europe. Drier than normal conditions take place in the south-west of Iberian Peninsula, south-eastern Europe, Caucasus, Turkey and the northernmost part of Scandinavian Peninsula.

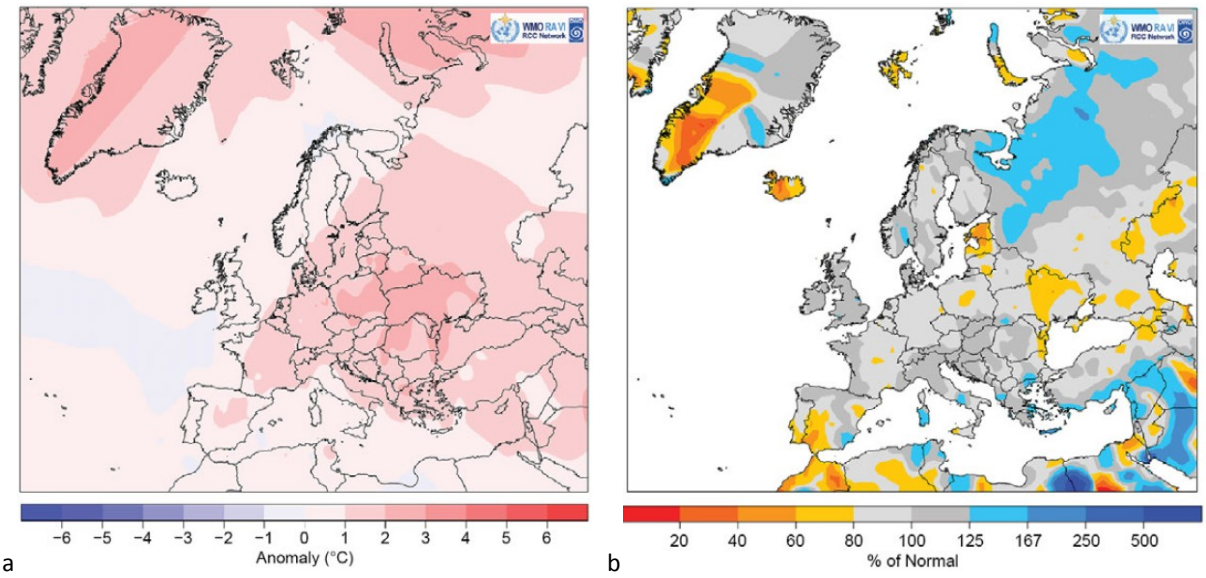

Fig. 3.1. *Anomaly of mean annual air temperature (a) and annual precipitation sum (b) in 2019 [Blunden and Arndt, 2020].*

Analysis of zonal and meridional atmospheric circulation indices shows that large-scale features of atmospheric circulation in the middle troposphere of the EMEP domain are close to the norm over the most part of the year [*HMCR*, 2020]. Intensity of zonal component of atmospheric circulation is weaker than norm in April, June, July and November and higher than norm in March. Meridional transport is stronger than norm in February, April and June.

In 2019 annual sums of precipitation vary from 400 to 1000 mm over most part of the EMEP land area (Fig. 3.2a). In mountainous regions, e.g., the Alps and Caucasus, as well as windward parts of the British Isles and Scandinavia, annual sums of precipitation exceed 2000 mm. Over the central Asian countries precipitation may drop below 200 mm. Besides, relatively low precipitation sums (400-500 mm) are noted for the southern part of Russia, Spain and several regions in central and south-eastern parts of Europe. Difference between precipitation sums in 2019 and 2018 is expressed in percent relative to 2018. Positive values of the difference mean increase of the precipitation in 2019 compared with 2018, and vice versa. Precipitation sums in 2019 are considerably higher (15-50%) than those in 2018 over the northern part of Europe, including Scandinavia, north of Germany and the British Isles (Fig. 3.2b). The increase of precipitation exceeding 50% also takes place in the European part of Russia and the western part of Central Asia. Besides, precipitation sums have risen in the particular regions of Central Europe, such as north of Italy, west of Austria, Switzerland, Slovakia. Marked decline of precipitation in 2019 compared with 2018 takes place over most of Iberian and Balkan Peninsulas, France, Italy, Turkey. Large areas of the decline also occur over the southern part of Russia, Ukraine, Caucasus and the eastern part of Kazakhstan.

Mean annual air temperature in 2019 averaged over the vertical within atmospheric boundary later ranges from -5°C in the Arctic to 20°C in the southern part of Central Asia and over the Mediterranean Sea (Fig. 3.3a). The isotherms follow zonal distribution with the exception of mountainous regions. Compared with 2018, the increase of air temperature in the central and eastern parts of Europe is up to 1°C, and more than 1-1.5°C in the eastern part of Central Asia. Besides, some increase of the temperature is noted for Iberian Peninsula (Fig. 3.3b). Small decline (up to -1°C) of air temperature takes place in the western part of Europe, over the Mediterranean Sea and over most of Scandinavia. Over north of Scandinavia , Kola Peninsula and the European part of the Arctic Ocean the decline exceeds -1.5°C.

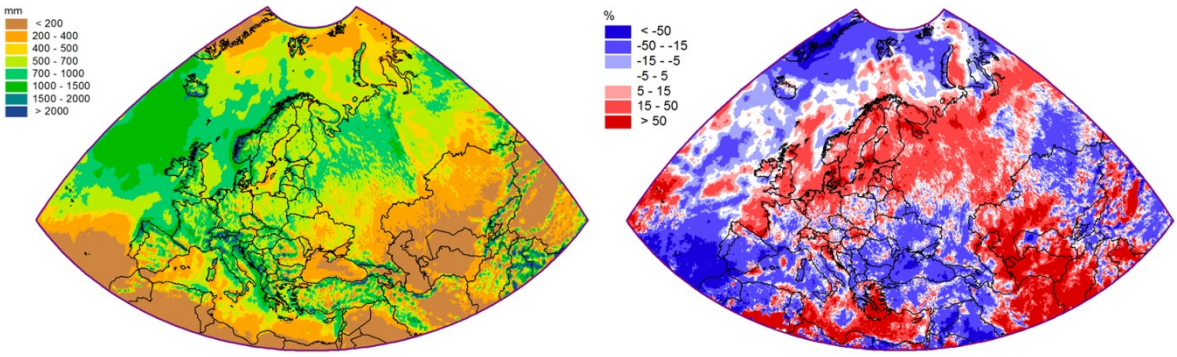

Fig. 3.2. *Annual precipitation sums in 2019 (a) and relative difference between precipitation in 2019 and 2018 (b). Positive values mean increase and negative – decrease of precipitation in 2019 relative to 2018.*

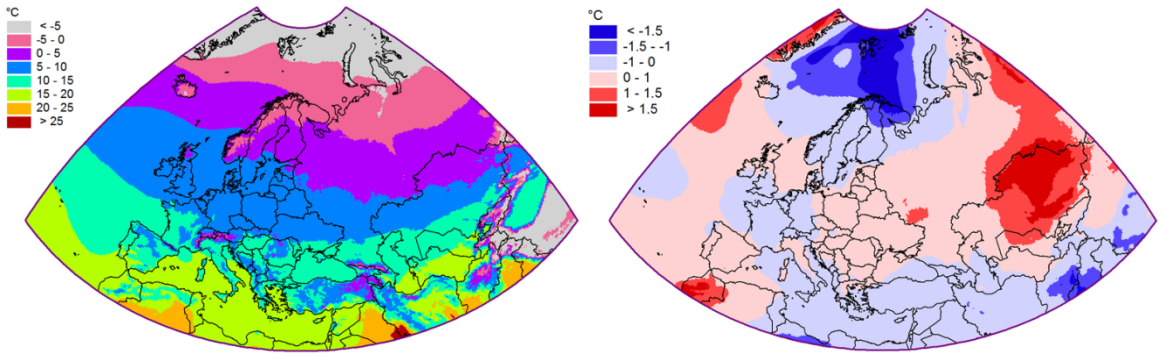

Fig. 3.3. *Annual mean air temperature averaged over atmospheric boundary layer (~1 km) in 2019 (a) and difference between the temperatures in 2019 and 2018 (b).*

3.2. Model setup

The operational model assessment of heavy metal and POP pollution in 2019 has been performed using the GLEMOS model, version v2.2.1. Description of the current stable version of the model is available at the MSC-E website (http://en.msceast.org/index.php/j-stuff/glemos). New research directions aimed at improvement of the model parameterizations, which will be included to the next versions of the model, are discussed in Chapter 4 of the report.

Modelling of pollution levels in the EMEP countries as well as the transboundary transport between them (source-receptor relationships) have been carried out within the new EMEP domain (https://www.ceip.at/the-emep-grid). Anthropogenic emission data for modelling of all pollutants have been prepared based on the gridded emissions fields provided by CEIP (Section 1.1) and complemented by additional emission parameters required for model runs (Section 1.2). Data on wind re-suspension of partide-bound heavy metals (Pb and Cd) from soil and seawater has been generated using the dust pre-processor [*Gusev et al.*, 2006; 2007].

Meteorological information for model simulations has been generated from the operational analysis data of the European Centre for Medium Range Weather Forecasts [*ECMWF*, 2020] using the meteorological pre-processor based on the Weather Research and Forecast modelling system (WRF) [*Skamarock et al.*, 2008]. Atmospheric concentrations of chemical reactants (O_3, OH, SO_2, NO_3 and Br) and particulate matter (PM2.5), which are required for description of Hg and POP chemistry, were derived from the MOZART and p-TOMCAT models [*Emmons et al.*, 2010; *Yang et al.*, 2005; 2010].

Boundary conditions for the regional scale simulations of all considered pollutants have been obtained from the GLEMOS model runs on a global scale (Section 3.7). Initial conditions for the evaluation of pollution levels of long-living POPs (e.g. PCBs, HCB, and PCDD/Fs) in the EMEP region were prepared from a long-term global model spin-up based on expert estimates of historical emissions.

3.3. Levels of Heavy Metal and POP pollution

3.3.1. Pollution summary

Pollution levels of heavy metals and POPs in the EMEP region are assessed on the basis of measurement data and the results of transboundary transport modelling. The assessment of pollution levels includes analysis of spatial distribution of air concentrations and deposition fluxes and information about source apportionment for the EMEP countries. Modelling results are based on meteorological information for 2019 and emission data for 2018. Update of the modelling results simulated with the most recent emission data for 2019 is presented in Annex B. More detailed information on pollution levels of each of considered pollutant is available in Sections 3.3.2-3.3.6.

Pollution levels depend on a number of factors, including physicochemical properties of pollutants, meteorological conditions, magnitude and spatial distribution of emission sources, characteristics of the underlying surface, etc. The purpose of this section is to deduce and summarize common features in pollution levels of considered pollutants (Pb, Cd, Hg, PAHs, PCDD/Fs, HCB, PCB-153) in 2019. Pollution levels of these contaminants and their changes are analyzed for six sub-regions of the EMEP domain, namely Western Europe, Southern Europe, Northern Europe, Eastern Europe, Central Europe and Caucasus and Central Asia (Fig. 3.4). The same sub-regions were used in the analysis of pollution levels of particular pollutants presented in sections 3.3.2-3.3.6. For the purpose of comparability deposition fluxes to the sub-regions are normalized and converted to dimensionless form. Overall pollution load is the highest in the Central Europe sub-region (Fig. 3.5a). This sub-region is characterized by the highest regional-mean deposition fluxes of Pb, Cd, Hg and PAHs, and ranks second for PCB-153 and the other pollutants. The highest PCB-153, HCB and PCDD/Fs deposition fluxes take place in Western, Eastern and Southern Europe, respectively. At the same time, relatively low levels of pollution occur in Northern Europe and Caucasus and Central Asia.

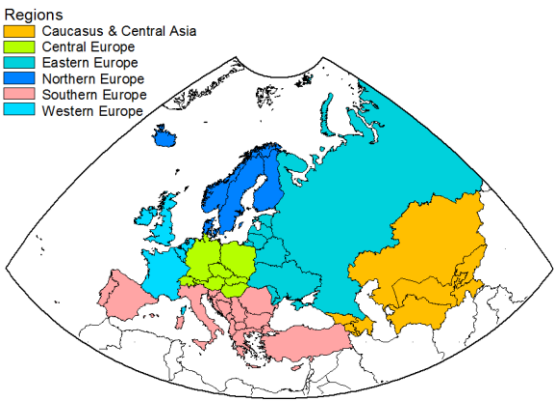

Fig. 3.4. *Definition of sub-regions of the EMEP region used in the report*

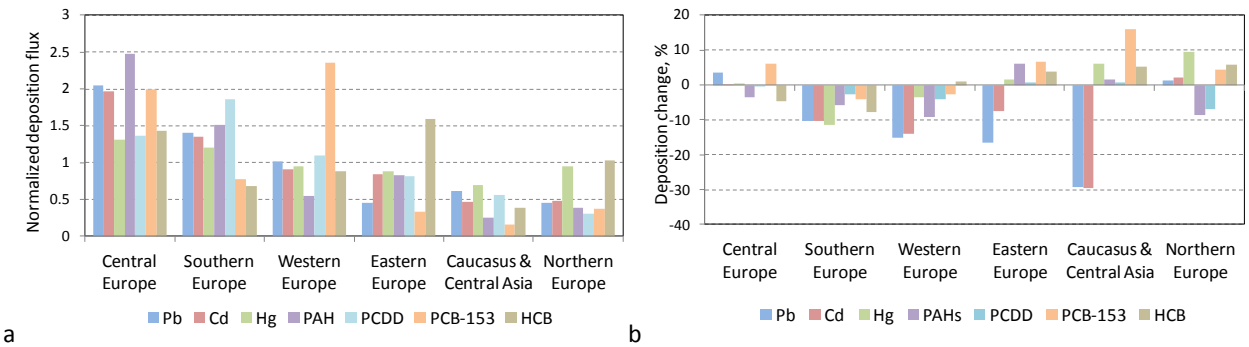

a b

Fig. 3.5. *Normalized mean deposition flux (a) and relative changes of heavy metals and POP deposition between 2019 and 2018 (b) in sub-regions of the EMEP region.*

In order to evaluate changes caused by inter-annual meteorological variability, the pollution levels based on the same emission data were compared. Relative change between the results for 2018 and 2019 is calculated as difference between the levels (X) from current (2019) and previous (2018) year related to the level in previous (2018) year according to the formula:

$$\Delta = \frac{(X_{2019} - X_{2018})}{X_{2018}} \cdot 100\%$$

Therefore, positive value of the change means the increase of pollution level in 2019, and vice versa. The same interpretation of pollution level change is used in Sections 3.3.2 - 3.3.6 describing pollution levels of the particular heavy metals and POPs.

Pollution levels of all considered contaminants declined in Southern Europe, and almost all – in Western Europe (Fig. 3.5b). In Central and Northern Europe both positive and negative changes for different pollutants take place. However, the magnitude of the changes in these two sub-regions is relatively low (within ±10%). In Eastern Europe and Caucasus and Central Asia deposition of most of pollutants increased. The exception is the changes of Cd and Pb. The levels of Pb and Cd significantly declined in most of sub-regions. Especially large decline (around 30%) is noted for Central Asia due to decrease of contribution of wind re-suspension in 2019.

More detailed information on evaluation of modelling results against measurements, source-receptor relationships, ecosystem-dependent deposition is summarized in Supplementary Data Reports for heavy metals [*Strizhkina et al.*, 2021a] and POPs [*Strizhkina et al.*, 2021b].

3.3.2. Lead

In the atmosphere lead is present in the particulate form. Consequently, the processes of Pb dispersion in air, as well as its removal from the atmosphere, are determined by properties of the particles with which it is associated. It should be noted that the partides containing lead are considered without taking into account chemical forms of Pb (oxides, salts, etc.).

Air concentrations

Spatial distributions of annual mean modelled and observed atmospheric concentrations of Pb in 2019 are presented in Fig. 3.6a. The concentrations of Pb vary over a wide range, from less than 0.3 ng/m^3 in remote areas (e.g., in the Arctic, in the northern part of Russia) and in Northern Europe to more than 30 ng/m^3 in some regions of Poland and Italy. Generally, the highest Pb concentrations in 2019 are noted for Central Europe, followed by Southern and Western Europe (Fig.3.6b). Besides, relatively high Pb concentrations take place in some regions of Central Asia (north-east and south of Kazakhstan, east of Uzbekistan and north of Tajikistan).

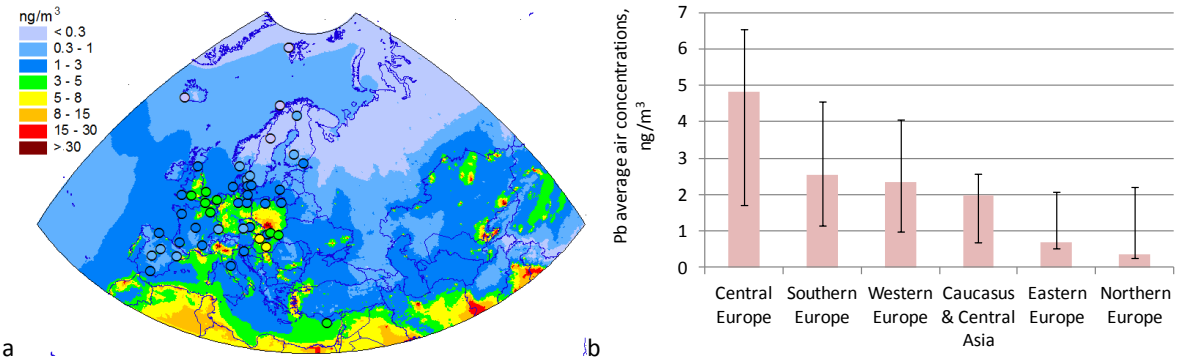

Fig. 3.6. *Annual mean air concentrations of Pb (circles on the map show observed values in the same colour scale) (a) and average air concentrations of Pb to EMEP sub-regions (b) in 2019. Whiskers show the range of concentrations in particular countries of the sub-region.*

Comparison of Pb modelled concentrations with the data of EMEP measurements shows satisfactory agreement between the modelled and observed values with high spatial correlation (about 0.77) and mean relative bias about 4%. The deviations of modelled concentrations from measurements are within a factor of two for more than 80% of stations. More detailed information on agreement between the modelled and observed concentrations of Pb is given in Supplementary Data Report [*Strizhkina et al.*, 2021a].

Deposition fluxes

Spatial distribution of total deposition fluxes of Pb calculated for 2019 is presented in Fig. 3.7a. The highest deposition fluxes are usually observed in areas of significant anthropogenic emissions or wind re-suspension. Total deposition of Pb consists of wet and dry components. For the EMEP countries, the average contribution of wet deposition is about 80%. However, in the Central Asian region this contribution is much lower due to climatic conditions (arid climate). Similar to air concentrations, the highest spatially mean Pb deposition flux takes place in Central Europe, while the lowest Pb deposition flux is noted for Eastern and Northern Europe (Fig. 3.7b).

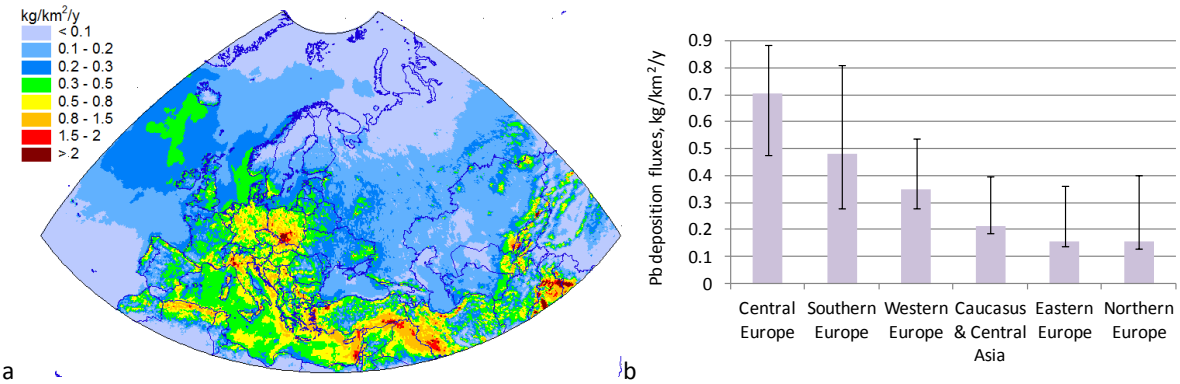

Fig. 3.7. *Annual total deposition flux of Pb (a) and average total deposition fluxes of Pb to EMEP sub-regions (b) in 2019. Whiskers show the range of deposition fluxes in particular countries of the sub-region.*

Modelling results are compared with data on measured wet deposition fluxes from EMEP monitoring network. In general, there is a satisfactory agreement between modelled and observed values. However, the model tends to underestimate the observed values on average by 30%. Inconsistencies may be explained by the model intrinsic uncertainty and measurement uncertainties. The largest underestimation of the observed wet deposition fluxes is noted for Northern Europe. For 70% of stations, deviations of modelled annual mean deposition fluxes from the observed values are within a factor of two. More detailed evaluation of modelling results against the monitoring data of EMEP is presented in Supplementary Data Report [*Strizhkina et al.,* 2021a].

The deposition of Pb within the EMEP region from different groups of sources is shown in Fig. 3.8. These groups include EMEP anthropogenic emissions, wind re-suspension of dust particles containing Pb, and emissions from sources located outside the EMEP region (non-EMEP sources).

Spatial distribution of Pb deposition from anthropogenic sources of the EMEP countries is a result of dispersion of emissions due to the influence of meteorological conditions (in particular, wind patterns, wet scavenging etc.) (Fig. 3.8a). In 2019, relative contribution of the EMEP anthropogenic sources to total Pb deposition is the largest (up to 60% of total deposition) in Central Europe (Fig. 3.8d).

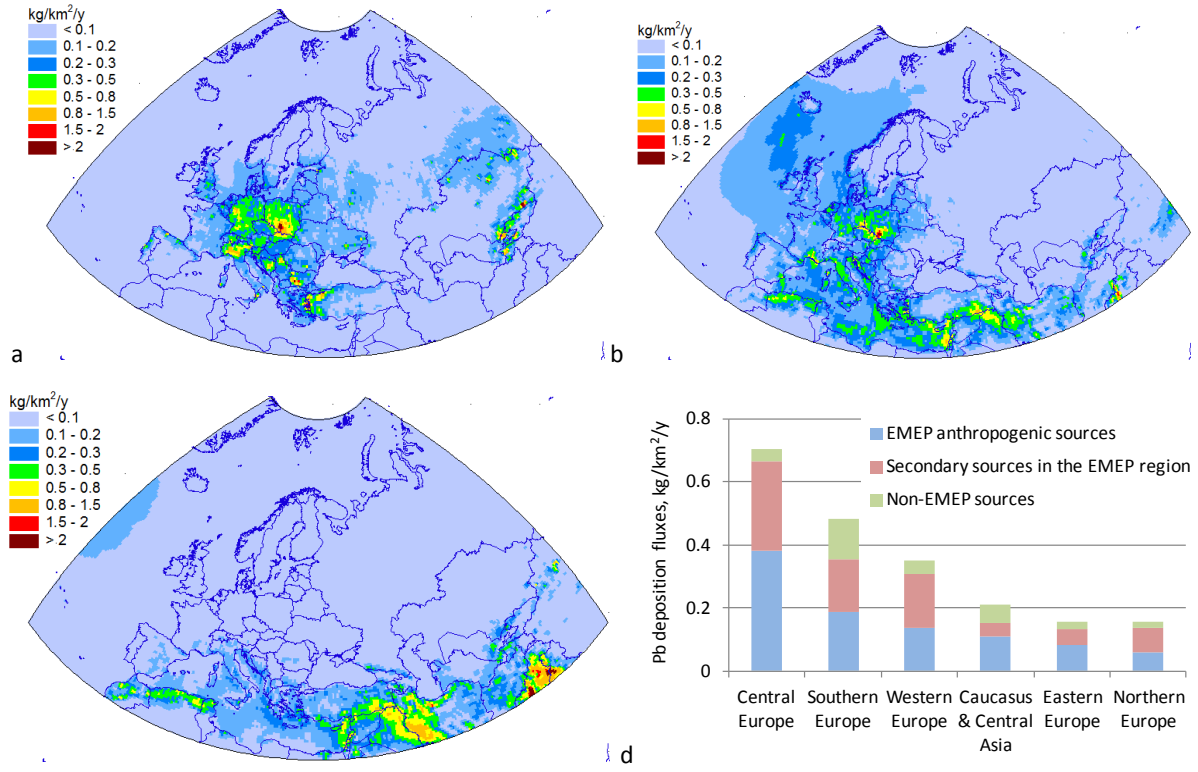

Fig. 3.8. *Annual deposition of Pb in 2019 from EMEP anthropogenic sources (a), secondary sources (wind re-suspension) (b) and non-EMEP anthropogenic sources (c), and mean deposition fluxes from these sources to the EMEP sub-regions (d).*

The spatial distribution of lead deposition from wind re-suspension is determined by a number of factors, such as Pb concentrations in soils, soil moisture, wind, etc. Generally, deposition from re-suspension accounts for 30-40% of the total Pb deposition in Eastern Europe, Southern Europe and

Central Europe; about 20% - in Caucasus and Central Asia (Fig. 3.8d). In Northern and Western Europe, levels of deposition from re-suspension are comparable to those from EMEP anthropogenic sources (about 50%). Some of the countries (e.g., Germany, Poland, Czechia, Italy) are characterized by relatively high contribution of re-suspension to deposition flux (Fig. 3.8b) due to elevated Pb concentrations in soil that arise from long-term accumulation of previously deposited Pb. Deserts of North Africa and Central Asia are characterized by relatively low enrichment by Pb but high wind-blown dust suspension. It results to high level of Pb deposition from wind re-suspension over the eastern part of the Mediterranean Sea.

Contribution of non-EMEP sources in most of the EMEP sub-regions is relatively low. The highest level of deposition from this group of sources is observed along the southern border of the EMEP region. This can be explained by the atmospheric transport from anthropogenic sources of Asia, in particular, from Iran, Iraq, India, etc. (Fig. 3.8c). Mean contribution of non-EMEP sources varies from 5% in Central Europe to about 25% in Southern Europe and almost 30% in Caucasus and Central Asia (Fig. 3.8d).

More detailed information on the contributions from the EMEP anthropogenic sources, wind re-suspension and non-EMEP anthropogenic sources to Pb deposition in 2019 in the particular EMEP countries can be found in Supplementary Data Report [*Strizhkina et al.,* 2021a].

Changes of the pollution levels in 2019

Changes of Pb concentrations in air in 2019 compared with the previous (2018) year over the EMEP domain due to the change of meteorological conditions are presented in Fig. 3.9. The Caucasus and Central Asia and Eastern Europe sub-regions show the most significant changes (45% and 12% declines, respectively) (Fig. 3.9b). In Western and Northern Europe, the average decrease in Pb concentrations does not exceed 6%. At the same time, Central and Southern Europe are characterized by slight increase of Pb concentration (1-2%). It should be noted that the range of the changes in particular countries can be higher lying within ±50% (Fig. 3.9a). For example, a 20-50% increase is observed in the regions of eastern Spain, southern Norway, western Italy, eastern Poland and some others.

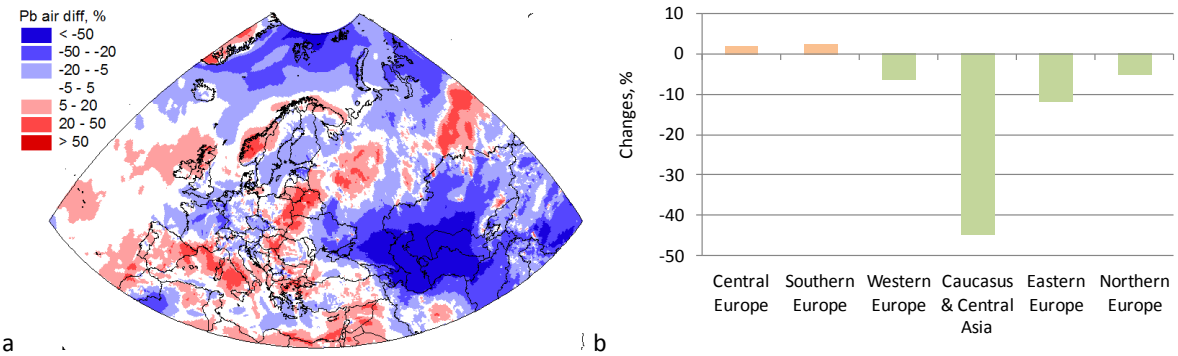

Fig. 3.9. *Relative changes of Pb air concentrations between 2019 and 2018 over the EMEP domain (a) and in various sub-regions (b).*

Changes in total Pb deposition fluxes in 2019 compared with previous (2018) year vary within ±50% over most of the EMEP area (Fig. 3.10a). Mean sub-region changes of the fluxes range from about -30% in Caucasus and Central Asia to 3.5% in Central Europe (Fig. 3.10b). Among the particular countries, the increase is observed in Poland, northern Norway and southern Spain (20-50%). At the same time, France, Portugal, Czechia and southern Russia are characterized by a decrease in the total Pb deposition fluxes.

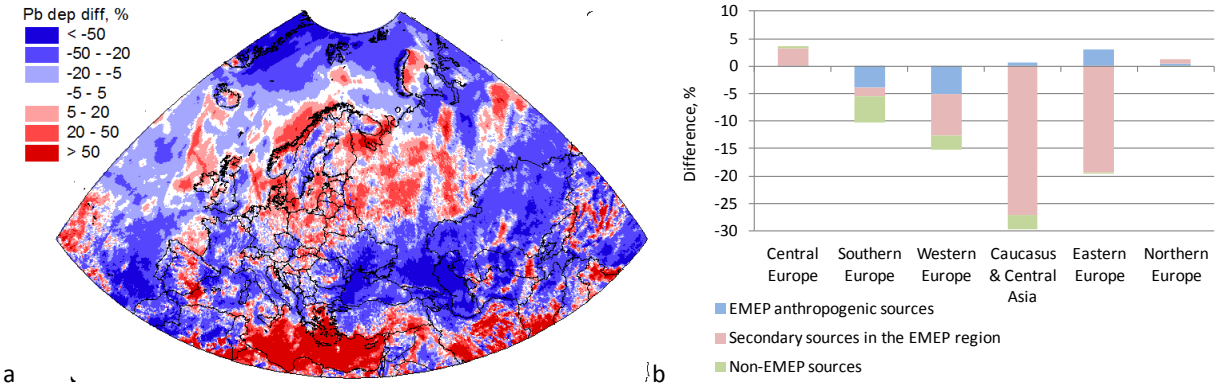

Fig. 3.10. *Relative changes of Pb deposition between 2019 and 2018 over the EMEP domain (a) and in various sub-regions (b).*

The changes in pollution levels in 2019 relative to 2018 are explained by changes in meteorological conditions. Increase in annual precipitation sums in 2019 over Northern Europe and over the large parts of Central Europe (Fig. 3.2) resulted in slight (1-3%) increase of total Pb deposition in these sub-regions of the EMEP domain. General decline of precipitation in Southern Europe is responsible for a 10% decrease of Pb deposition in this sub-region. In Central Asia and Caucasus, the increase in annual precipitation sums coincides with the a marked (almost 30%) decline of total deposition. Significant contribution to Pb deposition in this sub-region in previous year is made by wind re-suspension of natural or historical Pb. Previous year (2018) was known for anomalously low (40-80% of norm) precipitation amounts in the western part of Central Asia [*Blunden and Arndt,* 2019], while precipitation sums in 2019 were closer to the climatic norm [*Blunden and Arndt,* 2020]. Rise of precipitation over the western part of Kazakhstan, Turkmenistan and most part of Uzbekistan from 2018 to 2019 led to increase of soil moisture, which favours substantial reduction of wind re-suspension flux. As a result, the decline of total deposition and concentrations in air is mainly caused by the reduction of deposition from re-suspension component (Fig. 3.10). The atmospheric transport of re-suspended Pb from Central Asia and Caucasus to Eastern Europe also decreased, which also led to overall decline of deposition and air concentrations in Eastern Europe. However, anthropogenic component of Pb deposition in Eastern Europe and Central Asia and Caucasus sub-regions increased. For Western Europe, the overall decrease in deposition is amounted to 15%, and air concentrations declined by about 6%. Simultaneous decrease of the both parameters is explained by changes in the atmospheric transport patterns. In 2019 atmospheric transport from emission sources of Central Europe decreased compared with 2018, which favoured decline of both air concentrations and deposition fluxes in Western Europe.

Transboundary transport

In general, the effect of transboundary transport on Pb pollution levels in the particular country is determined by relative contribution of national and foreign sources to total anthropogenic deposition of Pb. The contribution of transboundary transport ranges from 10-20% in Portugal, Turkey and Italy to more than 95% in Montenegro, Liechtenstein and Monaco. On the whole, the relative contribution of Pb deposition from foreign sources exceeds 50**%** in 38 countries and 75**%** in 27 countries. An example of two countries with different contributions of transboundary transport is presented in Fig. 3.11. In the Netherlands anthropogenic deposition of Pb is mainly caused by foreign sources (about 90%). The largest contributors are Germany (32%), France (19%), the United Kingdom (16%) and Belgium (15%) (Fig. 3.11a). In contrast, Pb anthropogenic deposition in Germany is mainly determined by national sources (70%). Among the most significant foreign contributors to Pb deposition in Germany, Poland and France are noted (Fig. 3.11b). Detailed information on contributions of transboundary transport to Pb anthropogenic deposition for each EMEP country is presented in Supplementary Data Report [*Strizhkina et al.*, 2021a].

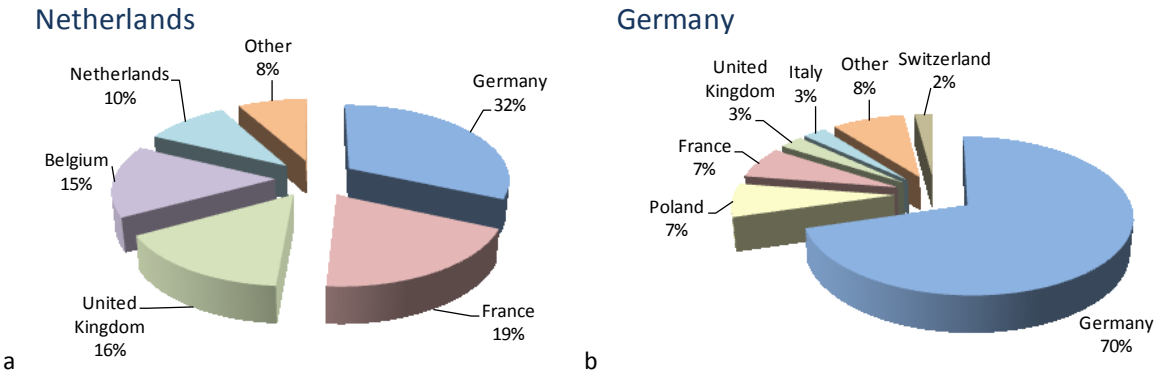

Fig. 3.11. *Contribution of transboundary transport and national sources to anthropogenic Pb deposition in the Netherlands and Germany in 2019.*

Changes of Pb deposition from particular source countries to receptor country can be obtained from source-receptor matrices for 2018 and 2019 (*http://en.msceast.org/index.php/pollution-assessment/emep-domain-menu/data-hm-pop-menu*). The differences are explained by inter-annual variations of atmospheric circulation and other meteorological parameters. An example of such changes in Estonia is shown in Fig. 3.12. The total anthropogenic Pb deposition in Estonia in 2019 amounted to 7300 kg/y that is 330 kg/y more than in the previous (2018) year (Fig. 3.12a). The contribution of national emission sources was 40% (2900 kg/y). The increase of deposition is associated with an increase in deposition from other countries by 490 kg/y and decrease of deposition from 160 kg/y (Fig. 3.12b).

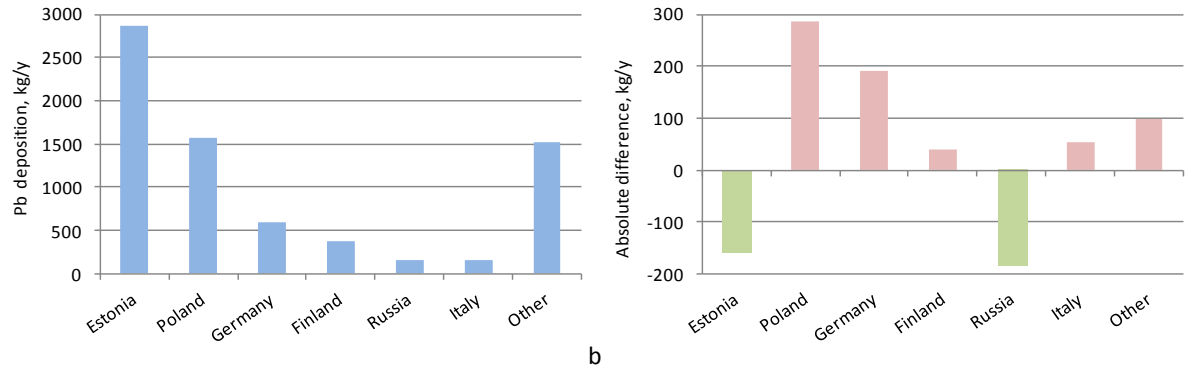

a b

Fig. 3.12. *Major contributors of Pb anthropogenic deposition in Estonia in 2019 (a) and absolute difference of Pb deposition between 2019 and 2018 (b).*

Each EMEP country is both a receptor and a source of transboundary pollution. Contribution of a particular country to transboundary Pb pollution in other regions depends on the national emissions, size and geographical location of the country. It should be noted, that emission sources of about 10 countries contribute up to 70% of Pb deposition in the EMEP region. The largest total Pb deposition to territories of other EMEP countries are noted for Kazakhstan (about 230 t/y), followed by Poland (about 135 t/y) and Uzbekistan (about 85 t/y). The deposition to own territory of these countries amounted to 240, 120 and 25 t/y, respectively. For illustration, the contributions of the Polish sources to own territory as well as to other countries in 2019 are presented in Fig 3.13a. The spatial distribution of Pb deposition from Poland in the EMEP region is shown in Fig. 3.13b.

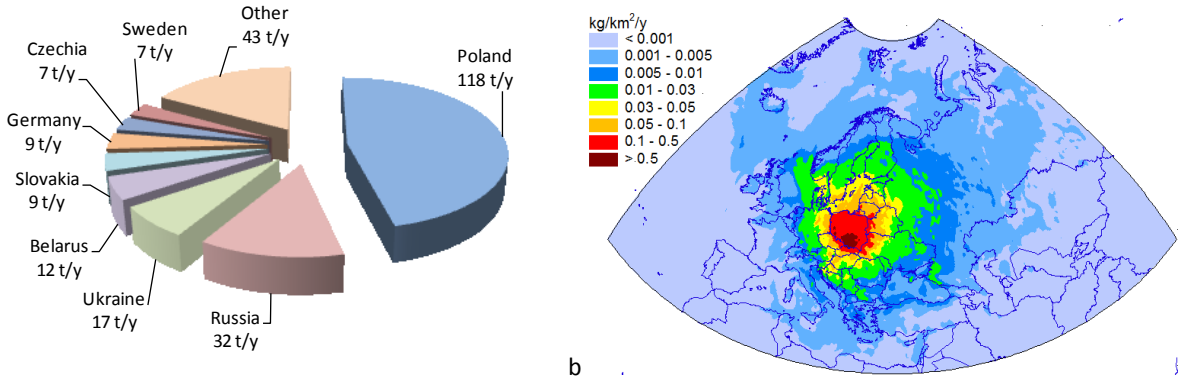

a b

Fig. 3.13. *Deposition of Pb from Polish anthropogenic sources to the EMEP countries in 2019 (a) and map of Pb deposition from Polish sources in the EMEP region (b).*

Deposition from a country to territories of other countries varies from year to year. For instance, such changes between 2019 and 2018 for France are shown in Fig. 3.14. In 2019, the deposition of Pb from France to own territory was 41 t/y (55%), while the remaining 34 t/y (45%) deposited in other EMEP countries (Fig. 3.14a). In comparison with the previous year, deposition of Pb from the French sources to own territory decreased by 5.5 t/y and to Spain - by 1 t/y. At the same time, deposition from France to Germany increased by 2 t/y, and to Belgium and the Netherlands by 0.5 t/y . A slight increase of deposition from the French sources is also observed in some other countries, e.g., Italy, Belgium, the Netherlands (Fig. 3.14b).

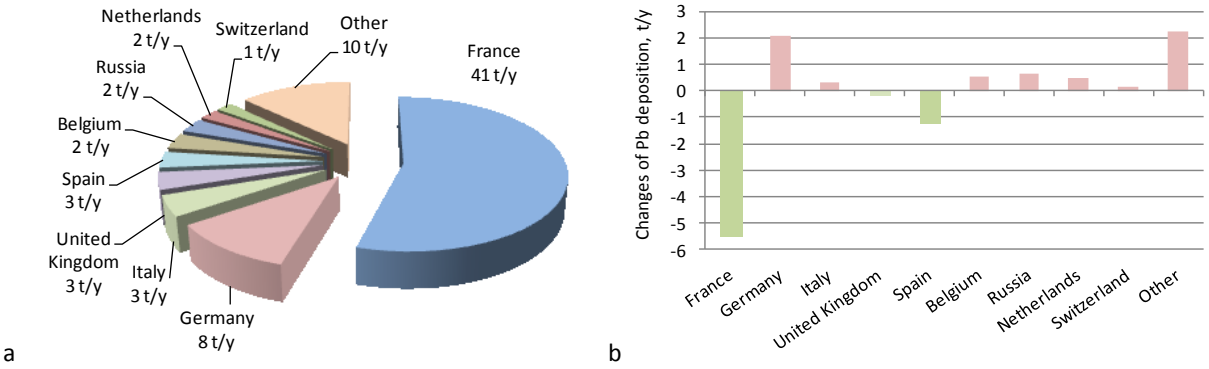

Fig. 3.14. *Deposition of Pb from French anthropogenic sources the EMEP countries in 2019 (a) and the deposition changes between 2019 and 2018 (b)*

The main contributors to deposition in most of the EMEP countries are EMEP anthropogenic and secondary sources. Inter-annual variability of meteorological conditions resulted to significant decline of Pb deposition in Caucasus and Central Asia as well as in Eastern, Western and Northern Europe.

3.3.3. Cadmium

Cadmium in the atmosphere is associated with particulate matter. Therefore, atmospheric transport, dry deposition and wet scavenging of this heavy metal are determined by properties of the particles containing Cd. Chemical forms of Cd (oxides, salts, etc.) in the particles do not affect properties of the particles from viewpoint of their atmospheric transport and deposition.

Air concentrations

Annual mean concentration of Cd in 2019 varies from 0.01 to 0.2 ng/m^3 over most part of the EMEP region (Fig. 3.15a). Much higher levels (>0.4 ng/m^3) are noted for numerous hot-spots in the western part of Germany, the south-western part of Poland, the central part of Russia, Turkey and the southern part of Italy. The lowest concentrations (below 0.01 ng/m^3) have been simulated for the northern part of Eurasia. Central Europe is characterized by the highest regional-mean concentrations in the EMEP region followed by Southern Europe and Western Europe (Fig. 3.15b). However, the comparison of whiskers for each sub-region reveals that the highest country-mean concentrations of Cd take place in Western Europe. EMEP monitoring stations measuring concentrations of Cd in air are located in the northern, central, western and southern parts of Europe. Mean relative bias between modelled and observed concentrations in air is 23%, indicating the tendency to somewhat overestimate the observed levels. This overestimation is revealed at stations in Belgium, the Netherlands and mountainous station DE3 in Germany. For about 75% of stations modelled levels agree with the observed concentrations within a factor of two. More detailed information on the agreement between modelled and observed concentrations is given in Supplementary Data Report [*Strizhkina et al.*, 2021a].

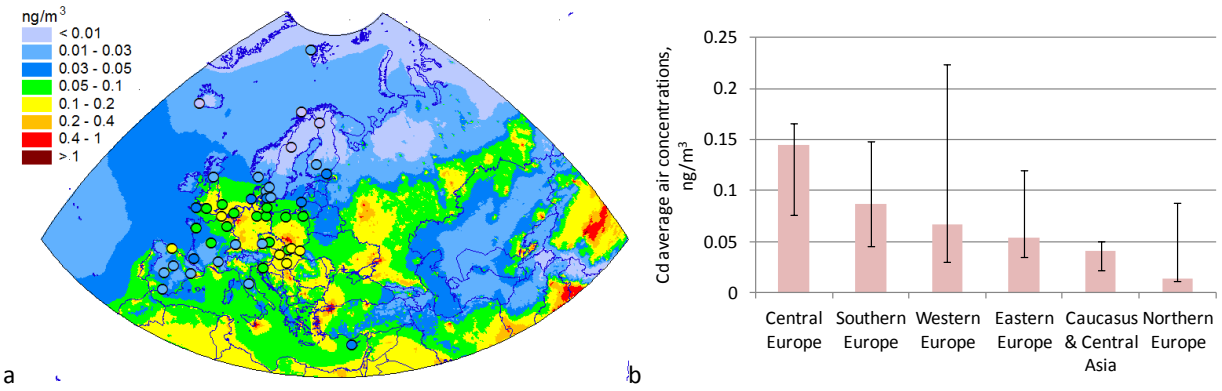

Fig. 3.15. *Annual mean air concentrations of Cd (circles on the map show observed values in the same colour scale) (a) and average air concentrations of Cd to EMEP sub-regions (b) in 2019. Whiskers show the range of concentrations in particular countries of the sub-region.*

Deposition fluxes

Total deposition flux of Cd in 2019 ranges from 5 to 40 g/km^2/y over major part of the EMEP domain (Fig. 3.16a). The levels below 5 g/km^2/y occur in Scandinavian Peninsula and in the Russian Arctic because of low emissions in these regions. Besides, similar low levels are noted for Central Asia due to low precipitation amount. Similar to concentrations in air, hot-spots of Cd deposition fluxes present in Germany, Poland, Russia and Turkey. These hot-spots are associated with regions of significant anthropogenic emissions. Central Europe is characterized by the highest regional-mean deposition (about 25 g/km^2/y) of Cd. The lowest fluxes (about 6 g/km^2/y) occur in the Northern Europe and Caucasus and Central Asia.

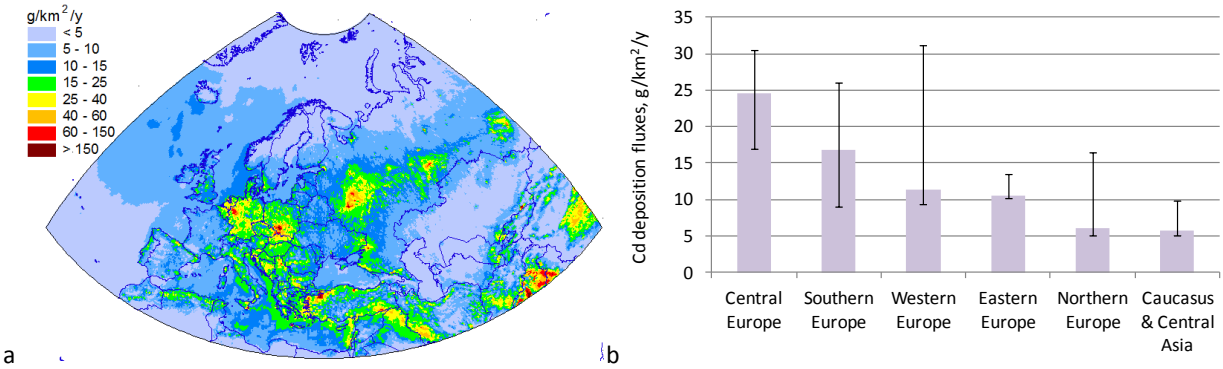

Fig. 3.16. *Annual total deposition flux of Cd (a) and average total deposition fluxes of Cd to EMEP sub-regions (b) in 2019. Whiskers show the range of deposition flux values in particular countries of the sub-region.*

Total deposition of Cd consists of wet and dry components. Wet deposition of Cd constitutes about 70% of total deposition for the EMEP region as a whole. Quality of the model performance strongly varies among particular stations. Mean relative bias between the modelled and observed wet deposition fluxes is around -35%. Therefore, the model underestimates the observed levels in the EMEP countries where measurements are available. At about 60% of stations the difference between modelled and observed fluxes lies within a factor of two. The modelled and observed monthly and

annual mean values from all the stations are available in Supplementary Data Report [*Strizhkina et al.*, 2021a].

Model assessment of Cd atmospheric pollution considers three groups of emission sources. They include anthropogenic emissions in the EMEP countries, wind re-suspension, and emissions from the sources located outside the EMEP countries (non-EMEP sources). Spatial distribution of deposition fluxes from these groups and their contributions to mean fluxes in the sub-regions of EMEP domain are shown in Fig. 3.17.

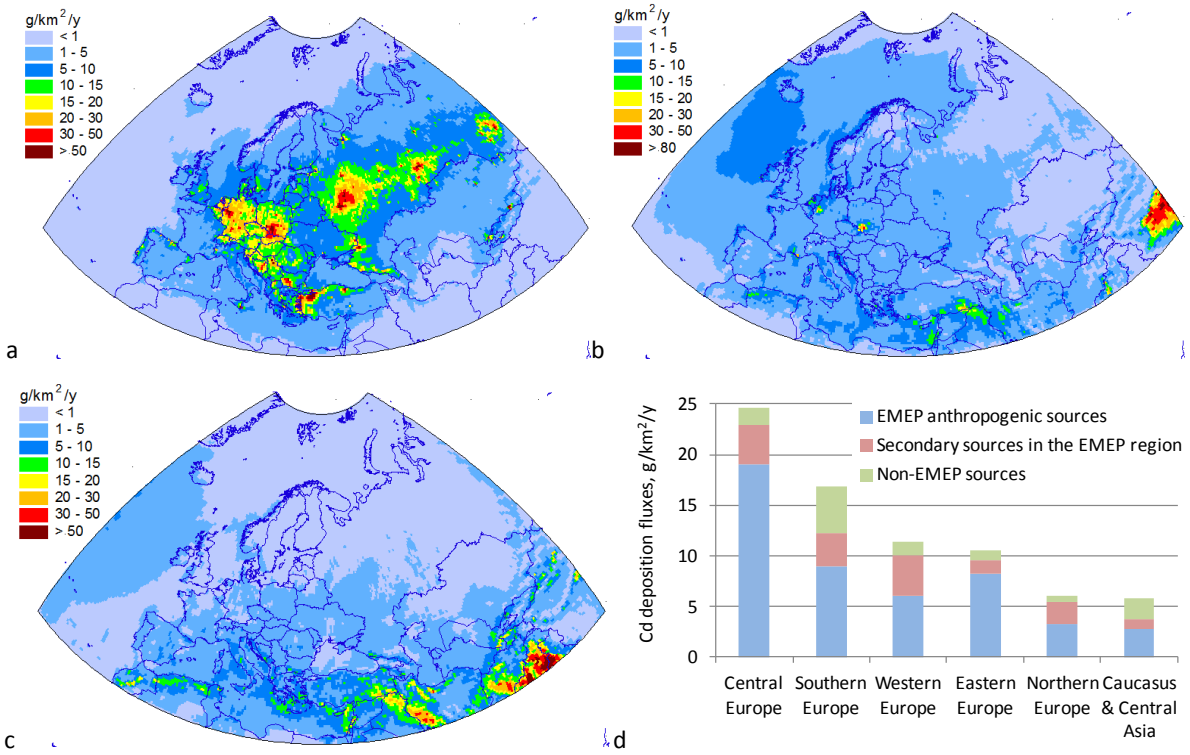

Fig. 3.17. *Annual deposition of Cd in 2019 from EMEP anthropogenic sources (a), secondary sources (wind re-suspension) (b) and non-EMEP anthropogenic sources (c) and mean deposition fluxes from these sources to the EMEP sub-regions (d).*

Spatial distribution of deposition from anthropogenic sources is determined by location of emission sources and by dispersion of the emitted Cd by atmospheric flows and turbulent mixing. Location of maximum values of deposition corresponds to regions with the most significant anthropogenic emission sources (Fig. 3.17a). Relative contribution of the EMEP anthropogenic emissions to Cd deposition in the considered sub-regions varies from almost 50% in Caucasus and Central Asia to almost 80% in Central Europe (Fig. 3.17d).

Re-suspension flux of Cd depends on concentrations of Cd in soils, meteorological conditions (wind velocity, soil moisture), soil texture (relative content of sand, silt and clay) and land-cover. It is assumed that concentration in soil is enriched with Cd in regions with relatively high atmospheric pollution. Therefore, comparatively high deposition of re-suspended Cd takes place in such regions , e.g. the south-eastern part of Poland and the western part of Germany. The highest mean deposition flux from re-suspension (around 4 g/km^2/y) is noted for Central and Western Europe. The highest

contribution of wind re-suspension to total flux (about 35%) is indicated for Western and Northern Europe. Considerable relative contribution of re-suspension to Northern Europe is explained by low anthropogenic emissions in countries of Northern Europe and by transboundary transport of Cd re-suspended from more polluted sub-regions, e.g., from Central Europe.

The most significant impact of non-EMEP sources is revealed in countries in the southern and south-eastern part of the EMEP domain, e.g., Greece, Turkey, Transcaucasian and Central Asian countries (Fig. 3.17c). On average, the contribution of non-EMEP sources varies from 0.6 g/km^2/y in Northern Europe to 4.6 g/km^2/y in Southern Europe (Fig. 3.17d). The highest contribution of non-EMEP sources to total deposition is noted for Caucasus and Central Asia (35%) followed by Southern Europe (about 30%).

More detailed information on the contributions from EMEP anthropogenic sources, wind re-suspension and non-EMEP anthropogenic sources to Cd deposition in 2019 in the particular EMEP countries can be found in Supplementary Data Report [*Strizhkina et al.,* 2021a].

Changes of the pollution levels in 2019

Changes of Cd air concentrations in 2019 compared with 2018 are demonstrated in Fig. 3.18a. Areas with increased air concentrations include the United Kingdom, Norway, Russia, Germany, the eastern part of Poland, the north-eastern part of Spain and the southern parts of Italy and France. The decline of concentrations takes place in France, the Baltic region, Central Asia and in a number of regions of Central and Eastern Europe. The highest decline of mean concentrations is noted for Caucasus and Central Asia (about -50%), while in other sub-regions the concentration change is much lower (from 1% to -7%) (Fig. 3.18b).

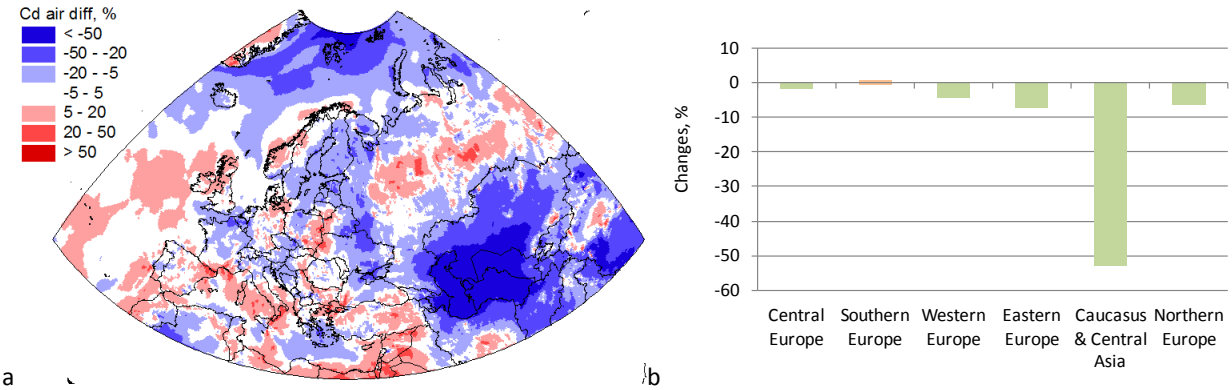

Fig. 3.18. *Relative changes of Cd air concentrations between 2019 and 2018 over the EMEP domain (a) and in various sub-regions (b).*

Over most part of the EMEP countries the relative changes of total deposition flux between 2018 and 2019 range within ±50% (Fig. 3.19a). Increase of deposition takes place in the central part of Norway, central part of Russia, some regions of the Baltic region, north of Germany and the western part of the Mediterranean. In France, Iberian Peninsula, eastern Mediterranean, south-eastern Europe and

Central Asia Cd deposition in 2019 decreased. The highest relative decline of mean deposition (-30%) occurs in Caucasus and Central Asia sub-region (Fig. 3.19b). The main contribution to this decline is made by deposition changes from secondary sources, while the contribution of anthropogenic and non-EMEP sources slightly increased. Overall decline (from -7% to -14%) of total Cd deposition also occurs in Southern, Western and Eastern Europe. In Central and Northern Europe the changes are insignificant.

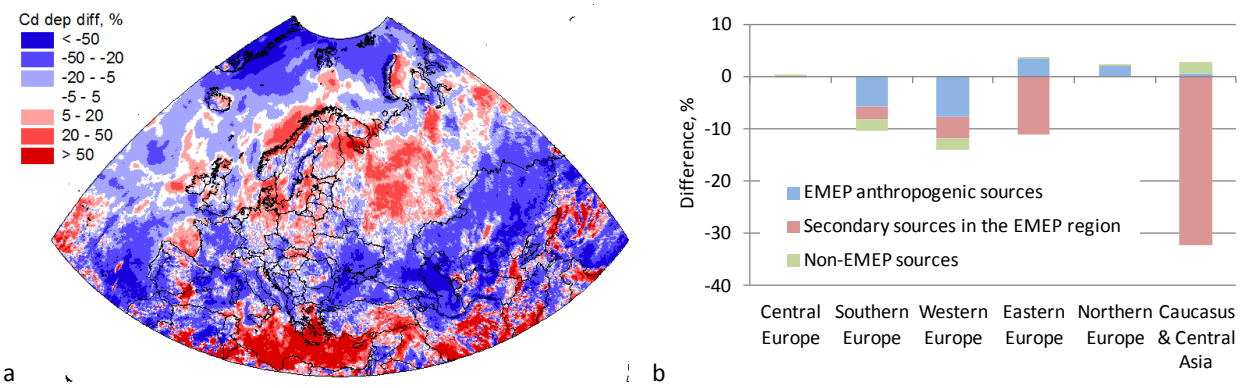

***Fig. 3.19**. Relative changes of Cd deposition between 2019 and 2018 over the EMEP domain (a) and in various sub-regions (b).*

The changes of Cd pollution levels between 2018 and 2019 are explained by inter-annual variability of meteorological parameters, first of all, annual sums of precipitation and atmospheric transport patterns. In Southern Europe the general decline of precipitation results to 10% decrease of total deposition (Fig. 3.19b). In Western Europe the decline of mean deposition flux is 14%. It can partly be explained by the decline of precipitation amounts over most part of France (Fig. 3.2). However, in some countries of Western Europe sub-region (e.g., the United Kingdom, Belgium) the deposition declined in spite of the increase of annual precipitation. Comparison of the results of source-receptor calculations in 2018 and 2019 reveals that in these countries the deposition from national sources increased but that from the foreign sources decreased. Therefore, the deposition in these countries declined due decrease of transboundary transport component. The highest decline of total deposition in 2019 occurred in the Caucasus and Central Asia. Annual precipitation sums in 2018 are significantly lower than climatic norm in the western part of Central Asia [*Blunden and Arndt*, 2019], while precipitation in 2019 were closer to the norm. Higher precipitation in 2019 leads to wetter soil and, hence, suppresses generation of wind-blown re-suspension of Cd. Therefore, the decline of deposition in 2019 in Central Asia is a consequence of significant reduction of Cd input to the atmosphere. At the same time, the deposition from other groups of sources, such as anthropogenic emissions and non-EMEP sources, increased in 2019. The smaller re-suspension of Cd in Central Asia in 2019 compared with 2018 resulted to lower deposition to the eastern part of Europe because of long-range transport of re-suspended Cd from Central Asia. Therefore, in the Eastern Europe the deposition from secondary sources declined by around 10%. Deposition from anthropogenic sources increased mostly due to increase of annual precipitation. Changes of mean deposition fluxes in Northern and Central Europe are insignificant. However, the changes in particular countries or country's provinces can considerably exceed average values for the sub-regions.

Transboundary transport

The contribution of transboundary transport to Cd pollution levels in the EMEP countries is considered as a relative fraction of deposition originated from foreign anthropogenic sources to total deposition from the EMEP anthropogenic sources. In 2019 the contribution of transboundary transport to anthropogenic deposition varied from 12% in Portugal to more than 98% in Malta, Iceland, Liechtenstein and Monaco. Contribution of transboundary transport to deposition exceeds 50% in 39 countries and 75% in 18 countries. In this section afew examples concerning evaluation of transboundary pollution in the EMEP countries are presented. Detailed information on source-receptor relationships between the EMEP countries is available on the Internet (*www.msceast.org*) and in Supplementary Data Report [*Strizhkina et al.*, 2021a].

Fig. 3.20 demonstrates examples of contributions of national and foreign sources to Cd deposition in Lithuania and Poland. Lithuania is characterized by relatively low national emissions. Therefore, only 9% of Cd, deposited to Lithuania from anthropogenic sources, is caused by national emissions, and 91% comes from the sources located in other EMEP countries (3.20a). Among them the main contributor is the emission of neighboring Poland (29%). In Poland the distribution between the contributions of national and foreign sources to deposition is strongly different. Compared to other EMEP countries, Cd emissions in Poland are high. Therefore, most of Cd deposition (64%) in Poland is caused by national emission sources (Fig. 3.20b). Main sources of transboundary transport to Poland are emissions of Germany (13%), Czechia (4%) and Slovakia (4%).

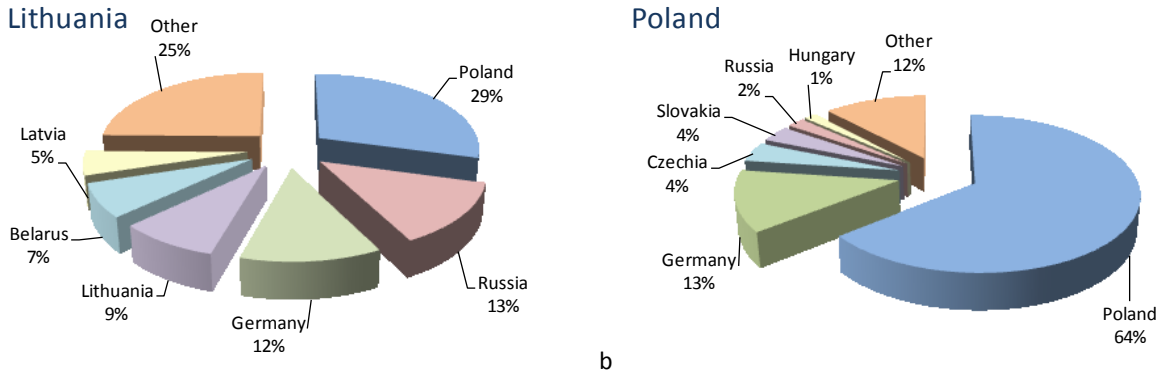

Fig. 3.20. *Contribution of transboundary transport and national source to anthropogenic Cd deposition in Lithuania and Poland in 2019.*

Changes of contribution of transboundary transport and national sources to deposition in particular countries, caused by variability of meteorological conditions, are estimated by the comparison of source-receptor matrices for 2018 and 2019. Analysis of the changes is presented for North Macedonia as example, but could be carried out for any other EMEP country. Total deposition of Cd to North Macedonia in 2019 is about 120 kg, which is about 15 kg less than the deposition in 2018 (Fig. 3.21). It corresponds to a decrease in precipitation amount over the country between 2018 and 2019. Besides, substantial decline of deposition from Bulgarian sources also takes place. At the same time, deposition from a number of countries, e.g., Greece, Turkey, Serbia increased. For example, Cd deposition caused by the Turkish sources in 2019 increased by 10 kg (about 45%). Since precipitation amount over Turkey in 2019 reduced, smaller fraction of Turkish emissions deposited to own

territory and more emitted Cd entered transboundary transport affecting neighboring or closely located countries.

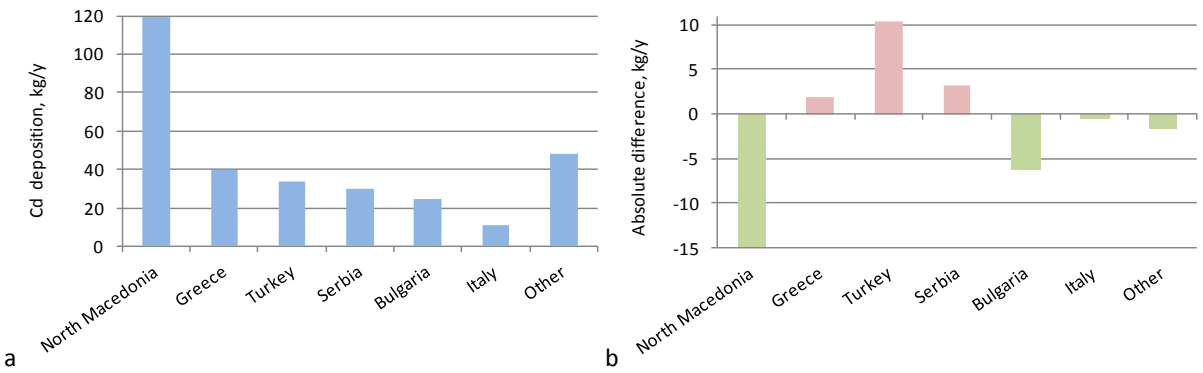

Fig. 3.21. *Cadmium deposition in North Macedonia from main countries-contributors in 2019 (a) and absolute difference of Cd deposition between 2019 and 2018 (b).*

Each EMEP country is considered not only as a receptor, but also as a source of transboundary pollution in the EMEP region. As much as 75% of anthropogenic deposition to the EMEP countries are caused by the emission sources from seven EMEP countries. The largest deposition to foreign EMEP countries is caused by sources of Russia (about 8 tonnes), followed by Germany (about 5 tonnes) and Poland (4 tonnes). Deposition of Cd from national sources to the territories of their own countries amounts to 48, 5 and 4 tonnes, respectively. Pie chart (Fig. 3.22a) and map (Fig. 3.22b) demonstrate contribution of German emission sources to Cd deposition to other EMEP countries in 2019.

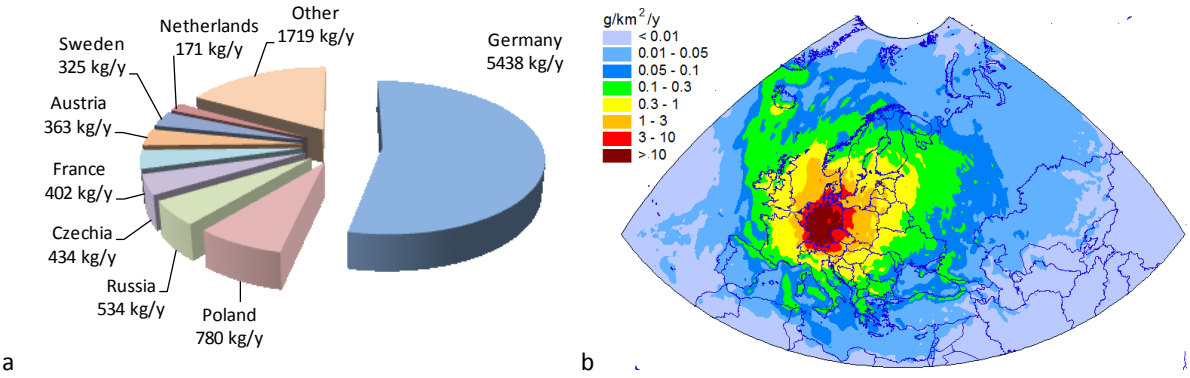

Fig. 3.22. *Deposition of Cd from German anthropogenic sources to the EMEP countries in 2019 (a) and map of Cd deposition from German sources in the EMEP region (b)*

Inter-annual meteorological variability results to changes of deposition from country's sources to own territory and territories of other countries. For example, total Cd deposition from the Dutch sources to territories of the EMEP countries is 1480 kg/y. Among them the deposition to own territory is 361 kg/y (23%), to Germany – 456 kg/y (31%) etc. (Fig. 3.23a). Compared with 2018, deposition from the Dutch sources to own territory and to a number of other countries (e.g., Germany, Sweden, Russia, Poland, Denmark) increased (Fig. 3.23b). On the contrary, deposition to France, the United Kingdom and Belgium from the Dutch sources declined by 10 – 50%.

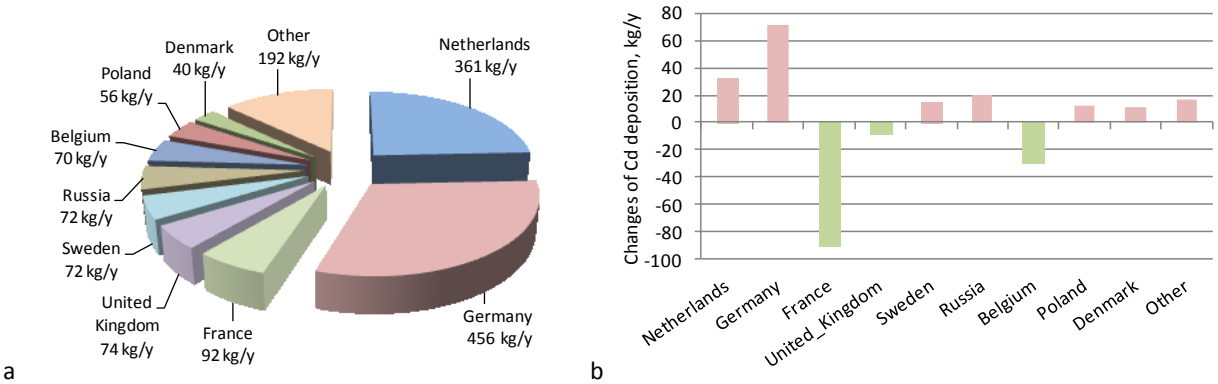

Fig. 3.23. *Deposition of Cd from Dutch anthropogenic sources the EMEP countries in 2019 (a) and the deposition changes between 2019 and 2018 (b)*

The main contributor to Cd atmospheric pollution in most of the EMEP countries is anthropogenic emissions of the EMEP countries followed by secondary sources. Inter-annual variability of meteorological conditions resulted to decline of Cd total deposition in Caucasus and Central Asia, Southern, Western and Eastern Europe.

3.3.4. Mercury

Mercury is present in the atmosphere predominantly in elemental gaseous form (Hg^0), in contrast to other heavy metals (Pb and Cd), which occur in the atmosphere being associated with aerosol particles. Besides, chemical transformations of Hg^0 lead to formation of oxidized Hg species, which can occur in both gaseous and particulate forms. The dispersion of Hg in the atmosphere, its transboundary transport and deposition are determined by the complex chemical cycling of Hg compounds in the atmosphere.

Air concentrations

Air concentration of Hg^0 is evenly distributed throughout the EMEP region due to its long residence time in the atmosphere. The concentrations of Hg^0 range from less than 1.4 ng/m^3 in remote regions (e.g., the Arctic, Northern Sweden, the Himalayas etc.) up to 1.8 ng/m^3 in Southern Europe, the Caucasus and Central Asia (Fig. 3.24a). Southern Europe and some countries of Central Asia are characterized by higher emission of Hg from natural and secondary sources, resulting in higher Hg concentrations in these regions (Fig. 3.24b). The large concentrations of Hg^0 (over 2.0 ng/m^3), which occur in the Caucasus, are caused by high anthropogenic emissions reported by Armenia (see Annex A in *O.Travnikov et al.* [2020]). Relatively low Hg concentrations are noted for France, Northern and Eastern Europe, Kazakhstan, Kyrgyzstan and Tajikistan. Modelling results are in agreement with measured background Hg^0 concentrations, obtained from the EMEP monitoring network, with relative bias ranging from -10% to 20%. Detailed information on agreement between modelled and observed concentrations is presented in Supplementary Data Report [*Strizhkina et al.*, 2021a].

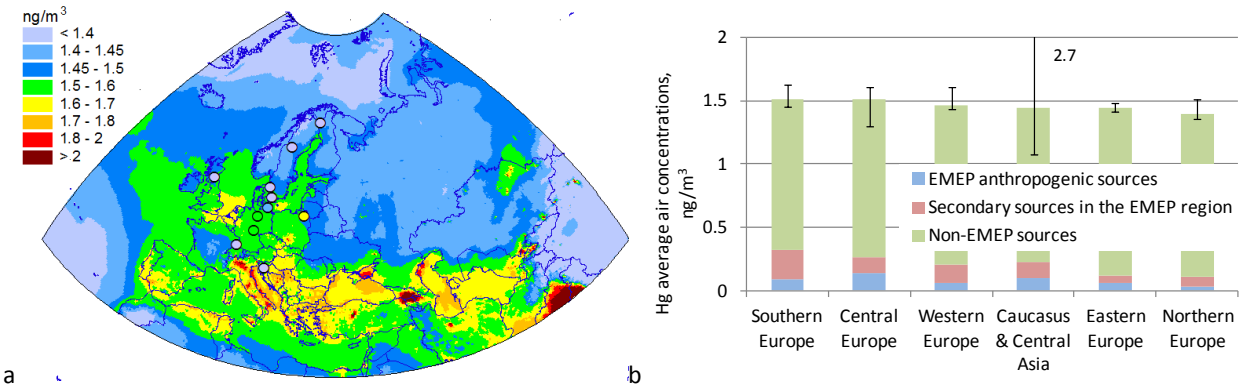

Fig. 3.24. *Spatial distribution of annual mean Hg^0 air concentration over the EMEP domain (a) and average Hg^0 concentration in various sub-regions (b) in 2019. Circles on the map show observed values in the same colour scale. Whiskers show the range of concentrations in particular countries of the sub-region.*

Changes of meteorological conditions caused slight variation in Hg^0 air concentration (±5%) in 2019 compared to the previous year (Fig. 3.25a). Mercury near-ground concentrations in Southern Europe and the Mediterranean declined on average by 0.7% (up to 3% in some areas) because of higher vertical mixing leading to decrease of contribution of local anthropogenic and natural/secondary emissions, which was partly balanced by increase of contribution from non-EMEP sources (Fig. 3.25b). On the contrary, the Caucasus and Central Asia were characterized by decrease of contribution of non-EMEP sources and increase of contribution of anthropogenic and secondary sources. The increase (up to 5%) of the surface air concentration of Hg^0 in Eastern Europe (particularly, in the European part of Russia) was largely caused by decreased Hg^0 dry deposition in this sub-region.

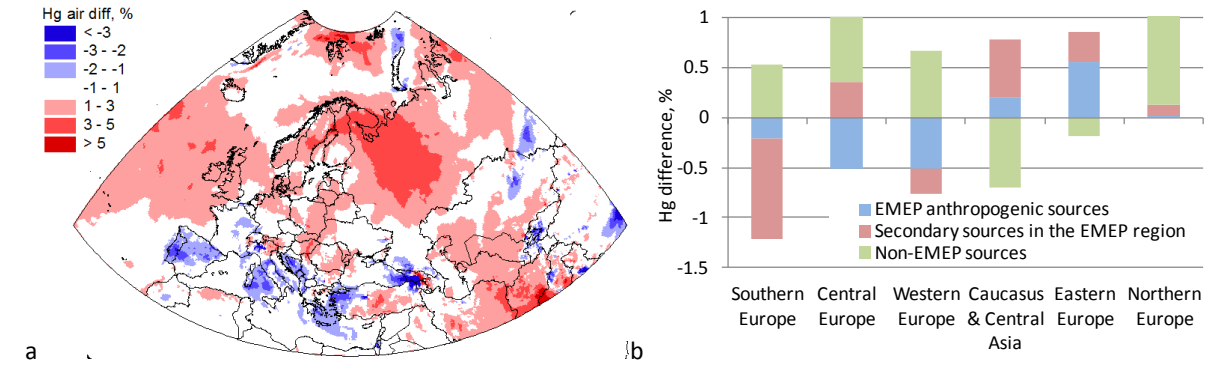

Fig. 3.25. *Relative changes of Hg^0 air concentrations between 2019 and 2018 over the EMEP domain (a) and in various sub-regions (b).*

Deposition fluxes

Deposition of Hg is largely determined by oxidized Hg forms that are emitted and formed chemically in the atmosphere. Thus, the spatial pattern of Hg deposition is affected by a number of factors, which include spatial distribution of emissions, variability of meteorological conditions and the distribution of zones of intensive atmospheric oxidation. Spatial pattern of Hg deposition is shown in

Fig. 3.26a. The model assessment shows high deposition fluxes (more than 17 g/km^2/y) in some countries of Southern and Central Europe (e.g., Poland, Slovakia, Czechia, Italy, Croatia). Elevated Hg deposition (more than 25 g/km^2/y) also occurs in some countries of Caucasus and Central Asia (particularly, Armenia and Georgia) due to high Hg anthropogenic emissions reported by Armenia in 2020 (see Annex A in *O.Travnikov et al.* [2020]). In addition, intensive oxidation of Hg^0 in spring during the Atmospheric Mercury Depletion Events (AMDEs) leads to relatively high Hg deposition in the high Arctic. At the same time, it should be noted that significant part of Hg deposited to snow is thereafter re-emitted to the atmosphere.

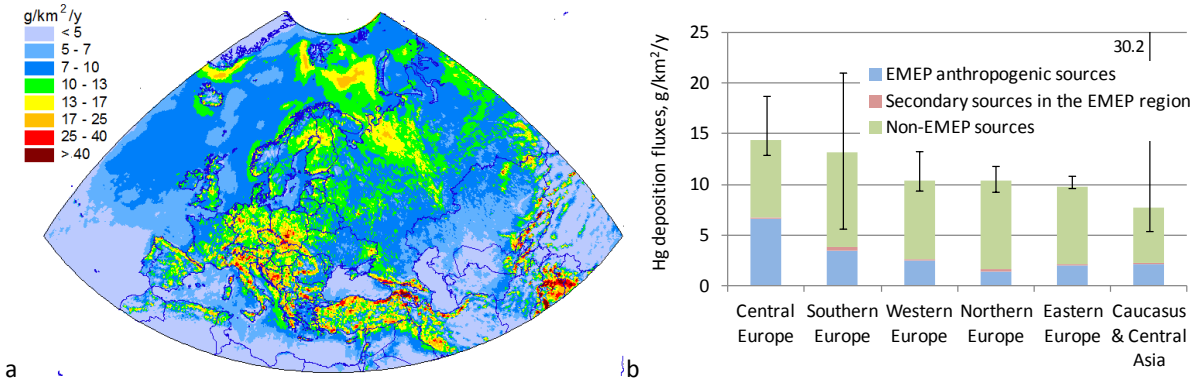

Fig. 3.26. *Spatial distribution of annual Hg deposition flux over the EMEP domain (a) and average Hg deposition in various sub-regions (b) in 2019. Whiskers show the range of deposition fluxes in particular countries of the sub-region.*

The relative contribution of EMEP anthropogenic sources to Hg deposition is the largest (over 45%) in Central Europe (Fig. 3.26b). For all the sub-regions, the contribution of secondary and natural sources to Hg deposition does not exceed 2.5%. Mercury emitted from these sources is mainly carried out of the region. On the contrary, the contribution of non-EMEP sources is large and amounts to 50-97% of total Hg deposition to particular countries. However, these non-EMEP sources may also include some input of Hg from the EMEP sources that have been transported through the borders, mixed with Hg from other sources and returned back to the region.

Figure 3.27 shows annual deposition of Hg from different groups of sources in the EMEP region. Generally, the spatial patterns of Hg deposition from EMEP anthropogenic as well as natural/secondary sources are consistent with the distribution of respective emission sources. The industrial regions of Central and Southern Europe, as well as some areas of Eastern Europe, are characterized by the most significant Hg deposition from anthropogenic sources (Fig. 3.27a). Deposition of Hg from natural and secondary sources is much lower in all the sub-regions (less than 1.7% of total deposition flux), only in Southern Europe contribution of this source type exceeds 2% (Fig. 3.27b). The highest deposition fluxes from non-EMEP sources take place in the high Arctic, Southern Europe and Middle East (Fig. 3.27c). It should be noted, that the spatial distribution of Hg deposition from non-EMEP sources is largely influenced by chemical transformations of Hg compounds as well as meteorological and surface conditions.

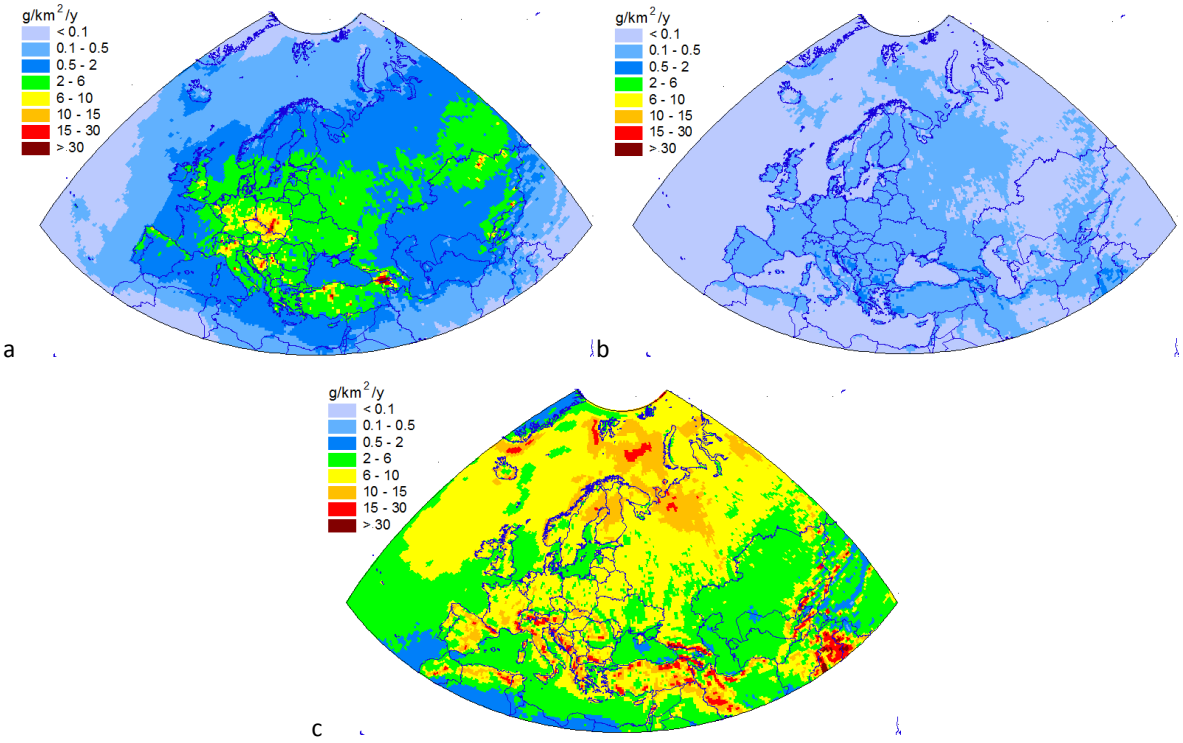

Fig. 3.27. *Annual deposition of Hg in 2019 from EMEP anthropogenic sources (a) natural/secondary sources (b) and non-EMEP sources (c).*

Changes in the Hg deposition pattern in 2019 compared to 2018 due to variability in meteorological parameters are shown in Figure 3.28. In Northern Europe, the Caucasus and Central Asia, Hg deposition flux increased by 9% and 6%, respectively, mainly due to increase of deposition from EMEP anthropogenic sources. One of the key factors influencing the increase of Hg deposition flux in Northern Europe is considerable increase of precipitation in this region (Section 3.1), which determines wet deposition of Hg. Decrease in deposition occurred in Southern and Western Europe, in the high Arctic and the western part of Mediterranean regions. This can be explained by significant decrease of precipitations in these sub-regions. In Central and Eastern Europe, the changes of Hg deposition have more mosaic character, where areas of increased deposition alternate with those of decreased deposition depending on changes of local conditions (e.g. precipitation amount, vertical mixing and concentration of chemical reactants).

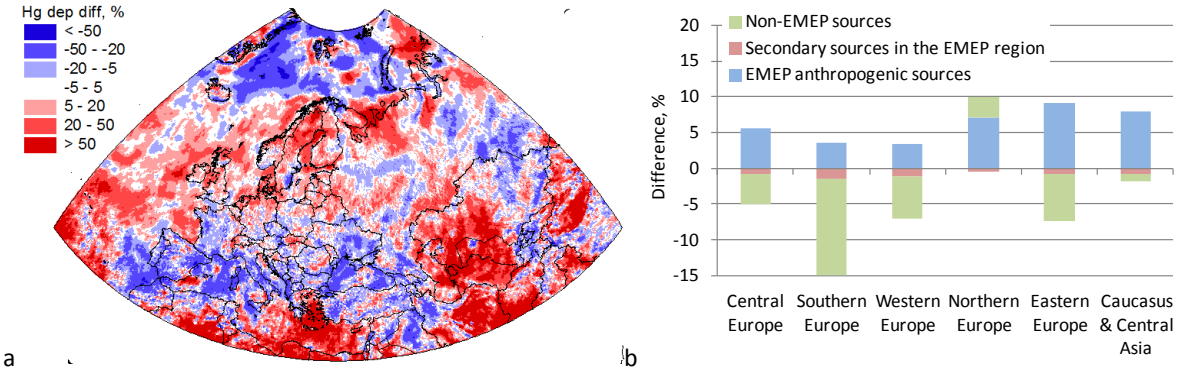

Fig. 3.28. *Relative changes of Hg deposition between 2019 and 2018 over the EMEP domain (a) and in various sub-regions (b).*

Evaluation of simulated Hg deposition can be partly carried out by comparing of the modelled and observed wet deposition fluxes. The comparison of the modelling results with the EMEP measurements shows satisfactory agreement of the modelled and observed values with high spatial correlation (0.73) and deviations being mostly within a factor of two (Supplementary Data Report [*Strizhkina et al.*, 2021a]). However, the model tends to overestimate the observed values. This discrepancy can be explained by uncertainties in speciation of Hg anthropogenic emissions and insufficient knowledge about the mechanisms of chemical reactions of Hg species in the atmosphere. It should be mentioned that information on speciation of Hg emissions is not the mandatory parameter to be included in the annual reporting of the EMEP countries. Therefore, preparation of emission data for modelling is carried out using simplified expert estimates. Model experiments with an updated version of GLEMOS, which include updated global Hg emissions inventory for boundary conditions, new input dataset of chemical reactants and revised Hg emission speciation scheme, demonstrate considerably better model performance in comparison with observations (Section 4.5). This renewed model version is planned to be used for the EMEP operational modelling of Hg in future.

Transboundary transport

The model assessment of long-range transport of Hg demonstrates the significant effect of transboundary pollution in the EMEP countries. This effect in a particular country can be estimated using the ratio of the contributions of national and foreign anthropogenic sources to Hg deposition. The relative contribution of foreign sources ranges from 8-20% for Armenia and Turkey to over 98% for Georgia, Monaco and Liechtenstein. Generally, the contribution of foreign sources to Hg deposition exceeds 50% in 41 EMEP countries and 75% in 25 EMEP countries.

Fig. 3.29 demonstrates an example of two countries with different contributions of transboundary transport (Spain and Sweden). In Spain, anthropogenic deposition of Hg is largely determined by national sources (66%). About 25% of Hg deposition is made by Portugal, Italy, France, Germany, and the United Kingdom. In contrast, in Sweden, transboundary transport accounts for almost 90% of total anthropogenic Hg deposition. The largest contributions are made by Germany (20%), Poland (18%), the United Kingdom (8%), Finland (5%) and Denmark (4%). Detailed information on transboundary pollution for each EMEP country is presented in Supplementary Data Report [*Strizhkina et al.*, 2021a].

Variations of atmospheric circulation and other meteorological conditions lead to changes in transboundary transport patterns from year to year. Figure 3.30 illustrates an example of changes in the contribution of other EMEP countries to Hg deposition in Belgium between 2019 and 2018. In 2019, the contribution of national emission sources in this country to Hg deposition is about 50% (78 kg/y). Germany, France, the United Kingdom, Netherlands and Poland are the main foreign contributors of Hg anthropogenic deposition in Belgium. Compared to 2018, the contribution of Germany to Hg deposition in Belgium in 2019 decreased from 43 to 29 kg/y. In contrast, the contribution of France increased from 18 to 26 kg/y and the contribution of the United Kingdom increased from 8 to 14 kg/y.

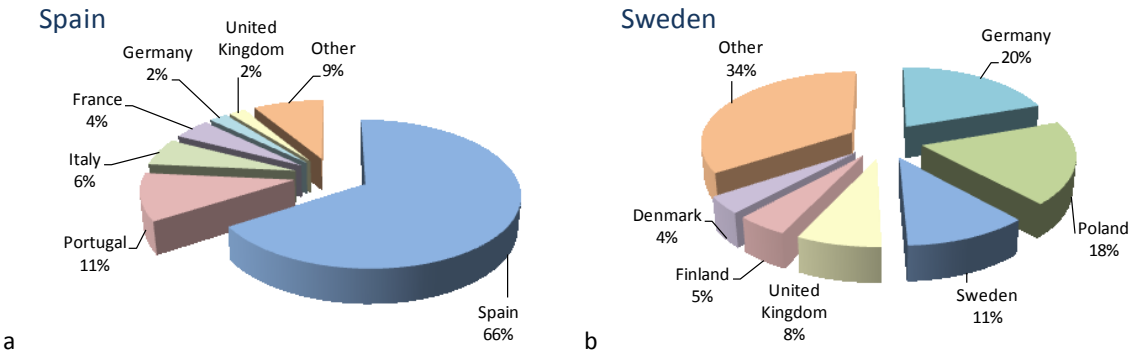

Fig. 3.29. *Contribution of transboundary transport and national sources to anthropogenic Hg deposition in Spain and Sweden 2019.*

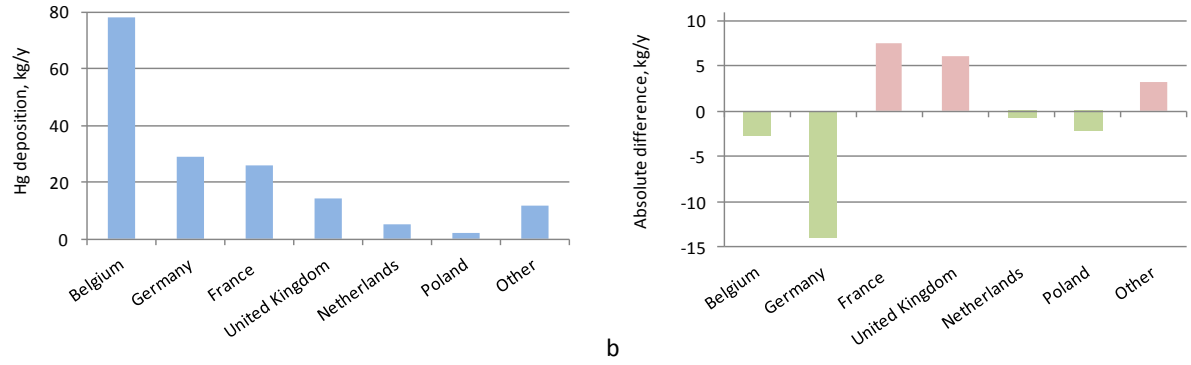

Fig. 3.30. *Major contributors of Hg anthropogenic deposition in Belgium in 2019 (a) and absolute difference of Hg deposition between 2019 and 2018 (b).*

Each country acts as a source of Hg pollution of its own territory as well as of the territories of other countries. The contribution of a particular EMEP country to transboundary pollution is determined by the national emissions, the size and location of the country. It should be noted, that 10 major source countries (Kazakhstan, Russia, Turkey, Poland, Germany, Armenia, Ukraine, Italy, the United Kingdom and Czechia) contribute about 75% of Hg deposition in the EMEP region. For most of these countries, Hg deposition to their own territory is comparable to their contribution to transboundary pollution. However, in Russia, deposition to its own territory exceeds deposition to the territories of other countries by a factor 4.6. In contrast, in Armenia, the contribution to transboundary transport exceeds deposition to its own territory by a factor 5.3.

Changes in deposition of national emissions in Czechia to other countries between 2019 and 2018 due to interannual meteorological variability are shown in Fig.3.31. Deposition of Hg from the Czech sources to the territories of other countries increased by 164 kg/y between 2018 and 2019, while deposition from Czechia to its own territory decreased by 21 kg/y. At the same time, changes in meteorological conditions have led to some decline of Hg deposition from the Czech sources outside of the EMEP region. Increase of Hg deposition from Czech sources occur in Poland, Russia, Slovakia, Austria, Ukraine, Sweden and Hungary. Decrease of Hg deposition from Czechia by 30 kg/y is noted for Germany (Fig. 3.31b).

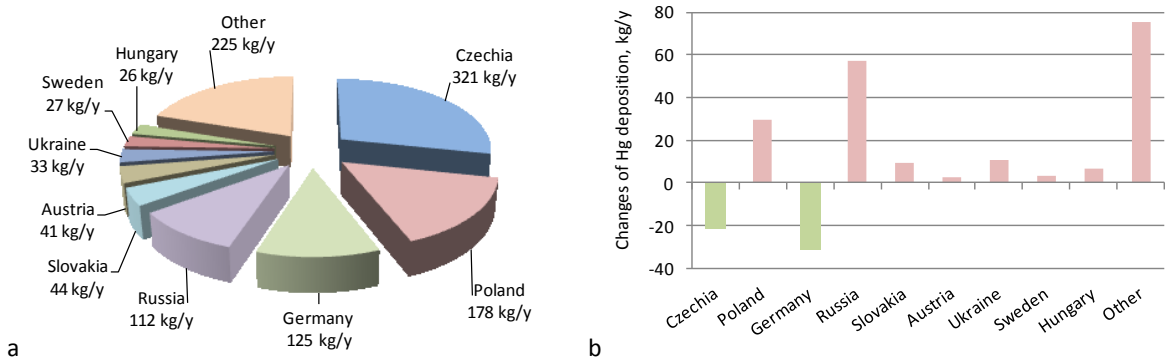

Fig. 3.31. *Deposition of Hg from Czech anthropogenic sources the EMEP countries in 2019 (a) and the deposition changes between 2019 and 2018 (b)*

Mercury deposition in the EMEP countries is largely determined by EMEP anthropogenic emissions and emissions (both direct anthropogenic and secondary/natural) transported from other regions. The impact of regional secondary/natural sources is insignificant. Inter-annual variability of meteorological conditions between 2018 and 2019 resulted in an increase of Hg deposition in Northern Europe and Caucasus and Central Asia, and a decrease in Southern and Western Europe.

3.3.5. Polycyclic Aromatic Hydrocarbons (PAHs)

Polycyclic Aromatic Hydrocarbons comprise a large group of pollutants that are emitted into the atmosphere during incomplete combustion of fossil fuels and biomass. Many PAHs pose a serious risk to human health due to their carcinogenic, mutagenic, and teratogenic properties, liver and kidney toxicity, hematological, pulmonary and respiratory effects, and neurotoxicity. Besides, many PAHs are hazardous to the environment. For assessment of PAH pollution levels and exceedances of air quality target values established in EU, modelling of transboundary transport of 4 selected PAHs (namely benzo(a)pyrene, benzo(b)fluoranthene, benzo(k)fluoranthene, and indeno(1,2,3-cd)pyrene, targeted by the Protocol on POPs) as well as monitoring of their atmospheric concentrations are carried out. This section provides information on air pollution in the EMEP region for 2019 by sum of 4 selected PAHs. Information on the levels of air pollution by particular PAHs is presented in Supplementary Data Report [*Strizhkina et al.*, 2021b].

Air concentrations

Spatial distribution of annual mean values of modelled concentrations of sum of 4 PAHs in 2019 is shown in Fig. 3.32. The observed air concentrations reported by EMEP monitoring stations are mapped with model estimates. In general, the concentrations of PAHs in the EMEP region vary over a wide range. According to the model estimates, the highest concentrations of 4 PAHs are noted for the countries of Central, Southern, and Eastern Europe, including Poland, Czechia, Slovakia, Hungary, and Greece. High levels of PAH pollution are also estimated for northern Italy, eastern Croatia, Serbia, Ukraine, Romania, Bulgaria, and Russia (Fig. 3.32a). The lowest concentrations of sum of 4 PAHs in 2019 take place in Northern Europe and in Caucasus and Central Asia (Fig. 3.32b). Air

concentrations of individual PAHs in some regions exceed the air quality standards established in the EU. Detailed analysis of these exceedances is presented in Section 3.4.2.

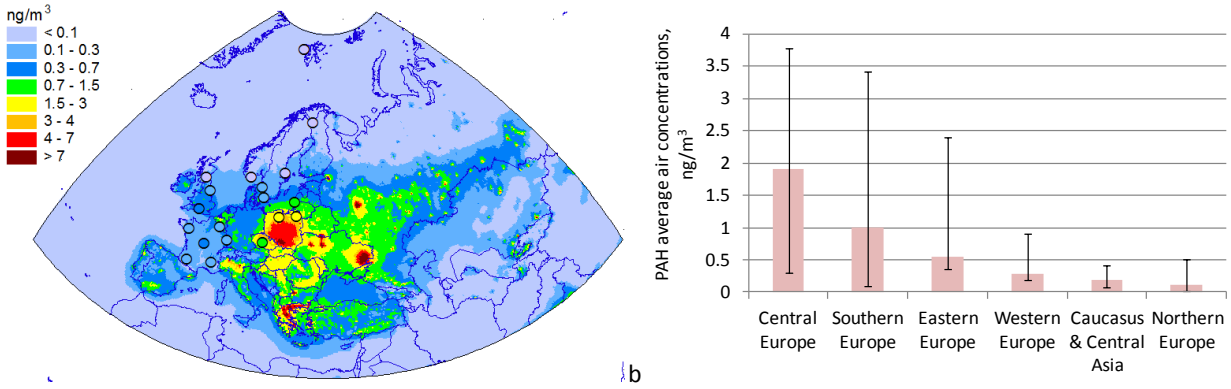

Fig. 3.32. *Spatial distribution of modelled and observed annual mean air concentrations of sum of 4 PAHs over the EMEP domain (a) and average air concentrations of sum of 4 PAHs in various sub-regions(b) in 2019. Circles on the map show observed values in the same colour scale. Whiskers show the range of concentrations in particular countries of the sub-region.*

In 2019, measurements of 4 PAHs were carried out at 36 monitoring sites in 7 EMEP countries. Evaluation of modelling results against EMEP measurements shows generally reasonable agreement of modelled and observed concentrations of the sum of 4 PAHs with significant spatial correlation (0.96). (Fig. 3.32a). The model tends to over-predict observed annual mean air concentrations of the sum of 4 PAHs with mean relative bias of about 24%. For about 70% of the monitoring sites, the difference between the modelling results and measured concentrations is within a factor of 2. A more significant overestimation is noted for the stations in Sweden and France (about factor of 2-3).

Evaluation of modelling results for individual PAH compounds against the EMEP measurements shows almost no bias for B(a)P and IcdP while for B(b)F and B(k)F some overestimation of observed air concentrations is obtained (about 60% and 23%, respectively). The model reproduced the spatial distribution of observed B(a)P, B(B)F, B(b)F, and IcdP air concentrations with correlation coefficient about 0.9. More detailed evaluation of modelling results against the monitoring data of EMEP is given in Supplementary Data Report [*Strizhkina et al.*, 2021b].

In addition to this, model predictions of B(a)P air concentrations for 2019 were compared with the measurements of EU EEA Air Quality e-Reporting (AQ e-Reporting). Monitoring of B(a)P air concentrations in 2019 was carried out at more than 700 national stations in 29 European countries. The model tends to underestimate the observed values of B(a)P concentrations, especially for industrial, background urban and suburban monitoring sites. The most significant underestimation is noted for the monitoring stations in Poland, Austria, Estonia, and France (about a factor of 3 on average). For about a half of the European countries, provided national B(a)P measurements, the model reasonably reproduces spatial distribution of the observed B(a)P concentrations (with correlation coefficients about 0.4-0.7). For other countries weak spatial correlation is obtained that can be attributed to uncertainties in spatial distribution of B(a)P emissions, as well as uncertainties in the model parameterization.

Model simulations of PAH pollution for 2019 were compared with modelling results for 2018 calculated with the same set of anthropogenic emissions for 2018. Differences in the obtained modelling results illustrate the effect of inter-annual variations of meteorological conditions on the pollution levels. Changes between the air concentrations in 2019 and 2018 within the EMEP domain are presented in Fig. 3.33.

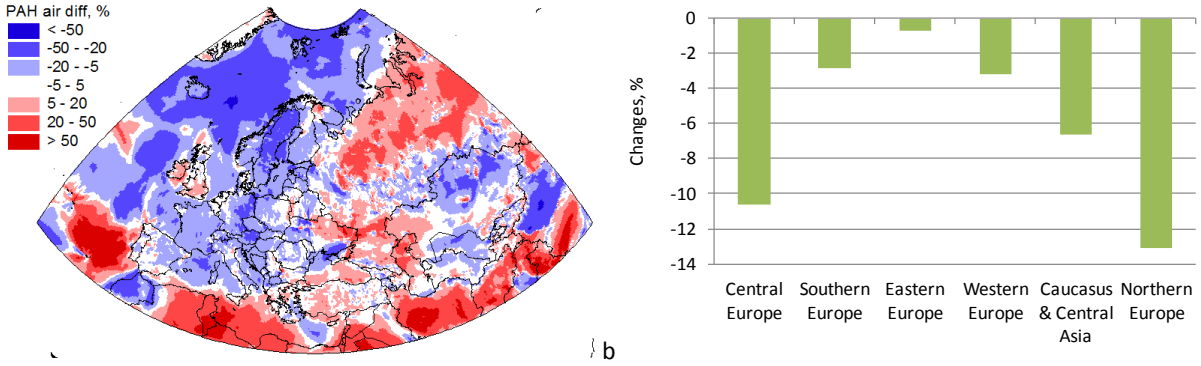

Fig. 3.33. *Spatial distribution of relative changes of sum of 4 PAH air concentration between 2019 and 2018 due to inter-annual variability of meteorological conditions (a) and relative changes of averaged air concentrations over different sub-regions of the EMEP domain (b).*

Generally, in all sub-regions of the EMEP domain, the sum of the air concentration of 4 PAHs decreased between 2019 and 2018 (Fig. 3.33b). The largest decrease (~13%) is indicated for Northern Europe followed by Central Europe (~10%) and Caucasus and Central Asia (~7%). At the same time, some particular countries are characterized by the increasing PAH concentrations. For example, it can be noted for the United Kingdom, Ireland, Russia, Greece, Turkey, and the western part of Kazakhstan (Fig. 3.33a).

Deposition fluxes

Spatial distribution of the total deposition fluxes of sum of 4 PAHs, estimated for 2019, is presented in Fig. 3.34. Areas of the highest annual mean deposition fluxes are estimated for Central and Southern Europe, which are also characterized by the highest air concentrations. Countries with the highest average deposition fluxes include Greece, Poland, Slovakia and Czechia. Detailed information on the deposition fluxes for particular PAHs can be found in Supplementary Data Report [*Strizhkina et al.*, 2021b].

Source apportionment of PAH pollution was performed taking into account contributions of anthropogenic emission sources of the EMEP region, EMEP secondary sources, and emission sources located outside the EMEP domain. The contribution of non-EMEP anthropogenic sources to total PAH deposition fluxes is estimated using global-scale modelling based on the global PAH emission inventory [*Shen et al.*, 2013]. Relative contributions of the three main groups of emission sources of PAHs to annual total deposition, averaged over different sub-regions of the EMEP domain, are shown in Fig. 3.34b. The contribution of the EMEP anthropogenic sources ranges from about 70% in

Caucasus and Central Asia to over 80% in Central Europe. Relative contribution of secondary sources and non-EMEP anthropogenic sources is much lower accounting for about 20% and less than 10%, respectively.

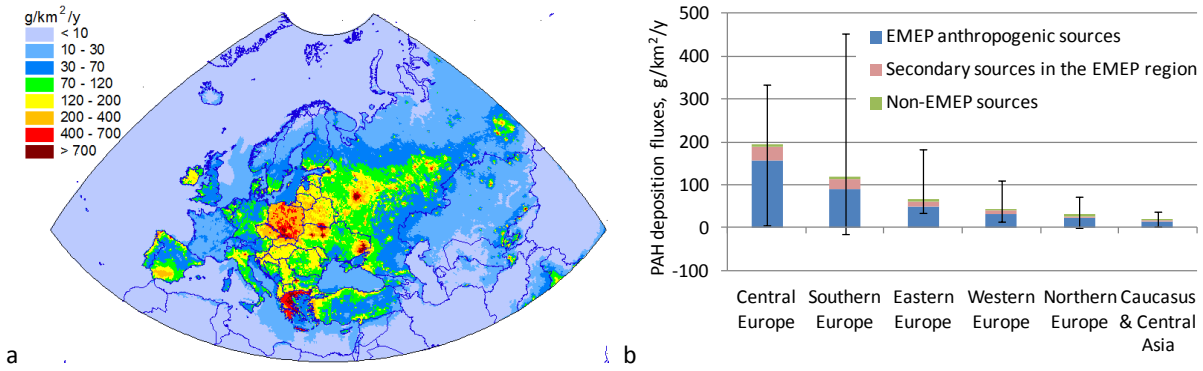

Fig. 3.34. *Spatial distribution of modelled total deposition fluxes of sum of 4 PAHs in the EMEP domain for 2019 (a) and deposition fluxes of sum of 4 PAHs in 2019 from EMEP anthropogenic sources, secondary sources and non-EMEP anthropogenic sources for different sub-regions of the EMEP domain. Whiskers show the range of deposition fluxes in particular countries of the sub-region (b).*

Differences of total deposition fluxes of 4 PAHs between 2018 and 2019 are shown in Fig. 3.35. An increase in PAH deposition fluxes is noted for Eastern Europe (including Russia, Lithuania, Estonia, Latvia) (~6%) and Caucasus and Central Asia (~2%). At the same time, PAH deposition fluxes decreased in Western, Northern, Southern and Central Europe, by 9%, 8%, 6% and 4%, respectively. It should be mentioned that these sub-regions are characterized by different direction of changes in the particular countries. Modelling results showed increasing deposition fluxes in Finland, Poland, Slovakia (Fig. 3.35a). Estimated changes in PAH pollution levels from 2018 to 2019 may be associated with inter-annual variations of meteorological conditions (precipitation and atmospheric circulation).

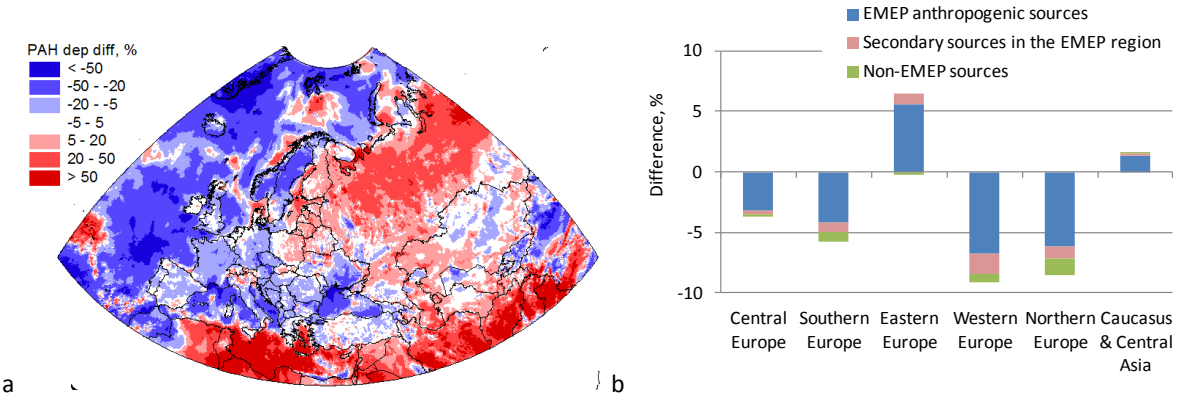

Fig. 3.35. *Spatial distribution of relative changes of sum of 4 PAH total deposition between 2019 and 2018 due to inter-annual variation of meteorological conditions (a) and relative changes of averaged total deposition in different sub-regions of the EMEP domain (b).*

Transboundary transport

The model simulations of PAH long-range transport showed significance of transboundary pollution in the EMEP countries. The influence of transboundary transport is characterized by relative contributions of national and foreign emission sources to total PAH deposition in the particular countries. Thus, the contribution of foreign sources varies from 3-10% in Spain, Ireland and Greece to more than 97% in Liechtenstein, Montenegro and Monaco. PAH deposition from transboundary transport exceeds deposition from national sources in 26 EMEP countries. The contribution of foreign sources exceeds 75% in 8 EMEP countries. A model assessment of transboundary pollution was also carried out for individual PAHs (B(a)P, B(b)F, B(k)F, IcdP). Examples of two countries with different contributions of foreign and national sources to total deposition flux of B(a)P are illustrated in Fig. 3.36. In Armenia, the contribution of foreign sources to the B(a)P pollution of the country is about 76%. The largest contributors are Georgia (43%) and Turkey (30%). In contrast, in Hungary, the effect of transboundary transport from other countries is less important and the contribution of national sources to anthropogenic deposition of B(a)P is almost 70%. Detailed information on transboundary pollution for each EMEP country and for all selected PAHs is presented in Supplementary Data Report [*Strizhkina et al.*, 2021b].

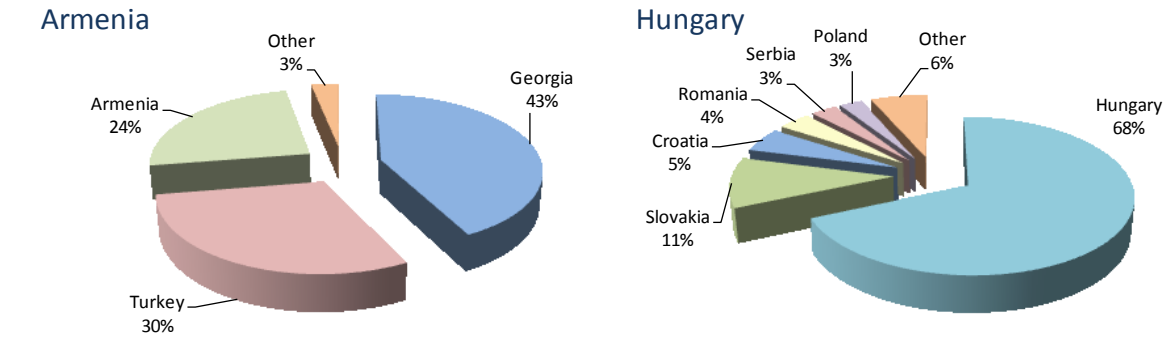

Fig. 3.36. *Contributions of transboundary transport and national emission sources to B(a)P deposition in Armenia and Hungary in 2019.*

Patterns of transboundary transport can vary considerably from year to year due to inter-annual variations of meteorological conditions. Fig. 3.37 presents an example of total annual deposition of B(a)P in Austria in 2019 from national and foreign sources and their changes from 2018 to 2019. National sources contributed about 40% (about 450 kg/y) to B(a)P deposition in Austria in 2019. The main foreign contributors are Germany, Czechia, Slovenia, Hungary and Slovakia. The contributions of Germany and Slovenia to B(a)P deposition in Austria increased by 30% and about 5%, respectively. At the same time, the contributions of Czechia, Hungary and Slovakia ranges from about 5% to 20% (Fig. 3.37b).

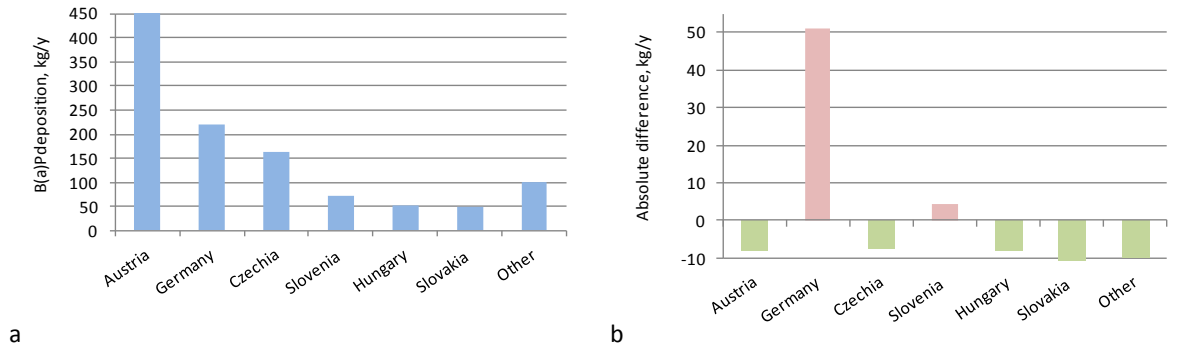

a b

Fig. 3.37. *B(a)P deposition in Austria from main countries-contributors in 2019 (a) and absolute difference of B(a)P deposition between 2019 and 2018 (b).*

PAH transboundary pollution can also be characterized by the amount of PAHs, emitted in the particular country, and deposited to its own territory and to the territories of other EMEP countries. Model estimates for 2019 show that in 20 from 51 EMEP countries, deposition from national emission sources to other countries exceeds deposition to their own territory. The largest contribution to transboundary PAH pollution in the EMEP region are made by the countries with high emissions, namely, Poland, Russia, Czechia, Romania, Ukraine, and Turkey. The distribution of total B(a)P deposition, originated from national anthropogenic emission sources of Czechia, is shown in Figure 3.38. The largest part (about 65%) is deposited to Czechia followed by Poland, Germany, Slovakia, and Austria. Detailed information on deposition fluxes of selected PAHs from other EMEP countries is presented in Supplementary Data Report [*Strizhkina et al.*, 2021b].

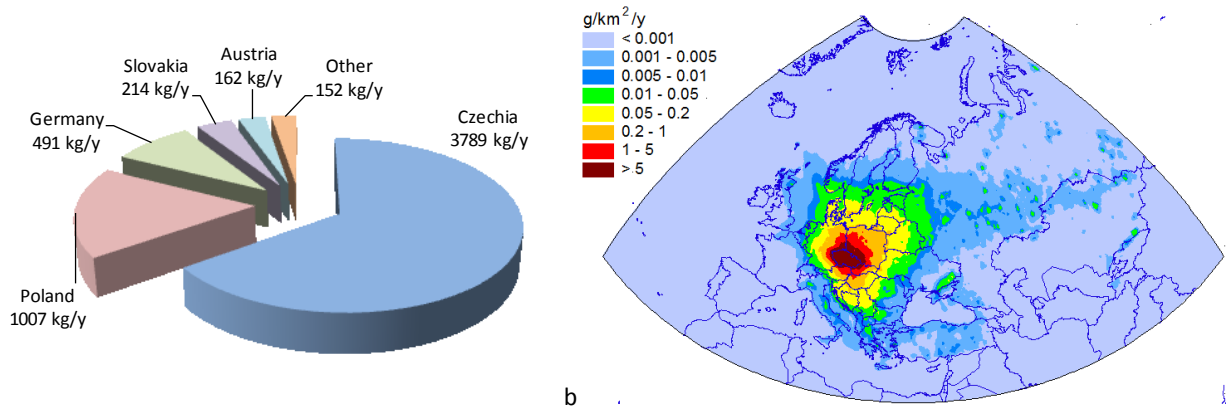

a b

Fig. 3.38 *Deposition of B(a)P from Czech anthropogenic sources to the EMEP countries in 2019 (a) and map of B(a)P deposition from Czech sources in the EMEP region (b).*

Changes of distribution of annual total B(a)P deposition, emitted by the sources of Slovakia, from 2018 to 2019 are presented in Fig. 3.39. B(a)P deposition from Slovak anthropogenic emission sources to Poland and its own territory increased by almost 45% and 30%, respectively. At the same time, amount of B(a)P deposited to Austria, Hungary, and Czechia decreased by about 10%. Thus inter-annual variability of meteorological conditions noticeably affects distribution of B(a)P pollution originated from particular EMEP countries.

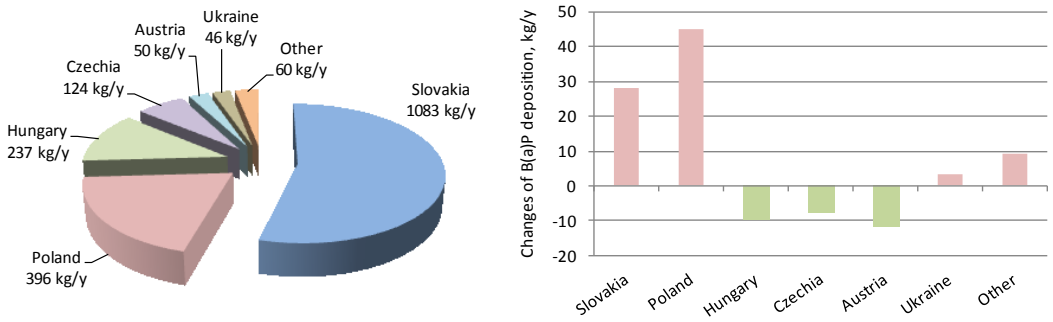

a b

Fig. 3.39. *Deposition of B(a)P from Slovak anthropogenic sources the EMEP countries in 2019 (a) and the deposition changes between 2019 and 2018 (b)*

3.3.6. PCDD/Fs, PCBs and HCB

This section provides a summary of information on PCDD/Fs, PCBs, and HCB pollution levels in 2019 in the EMEP region. These pollutants are persistent in the environment and pose risk to human health and biota [*WHO*, 2000; 2003a; *Starek-Świechowicz et al.,* 2017]. PCDD/Fs, PCBs, and HCB are formed as unintentional by-products of various anthropogenic activities and then released into the atmosphere. In addition to anthropogenic emissions, secondary emissions from the terrestrial and aquatic compartments make a significant contribution to the pollution by these POPs due to long-term accumulation of these pollutants in the environment.

Air concentrations of PCDD/Fs, PCB, and HCB in 2019

The spatial distributions of the annual mean modelled air concentrations of PCDD/Fs, HCB, and PCBs (PCB-153) in 2019 are shown in Fig. 3.40. Modelled concentrations of PCDD/Fs and PCB-153 in the EMEP countries vary in a wide range. At the same time, the spatial distribution of annual mean concentrations of HCB in air is more homogeneous, which may be due to its high persistence in the atmosphere.

According to the modelling results, the highest annual mean air concentrations of PCDD/Fs in 2019 are noted for the countries of Southern and Central Europe (Fig. 3.40 a, b), while significant levels of HCB are estimated in the countries of Central and Eastern Europe (Fig. 3.40 c,d). For PCB-153, the highest concentrations are noted for Western and Central Europe (Fig. 3.40e, f). Thus, Central Europe is among the two most polluted regions for all three considered pollutants. Northern Europe, the Caucasus and Central Asia are characterized by the lowest air concentrations of PCDD/Fs, HCB and PCB-153.

Comparison of the modelling results with observed PCB-153 and HCB concentrations from EMEP monitoring network shows reasonable agreement between the measurements and modelled concentrations. For most of the stations, the model predictions are within a factor of 2 compared to measured concentrations. For PCB-153, the differences higher than a factor 2 were found for two stations (CZ0003R and NO0042R). For HCB such differences were noted for DE0001R, DE0002R, DE0009R and NO0042G. Relative bias between modelled and observed concentrations is about 30% for PCB-153 and HCB.

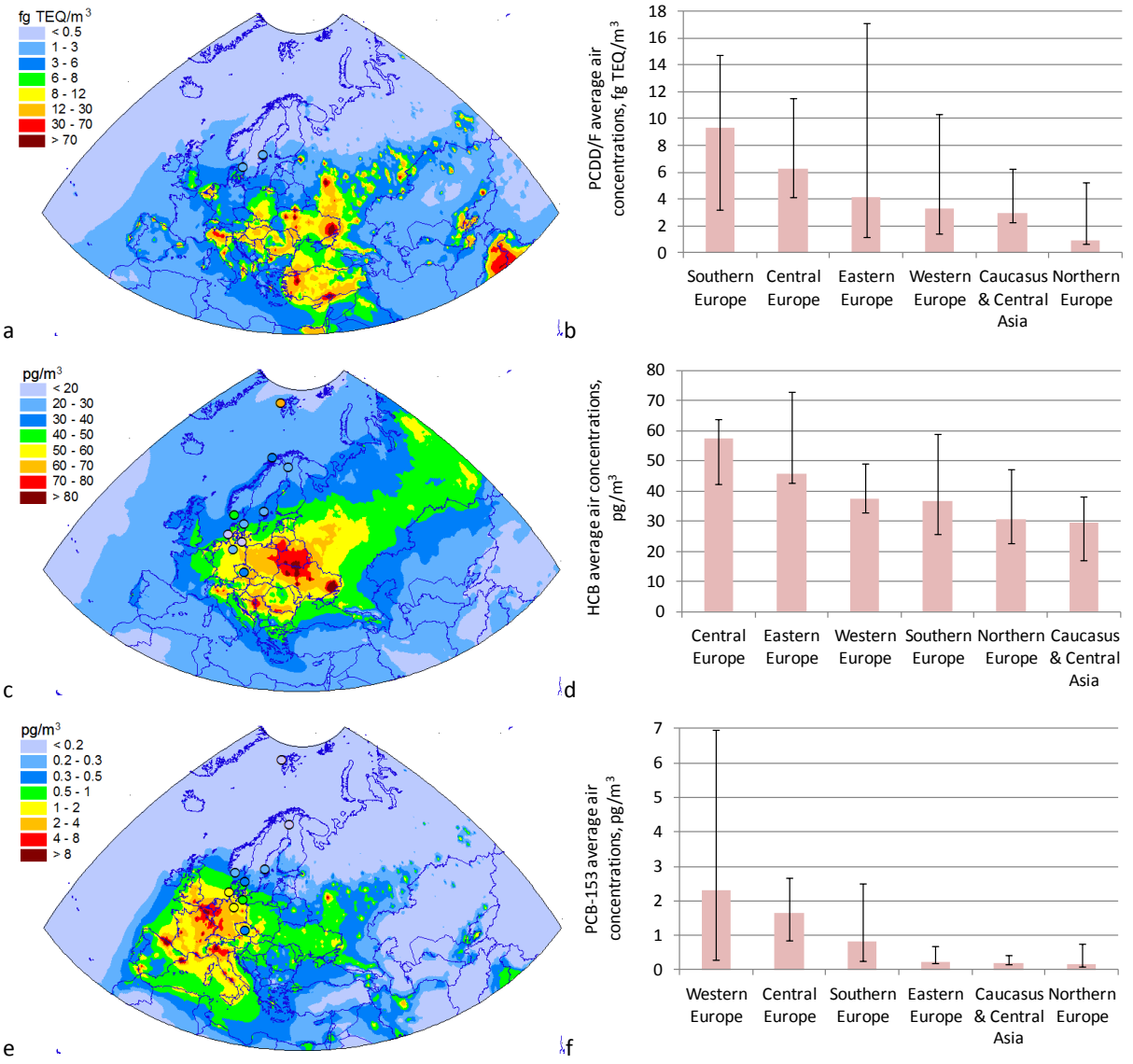

Fig. 3.40. *Spatial distribution of modelled and observed annual mean air concentrations in 2019, and annual mean air concentrations, averaged over different sub-regions of the EMEP domain, of PCDD/Fs (a,b), HCB (c,d), and PCB-153 (e,f). Whiskers indicate the range of annual mean air concentrations in the countries of particular region.*

Measurements of PCDD/F concentrations in air in 2019 were carried out at two EMEP stations (SE0014R and SE0022R). Comparison of predicted and observed air concentrations shows a reasonable agreement between measurements and modelling results. Some overestimation of measured concentrations takes place at the station SE0014R (relative bias of about 25%), and some underestimation is noted for the station SE0022R (relative bias of about -50%). More detailed information on agreement between modelled and observed concentrations of POPs is given in Supplementary Data Report [*Strizhkina et al.,* 2021b].

Relative changes in the spatial patterns of air concentrations of PCDD/Fs, HCB, and PCB-153 between modelling results for 2018 and 2019 are shown in Fig. 3.41. The calculations for these two years were carried out using the same set of emission data for 2018, therefore difference in the results illustrates the influence of interannual variability of meteorological parameters on temporal changes

of pollution levels (Section 3.1). For PCDD/F, all sub-regions of the EMEP domain are characterised by decline of averaged air concentrations from 2018 to 2019 (Fig. 3.41 a, b). However, some increases in PCDD/F air concentrations are noted in particular areas of the United Kingdom, Norway, Turkey and Russia. For HCB, increasing concentrations are estimated for Eastern and Northern Europe, as well as for Caucasus and Central Asia. Other sub-regions are characterised by some decline of HCB pollution levels (Fig. 3.41c, d). For PCB-153, the modelling results show increase of pollution levels for Caucasus and Central Asia, Central and Eastern Europe. For other sub-regions, decreasing averaged concentrations are estimated (Fig. 3.41e, f). It can be seen that the spatial patterns of the changes in the air concentrations of PCDD/Fs, HCB, and PCB-153 differ significantly from each other. These differences can be explained by the different spatial distributions of emissions of these pollutants, as well as by the differences in their physico-chemical properties.

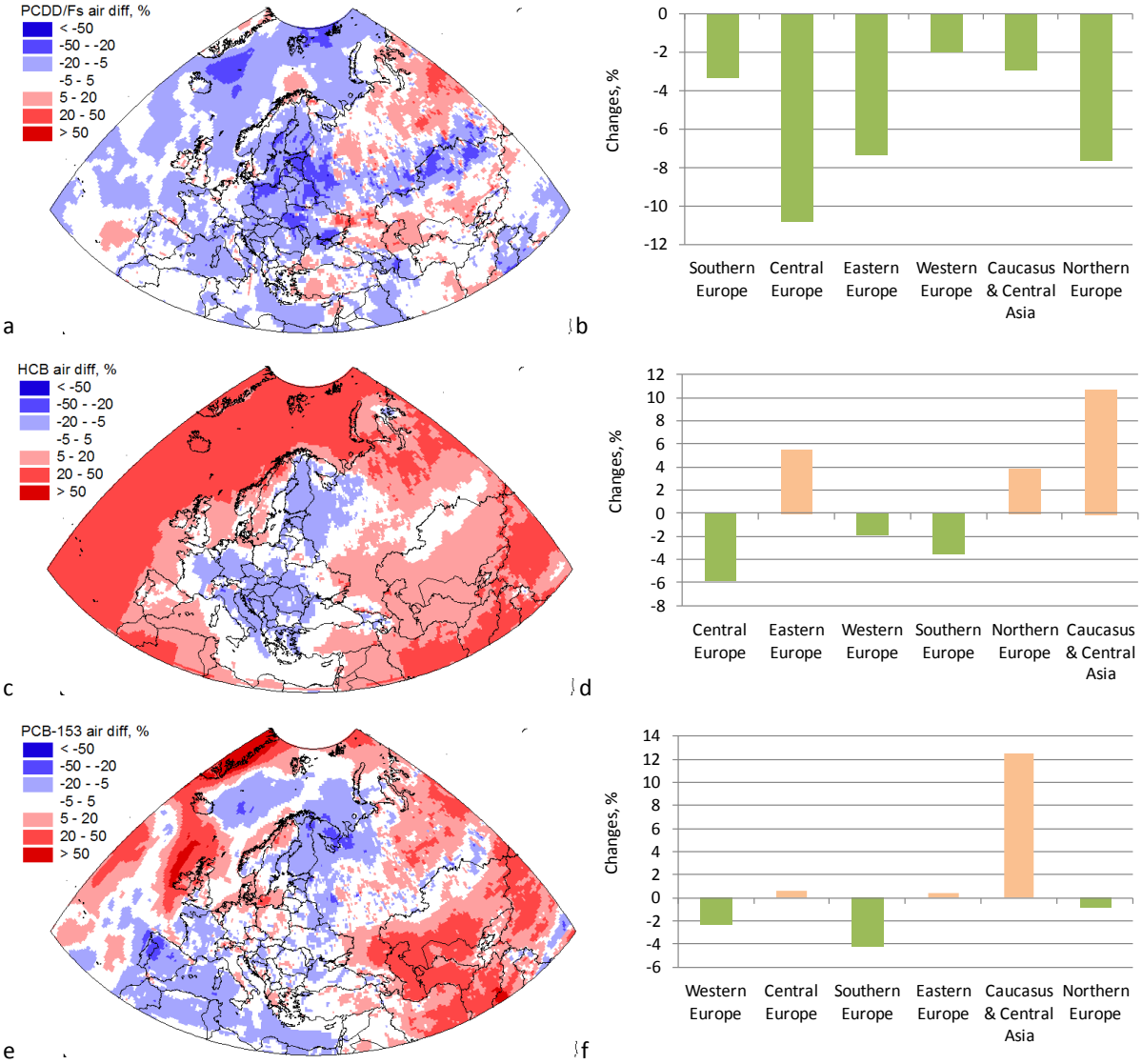

Fig. 3.41*. Spatial distribution of relative changes of air concentrations between 2019 and 2018 and relative changes of averaged air concentrations over different sub-regions of the EMEP domain for PCDD/Fs (a,b), HCB (c,d), and PCB-153 (e,f).*

Source apportionment of PCDD/F, PCB-153, and HCB pollution

Average annual total deposition fluxes for different EMEP sub-regions for PCDD/Fs, HCB, and PCB-153 are illustrated in Fig. 3.42. The highest average annual deposition fluxes of PCDD/Fs take place in Southern and Central Europe. High deposition fluxes of PCB-153 are predicted in Western and Central Europe. The highest values of HCB deposition fluxes are noted for Eastern and Central Europe. In whole, for all three pollutants, the areas with the highest average annual deposition fluxes are located in the sub-regions that also have high air concentrations (Fig. 3.40).

Source apportionment of PCDD/F, PCB-153, and HCB pollution is carried out taking into account contributions of EMEP anthropogenic and secondary sources as well as non-EMEP sources. According to the modelling results, the contribution of anthropogenic sources to total deposition in the considered sub-regions is 20-50% for PCDD/Fs, 15-40% for PCB-153, and 1-3% for HCB (Fig. 3.42 a,c,e). The largest contribution of PCDD/F anthropogenic emissions is noted for Eastern Europe (about 50%), PCB-153 for Western Europe (about 40%), and HCB for Southern Europe (3%). The contribution of secondary emission sources in the EMEP countries is about 60% for PCDD/Fs, about 70% for PCB-153 and about 75% for HCB. Non-EMEP emission sources contribute to total deposition about 10% for PCDD/Fs, 5% for PCB-153, and about 20% for HCB.

Inter-annual meteorological variability between 2018 and 2019 led to changes in PCDD/F total deposition fluxes in the EMEP sub-regions from about -7% in Northern Europe to 1% in Eastern Europe and Caucasus and Central Asia (Fig. 3.42b). For all the sub-regions, the PCDD/F deposition from non-EMEP sources in 2019 is lower than in 2018. The contributions of primary EMEP anthropogenic sources decreased in all sub-regions excluding Eastern Europe, where some increase takes place. The deposition from secondary sources increased in Central Europe, and Caucasus and Central Asia; other sub-regions are characterised by decrease in the deposition from this group of sources.

Changes in total annual deposition fluxes of PCB-153 range from -4% in Southern Europe to 16% in Caucasus and Central Asia (Fig. 3.42d). The main contribution to these changes was made by changes in secondary emission. For HCB, changes in total deposition fluxes in 2019 compared with 2018 for all sub-regions are characterised by an increase of deposition from non-EMEP sources, together with a decrease of deposition from EMEP secondary emissions (Fig. 3.42f).

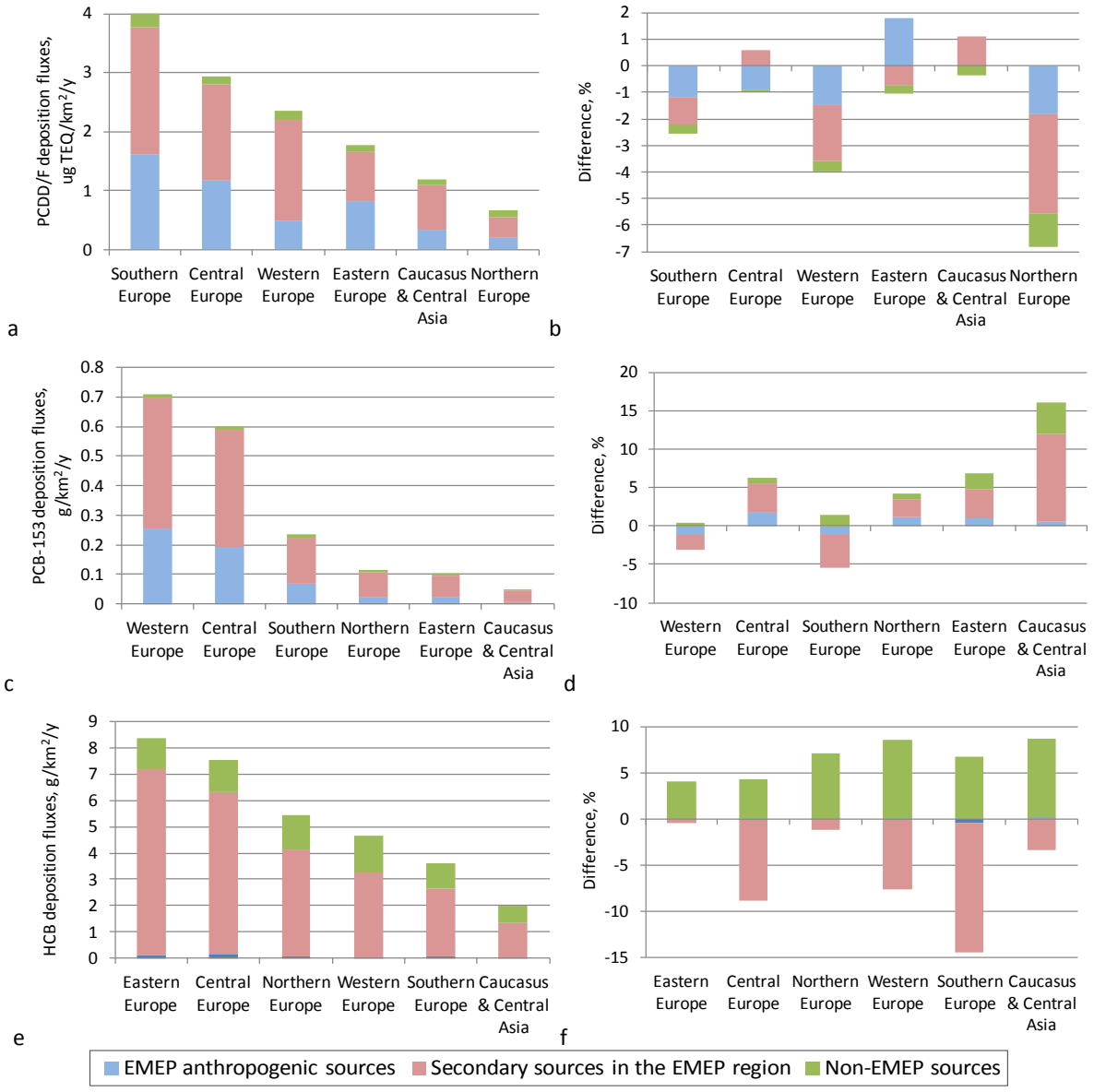

Fig. 3.42. *Deposition fluxes from EMEP anthropogenic sources, secondary sources, and non-EMEP anthropogenic sources in 2019 and relative difference in deposition fluxes between 2019 and 2018 normalized by total deposition in 2018 for different sub-regions of the EMEP domain for PCDD/Fs (a,b), PCB-153 (c,d), and HCB (e,f).*

Transboundary transport

The effect of transboundary transport for the country's pollution can be illustrated using the ratio of contributions of national and foreign anthropogenic sources to deposition in the particular country. Model assessment of long-range transport of PCDD/F, PCB-153, and HCB shows a significant role of transboundary pollution. For HCB, in 2019, deposition from transboundary transport exceeds deposition from national emissions in 40 (78%) countries. For PCDD/Fs and PCB-153, relative contribution of foreign sources to deposition exceeds 50% in 22 (43%) countries and 34 (67%) countries, respectively.

Examples of two countries with different contributions of national and foreign sources to total deposition flux of HCB are shown in Fig. 3.43. In Serbia, the contribution of foreign sources to the HCB pollution of the country is over 90%. The largest contributors are Bosnia and Herzegovina (47%) and Ukraine (21%). On the contrary, in France, the contribution of national sources to anthropogenic deposition of HCB is 62%, while the contribution of transboundary transport from other countries is less important. More information on transboundary pollution for each EMEP country and for each of three pollutants is available in Supplementary Data Report [*Strizhkina et al.*, 2021b].

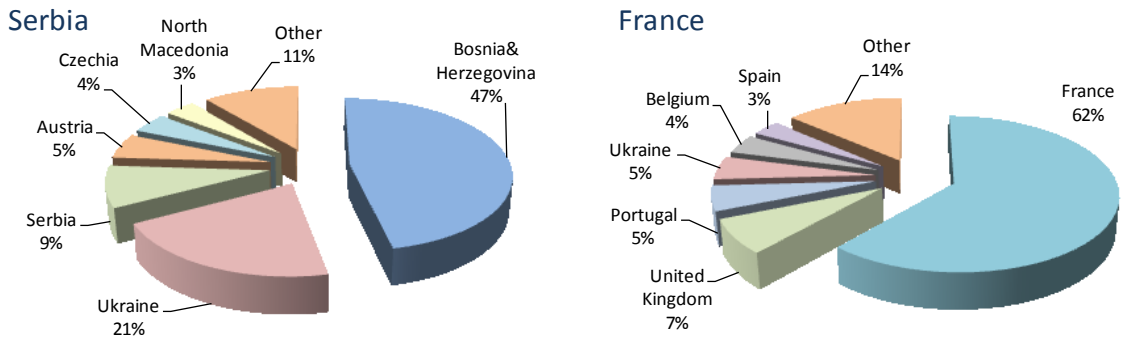

a b

Fig. 3.43. *Contributions of transboundary transport and national sources to HCB deposition in Serbia and France in 2019.*

Inter-annual variations in meteorological conditions lead to changes in the patterns of transboundary transport from year to year. Fig. 3.44 illustrates an example of total annual deposition of PCB-153 in Czechia in 2019 from national and foreign sources and their changes from 2018 to 2019. PCB-153 deposition from national sources contributed about 50% (6.7 kg/y) to total PCB-153 deposition in Czechia in 2019. The main foreign contributors are Germany, France, Austria, Slovakia, and Poland. The contributions of Germany, France and Austria to PCB-153 deposition in Czechia increased . At the same time, the contribution of Czechia, Poland and Slovakia decreased (Fig. 3.44b).

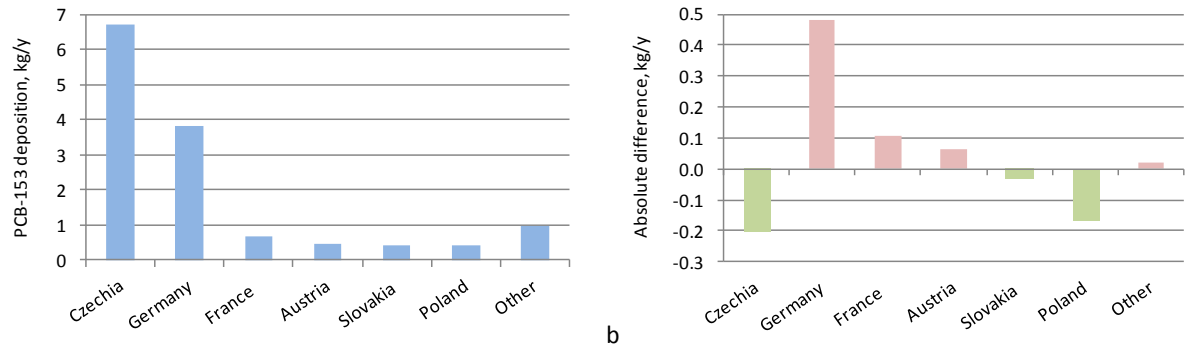

a b

Fig. 3.44. *PCB-153 deposition in Czechia from main countries-contributors in 2019 (a) and absolute difference of PCB-153 deposition between 2019 and 2018 (b).*

PCDD/F, PCB-153, and HCB emitted by national sources of a particular country are partially deposited over the own territory of this country and contribute to transboundary pollution of territories of

other countries. For HCB, the deposition of the pollutant to territories of other countries is higher than the fraction, deposited to own territory, for 32 (63%) countries. For PCDD/Fs and PCB-153, this ratio is estimated for 14 (27%) and 16 (31%) countries, respectively.

Figure 3.45 shows the distribution of PCB-153 deposition, originated from Belgian anthropogenic emission sources, to the territory of Belgium and other EMEP countries. About a half of PCB-153 (48%) deposited to the territory of Belgium, followed by France, Germany, and Netherlands. More detailed information on transboundary pollution for each EMEP country is presented in Supplementary Data Report [*Strizhkina et al.*, 2021b].

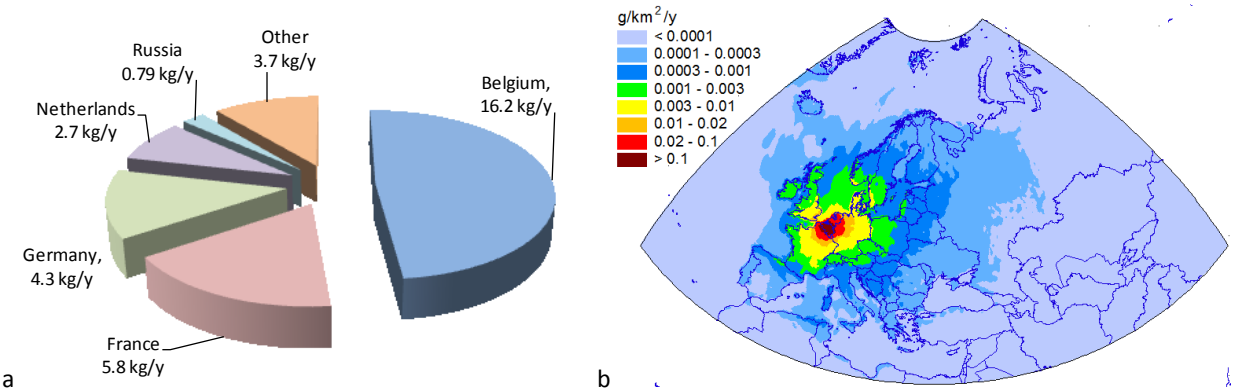

Fig. 3.45 *Deposition of PCB-153 from Belgian anthropogenic sources to the EMEP countries in 2019 (a) and PCB-153 map of deposition from Belgian sources in the EMEP region (b).*

Changes of distribution of annual total HCB deposition, originated from the sources of Czechia, between 2018 to 2019 are presented in Fig. 3.46. HCB deposition from Czech anthropogenic emission sources to Poland, Slovakia, Russia, and Belarus increased by about 5 - 45%. At the same time, HCB deposition to Germany and Austria from Czechia decreased by around 40 - 60%. Thus inter-annual variability of meteorological conditions noticeably affects distribution of HCB pollution originated from particular EMEP countries.

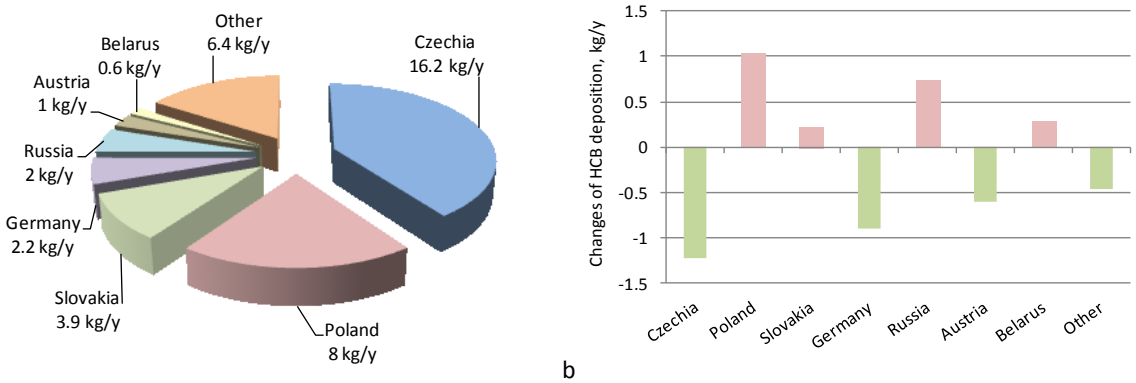

Fig. 3.46. *Deposition of HCB from Czech anthropogenic sources to the EMEP countries in 2019 (a) and the deposition changes between 2019 and 2018 (b).*

3.3.7. Country-specific information

Dissemination of the assessment results and other relevant information, aimed at support of political decisions, is of high importance. Annual reports containing current status of heavy metals and POPs pollution within the EMEP region are supplemented by presentation of information on the web. It provides more flexible and targeted assistance to national experts and authorities with data required for the environment protection regulations.

Detailed information on heavy metals and POPs pollution is given for each individual EMEP country. This country-specific information includes variety of data on the model assessment for particular country collected in one place to make easier access to information and its analysis by national experts. Information is presented in the form of diagrams, maps and data files for all the EMEP countries at the MSC-E website (http://en.msceast.org/index.php/pollution-assessment/emep-countries-menu). In addition, the country-specific information for the EECCA countries is also available in Russian (http://www.ru.msceast.org/index.php/pollution-assessment/eecca-countries-menu).

Country-specific information includes the following elements:

- Spatial distribution of pollution levels;
- Transboundary pollution of a country;
- Contribution of national sources to transboundary transport;
- Ecosystem-specific deposition (17 land cover categories).

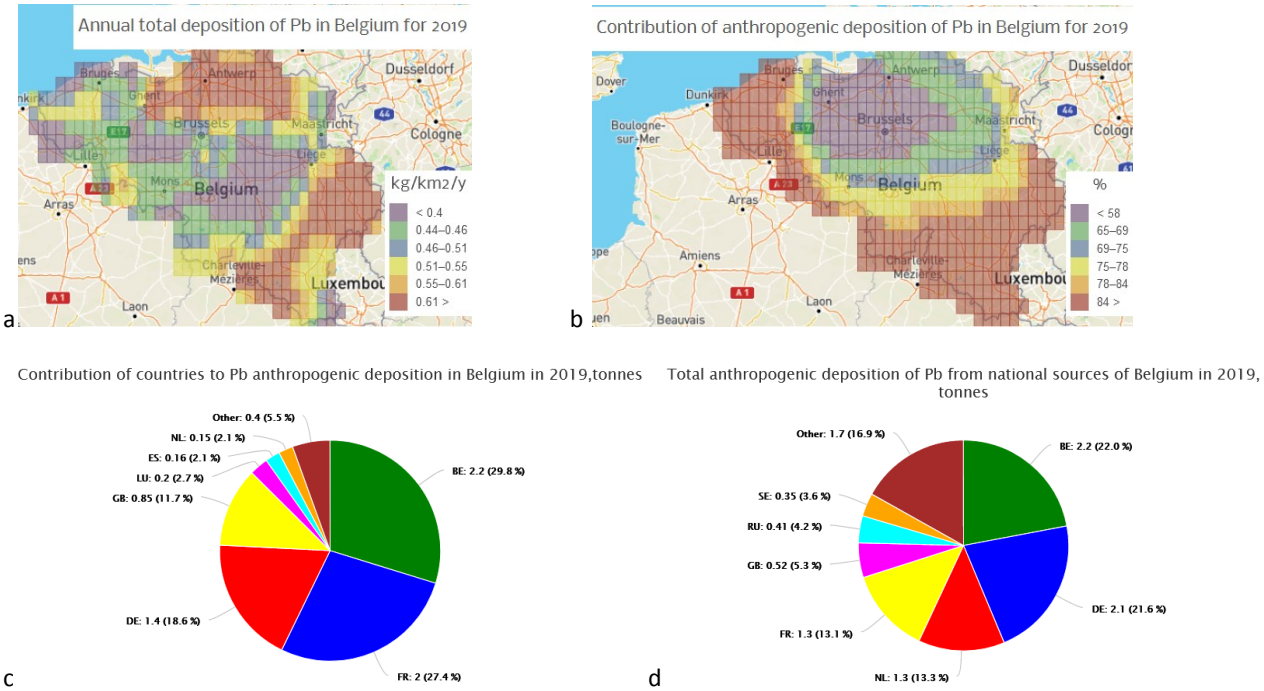

Fig. 3.47. *Characteristics of transboundary transport of Pb to France: (a) –deposition map, (b) – relative contributions of foreign sources; (c) – main contributors to anthropogenic deposition in the country; (d) main receptors of deposition from the country.*

Detailed information on transboundary pollution of individual countries includes maps of total deposition flux to a country's territory (Fig. 3.47a) and relative contributions of foreign sources to anthropogenic deposition (Fig. 3.47b). Besides, source apportionment of anthropogenic deposition to the country's territory is presented (Fig. 3.47c). Each country contributes to atmospheric pollution of other EMEP countries. Spatial distribution of deposition caused by country's sources is available for the entire EMEP region. Besides, country's total deposition to main receptor regions and its fraction of deposition within the EMEP region are indicated (Fig. 3.47d).

Detailed information on source-receptor relationships between all EMEP countries is also available in the database on the website along with other data on heavy metals and POP pollution of the EMEP domain (http://en.msceast.org/index.php/pollution-assessment/emep-domain-menu/data-hm-pop-menu).

3.4. Information for exposure assessment

3.4.1. Ecosystem-specific deposition of heavy metals

Adverse effects of heavy metals on human health and natural environment have been studied and documented in both scientific literature and in the reports of international organizations [e.g., *ECHA*, 2013, *ECHA*, 2018, *WHO*, 2003b, *Rice et al.*, 2014]. In order to establish link between heavy metal pollution levels and their effects on human health and biota the Working Group on Effects (WGE) of the Convention developed the critical loads approach. This approach allows identification of areas where long-term adverse effects of heavy metal and POP pollution most likely occur [*de Vries et al.*, 2015a,b]. Technical information on the use of this approach is presented in Manual [*CLRTAP*, 2017]. At the same time, alternative approaches to evaluate critical loads are also being developed, e.g., [*Feng et al.*, 2020].

In order to support this activity of WGE, MSC-E calculates deposition fluxes to different types of land cover (forests, shrubs, grasslands, crops, water bodies, etc.) within the EMEP domain or regular basis. Data on the calculated Pb, Cd and Hg deposition to 17 land-cover types in 2019 is available on the MSC-E website [http://en.msceast.org/index.php/pollution-assessment/emep-domain-menu/land-use-menu] and in Supplementary Data Report [*Strizhkina et al.*, 2021a]. When deposition flux is compared with the critical load to particular ecosystems, an exceedance of critical loads is determined. Positive values of the exceedances mean that heavy metal levels in soils or aquatic ecosystems may be harmful for humans or biota.

Fluxes of atmospheric deposition depend on a number of factors such as location of emission sources, atmospheric transport patters and precipitation amounts. Besides, dry deposition strongly depends on properties of the underlying surface. Dry deposition velocity to high vegetation (e.g., forests) is much higher than that to grasslands or bare lands under the same meteorological conditions [*Travnikov and Ilyin*, 2005]. It is the reason why deposition fluxes for the effect assessment purposes are simulated for various types of the underlying surface. It is also worth mentioning that other sources beside the atmospheric deposition can contribute to pool of heavy

metals in soil. In particular, significant contribution to Cd content in the agricultural soils is made by application of phosphate fertilizers. According to [*Nicholson et al.*, 2003], Cd inputs to the British agricultural soils due to atmospheric deposition and application of the fertilizers are comparable. In [*Belon et al.*, 2012; *Six and Smolders*, 2014] it is stated that the contribution of the fertilizers exceeds the contribution of atmospheric deposition by 2-3 fold in France and in the European Union.

Example of Cd mean deposition flux to different land-cover types is demonstrated in Fig 3.48. The highest fluxes occur over evergreen broadleaf, deciduous broadleaf and mixed forests. Smaller mean fluxes to evergreen and deciduous needleleaf forests compared to other forest types is explained by their location in relatively clean areas of the EMEP region, e.g., Scandinavian Peninsula. However, their maximum values of deposition fluxes are comparable with the fluxes to other types of forests. Deposition fluxes to croplands and urban areas are higher than the deposition to deciduous needleleaf forests. On one hand, dry deposition velocity to croplands and urban land cover types is smaller than that to needleleaf forest ecosystems. On the other hand, croplands and urban areas are located closer to regions of significant emissions, which favours increase of deposition fluxes to these land cover types.

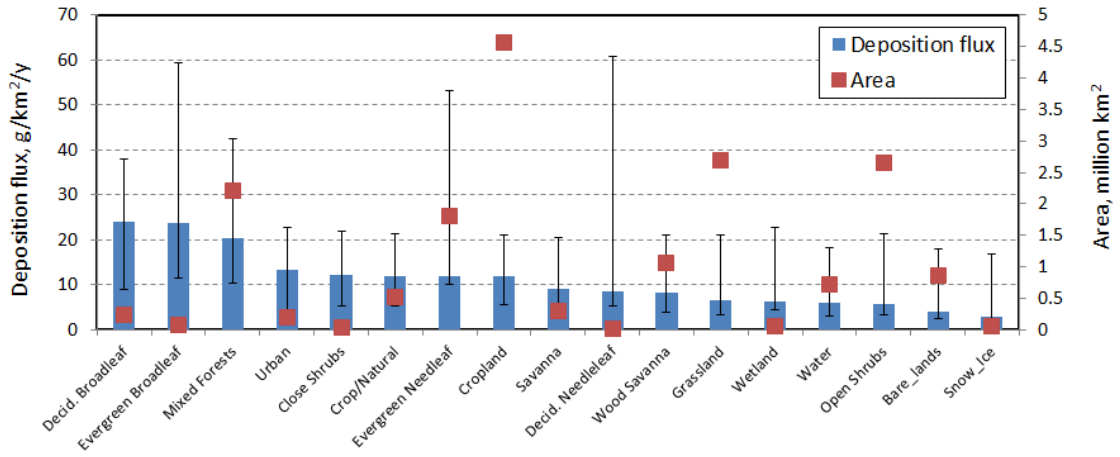

Fig. 3.48. *Deposition of Cd to various ecosystem types within the EMEP domain in 2019. Bars show average value for all EMEP countries; whiskers show range of deposition flux variation (5th -95th percentile) among the EMEP countries.*

Difference in deposition fluxes to areas covered with high and low vegetation is demonstrated in Fig. 3.49. Cd deposition flux to croplands varies from 5 to 20 g/km^2/y over most of the EMEP countries (Fig. 3.49a). In the most polluted areas (western Germany, Central Russia, southern Poland, etc.) the flux exceeds 80 g/km^2/y. Deposition fluxes to mixed forests are 2-3 fold higher than those to croplands. Except for northern Russia and Scandinavian Peninsula, the fluxes to mixed forests exceed 10 g/km^2/y (Fig. 3.49b). In the most contaminated regions they can even exceed 150 g/km^2/y. Similar peculiarities of spatial distribution of ecosystem-dependent deposition are noted for other heavy metals and for POPs.

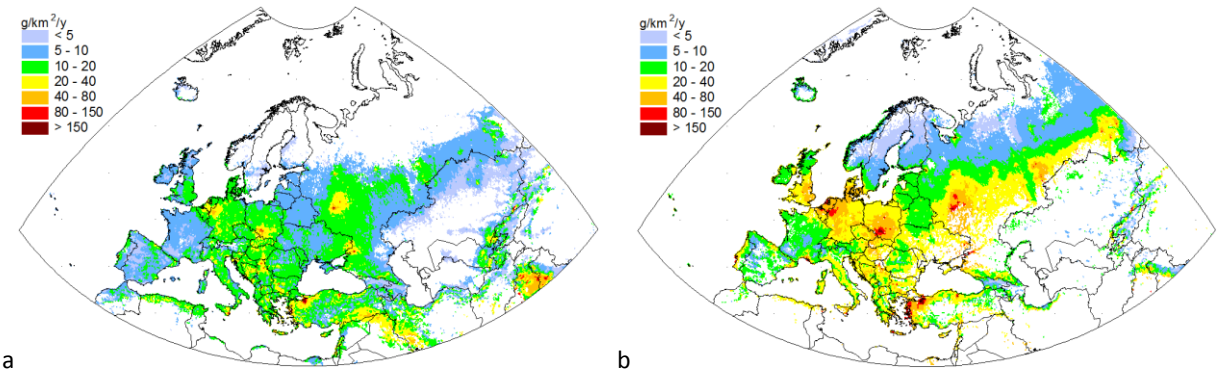

Fig. 3.49. Annual deposition flux of Cd to croplands (a) and mixed forests (b) in 2019.

It is important to draw attention to the fact that the most recent estimates of the adverse effects on human health and biota relate to 2010 and can hardly reflect present status of pollution [*de Wit et al.,* 2015]. Therefore, more efforts of the effects community in the field of evaluation of heavy metal and POP pollution adverse impacts are needed.

3.4.2. Exceedances of air quality standards (PAH)

Many of PAHs are characterized by carcinogenic, mutagenic, and/or teratogenic properties [*Abdel-Shafy et al.*, 2016].To assess the risk of population exposure to PAHs, several threshold values were established in European Union. These values were set up for B(a)P as an indicator compound due to availability of studies related to B(a)P adverse effects. These thresholds include target value of B(a)P air concentration equal to 1 ng/m^3, along with the upper and lower assessment thresholds (UAT and LAT) set up to 0.6 and 0.4 ng/m^3 respectively (European Directive 2004/107/EC). In addition, the reference level of 0.12 ng/m^3 for B(a)P has been defined by World Health Organization (WHO) as a level of air concentrations corresponding to the excess lifetime cancer risk level of 10^{-5} [*WHO*, 2017].

Modelled B(a)P air concentrations for 2019 (Fig. 3.50a) were used to evaluate the amount of population living in areas where levels of concentration exceed air quality guidelines (Fig. 3.50b).

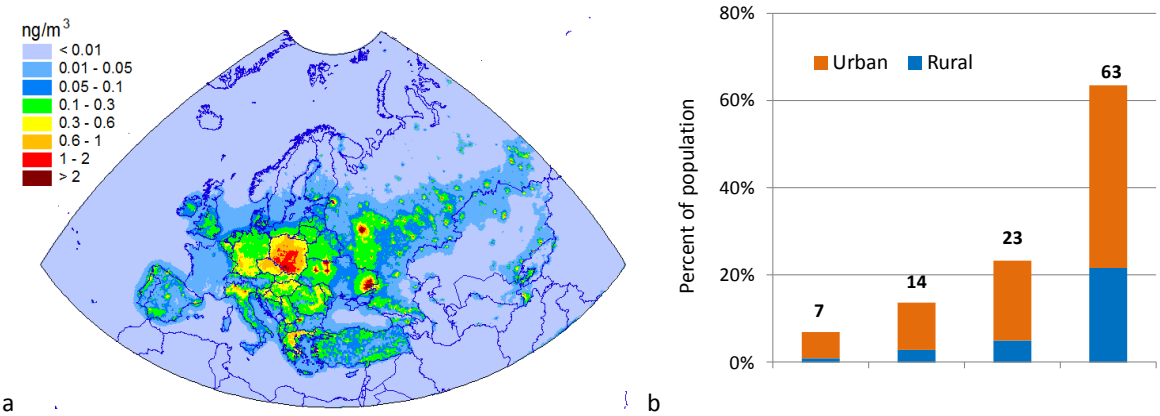

Fig. 3.50. Spatial distribution of annual mean B(a)P air concentrations for 2019 (a) and percentage of urban and rural population of the EMEP countries in the areas with annual mean B(a)P air concentrations in 2019 exceeding the EU limit values and WHO reference level (b).

Modelling results indicate that about 7% of the population of EMEP countries in 2019 lived in areas with exceeded EU target level for annual mean B(a)P air concentrations. The upper assessment thresholds (UAT) and lower assessment thresholds (LAT) values were exceeded in the areas with about 14% and 23% of population, respectively. The WHO Reference level was exceeded for about 63% of population of EMEP countries.

PAHs are emitted to the atmosphere as mixtures of various PAH compounds. To evaluate population exposure to mixture of toxic PAHs the approach based on toxic equivalency factors can be used [*Liu et al.*, 2019]. Each of the PAH compounds that contribute to the toxicity of PAH mixture has a specific toxic equivalence factor (TEF) that weights its toxicity relative to that of B(a)P [*ALS*, 2013]. The TEFs can be applied to characterize the carcinogenic potency of each considered PAH and calculate B(a)P equivalent concentration of PAH mixture. To illustrate this, equivalent B(a)P concentration of the four PAH compounds (namely, B(a)P, B(b)F, B(k)F, IcdP) was estimated for the EMEP domain (Fig. 3.51a).

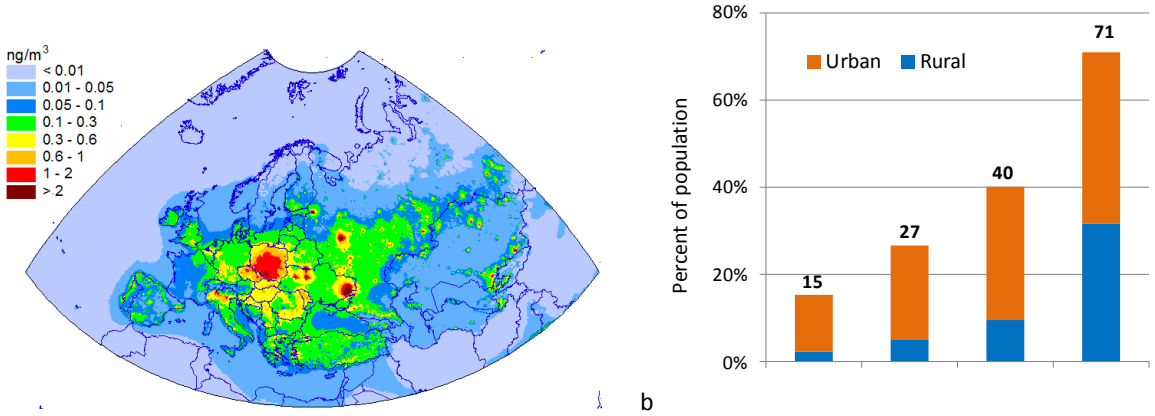

***Fig. 3.51**. Calculated B(a)P equivalent concentrations in the EMEP region (a) and percentage of urban and rural population of the EMEP countries in the areas with equivalent B(a)P air concentrations exceeding the EU limit values and WHO reference level in 2019 (b).*

The map represents the sum of concentrations of individual PAHs multiplied by corresponding values of TEFs. Estimated equivalent B(a)P concentrations differ significantly from the above results for B(a)P only. In particular, the share of population living in the regions with equivalent B(a)P concentrations exceeding EU target value is evaluated as 15% in comparison with 7% calculated on the basis of B(a)P.

The results of the model simulations are confirmed by PAH measurement data. The results of evaluation of B(a)P concentrations based on measurement data from EEA air quality database are illustrated by Fig. 3.52.

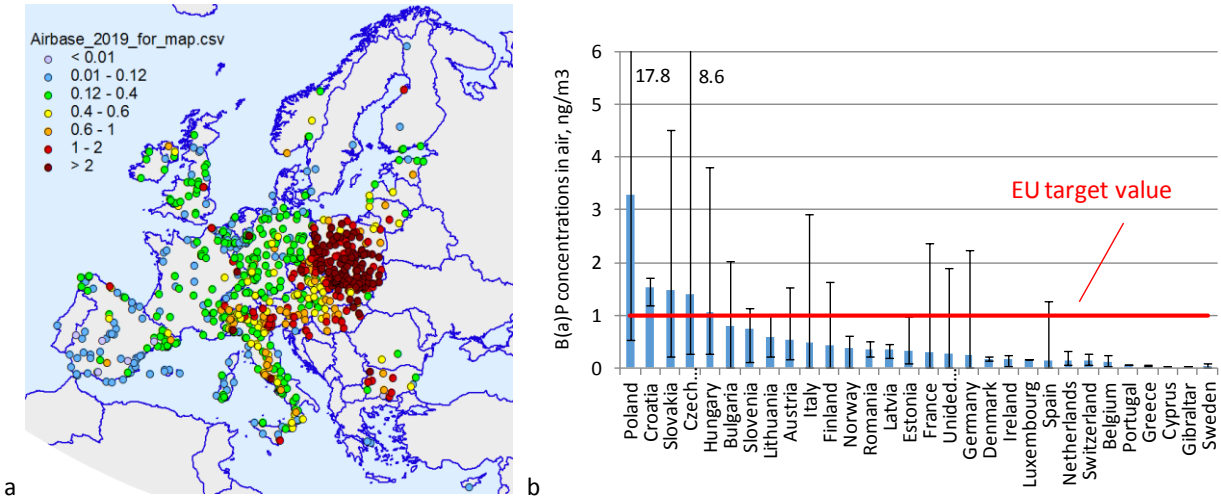

Fig. 3.52. *Spatial distribution of B(a)P air concentrations observed at EEA monitoring sites in 2019 (a) and average values of measured annual mean B(a)P air concentrations in the EU countries in 2019 (b). Whiskers denote the range from minimum to maximum of measured concentrations.*

According to these data, B(a)P air concentrations, averaged over the monitoring sites of particular country, were above the EU target value in 5 EU countries, namely, Poland, Croatia, Slovakia, Czechia, and Hungary. In addition, exceedances of EU target values take place in at least one of measurement sites in 15 EMEP countries. Exceedances of the EU target value were observed mostly at the urban background stations. In case of WHO reference level exceedances of average B(a)P concentrations in 2019 took place in 24 countries from 30 countries performing regular monitoring of B(a)P pollution levels. The information on exceedances of the EU and WHO air quality guidelines for B(a)P as well as data on B(a)P equivalent air concentrations of PAHs can be used to support activities of the Task Force on Health and Working Group on Effects with regard to the analysis of population exposure to toxic substances and their impacts on human health.

3.5. Atmospheric loads to the marginal seas

The protection of marine environment is governed by a number of national and international regulations, including regional conventions such as HELCOM, OSPAR, Barcelona Convention, Bucharest Convention, and Tehran Convention. Besides, in 2021 European Commission has published a roadmap for the review of the Marine Strategy Framework Directive. The concern of marine pollution was also highlighted at the Bureau meeting in March, 2021.

This section provides brief information on atmospheric inputs of heavy metals and POPs to the marginal seas surrounding the EMEP region for 2019. These are the Baltic, Black, Caspian, Mediterranean and North Seas. More detailed information is available in Supplementary Data Reports [*Strizhkina et al.*, 2021a,b]. In addition, the modelling results of heavy metal and POP deposition to the Baltic Sea, prepared for HELCOM, are overviewed in Section 5.2.4.

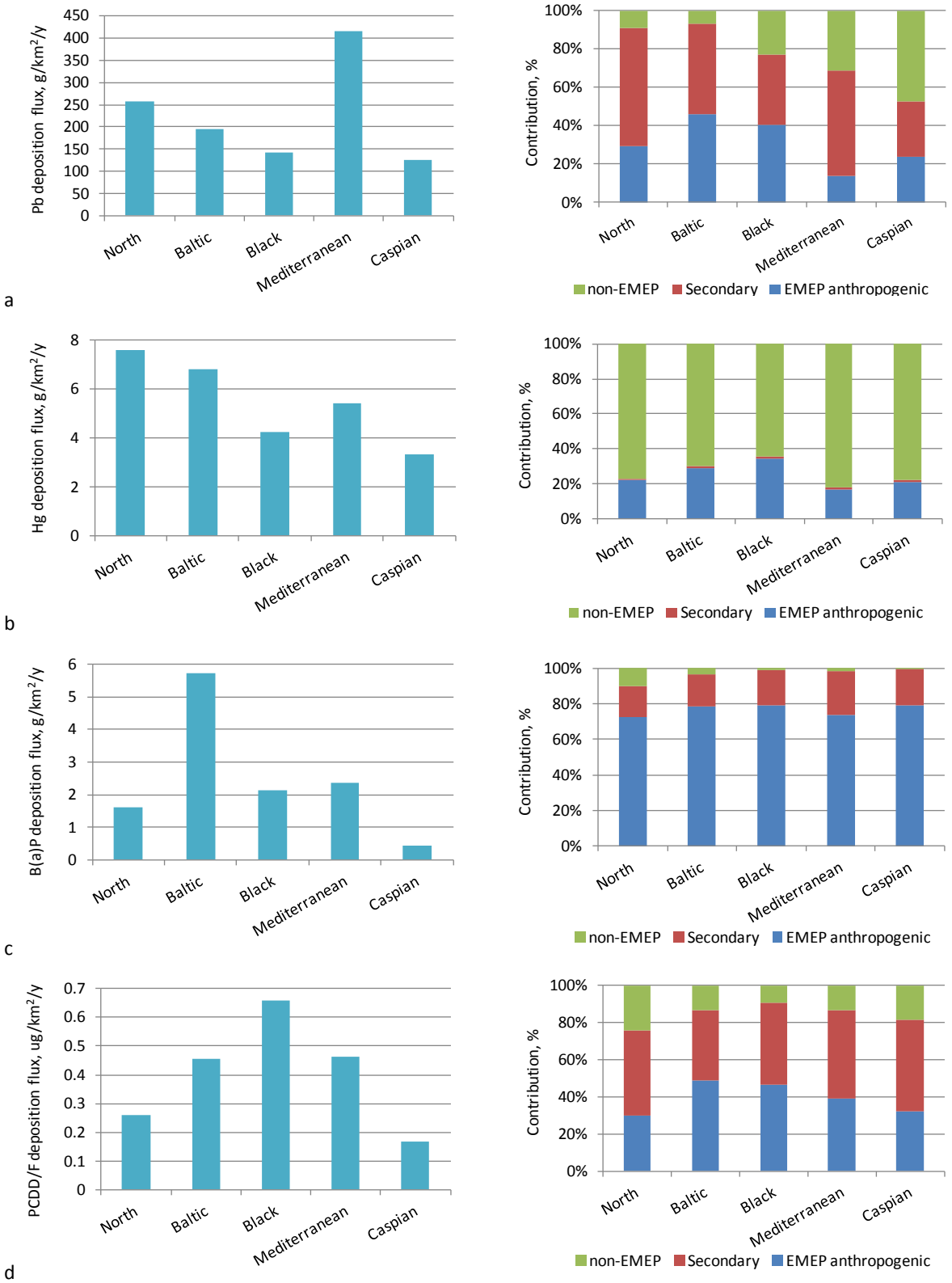

Fig. 3.53. *Mean deposition fluxes (left) and relative contribution of various source types to deposition (right) of Pb (a), Hg (b), B(a)P (c) and PCDD/Fs (d) to the marginal seas of the EMEP region in 2019.*

The deposition fluxes of heavy metals and POPs to the considered seas differ significantly depending on location of emission sources and meteorological conditions. For Pb, the highest spatially averaged

deposition fluxes are estimated for the Mediterranean Sea, followed by the North and Baltic Seas. The Black and Caspian Seas are characterized by lower fluxes (Fig. 3.53a, left). This can be explained by predominant contribution of secondary and non-EMEP sources for the Mediterranean Sea, and high contribution of secondary sources, combined with the significant impact of anthropogenic sources of Pb, to deposition to the North Sea (Fig. 3.53a, right). Similar to Pb, the highest deposition flux of Cd takes place for the Mediterranean Sea and the lowest – for the Caspian Sea.

The highest Hg deposition fluxes take place in the North Sea, followed the Baltic and Mediterranean Seas, while the lowest Hg flux is estimated for the Caspian Sea (Fig. 3.53b, left). For regions remote from anthropogenic sources, the main process for removing Hg from the atmosphere is the oxidation of elemental mercury with further wet deposition or dry uptake of oxidized Hg. Wet deposition is strongly dependent on atmospheric precipitation. Consequently, the higher deposition to the North and Baltic Seas in comparison with the Black and Caspian Seas is caused by spatial distribution of precipitation (Section 3.1). In contrast to Pb and Cd, the main contribution to Hg deposition is made by non-EMEP sources (Fig. 3.53b, right). However, the contribution of Hg non-EMEP sources, calculated at the regional scale, may be overestimated as these sources include mercury emitted by the EMEP sources that leaves the region and then returns as 'non-EMEP' Hg.

The highest deposition of POPs is estimated for the Baltic and Black Seas, while the lowest flux is noted for the Caspian Sea (Fig. 3.53c,d left). For example, PCDD/Fs deposition to the Black Sea is about 4-fold higher than that to the Caspian Sea. The relatively high deposition of PCDD/Fs to the Black Sea can be attributed to the presence of significant emission sources in Turkey, Romania, and countries of Eastern Europe. As seen in Fig. 3.53d (right), the contributions of different types of PCDD/F sources are comparable for the considered seas (30-50% for EMEP anthropogenic sources, 35-50% for secondary sources and 10-25% for non-EMEP sources).

Spatial distribution of heavy metal and POP deposition to the considered seas is determined by a number of factors, such as distribution of emissions, meteorological conditions and physico-chemical properties of pollutants. For example, B(a)P deposition to the North Sea demonstrates distinct gradient from more polluted coasts of the countries of Western and Northern Europe to lower levels in the central and northern parts of the sea (Fig. 3.54a). This is explained by the relatively high contribution of the emission sources located on the land, while the contribution of marine sources, including shipping, is relatively low. At the same time, the spatial distribution of Hg deposition to the North Sea differs markedly from that of B(a)P. In addition to the spatial distribution of emission sources, Hg deposition is strongly influenced by chemical processes resulting in the transformation of relatively inert elemental Hg to easily scavenged oxidized species. Thus, the highest Hg deposition flux to the North Sea is estimated for the western coasts of Norway and Denmark, which are characterized by high annual precipitation, intensively washing out oxidized Hg. Spatial distribution maps for atmospheric input of all pollutants (Pb, Cd, Hg, PAHs, HCB, PCB-153, and PCDD/Fs) to all considered seas are available in Supplementary Data Reports [*Strizhkina et al.*, 2021a; 2021b].

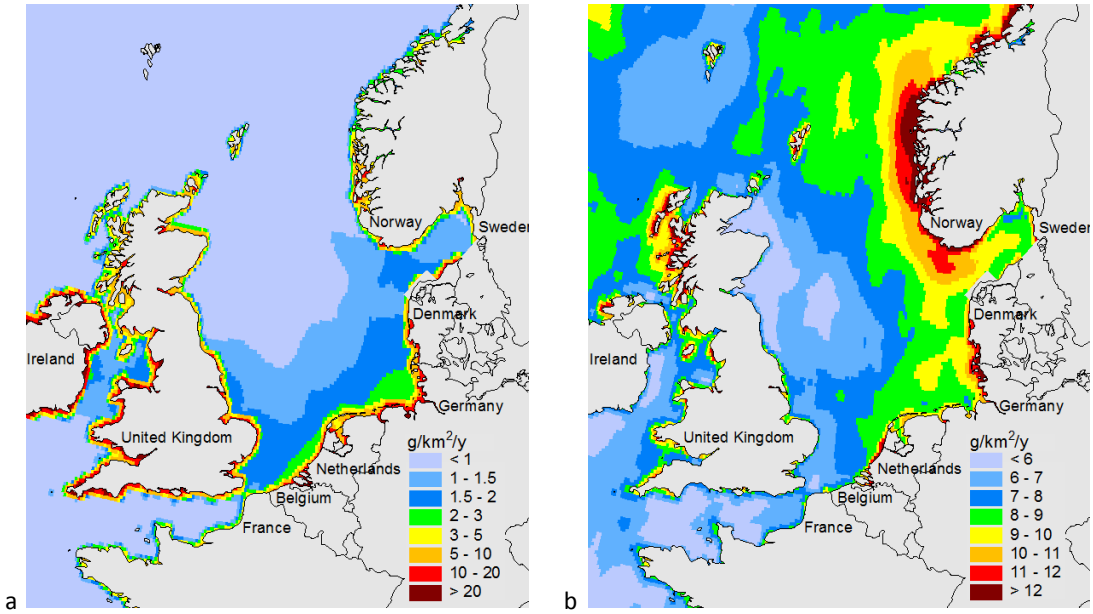

Fig. 3.54. *Total deposition flux of B(a)P (a) and Hg (b) to the North Sea in 2019.*

3.6. Pollution of the Arctic

This section provides information on the pollution of the Arctic by heavy metals (Pb, Cd, Hg) and POPs (PAHs, PCDD/Fs, HCB, PCBs) in 2019. This information includes the spatial distribution of total deposition of heavy metals and POPs and net Hg flux for the Arctic zone within the AMAP region, which were estimated using global-scale modelling. Besides, an assessment of the contributions of different types of sources to Arctic pollution and the source-receptor relationships was carried out for the Arctic territory within the EMEP domain.

In general, the deposition fluxes of heavy metals in the Arctic are significantly lower than in temperate latitudes due to the remoteness of the Arctic from the main sources of emissions of Europe, Asia and North America, as well as the relatively low amounts of precipitation (Fig. 3.55). For example, the deposition flux of Cd in the Arctic is 0.1-10 g/km^2/y, whereas the flux over most of the EMEP area ranges from 5 to 40 g/km^2/y. A similar contrast is noted for Pb: the deposition flux is 10-100 g/km^2/y in the Arctic and more than 250 g/km^2/y in middle latitudes. For Hg, the differences between net deposition fluxes in the Arctic and in the other parts of the EMEP region are smaller due to the global character of Hg pollution.

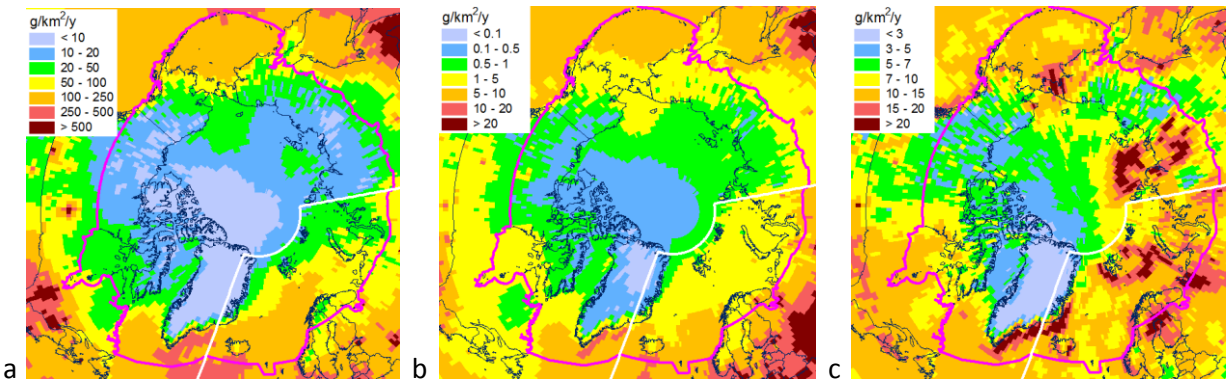

Fig. 3.55. *Total deposition fluxes of Pb (a), Cd (b) and Hg (c) to the Arctic in 2019. Purple line denotes the border of the Arctic region adopted by AMAP, and white line denotes a border of the EMEP domain.*

Deposition fluxes of POPs in the Arctic are also much lower than those in temperate latitudes. For example, B(a)P deposition fluxes in the Arctic range from 0.1 to 5 g/km^2/y, while the fluxes over most of the EMEP area are 2-150 g/km^2/y. Exceptions are hotspots of elevated deposition fluxes of B(a)P in some regions of the Arctic, such as Kola Peninsula, the eastern part of Russia and northern Canada, which can be attributed to significant emission sources in these regions (Fig. 3.56). The situation is similar for PCDD/Fs: in general, deposition fluxes in the Arctic are significantly lower than in mid-latitudes, but some hotspots take place.

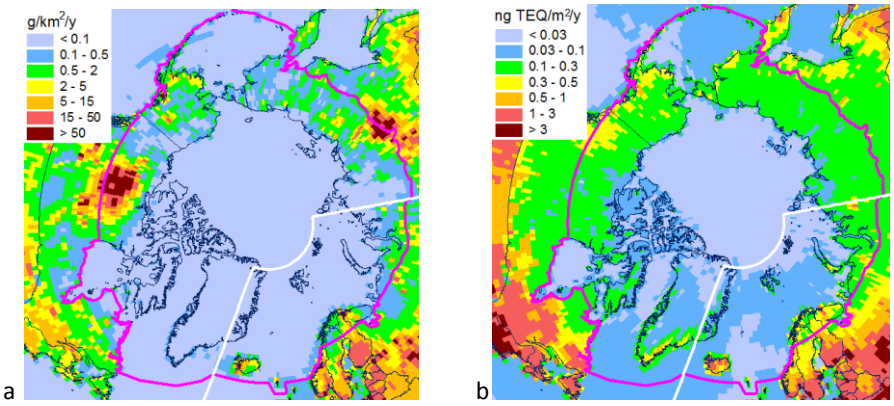

Fig. 3.56. *Total deposition fluxes of B(a)P (a) and PCDD/Fs (b) to the Arctic in 2019. Purple line denotes the border of the Arctic region adopted by AMAP, and white line denotes a border of the EMEP domain.*

Similar to the calculations for the EMEP region, three groups of sources responsible for the deposition of pollutants in the Arctic are considered. These are anthropogenic emissions from EMEP countries, secondary (historical)/natural sources and non-EMEP sources. The largest contribution (over 50%) to Pb deposition in the Arctic within the territory of the EMEP domain is made by secondary sources due to significant re-suspension from the sea surface, and low anthropogenic emissions in or close to the Arctic region. (Fig. 3.57). The contribution of the EMEP anthropogenic sources to deposition of Pb is about 30%. Significant contribution of secondary sources is also noted for PCDD/Fs (about 45%), PCB-153 (65%) and HCB (about 70%), which can be explained by the re-emission of historically accumulated pollutants in soils. For B(a)P and Cd, the largest contribution to

the deposition in the Arctic is made by EMEP anthropogenic sources (74% and 54%, respectively). The contribution of non-EMEP sources in the Arctic region is the largest for Hg (over 90%), while for the other pollutants the contribution of this group of sources ranges from 4% to 29%.

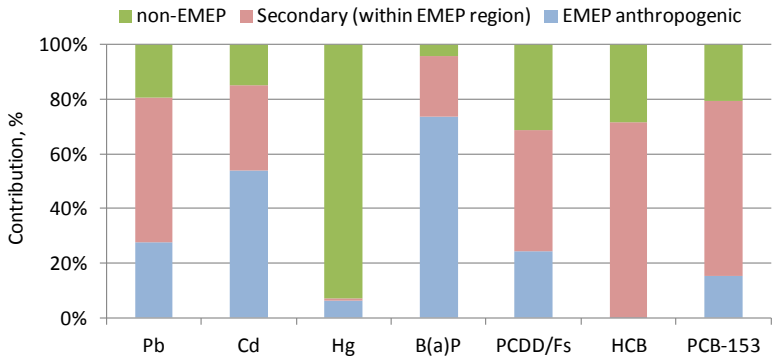

Fig. 3.57. *Relative contributions of the EMEP anthropogenic, secondary and non-EMEP sources to deposition in the Arctic (within the EMEP domain) in 2019.*

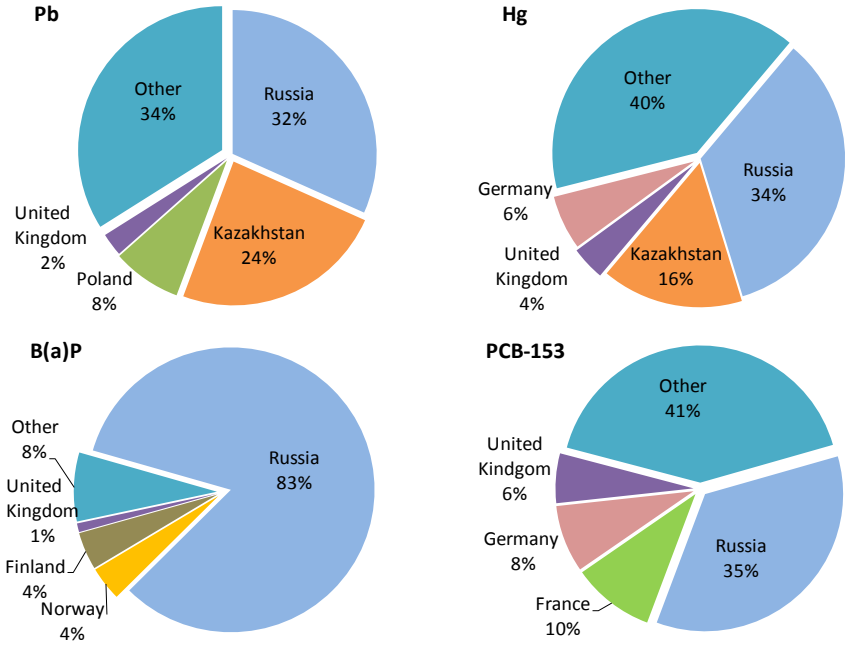

Fig. 3.58. *Source apportionment of heavy metal and POP anthropogenic deposition to the Arctic (within the EMEP domain) in 2019.*

The contribution of emission sources from various EMEP countries to deposition to the Arctic within the EMEP domain is exemplified for land areas (Fig. 3.58). This contribution is determined by a number of factors, including the size and distance of the sources from the Arctic, the physico-chemical properties of pollutants, meteorological conditions, etc. For all considered pollutants, Russia is the main contributor to air pollution in the Arctic (Fig. 3.58), since large part of the territory of Russia is located within the Arctic region. Another significant contributor for Pb and Hg is Kazakhstan, which has one of the highest emissions of heavy metals among the EMEP countries. The noticeable contribution of French and German sources to deposition of PCB-153 in the Arctic can be explained by similar reasons. For B(a)P, substantial contribution is made by sources of Norway, Finland and the United Kingdom, which are located partly within or close to the Arctic region.

3.7. Global scale pollution by heavy metals and POPs

Air concentrations and deposition of heavy metals and POPs to the EMEP countries are caused by sources located both inside and outside the EMEP domain. In case of pollutants, which are characterized by long residence time in the atmosphere (e.g., Hg and some POPs), intercontinental atmospheric transport can contribute substantially to the pollution levels in the EMEP countries. In order to take into account the contribution of non-EMEP sources to concentrations and deposition in the EMEP region, global-scale modelling is performed. Air concentrations of the pollutants derived from global-scale modelling are used as boundary conditions for model simulations over the EMEP region. Besides, results of the global-scale pollution assessment are disseminated to other international conventions and programmes (e.g. Stockholm and Minamata Conventions, AMAP, etc.) in a framework of bilateral or multilateral co-operation (see Section 5.2 for details).

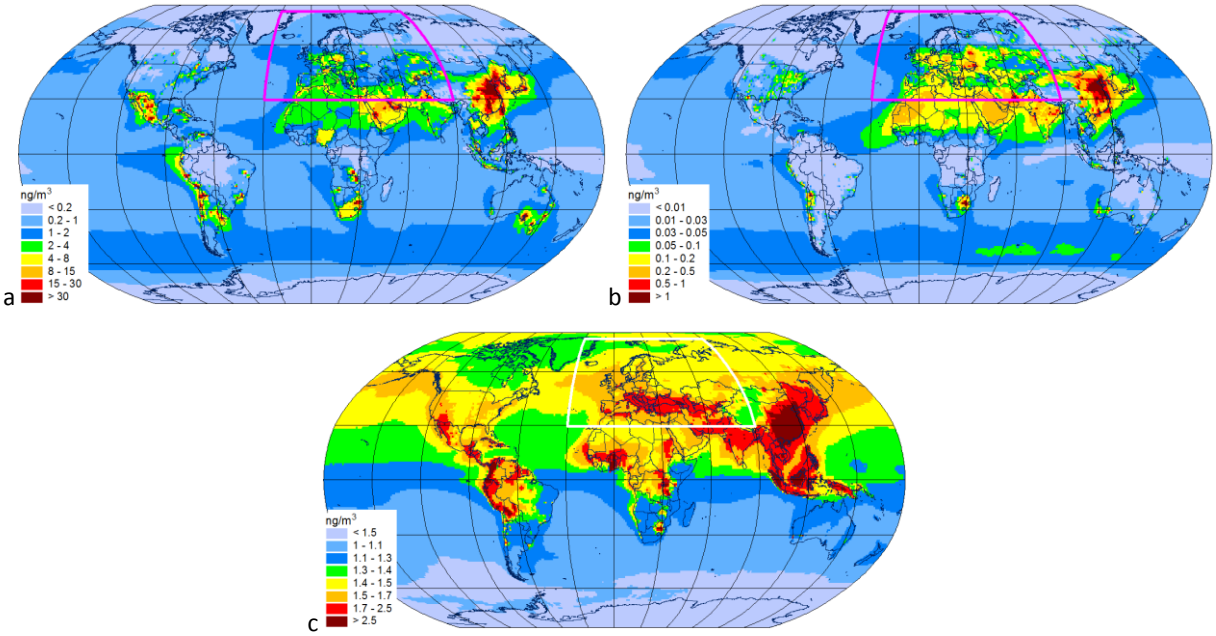

Fig. 3.59. *Global distributions of annual mean air concentration of Pb (a), Cd (b) and Hg^0 (c) in 2019. White line depicts boundary of the EMEP region.*

Global scale model simulations indicate the highest levels of Cd and Pb concentrations in 2019 for the eastern and south-eastern parts of Asia because of large emissions in China (Figs. 3.59a and b). Considerable concentrations of Pb and Cd in North Africa and Middle East are caused by both anthropogenic emissions and by high re-suspension fluxes of wind-blown dust containing these metals. Relatively low concentrations of Pb and Cd take place over oceans, central parts of South America, Africa and Australia, and over the Arctic. Concentrations of Pb and Cd near the western, northern and eastern borders of the EMEP domain are lower by an order of magnitude than those in its inner part. However, the concentrations along the southern border of the domain are comparable with the levels in the EMEP countries. Therefore, anthropogenic emissions and wind re-suspension in North Africa and Middle East can considerably affect Pb and Cd pollution levels in the southern part of the EMEP domain.

Air concentrations of Hg are distributed more evenly over the globe compared to those of Pb and Cd (Fig. 3.59c). The reason for that is long residence time of Hg^0 in the troposphere allowing mixing over the Northern Hemisphere. Concentrations of Hg exhibit distinct gradient between the Northern and Southern Hemispheres. It is explained by the fact that most of Hg anthropogenic emission sources are located in the Northern Hemisphere. Relatively high levels (1.7-2.5 ng/m^3 or even more) in East and South Asia are caused by industrial sources. Significant contribution to high Hg levels in South America, Northern Africa and South-East Asia is made by emissions from artisanal and small-scale gold mining. Natural and legacy Hg emissions significantly contribute to elevated Hg concentrations in the southern part of the EMEP region and the western parts of North and South Americas.

The highest levels of global-scale B(a)P air concentrations (exceeding than 1 ng/m^3) are estimated for the South, East and South-East Asia (Fig. 3.60a). The EMEP domain is characterized by relatively lower B(a)P concentrations varying from 0.02 to 1 ng/m^3 over the most of its part. Similar levels are noted for Africa and the eastern parts of North and South America. Concentrations of B(a)P along the borders of the EMEP domain are much lower than in its inner parts. The exception is the south-eastern corner of the region where higher levels caused by emission sources of South Asia occur. Similar features are also noted for global-scale spatial distributions of other modelled PAHs (B(k)F, B(b)F and IcdP).

The most significant PCDD/F air concentrations are predicted for South Asia (north-east of India, Bangladesh), South Korea and Japan (Fig. 3.60b). Another region with relatively high levels of PCDD/Fs is noted for the central part of Africa. Within the EMEP domain PCDDF concentrations range from 2 to 25 fg TEQ/m^3 in the central and southern parts of the EMEP region, and from 0.2 to 2 fg TEQ/m^3 in its northern part. Comparable levels are noted for the eastern part of North and South Americas. Concentrations near the eastern, northern and western borders of the EMEP domain are much lower than those in its central part. However, the concentrations along the southern border and in the European part of the EMEP domain are comparable. Therefore, contribution of the emission sources of Northern Africa and Middle East to the southern parts of the EMEP domain (e.g., the Mediterranean Sea, Caucasus and Central Asia) is expected to be substantial.

Compared to PAHs and PCDD/Fs, PCB-153 and HCB are characterized by higher potential to long-range atmospheric transport. Therefore, intercontinental transport of PCB-153 and HCB has stronger effect on the pollution levels over the globe. The highest levels of PCB-153 occur in Europe (up to 6 pg/m^3) and the eastern part of North America (0.6 – 3 pg/m^3) (Fig.3.60c). In the Northern Hemisphere the concentrations vary from 0.2 to 0.8 pg/m^3 over the most part of land areas, and from 0.01 to 0.2 pg/m^3 over oceans. In the Southern Hemisphere air concentrations of PCB-153 are 2-3-fold lower than those in the Northern Hemisphere.

Relatively high HCB concentrations (more than 50 pg/m^3) take place in Europe and Eastern Asia (Fig. 3.60d). Over most part of land area and oceans of the Northern Hemisphere the concentrations are distributed relatively uniformly ranging from 15 to 35 pg/m^3. In the Southern Hemisphere air concentrations vary from 5 to 15 pg/m^3.

Spatial distribution of both PCB-153 and HCB is characterized by distinct sharp gradient between Northern and Southern Hemispheres. This gradient is explained by two main reasons. First of all,

main emission and re-emission sources of PCB-153 and HCB are located in the Northern Hemisphere. The second reason is associated with relatively long residence time of these pollutants in the atmosphere and peculiarities of global atmospheric circulation. Long residence time favours spreading of PCB-153 and HCB over the global scale. At the same time, intertropical convergence zone, located close to the equator, hampers exchange of air between Southern and Northern Hemispheres resulting to relatively sharp change in concentrations between the Hemispheres. Unlike PAHs and PCDD/Fs, concentrations of PCB-153 and HCB along the borders of the EMEP domain are comparable with the levels in the EMEP countries. Therefore, contribution of non-EMEP sources to the pollution levels in the EMEP countries is likely comparable with the contribution of the EMEP anthropogenic sources.

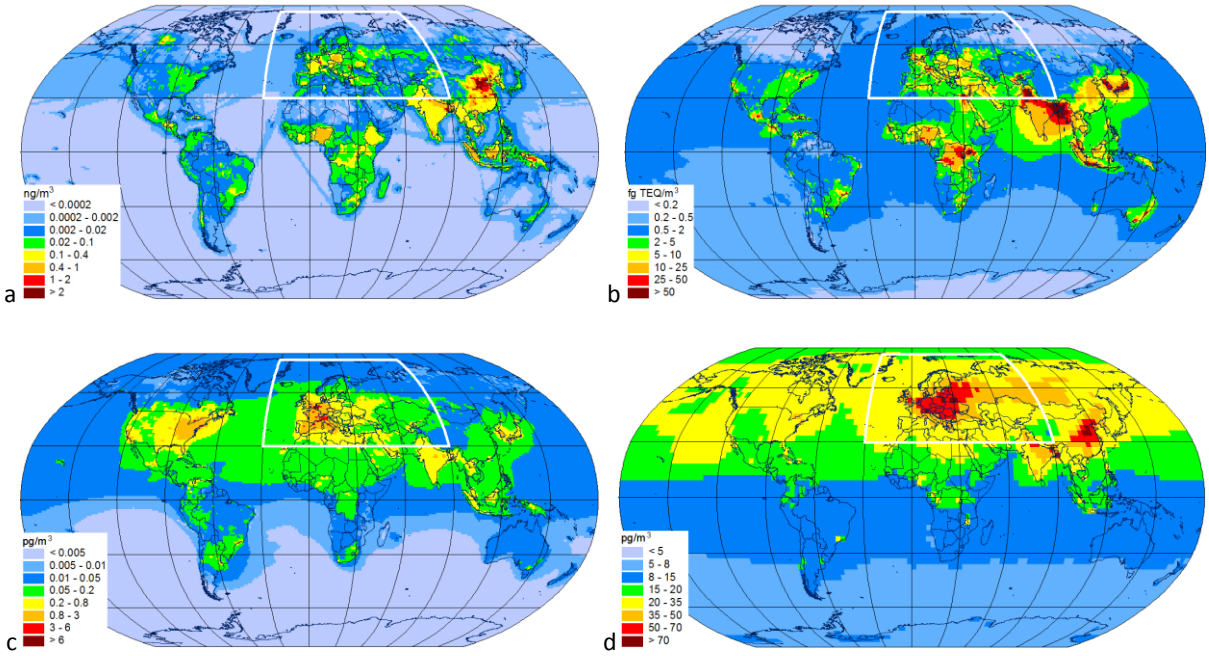

Fig. 3.60. *Global distribution of annual mean air concentration of B(a)P (a), PCDD/Fs (b), PCB-153(c), and HCB (d) in 2019. White line depicts boundary of the EMEP region.*

It is important to take into account that model simulations of heavy metal and POP levels over the global-scale require reliable and contemporary emission data. However, for a number of the considered pollutants (i.e., Pb, Cd, HCB, PCDD/Fs) gridded global-scale emission inventories are lacking. Available expert estimates of emissions applied to simulate their pollution levels over the globe are often based on insufficient input data and need revision (see Section 1.2). Thus, improvement of the global-scale assessment requires further development of global emissions inventories for heavy metals and POPs in co-operation with other international bodies (UN Environment, Stockholm Convention, Minamata Convention).

Chapter 4. RESEARCH ACTIVITIES

Research activities are aimed at improvement of atmospheric pollution assessment quality for the EMEP countries. Priority directions of the research and development in the field of heavy metals and POPs are formulated in the long-term strategy for the Convention and the bi-annual work-plan of EMEP [ECE/EB.AIR/144/Add.2]. The main directions of the research are presented in this chapter. They include attribution of long-term changes of Hg and POP pollution to regional and extra-regional sources, case study on B(a)P pollution assessment for Poland, analysis of long-term PAH trends in Europe, updates of the model parameterization of Hg and POP air-surface exchange, comparison of different land-cover datasets, evaluation of new global Hg emission inventory and data on chemical reactants, collection of information on microplastics relevant to evaluation of its potential to long-range transport.

4.1. Attribution of long-term changes of Hg and POP pollution: Pilot study

Analysis of long-term pollution trends involving both measurement data and modelling results is widely used for the effectiveness evaluation of the environment protection measures [e.g. *Colette et al.* 2016; *UNEP*, 2017; *AMAP/UNEP*, 2019]. Changes of pollution levels in particular regions are determined by possible reduction of anthropogenic emissions as a result of mitigation efforts as well as by other factors including changes in meteorological conditions, chemical properties of the atmosphere, surface characteristics etc. Thus, analysis of the factors responsible for pollution changes in the past can provide useful information for developing effective strategies of environmental protection in the future.

Directions of future research of Hg and POP pollution in the EMEP and other regions are currently discussed within the Task Force on Hemispheric Transport of Air Pollution (TF HTAP) (see Section 5.1.2). Attribution of long-term pollution trends is considered as one of the perspective directions of the Task Force future activities. Proposed objectives of such research include (i) retrospective analysis of Hg and POP pollution changes; (ii) the trends attribution to various factors (primary and secondary emissions, meteorology, chemistry, land cover, sea ice extent etc.); (iii) projection of future levels based emission scenarios. To facilitate the discussion and illustrate possible output of the study MSC-E performed pilot simulations and analysis of long-term changes of Hg and two PAHs with diverse properties (benzo(a)pyrene and fluoranthene) on a global scale. Preliminary results of the study are briefly discussed below. More detailed information is available in the MSC-E Technical Report 1/2021 [*Travnikov et al*., 2021].

The long-term Hg and POP simulations as well as trend attribution experiments were performed using the updated GLEMOS model. Description of the current stable model version 2.2.1 is available at the MSC-E website (*http://en.msceast.org/index.php/j-stuff/glemos*). The model updates include implementation of new input data on air concentrations of chemical reactants for a long period

generated by the GEOS-Chem model version 12.8.2 [*The International GEOS-Chem* ..., 2020] and multi-year land cover data (Section 3.4). The simulations were carried out on a global scale with the spatial resolution 3°×3° for the period 1990-2018. Time series of simulation results were evaluated against a limited set of measurement data. A number of the model sensitivity runs were also conducted to evaluate the influence of several anthropogenic and environmental factors (emissions, meteorological conditions, atmospheric content of major chemical reactants, and land cover distribution) on long-term changes of Hg and POP levels in various regions of the globe.

Meteorological input information for 1990-2018 time period has been generated from the operational analysis data of the European Centre for Medium Range Weather Forecasts [*ECMWF*, 2021] using the meteorological preprocessor based on the Weather Research and Forecast modelling system (WRF) [*Skamarock et al.*, 2008]. Land cover data were obtained from the International Geosphere-Biosphere Programme (IGBP) data layer of the Terra and Aqua combined Moderate Resolution Imaging Spectroradiometer (MODIS, Land Cover data product MCD12Q1, version 6) [*Friedl et al.*, 2019]. A global Hg emissions dataset for the considered time period was derived combining long-term time series of emission totals for various regions from [*Streets et al.*, 2019] and spatial distribution of emissions from the UNEP/AMAP inventories [*AMAP/UNEP*, 2019; *AMAP*, 2021]. For benzo(a)pyrene and fluoranthene the global scale inventory of PAH emissions developed by the research group of Peking University [*Shen et al.*, 2013] was used. Examples of time series of some input parameters for the European region are shown in Fig. 4.1. As seen there are noticeable changes in some anthropogenic and environmental parameters over the considered period. For instance, average annual air temperature over the European region has risen by almost 1°C (Fig. 4.1a). The built up area increased by 2000 km^2 from 2001 to 2018 (Fig. 4.1b). Anthropogenic emissions of fluoranthene have reduced by almost 50% during the period (Fig. 4.1c).

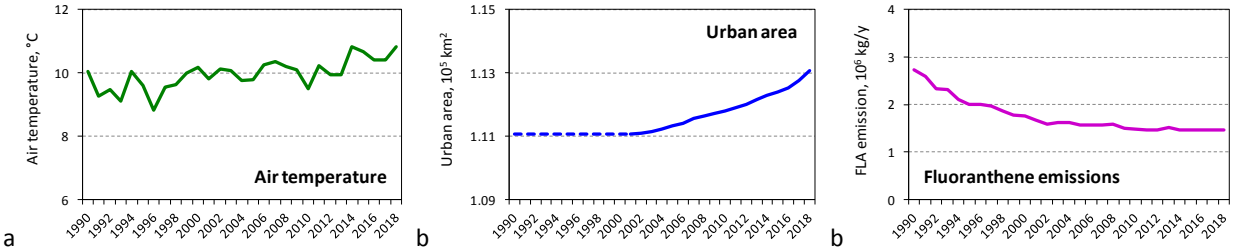

Fig. 4.1. *Changes of average air temperature (a), urban area (b) and fluoranthene emissions (c) in Europe.*

Results of the pilot simulations indicate gradual decrease in atmospheric concentrations of all three pollutants in Europe since 1991 after a small growth from 1991. The decreasing trend of Hg is smooth and continuous and lasts from 1991 to 2008 (Fig. 4.2a), in contrast to PAHs, which have a sharp decrease from 1991 to 2001 and a smoother decline until 2014 (Figs. 4.2b and c). Concentration levels of all three substances are almost unchangeable after 2014. The difference in the decrease rates of Hg and PAHs can be explained by different atmospheric properties and emissions dynamics. Benzo(a)pyrene and fluoranthene are mainly regional pollutants due to relative short residence time in the atmosphere. It is clearly seen by significant spatial variation of their concentration over the region. Therefore, the temporal changes of these pollutants are largely

determined by variation of anthropogenic emissions in Europe. In contrast, long-lived Hg can be transported globally and its concentration in Europe is affected by emissions in other regions. An additional factor that slows down the decrease of Hg concentrations is considerable contribution of natural and secondary sources, which change slowly in time.

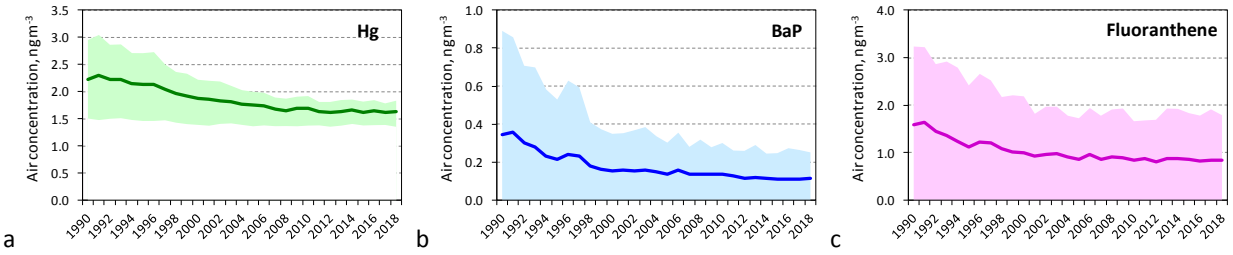

Fig. 4.2. *Long-term changes of Hg (a), B(a)P (b) and fluoranthene (c) air concentration in Europe. Line presents the average value and shaded area shows the 90%-interval of spatial variation over the region.*

An example of the trend attribution analysis is shown in Fig. 4.3. As seen the long-term dynamics of all three pollutants in Europe is primarily determined by changes in anthropogenic emissions. Source apportionment has shown that contribution of regional sources to PAHs levels in Europe remain predominant over the whole period [*Travnikov et al.*, 2021]. For Hg, prevailing contribution of regional sources decreases over the period and is replaced by increasing contribution of East Asian sources. Other factors also contribute to temporal variability of the pollutants concentrations. For instance, short-term increases of all pollutants concentrations in 1991 and 1996 are mostly caused by meteorological conditions. Change in atmospheric chemistry does not significantly affect concentrations of considered substances leading to some additional increase or decrease in particular years. Effect of land cover change on long-term variation of Hg and PAHs is negligible on a regional scale in Europe. However, more significant local effects can be expected. It should be noted that results of the study are highly sensitive to estimates of temporal changes of input parameters of the study. Besides, considered factors do not explain full temporal variability of the pollutants concentrations. Additional factors are to be identified and evaluated in future.

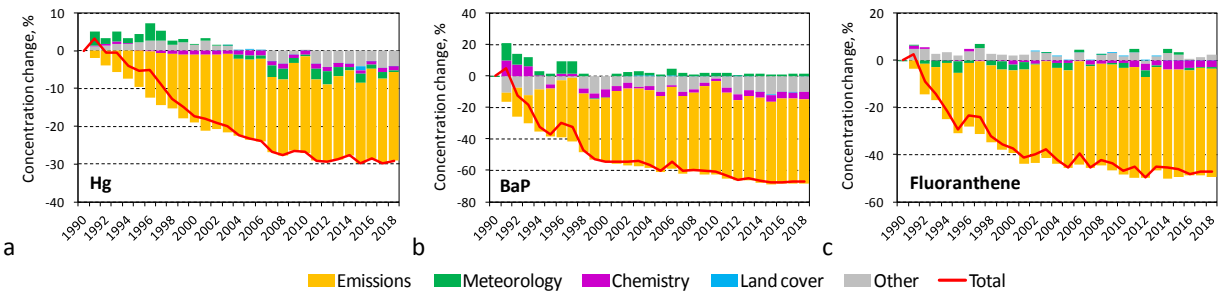

Fig. 4.3. *Relative change of average air concentrations of Hg (a), B(a)P (b) and fluoranthene (c) in Europe.*

Outcome of the pilot study shows that proposed trend attribution analysis can be applicable and useful for understanding of long-term pollution dynamics. However, the results are sensitive to uncertainties of input data on long-term changes of the key parameters affecting levels and variability of considered pollutants (first of all, anthropogenic emissions). Therefore, more efforts are needed to collect reliable input information for the analysis to obtain robust results of the trend attribution.

4.2. Assessment of regional and national scale PAH pollution levels

In accordance with the Long-term Strategy of the LRTAP Convention, MSC-E continued research activities to improve assessment of PAH pollution levels in the EMEP region and to contribute to the analysis of the effectiveness of measures to reduce unintentional releases of PAHs.

In particular, MSC-E continued analyzing long-term changes of the observed and modelled PAH concentrations in different parts of the EMEP region on the example of B(a)P. This activity includes evaluation of trends and analysis of temporal changes in the contribution of major emission sectors to the pollution levels. Besides, detailed analysis of national scale PAH pollution levels was performed in framework of the case study for Poland in cooperation with national experts. An overview of progress in the assessment of PAH pollution is presented in this section. More detailed information can be found in the MSC-E Technical Report on PAHs 2/2021 [*Gusev et al.*, 2021].

Analysis of long-term trends of the observed and modelled PAH concentrations

Time-series of modelled B(a)P air concentrations in different sub-regions of the EMEP domain for the period 1990-2018 are shown in Fig. 4.4. Model simulations were performed with the latest version of the GLEMOS model on the basis of officially reported emission data provided by the EMEP countries and processed by CEIP. Description of emission dataset applied for the analysis of B(a)P temporal variations is given in the technical report [*Gusev et al.*, 2021].

The analysis of modelling results shows in general decreasing trends of annual mean B(a)P air concentrations in most of the sub-regions with the exception of Caucasus and Central Asia. The model simulations indicate the most significant decrease in Western, Central, and Northern Europe (by 65%, 60%, and 40%, respectively). Relatively lower decrease is estimated for Southern and Eastern Europe (by 20% and 5%), whereas for Caucasus and Central Asia the model estimates demonstrate increase of B(a)P (by 65%). It should be noted however that emission data for this sub-region still incorporate relatively high uncertainties compared to other sub-regions.

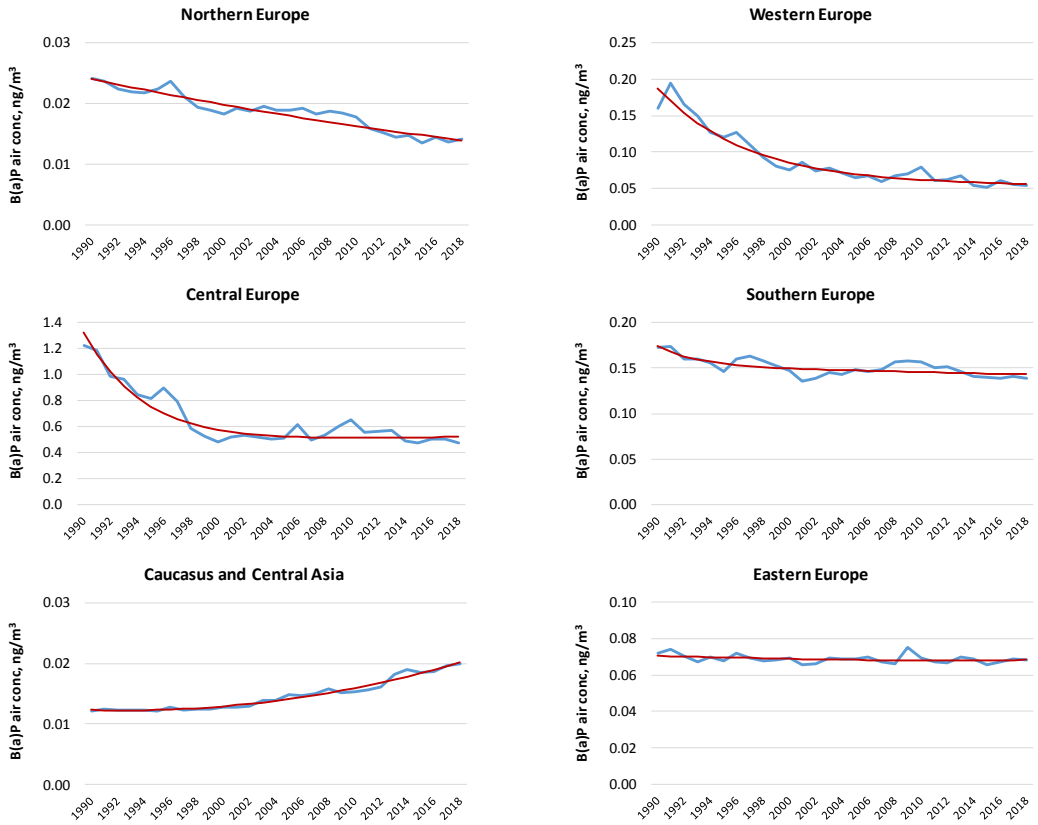

Fig. 4.4. *Long-term changes of B(a)P annual mean modelled air concentrations for the period 1990-2018, averaged across 6 sub-regions of the EMEP domain (Northern Europe, Western Europe, Central Europe, Eastern Europe, Southern Europe, and Caucasus and Central Asia) and bi-exponential approximation of temporal variations of B(a)P concentrations.*

The analysis of long-term trends of B(a)P air concentrations in the EMEP region for 1990-2018 was performed using the methodology based on fitting exponential law [*Shatalov et al.*, 2015]. The trend is expressed in terms of reduction rates that are assumed to be positive for a downward trend and negative for an upward trend. Bi-exponential approximations of B(a)P concentrations in different sub-regions are shown in Fig. 4.4. The highest reduction rate (about 4% per year on average) is estimated for Western Europe followed by Central and Northern Europe (3% and 2% per year, respectively). Noticeably lower reduction rates were in Southern and Eastern Europe (less than 1% per year), while increasing rate (about -2% per year) was obtained for Caucasus and Central Asia.

Comparison of annual mean modelled B(a)P concentrations for the period 1990-2018 with data of the available EMEP long-term measurements is shown in Fig. 4.5. Observed concentrations in the selected sub-regions of the EMEP domain were averaged across the monitoring stations and compared with the model estimates.

It is seen that long-term changes of modelled B(a)P concentrations generally correspond to the observed variations in Northern and Western Europe. In case of Central and Eastern Europe measured concentrations have higher inter-annual variability than that of the modelling results. The latter can be explained by lower amount of monitoring stations in these sub-regions as well as shorter periods of monitoring.

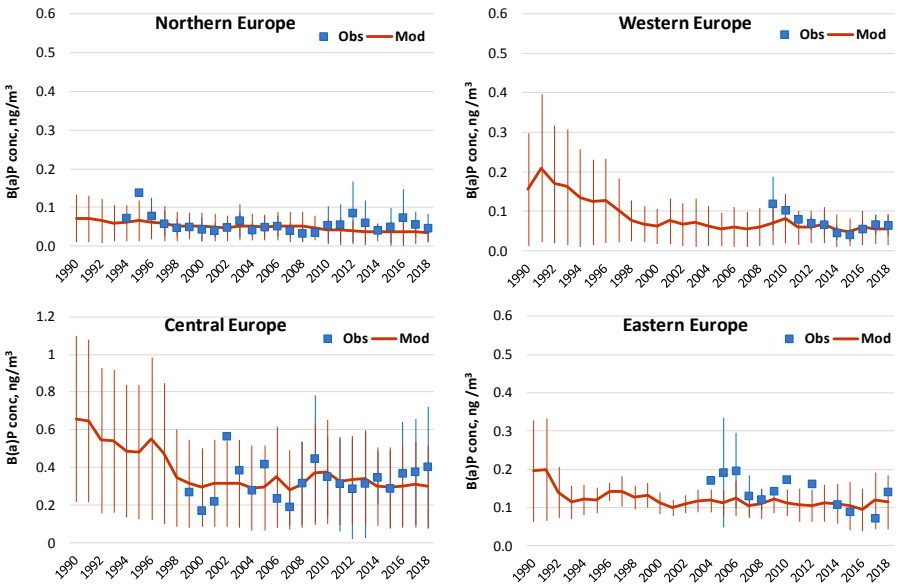

Fig. 4.5. *Modelled and observed B(a)P annual mean air concentrations for the period 1990-2018, averaged across 4 sub-regions of the EMEP domain, namely, Northern Europe (11 stations), Western Europe (12 stations), Central Europe (7 stations), Eastern Europe (5 stations). Whiskers indicate the range from minimum to maximum annual mean measured concentrations in particular sub-region.*

A number of model simulations were also performed to estimate the contribution of major emission sectors to B(a)P air concentrations and their variations across selected years in the period 1990-2018 (Fig. 4.6). It is seen that the *Residential Combustion sector* contributed the most to annual mean B(a)P air concentrations in all the sub-regions. Noticeable contribution was also made by the *Industry sector* in the beginning of the 1990s in Northern, Western and Southern Europe. However, later on its share decreased significantly. Besides, countries of Southern Europe are characterized by considerable contribution of the *Agriculture sector*.

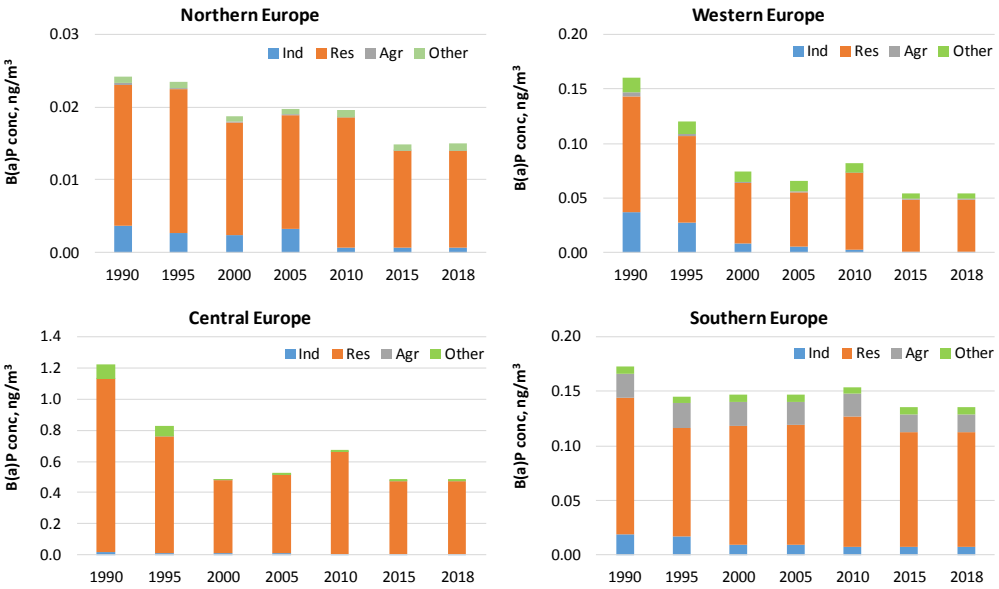

Fig. 4.6. *Long-term changes of the modelled B(a)P annual mean air concentrations for the period 1990-2018, averaged across 4 sub-regions of the EMEP domain (Northern Europe, Western Europe, Central Europe, and Southern Europe) with contribution of major emission sectors (Ind – Industry, Res – Residential combustion, Agr – Agriculture, and Other – other GNFR sector).*

Thus, similar to the previous stage of the study [*Gusev and Batrakova*, 2020], updated assessment of B(a)P pollution levels in the EMEP countries for the period 1990-2018 indicates the absence of significant changes in the pollution levels during the two recent decades and the dominating role of the *Residential Combustion* sector.

Case study of PAH pollution for Poland

The study for Poland continued a series of national scale case studies on PAHs [*Gusev et al.,* 2017; 2018; 2019] that followed the recommendation of the 2nd joint session of the Working Group on Effects and the Steering Body to EMEP (held in 2017). Current stage of the study is focused on the model assessment of PAH pollution in Poland. It was initiated in 2020 after the meeting of EMEP and national experts in modelling and emissions of B(a)P, held in November 2019 in Warsaw (Poland). Multi-model simulations for 2018 were planned to analyze levels of B(a)P/PAH air concentrations in Poland based on the new and previous national PAH emission inventories including comparison with measurements as well as with the EU and WHO air quality guidelines. Below preliminary modelling results obtained using the EMEP GLEMOS model are outlined. More detailed information can be found in the MSC-E Technical Report on PAHs 2/2021 [*Gusev et al.*, 2021].

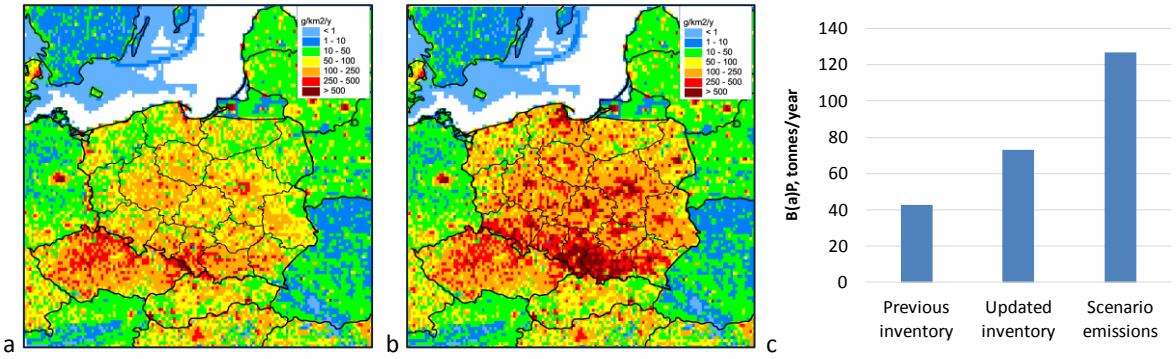

Fig. 4.7. *Spatial distribution of annual B(a)P emission fluxes in 2018 (g/km²/y) according to previous (a) and updated (b) B(a)P emission inventory (spatial resolution 0.1°x0.1°), and comparison of total annual B(a)P emission of Poland according to previous and updated emission inventories and scenario of B(a)P emissions(c).*

Three datasets of gridded anthropogenic B(a)P emissions for 2018 were prepared for the model simulations. The first one (*Previous Inventory*) was constructed using the previous national emission inventory of Poland (submission 2019) and emissions of other EMEP countries for 2018 provided by CEIP (submission 2020). In the second and the third datasets emissions of Poland were substituted by the new inventory (*Updated Inventory*) and by the scenario emissions (*Scenario Emissions*), respectively. The scenario emissions were prepared using the uncertainty range for the Residential Combustion sector (equal to 76%) defined in the inventory information report of Poland [*Bebkiewicz et al.*, 2020]. Constructed emission scenario represents possible maximum level of B(a)P emissions in the country. Spatial distributions of annual B(a)P emissions in the modelling domain, including data of the previous and new inventory of Poland, are presented in Fig. 4.7a and Fig. 4.7b, respectively. In

Fig. 4.7c comparison of annual total B(a)P emissions in Poland according to the previous and new inventory, and constructed scenario is shown.

Annual mean modelled B(a)P air concentrations for 2018, obtained in the model simulations with the three emission datasets are given in Fig. 4.8. The largest differences between the three sets of simulated air concentrations can be seen over the territory of Poland. In particular, the modelling results based on the new inventory show that B(a)P concentrations in most parts of the country are higher than 0.4 ng/m^3, and exceed the WHO reference level (0.12 ng/m^3). Area of B(a)P air concentrations above the EU target value (1 ng/m^3) is also significantly wider compared to the results based on the previous inventory. In case of the scenario emissions the area of concentrations above the EU target value covers the most of the country with the highest concentrations (over 2 ng/m^3) in its southern part.

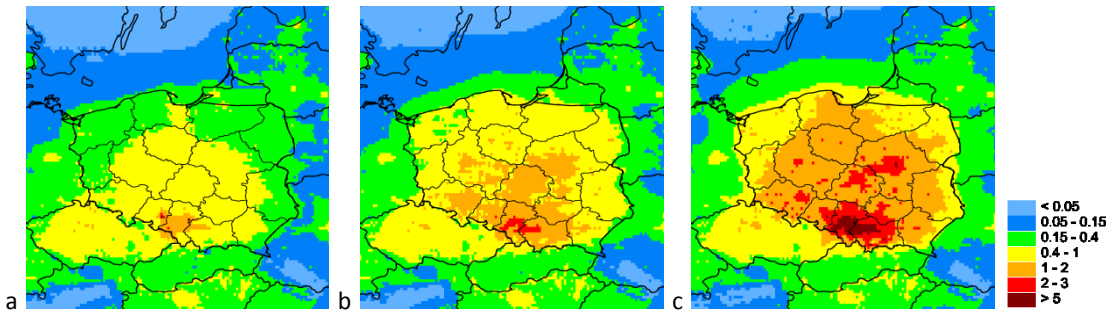

Fig. 4.8. *Annual mean modelled B(a)P air concentrations (ng/m³) in 2018 simulated using the B(a)P emissions including previous version of B(a)P emission inventory of Poland (a), the new B(a)P emission inventory (b), and scenario of B(a)P emission (c) (spatial resolution 0.1°x0.1°).*

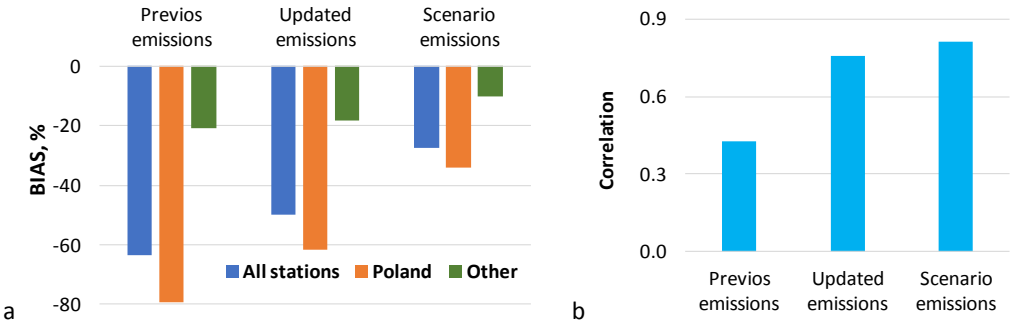

Fig. 4.9. *Mean relative bias (a) and spatial correlation (b) between the modelled and measured annual mean B(a)P air concentrations (ng/m³) for 2018 simulated using the B(a)P emissions that include previous and new B(a)P emission inventory, and scenario emissions. Mean relative bias is calculated for the three groups of monitoring stations: (1) all stations in the modelling domain, (2) stations in Poland, and (3) stations in other countries.*

Model estimates were compared with B(a)P air concentrations observed in 2018 at the EMEP and EEA Air Quality e-Reporting monitoring stations. In particular, rural, remote, and sub-urban stations in Poland and surrounding countries were selected for the comparison. Mean relative bias between the model estimates and measurements is shown in Fig. 4.9a for the three groups of monitoring stations, namely, all stations in the modelling domain, stations in Poland, and stations in other

countries. The use of the updated national emission inventory leads to significant decrease of the bias, both for the stations within and outside the country. Along with this, noticeable improvement of spatial correlation between the modelled and measured values is obtained (Fig. 4.9b). Model simulations with the scenario emissions showed further improvement of the agreement between the model and measurements indicating possible underestimation of B(a)P emissions.

Comparison of the modelled and observed seasonal variations of B(a)P air concentrations for 2018 shows in general satisfactory agreement between the model results and measurements. In Fig. 4.10 examples of the model predictions and measurements for the EMEP Polish monitoring sites PL0005R and PL0009R are presented. In general, the model simulations with scenario emissions better capture seasonal variations of the observed B(a)P air concentrations compared to the simulations using the new and previous inventory emissions. However, in some of the episodes, especially winter months in the beginning of the year, the model sometimes underpredicts measured B(a)P concentrations. Differences between the modelled and measured intra-annual variations of B(a)P concentrations may be explained by uncertainties of temporal disaggregation of B(a)P emissions which is currently based on the TNO estimates.

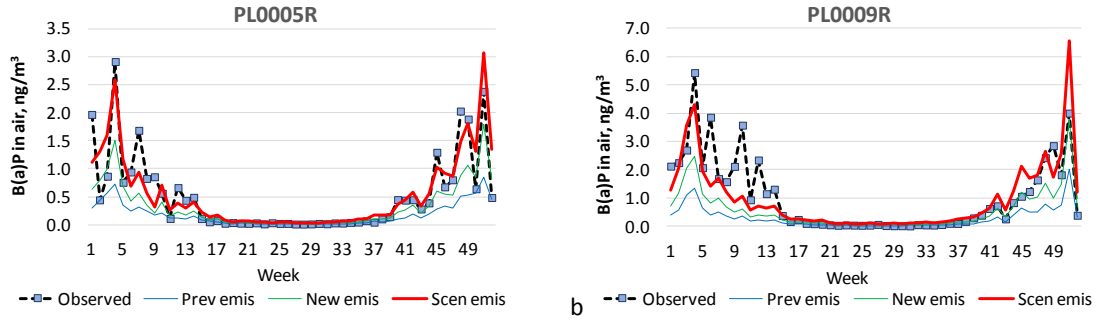

Fig. 4.10. *Seasonal variations of modelled B(a)P air concentrations (ng/m³) for 2018, calculated on the basis of the previous and new national B(a)P emission inventories and scenario emissions, against measurements of EMEP monitoring stations.*

Preliminary results of model simulations for 2018, based on the new national B(a)P emission inventory, showed better agreement with measurements compared to the previous inventory. At the same time, the model still tends to underpredict observed B(a)P air concentrations. The model simulations with the scenario emissions on the basis of emissions uncertainty range allow to further improve the agreement between the model and measurements indicating possible underestimation of national B(a)P emissions in Poland. At the same time, additional contribution to the model-measurement differences can be made by the uncertainties in currently applied model parameterizations of B(a)P degradation in the atmosphere and measurements of its concentrations. The model results and measurements indicate high level of annual mean B(a)P air concentrations, exceeding the EU target value (1 ng/m^3) and the WHO reference level (0.12 ng/m^3), in many areas of Poland. Possible future steps of the study can include multi-model simulations, application of more detailed temporal and spatial disaggregation of B(a)P emissions, and co-operation with national experts in monitoring, modelling, and emissions.

4.3. Update of model parameterizations for soil and vegetation compartments

Gaseous exchange of POPs and Hg between the atmosphere and vegetation is an important process that affects their distribution in the environment and can lead to human and wildlife exposure to harmful levels of their concentrations [*Barber et al.*, 2004; *Wang et al.*, 2014]. In order to evaluate transport and accumulation of these pollutants in the environment several modules describing their fate in surface compartments including inter-media exchange are being developed for the GLEMOS modelling system. This section presents a progress in the improvement of the GLEMOS model parameterization of the air-vegetation and air-soil exchange processes.

There are a few approaches that are implemented in the multi-compartment models to describe the air-vegetation exchange of POPs and Hg. The approach proposed in [*McLachlan and Horstmann*, 1998; *McLachlan,* 1999] considers vegetation as a single compartment with direct exchange of POPs between the atmosphere and vegetation. Developed one-compartment plant model has been found adequately describing semivolatile organic compounds uptake in the vegetation of a number of species. This approach is implemented in a number of multi-compartment models (e.g., [*Friedman and Selin,* 2012*; Lammel et al.,* 2009*; Sehili and Lammel,* 2007]) as well as in the current version of GLEMOS described in [*Travnikov et al.*, 2020].

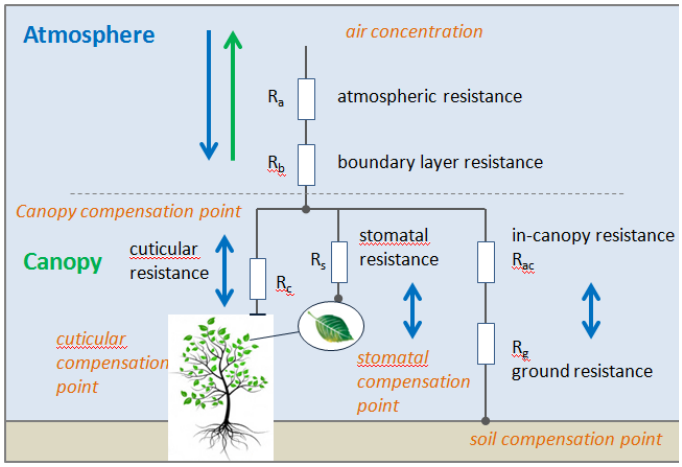

Fig. 4.11. *The scheme of gaseous air-vegetation-soil exchange parameterization, based on the resistance analogy following [Bash, 2010; Zhang et al., 2009; Wang et al., 2014].*

Another approach to the description of air-vegetation exchange considers vegetation and soil as parts of a single compartment (ecosystem) [*Sutton et al.*, 1998; *Sutton et al.*, 2007]. The exchange fluxes are controlled by the gradient between the pollutant air concentration and a compensation point representing concentration at the interface between the atmosphere and surface compartment. The compensation point is the value of air concentrations, for which the net gaseous exchange flux between considered medium and air changes its direction. This approach has been implemented in several studies of Hg air-surface exchange (e.g., [*Bash*, 2010; *Zhang et al.*, 2009; *Wang et al.*, 2014]). The scheme of model parameterization of gaseous air-vegetation-soil exchange of a pollutant, based on the resistance analogy, is presented in Fig. 4.11. On the basis of this approach a new parameterization of gaseous air-vegetation-soil exchange was developed for the GLEMOS model. Detailed description of developed model parameterization is given in Annex C.

The effect of the implementation of updated air-surface gaseous exchange parameterization in the GLEMOS model was evaluated using one-year simulations of PCB-153 for 2019. The model was run for the EMEP domain with zero initial conditions in the environmental compartments. Since stomatal uptake is believed to play minor role for air-vegetation uptake of heavy PCBs, this process was neglected in the model simulations. Annual mean PCB-153 concentrations in the atmosphere, soil, and vegetation, air-surface exchange fluxes as well as their seasonal variations, simulated with the currently used (old) and updated (new) air-surface gaseous exchange parameterization, were compared.

One-year simulations with the new parameterization indicated the biggest change of PCB-153 content for vegetation (about 40%) compared to the old parameterization while for the atmosphere and soil compartments the changes were smaller, -2% and -3%, respectively. The application of new parameterization based on compensation points leads to increasing of PCB-153 air-vegetation exchange and decreasing of air-soil exchange.

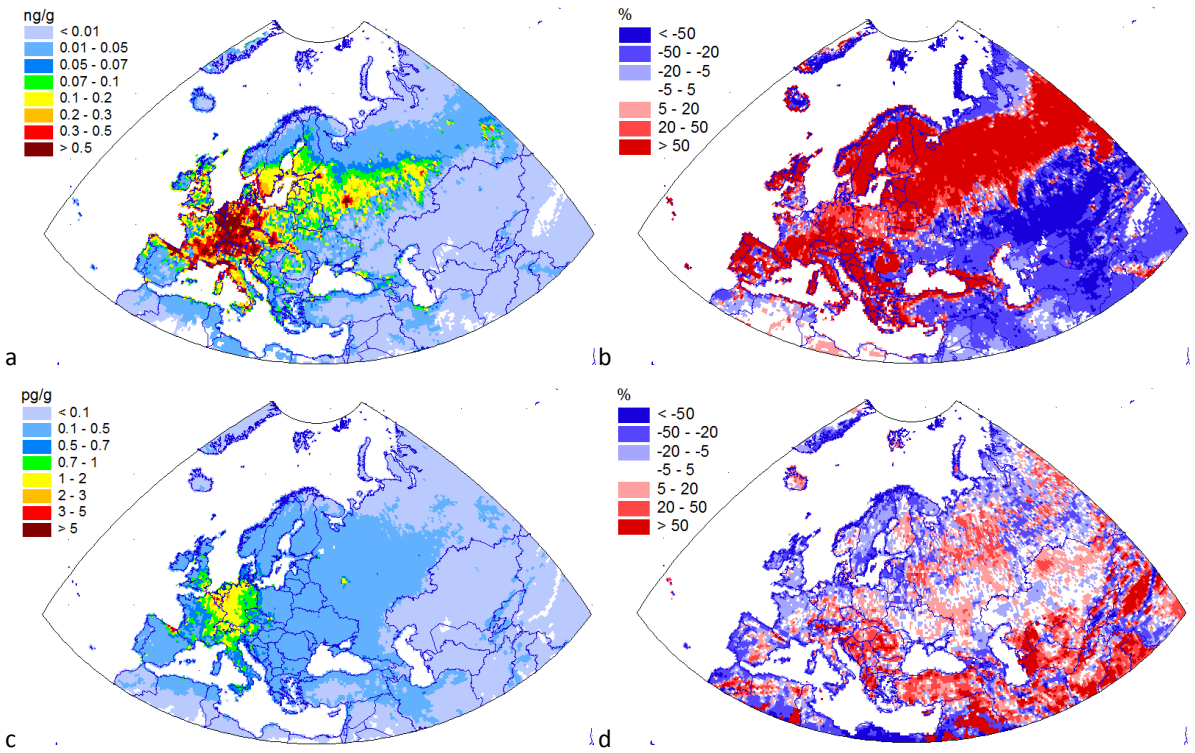

Fig. 4.12. *Absolute values of annual mean PCB-153 concentrations in vegetation (a) and soil (c) compartments for 2019 based on the new parameterization of air-surface exchange fluxes and relative changes ($(C_{new} - C_{old})/C_{old}$ x 100%) of PCB-153 concentrations between the model simulations with new and old parameterizations for vegetation (b) and soil (d) compartments.*

Spatial distribution of PCB-153 concentrations in vegetation is shown in Fig. 4.12a. The highest concentrations occur in the western and central parts of Europe (e.g., Germany, the Netherlands, Switzerland, Belgium, and France). Relatively high concentrations are noted for the north-eastern part of Europe and in the central part of Russia. Relative changes between the results with the new

and old parameterization indicate substantial differences in different parts of the EMEP domain (Fig. 4.12b). There is a large area of the positive change covering the most part of Europe and spreading from west to east of Russia following the distribution of vegetation cover. In the southern parts of Eastern Europe, Russia and in Central Asia the change is negative indicating that the usage of new parameterization leads to the decrease on modelled concentrations in areas with low amount of vegetation.

Spatial distribution of PCB-153 concentrations in soil is shown in Fig. 4.12c. The central and the western parts of Europe (Germany, Belgium, the Netherlands, east of France, north of Italy, Austria, Switzerland, south-east of the United Kingdom, north of Spain) are characterized by elevated concentrations of PCB-153 compared to other parts of the EMEP region. The use of the new parameterization results to an increase of PCB soil concentrations in the central and south-eastern parts of Europe, over the vast areas of Russia and Central Asia, the central part of Finland (Fig. 4.12d). Over the most part of Scandinavia and the western part of Europe modelled concentrations in soils decreased due to the change in the model parameterization.

Relative changes of seasonal variations of PCB-153 content in the environmental compartments demonstrate more significant effect of the update of air-surface model parameterization in the GLEMOS model (Fig. 4.13).

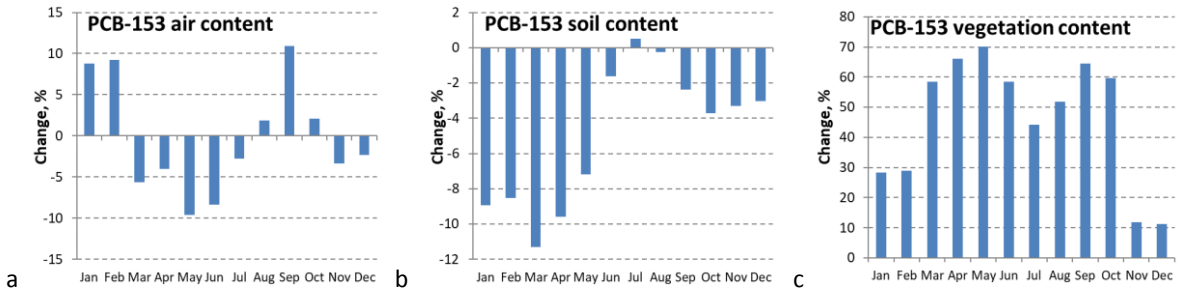

Fig. 4.13. *Relative changes ($(C_{new} - C_{old})/C_{old}$ x 100%) of seasonal variations of PCB-153 content in the atmosphere (a), soil (b), and vegetation (c) in the EMEP domain for 2019 based on the model simulations with new and old parameterizations of air-surface exchange fluxes in the GLEMOS model.*

Similar to the annual mean values of PCB-153 content in the model domain, the largest differences between the model simulations are seen for the vegetation compartment reaching 50-70% in the period from March to October (Fig. 4.13c). The use of the new parameterization results in more intensive exchange and accumulation of PCB-153 in vegetation. The change of PCB-153 content in the atmosphere is relatively low ranging within ±10% for most of the months (Fig. 4.13a) with relatively higher differences in May and September. The relative changes of PCB-153 content in soil compartment are mostly negative indicating decrease of PCB-153 uptake by soil with the largest differences in the beginning of the year. Although the changes in PCB-153 soil content may seem low, it is important to note that PCB-153 can be accumulated in soils over decades. Therefore, changes of modelling results between the new and old model parameterization over the longer period of time can be higher compared to that obtained in the one-year model run.

Analysis of changes in the modelling results induced by the update of air-vegetation and air-soil gaseous exchange parameterization has been initiated. Comparison of pilot modelling results for PCB-153 demonstrated that the changes in concentrations in air and soils in the EMEP region as whole are relatively low (around 10%), while the changes in concentrations in vegetation are more substantial (up to 70%). Besides, the changes vary over the EMEP domain markedly. Nevertheless, further testing of updated model parameterization is required for Hg and larger set of POPs as well as longer period of the model simulations. Furthermore, modelling results obtained with new and old model parameterizations need to be evaluated against available measurement data of POP content in vegetation and soil compartments.

4.4. Comparison of different land cover datasets

Information on land cover is important for modelling and essential for estimation of ecosystem-dependent deposition fluxes, because dry deposition velocities strongly depend on characteristics of the underlying surface. Furthermore, the land cover data are necessary for simulation of wind re-suspension of particle-bound pollutants, e.g., heavy metals.

Generally the GLEMOS simulations on both the global and regional scales use land cover information, which was obtained from the Moderate Resolution Imaging Spectroradiometer (MODIS) satellite dataset [*Strahler et al.*, 1999]. This dataset provides information on 17 land cover types with original spatial resolution of 30x30 arc seconds (about 1x1 km^2), which are designated according to the Annual International Geosphere-Biosphere Programme (IGBP) classification. Besides, in the recent country-specific case study on heavy metal pollution assessment in Germany more detailed land cover data from the CORINE dataset (release v18_5) were adapted and used [*Ilyin et al.,* 2020]. The CORINE dataset contains 44 land cover types of the underlying surface, which were matched with categories from the MODIS dataset to be used in the model. However, the CORINE dataset does not cover the whole EMEP region, so it cannot be used for regular calculations over the entire EMEP domain. Technical descriptions of the recent CORINE releases are available in [*Büttner et al.*, 2017].

Long-term changes in the surface conditions are considered to be one of the important factors which can possibly affect changes of heavy metal and POP levels in the EMEP and other regions. To study this impact as well as to evaluate the GLEMOS model behavior when using inconstant surface conditions another MODIS land cover data product was also used - The Terra and Aqua combined MODIS Land Cover Type (MCD12Q1, version 6) [*Friedl et al.*, 2019]. This product provides global distribution of land cover types at yearly intervals (2001-2018) with 500-m spatial resolution. For the implementation of continuity and compatibility with the parametrization of the model the data product layer derived from IGBP classification was utilized. Examples of spatial distribution of different types of forest, shrubs, non-irrigated arable lands and urban areas (discontinuous urban fabric) from the processed MODIS MCD12Q1 ICBP layer and CORINE dataset are shown in Fig. 4.14.

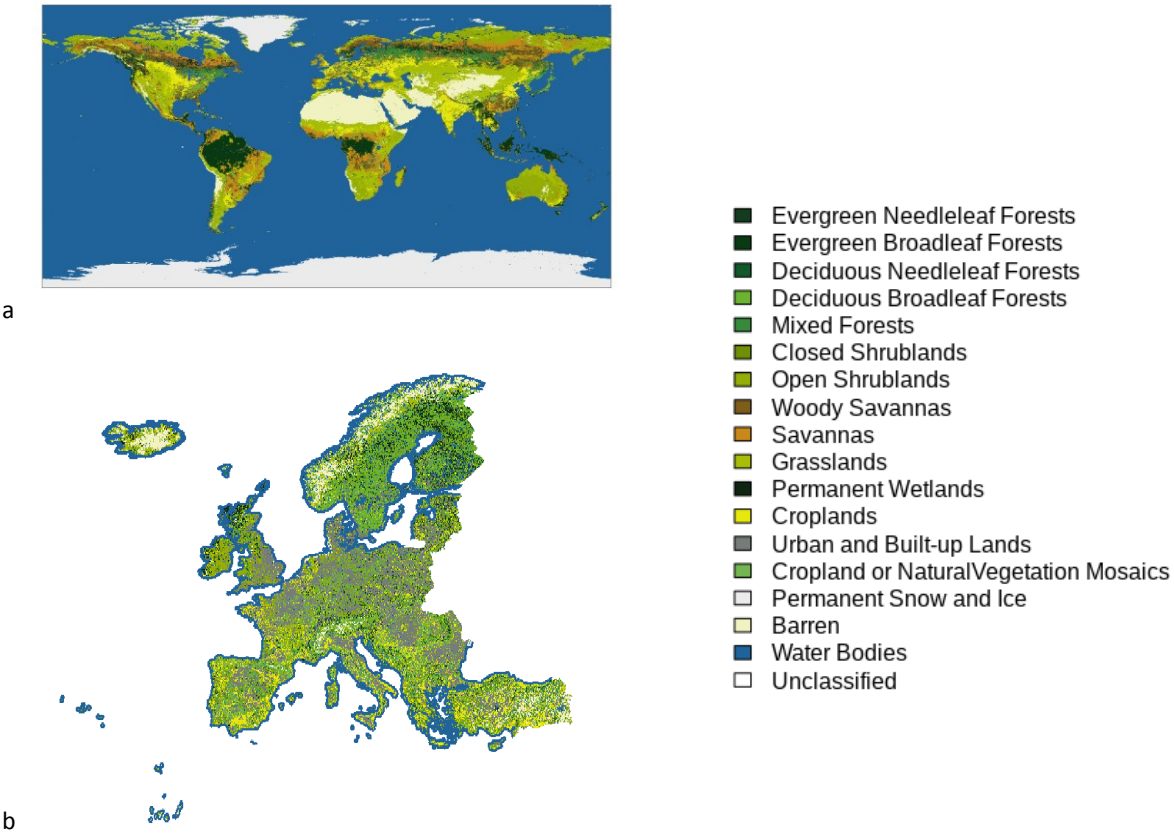

Fig. 4.14. *The processed MODIS MCD12Q1 ICBP layer for 2001 (a) and The CORINE dataset (b).*

Comparison of fractions of the underlying surface types between the standard GLEMOS land cover dataset, the preprocessed CORINE dataset and long-term IGBP layer from MODIS MCD12Q1 data product in the European region for the 2001-2018 time period is shown in Fig. 4.15. Differences between the two MODIS data products are well noticeable. The prevailing land cover types in all datasets include croplands, grasslands, shrublands and various types of forest. The classification applied in the long-term MODIS product partly differs from that of the currently used GLEMOS dataset, so a part of the forests is attributed to woody savannas (this type requires tree coverage 30-60%). Besides, a part of the forests, grasslands and shrublands is classified as savannas (which requires tree coverage 10-30%). There is also a decrease in the fractions of both croplands and urban areas in the long-term MODIS data product compared to the currently used one. The distribution of surface types in processed CORINE is generally similar to the distribution in MODIS products (Fig. 4.15). The main differences are that in processed CORINE there are more urban territories as well as barren and almost completely missing savannas and woody savannas fractions. More information, in particular on long-term changes of land cover in various regions and effect of these changes on the modelling results, is presented in MSC-E Technical Report [*Travnikov et al.*, 2021].

The necessity to use in the modelling such a wide variety of land cover datasets is explained by the fact that currently there is still no agreed land cover dataset to be used by the EMEP centres and Working Group on Effects. A harmonized dataset is crucial for assessment of ecosystem-dependent deposition fluxes and evaluation of ecosystem critical load exceedances.

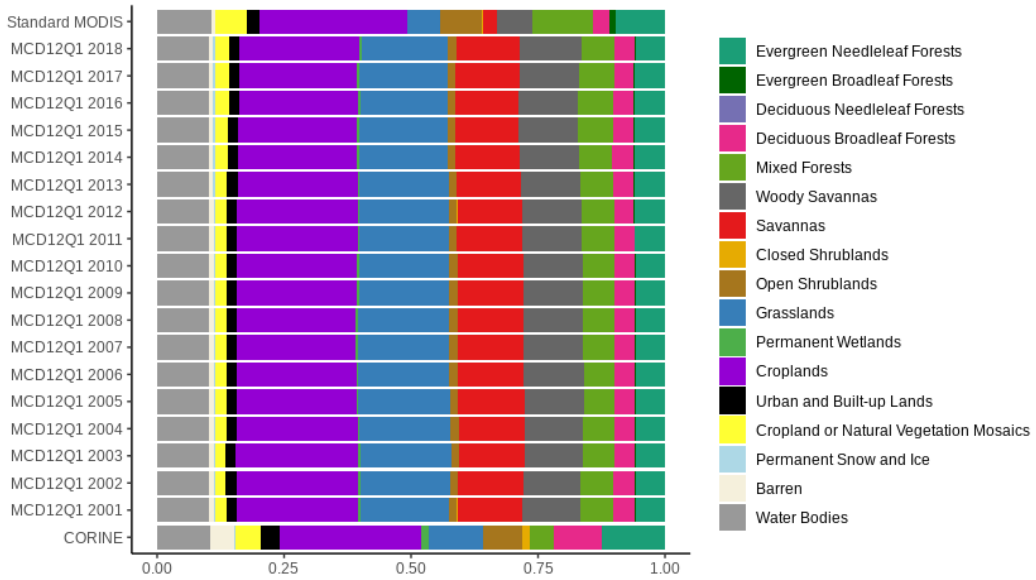

Fig. 4.15. *Comparison of fractions of underlying surface types between the basic GLEMOS land cover dataset, the preprocessed CORINE dataset and long-term IGBP layer from MODIS MCD12Q1 data product for 2001-2018 time period in the European region.*

4.5. Updates of Hg operational modelling with GLEMOS

Calculations of Hg pollution levels in the EMEP countries are performed using the operational version of the GLEMOS model (v2.2.1, http://en.msceast.org/index.php/j-stuff/glemos). The model assessment involves variety of input data needed for simulation of Hg atmospheric concentrations and deposition, which include anthropogenic, natural and secondary emissions, meteorological fields, concentrations of reactants involved in Hg chemical transformations, surface characteristics, etc. Both the model parameterisations and input data require periodical revisions and updates to keep the model in line with new findings of the scientific community.

Recent updates of the GLEMOS modelling system for Hg include utilizing a new global Hg emissions inventory for calculations of boundary conditions for the EMEP regional domain and an improved dataset of chemical reactants concentrations in the atmosphere. The multi-scale approach used for the operational EMEP simulations requires the model application on both regional and global scales to take into account possible effect of intercontinental transport on pollution levels in the EMEP countries. Therefore, a combination of the EMEP regional emissions dataset based on the officially reported data and a global emissions inventory is used for the modelling (Section 1.2). A new global Hg emissions inventory for 2015 developed as a part of the UNEP Global Mercury Assessment 2018 [*AMAP/UNEP*, 2019] has been tested and prepared for operational modelling along with revision of the estimates of Hg natural and secondary emissions. In addition, a new data on air concentration of substances (e.g. O_3, OH, Br, $PM_{2.5}$) that take part in Hg redox reactions in the atmosphere was derived from the GEOS-Chem model output [*Travnikov et al.*, 2020] and tested for Hg modelling. Evaluation of the GLEMOS updates against the original version of the model is discussed below.

Figure 4.16 shows comparison of simulated Hg^0 air concentrations on a global scale based on the original and updated versions of the model (Figs. 4.16a and b) as well as evaluation of both simulations against measurements (Fig. 4.16c). Two measurement datasets were used in the study – Hg^0 measurements for 2019 from the EMEP monitoring network in Europe [*EBAS*, 2021] and the most recent available measurement data for 2018 from the AMNet network in North America [*NADP/AMNet*, 2021]. The updated simulations provide generally lower levels of Hg^0 concentration in most regions of the globe than results of the original version. In particular, simulated Hg^0 concentrations decreased from 1.5-1.7 ng/m^3 to 1.4-1.5 ng/m^3 in Europe and from 1.4-1.6 ng/m^3 to 1.3-1.4 ng/m^3 in North America that better agrees with observations. As a result the updated simulations provide more realistic boundary conditions for the regional modelling.

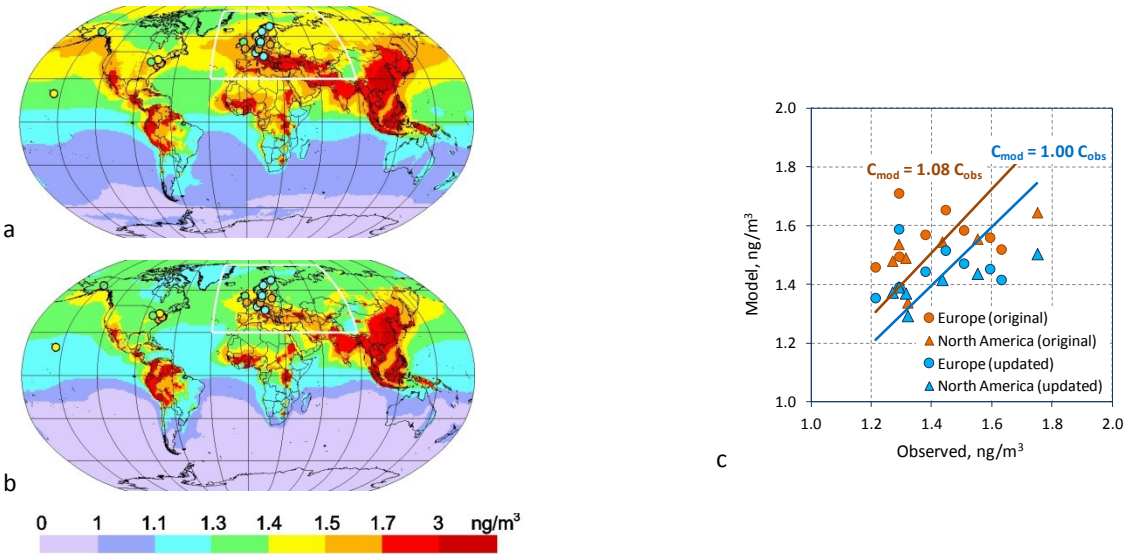

Fig. 4.16. *Global distribution of Hg^0 air concentration in 2019 according to calculations with the original (a) and updated (b) model, and evaluation of the modelling results against observations in Europe (EMEP) and North America (AMNet)(c). White line on the maps depicts boundary of the EMEP region.*

In addition to the improvement of Hg^0 concentrations, the model updates led to changes in simulated Hg wet deposition. Atmospheric chemistry determines *in situ* transformations of Hg^0 into more soluble and reactive Hg oxidated forms and, therefore, directly affects Hg wet deposition flux. Thus, utilizing more correct data on air concentrations of chemical reactants results in improvement of the modelled wet deposition. Comparison of the updated and original wet deposition flux in the EMEP region is shown in Fig. 4.17. As seen the updated results show lower wet deposition over most parts of the model domain than the original ones (Figs. 4.17a and b). As a consequence, a general overestimation (by 25%) of observed wet deposition values by the original version vanishes when the updated model version is used (Fig. 4.17c).

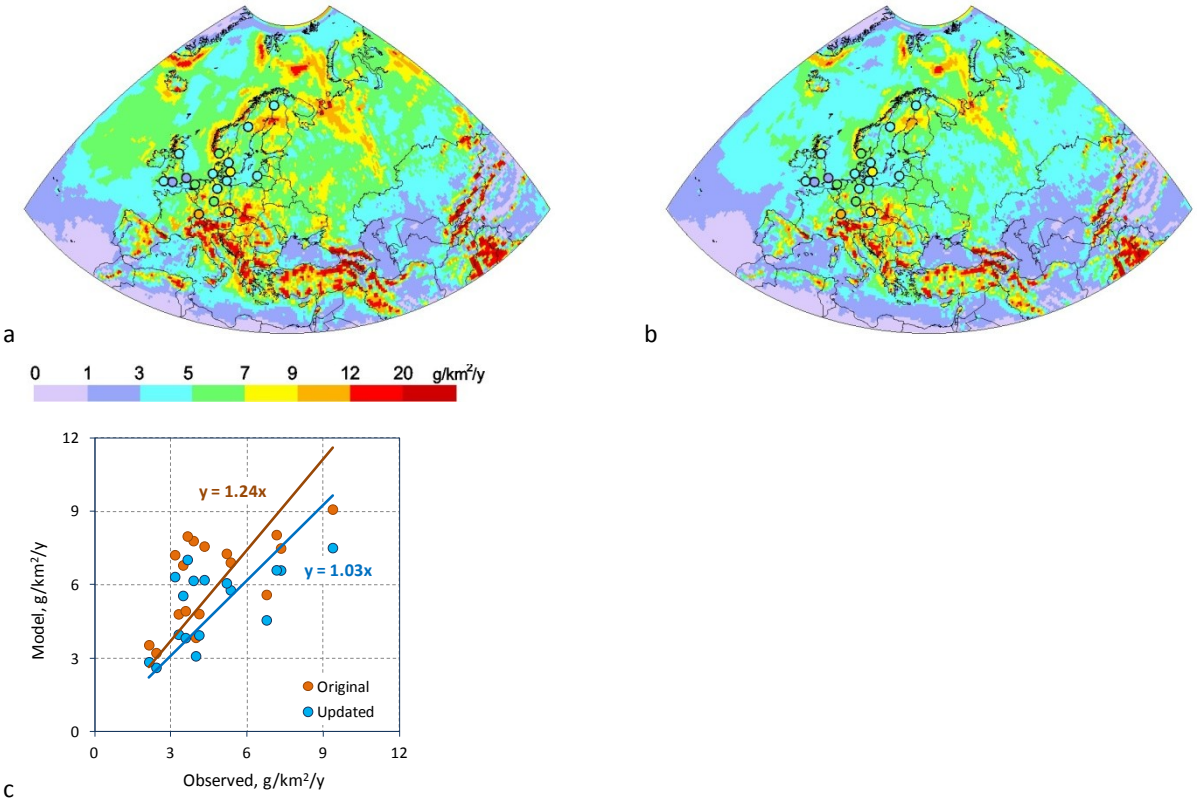

Fig. 4.17. *Distribution of Hg wet deposition in the EMEP region in 2019 according to calculations with the original (a) and updated (b) model, and evaluation of the modelling results against EMEP observations(c).*

Thus, the updated version of the model demonstrates better performance than the original one in terms of comparison with observations. Besides, it should be noted that the Centre continues research activities, focused on the study of Hg chemical mechanisms in the atmosphere, in collaboration with other scientific groups. In particular, a newly developed scheme of Hg photo-reduction in the atmosphere has been recently tested and evaluated [*Saiz-Lopez et al.*, 2020]. The study of Hg atmospheric chemistry is currently continued with a focus on Hg^0 heterogenic oxidation. The ultimate aim of the research is improvement of the model estimates of Hg pollution levels in the EMEP countries.

4.6. Potential of long-range transport of microplastics in the atmosphere

Pollution by microplastics is recognized as an urgent and global problem due to their high persistence and negative impact on human health and environment [*Plastics Europe*, 2018; *European Commission*, 2019; *European Parliament*, 2019; *Da Costa et al.*, 2020]. Besides, microplastics are regarded as emerging contaminants [*Hartl et al.*, 2015].

Human exposure to microplastics occurs through its ingestion with drinking water or from food chains [*WHO*, 2019; *Setälä et al.*, 2014; *Zhao et al.*, 2018; *Liu et al.*, 2019]. Recent studies have shown

that inhalation of atmospheric microplastic should also be considered [*Prata*, 2018; *Abbasi et al.,* 2019; *Liu et al.,* 2019]. The adverse health effects of microplastics may be related to the presence of toxic components such as monomers, pigments, plasticizers, flame retardants and other additives [*Gasperi et al.*, 2018; *Chen et al.*, 2019]. In addition to this, microplastics can absorb and accumulate other pollutants, including heavy metals and POPs, which pose health risks to human [*Jiang and Li*, 2020; *Wang et al.*, 2020].

According to the generally accepted definition, microplastics are particles less than 5 mm in size [*GESAMP*, 2015; *ECHA*, 2019]. Besides, for particles <1 µm in size, the term 'nanoplastics' is used [*Wagner and Reemtsma,* 2019; *Evangeliou et al,* 2020]. Atmospheric microplastics can be of various shapes, such as beads, fibres, films, flake, foam, fragments, pellets, spheres, etc. [*Zhang et al.*, 2020]. A number of studies indicate that fragments and fibres are predominant forms of microplastics in the atmosphere [*Cai et al.*, 2017; *Dris et al.*, 2015; *Klein et al.*, 2019; *Klein and Fischer*, 2019]. Based on chemical composition, microplastics can be classified into various types, including poly(vinyl acetate), poly(N-methyl acrylamide), polyurethane, rayon, teflon, ethylene vinyl acetate, polyethylene, terephthalate, epoxy resin, polyethylene, alkyd resin, polyacrylonitrile, polystyrene, polyester, polyamide, polypropylene [*Enyoh et al.*, 2019; *Liu et al.,* 2019]. Therefore, microplastics are characterized by a wide range of physicochemical characteristics that can influence their behavior in the atmosphere.

Possible sources of microplastics in the atmosphere and other environmental compartments include tire erosion, agricultural soil dust, waste incineration, sewage sludge, landfills, building materials, 3D printing, synthetic fabrics from clothing, household objects, abrasive powders, the re-suspension of urban dust [*Amato-Lourenço et al.*, 2020; *Catarino et al.*, 2018; *UNEP*, 2016; *Brahney et al.,* 2021]. At the moment, data on the quantitative characteristics of the emission of microplastics into the atmosphere are limited and further research is required. However, there are some estimates of emissions, for example, for microplastics produced by road traffic [*Evangeliou et al.*, 2020].

Once released into the atmosphere, microplastics can be transported over long distances, leading to their presence in remote regions without local sources of plastics. For example, microplastic particles have been found in the Arctic environments [*Bergmann et al.*, 2019], the Alps and the Tibetan glaciers [*Ambrosini et al.*, 2019; *Zhang et al.*, 2019], remote marine atmosphere [*Trainic et al.*, 2020]. However, the processes that determine the atmospheric transport of microplastics are poorly understood, and more research is needed [*Allen et al.,* 2019; *Dris et al.,* 2017].

It is planned to continue collection of information on microplastics relevant to the assessment of environment pollution as well as adverse effects on human health and ecosystems in cooperation with TFMM and TF HTAP.

Chapter 5. COOPERATION

Cooperation with the Subsidiary Bodies of the Convention, international and national organizations is highly important part of the MSC-E work. This work is aimed at dissemination of the Convention results. Besides, the cooperation favours improvement of the assessment of trans boundary pollution levels in the EMEP countries.

5.1. Subsidiary Bodies of the Convention

5.1.1. Task Force on Measurements and Modelling

An overview of the MSC-E activities in the field of assessment of heavy metal and POP pollution levels in the EMEP region and on a global scale was presented at the recent virtual TFMM meeting held in May, 2021.

Long-term changes of Hg and PAH pollution levels in Europe and other regions of the globe as well as main factors affecting the changes were evaluated. Model simulations showed that for the majority of regions the most important factor responsible for the long-term changes of pollution levels was changing of anthropogenic emissions. At the same time, in remote regions (e.g., the Arctic) other factors, such as changes of meteorological conditions and concentrations of atmospheric reactants, were also significant. Analysis of source attribution to long-term variability of pollution levels was carried out. It was demonstrated that from 1990 to 2018 the contribution of the European sources to Hg pollution levels in Europe and the Arctic was steadily decreasing while the contribution of the Asian sources was increasing . This work is being performed in cooperation with TF HTAP.

Long-term changes and source attribution of heavy metal and POP pollution were also investigated in the framework of cooperation with the regional marine conventions - HELCOM and OSPAR . Along with the pollutants, targeted by the Convention on regular basis, MSC-E performed model simulations for the second priority metals (Cu) and contaminants of emerging concern (PBDE). In addition to this, it was reported about contribution of MSC-E to the AMAP Mercury Assessment 2021. The MSC-E participated in the multi-model study aimed at the assessment of Hg pollution in the Arctic region. In addition to this, further development of the GLEMOS modelling system was presented. Finally, MSC-E has started collection of information on microplastics aimed at evaluation of its potential to long-range atmospheric transport.

Another direction of MSC-E activity was focused on the assessment of long-term changes of PAH pollution levels and contributions of major source categories in the EMEP region. It was shown that B(a)P concentrations in different parts of the EMEP region demonstrated slow decline or even some increase during the last two decades. Besides, the model estimates showed that the main contributor to the PAH levels in the EMEP region was the residential combustion emission sector. Furthermore, it was estimated that substantial part of population of the EMEP region in recent years was exposed to B(a)P concentrations exceeding the EU and WHO air quality guidelines. This work is

considered as a contribution to the analysis of POP Protocol effectiveness and to the activities of the Task Force on Health (TF Health) regarding assessment of PAH pollution health effects.

Along with this, main results of country-specific case study of PAH pollution in Poland were presented. In the framework of the study a new national inventory of B(a)P emissions in Poland was analyzed using fine resolution model simulations. Comparison of the modelling results with measurements indicated significant improvement of the quality of the model assessment due to updates of national emission data. Finally, a multi-model study of B(a)P pollution in Europe to be performed in the framework of TFMM/Eurodelta-Carb experiment, was outlined.

Directions of future research activities relevant to TFMM work were presented and discussed during the special sub-session of the meeting devoted to heavy metals, POPs, chemicals of emerging concern, and microplastics. In particular, it was suggested to improve understanding of sources of carbonaceous aerosols and toxic compounds (e.g. PAHs, PCDD/Fs, PCBs) from biomass burning and wildfires as well as re-suspension of heavy metals with the wind-blown dust on the base of the content of Al, Fe, Ti, Mn as tracers using combined monitoring and modelling studies. Besides, continuation of national scale case studies of heavy metal and POP pollution in the selected countries was discussed (e.g. continuation of B(a)P case study for Poland and other countries, initiation of Hg case study in cooperation with CCC based on the Hg monitoring activities in Norway). Besides, it was proposed to continue analysis of long-term trends of heavy metal and POP pollution levels in the EMEP region, involving measurement data and modelling results, with emphasis to regional seas in cooperation with HELCOM and OSPAR, and for the global scale in cooperation with TF HTAP. Finally, preparatory work for the analysis of pollution by the contaminants of emerging concern and of long-range transport of microplastics was discussed. Results of the discussion are intended to contribute to the development of future work plans of TFMM.

5.1.2. Task Force on Hemispheric Transport of Air Pollution

MSC-E is intensifying collaboration with the Task Force on Hemispheric Transport of Air Pollution (TF HTAP) on Hg and POP pollution assessment. In particular, the Centre and TF HTAP jointly hosted two workshops (online, 13 and 15 April 2021) to identify near-term opportunities and longer-term research needs to improve the scientific basis for assessment of Hg and POP pollution and trends. Specifically, the workshops were aimed at initiating cooperative research activities to better assess the regional and extra-regional contribution to long term trends of Hg and POPs as well as to identify additional issues or measures that might be addressed by the Convention to protect the environment and human health. Recognizing that the Hg and POP pollution is addressed by the Minamata and Stockholm Conventions as well as other regional bodies, including but not limited to the Arctic Council and the European Union, the future work of TF HTAP should be designed to both build upon the findings of recent efforts in other forums and provide useful information back to these forums to the extent possible. Thus, discussions at the workshops were particularly focused on:

- Reviewing progress made and anticipating assessment needs of CLRTAP, the Minamata and Stockholm Conventions, Arctic Monitoring and Assessment Programme, and other international forums;

- Identifying cooperative activities that can be undertaken in the short term (2 years) and longer term (5 years) to improve our understanding and ability to estimate Hg and POP pollution levels, trends and source attribution.

The workshops examined current work and efforts throughout the international science community aimed at addressing Hg and POP pollution problem on global and regional scales. Participants of the meetings explored potential synergies with the on-going activities within various international bodies and identified areas where new cooperative efforts under the Task Force could be the most impactful. Besides, a discussion of policy-relevant science questions was initiated to govern future co-operative research of Hg and POP regional and global pollution within TF HTAP.

A program of multi-model assessment and attribution of long-term Hg and POP pollution trends in the EMEP and other regions was proposed by MSC-E. The objectives of the assessment include retrospective analysis of pollution changes based on model estimates and measurement data, the trends attribution to changes in regional and extra-regional anthropogenic emissions, analysis of other factors affecting long-term pollution changes, as well as projection of future levels based on emission scenarios. Pilot results of a model assessment of Hg and POP pollution trends and their attribution to various factors (changes in anthropogenic emissions, meteorological conditions, atmospheric chemistry, land cover etc.) were presented to illustrate possible outcome of the study and input data required (see Section 4.1).

More detailed information on the TF HTAP Workshops on Hg and POP as well as description of the pilot simulations and analysis is available in the EMEP Technical Report 1/2021 [*Travnikov et al.*, 2021].

5.1.3. Task Force on Health

The twenty-fourth meeting of the Task Force on Health[7] (TF Health), attended by representatives from 34 Parties to the Convention, was held online on 10th and 11th May 2021. MSC-E took part in the meeting presenting the assessment of PAHs pollution levels in the EMEP region, key sources and trends. The assessment was prepared to contribute to the analysis of effectiveness of the Protocol on POPs in co-operation with the Task Force on Techno-economic Issues (TFTEI) and TF Health.

It was highlighted that biomass/fossil fuels combustion was the main source of PAHs emission, with the largest contribution made by residential combustion sector, and PAHs emissions did not change

[7] Task Force on the Health Aspects of Air Pollution (Task Force on Health) under the World Health Organization (WHO) European Centre for Environment.

significantly over the past 20 years. In relation to long-term changes of B(a)P pollution in the EMEP region, modelled B(a)P concentrations generally corresponded to the EMEP measurements, and no significant decrease of B(a)P concentrations in modelling results and measurement was found. Significant amount of population in the EMEP countries in recent years lived in the areas with exceeded EU target (1 ng/m^3) and WHO target (0.12 ng/m^3) values.

Recent studies of population exposure to PAHs indicated the need to evaluate joint toxicity of a mixture of different PAHs emitted to the atmosphere. Experimental model simulations of sixteen PAHs based on expert estimates of emissions showed that B(a)P-equivalent concentrations of sixteen PAHs exceeded EU target value in many countries. In relation to the contribution of PAHs to adverse effects of particulate matter (PM), air quality assessment for PM was often based on PM mass concentration without considering sources and chemical composition of particles. Impact of PM on human health might be more significant due to the presence of toxic constituents, including organic compounds, heavy metals, and other compounds [*WHO*, 2003c; 2013a; 2013b].

Ongoing and further EMEP research activities on PAHs were presented including analysis of trends and key sources of PAHs pollution in the EMEP region, case study on B(a)P pollution in Poland, and multi-model study of B(a)P pollution in the European countries under TFMM. The importance of data exchange with TF Health on B(a)P and PAHs concentration and exceedances of target values to assess population exposure and cooperation with international organizations was also highlighted.

5.2. International organizations

5.2.1. Arctic Monitoring and Assessment Programme (AMAP Assessment 2021)

EMEP continues co-operation with the Arctic Monitoring and Assessment Programme (AMAP). Recently, MSC-E participated in the AMAP Assessment of the Arctic pollution by Hg (AMAP Mercury Assessment 2021). The Centre contributed to the assessment providing the results of multi-model simulations and contributing to preparation of the report. In particular, MSC-E collected, processed and illustrated results of the multi-model simulations of Hg pollution levels in the Arctic based on the previous assessment [*AMAP/UN Environment*, 2019] and new modelling results. Four chemistry transport models for Hg from different institutions took part in the study – GLEMOS (EMEP/MSC-E), GEOS-Chem (Massachusetts Institute of Technology/Harvard University, USA), GEM-MACH-Hg (Environment and Climate Change Canada, Canada), DEHM (Institute of Atmospheric Pollution Research, Denmark). The modelling results include spatial patterns of Hg air concentration, wet and total deposition, source attribution of Hg deposition to the Arctic region, sub-regions and watersheds of large Arctic rivers.

Figure 5.1 shows simulated spatial distribution of Hg^0 air concentration in the Arctic in different seasons. Generally, seasonal average air concentrations of Hg^0 in the Arctic region vary within a relatively narrow range 1.1-1.6 ng/m^3 due long residence time of this Hg species in the atmosphere.

However, both spatial patterns and values of Hg^0 surface concentrations considerably alter among the seasons. In winter Hg^0 levels decrease gradually from the European and Siberian sectors of the Arctic (1.55 ng/m^3) to the high Arctic (1.4 ng/m^3) and further to the Hudson Bay (1.35 ng/m^3) (Fig. 5.1a). In spring average Hg^0 concentration declines down to 1.1 ng/m^3 over the high Arctic and the Canadian Archipelago because of the atmospheric Hg depletion events (AMDEs) (Fig. 5.2a). In contrast, during summer Hg^0 levels increase up to 1.5 ng/m^3 over the high Arctic due to intensive re-emission of Hg^0 from snow. At the same time Hg^0 concentration over terrestrial areas in Eurasia and North America decrease down to 1.3 ng/m^3 because of vegetation uptake. In fall concentrations remain relatively low (1.3-1.4 ng/m^3) over the most part of the Arctic. The modelled Hg^0 air concentrations in the Arctic well agree with available observations.

Spatial pattern of total Hg deposition reflects spatial variations of Hg scavenging by precipitation (wet deposition) and air-surface exchange (dry deposition). Both removal processes are largely determined by direct emissions of oxidised Hg forms from anthropogenic sources or oxidation of Hg^0 in the atmosphere. Wintertime is characterised by relatively low Hg deposition in the Arctic (below 3 μg/m^2/y) due to low oxidation capacity of the atmosphere during polar night and limited air-surface exchange (Fig. 5.2a). The deposition flux increases largely (above 15 μg/m^2/y) in the high Arctic in spring during AMDEs when atmospheric Hg^0 is intensively oxidized and removed to the surface (Fig. 5.2b). In summer Hg deposition significantly decreases over the Arctic ocean (down to 5 μg/m^2/y) and increases over terrestrial areas (above 20 μg/m^2/y) due to strong dry deposition via air-vegetation exchange of Hg^0 (Fig. 5.2c). Deposition decreases in fall down to 7-12 μg/m^2/y over the sub-Arctic territories and remains relatively low (below 5 μg/m^2/y) over the high Arctic (Fig. 5.2d).

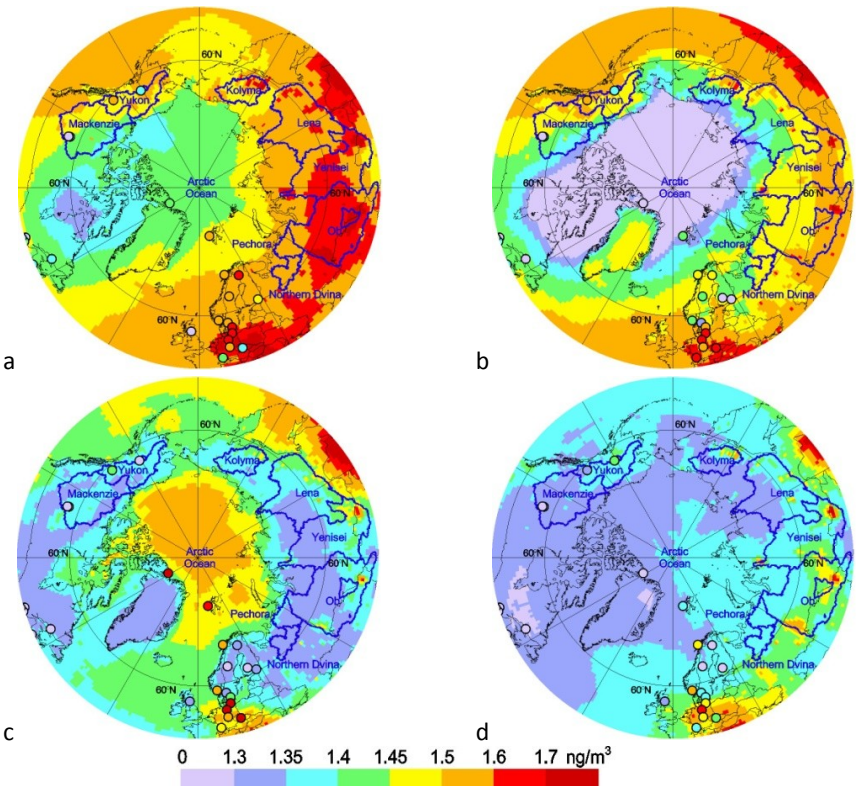

Fig. 5.1. *Model ensemble median Hg^0 air concentration in the Arctic in winter (a), spring (b), summer (c) and fall (d) of 2015. Circles show observations in the same color scale.*

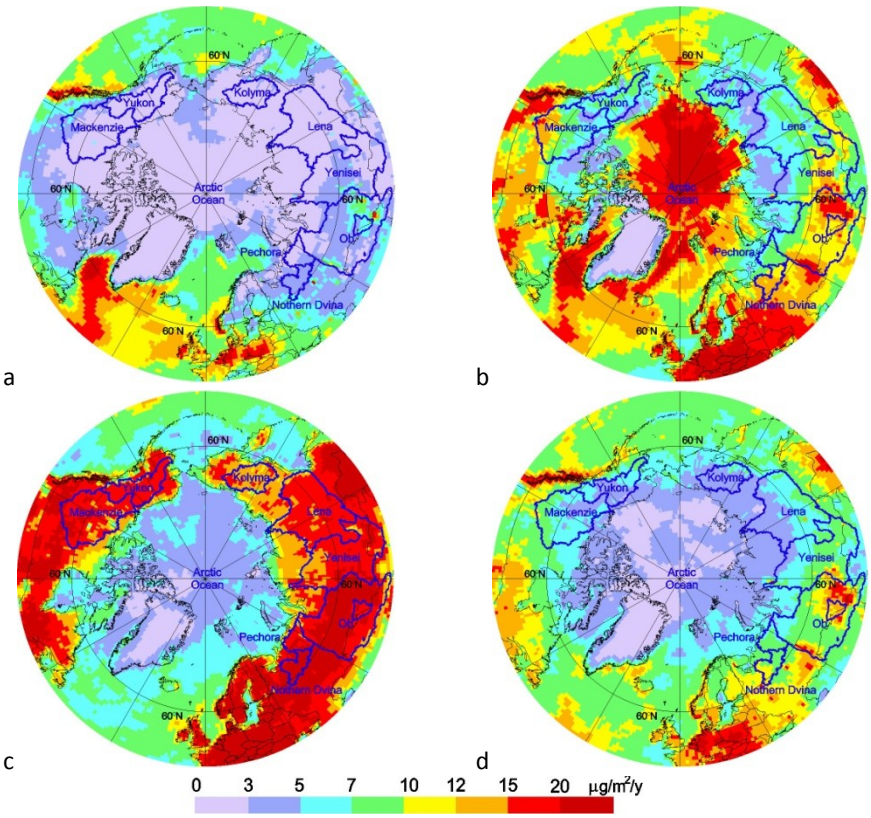

***Fig. 5.2**. Model ensemble median Hg deposition in the Arctic in winter (a), spring (b), summer (c) and fall (d) of 2015.*

Detailed discussion of various aspects of the Arctic pollution with Hg including emissions, atmospheric and oceanic transport, cycling and accumulation in aquatic and terrestrial ecosystems, as well as human and biota exposure is available in the AMAP Mercury Assessment 2021. The main findings of the assessment are also formulated in the policy-oriented summary [*AMAP*, 2021].

5.2.2. Minamata and Stockholm Conventions

EMEP continues co-operation with the Minamata Convention on Mercury. In particular, MSC-E took part in the Minamata Online Session "Multimedia modelling of global mercury movement" co-organized by the Minamata Convention Secretariat, UNEP Global Mercury Partnership and the International Conference on Mercury as a Global Pollutant (ICMGP). The session aimed to bridge the scientific community and international policy to better understand abilities of the multimedia mercury modelling for assessing the state of the environment and effectiveness of pollution control measures. The Centre presented the experience gained under the LRTAP Convention on atmospheric modelling of mercury transport and fate in the environment. It also participated in the discussion of the key uncertainties and further efforts needed to improve the model assessment. Closer integration of the relevant activities within CLRTAP and the Minamata Convention could facilitate resolving the Hg pollution problem both in the EMEP region and on a global scale.

In framework of co-operation with the Stockholm Convention, MSC-E took part in the online expert meeting that initiated the development of the third global monitoring report under the global monitoring plan (GMP) for POPs (held on 24-25 June 2021). The meeting discussed the general approach and format of the report including the strategy of its compilation and working plan. The report will synthesize information from the previous stages of the work under the GMP as well as current findings on POP concentrations at the global scale to support the effectiveness evaluation of the Stockholm Convention. Comparing to the previous reports, the present one will pay more attention to the detection of temporal trends for a larger number of chemicals. In addition, it is planned that the report will also address aspects relevant to long-range transport of POPs and climate change effects from a global perspective, and will include new information on all POPs from the newly implemented monitoring programmes.

5.2.3. European Commission

The international project "*Global Mercury Observation and Training Network in Support to the Minamata Convention*" (GMOS-Train, www.gmos-train.eu) has been recently launched as a part of the Marie Skłodowska-Curie Actions (Innovative Training Networks) of the European Commissions (EC). The objectives of the GMOS-Train project are (1) to provide urgently needed training of Early Stage Researchers in Hg science, and (2) to fill key knowledge gaps in biogeochemical Hg cycling linking anthropogenic emissions and Hg in marine food webs. With the purpose to better understand the global exchange of Hg between atmosphere, hydrosphere, lithosphere, and biosphere, the next generation of young researchers will gain expertise through a network-based, highly interdisciplinary research training programme including atmospheric chemistry and physics, aquatic chemistry, ecology, analytical chemistry, multimedia modelling, and the use of science results for policy making. An additional feature is the strong inter-sectoral collaboration involving academic and non-academic partners, non-governmental and international organizations.

MSC-E participates in the GMOS-Train project as an external partner contributing to the work of the Supervisory Board. In particular, the Centre took part in the kick-off meeting of the project (virtual, 7-8 December 2020) aimed at presentation of the project programme and discussion of practical steps and coordination of the research activities. Further co-operation of EMEP with the European Commission in the field of Hg research will improve Hg pollution assessment within the Convention and facilitate outreach of the gained expertise to EC and other national and international bodies.

5.2.4. Helsinki Commission

In accordance with the Memorandum of Understanding between the Baltic Marine Environment Protection Commission (HELCOM) and the United Nations Economic Commission for Europe (UN ECE) MSC-E is responsible for regular evaluation of atmospheric input of heavy metals and POPs to the Baltic Sea. This work is performed on the basis of the long-term contract between the EMEP Centres and HELCOM. According to the contract, during this year atmospheric deposition of selected heavy metals and POPs to the Baltic Sea was estimated for the period 1990-2018. This information is

based on the results presented to the Sixth Joint session of the Working Group on Effects and the Steering Body to EMEP, which took place on 14-18 September 2020.

Updated data on emissions of selected heavy metals and POPs, modelled deposition fields, and allocation budgets were presented in the Joint report of the EMEP Centres for HELCOM [*Gauss et al.,* 2020] as well as in the indicator fact sheets, published on the HELCOM website (*http://www.helcom.fi*). Unlike the previously published model estimates of heavy metal and POP deposition to the Baltic Sea [*Gauss et al.,* 2018, 2019], this year the model simulations were performed on the new latitude-longitude EMEP grid using the latest version of the GLEMOS model. Changes in the long-term deposition trends caused by the transition to the new modelling grid and the GLEMOS model were thoroughly examined and documented in the report.

Anthropogenic emissions of Cd, Hg, B(a)P and PCB-153 reduced from 1990 to 2018 by 50%, 63%, 42% and 80%, respectively. The most substantial decline of the emissions took place in 1990s, while after 2000-2005 the rate of emission reduction slowed down (Fig. 5.3). In 2018 the main contributions to Cd, Hg and B(a)P emissions among the HELCOM countries were made by Russia, Poland and Germany. Their emissions in total contributed more than 90% to total emissions of the HELCOM countries. In case of PCB-153, main contributors were Germany, Poland, and Russia with aggregated share amounting to almost 80%.

Model simulations indicated large decline of Cd , Hg, B(a)P, and PCB-153 deposition to the Baltic Sea from 1990 to 2018 by 73%, 35%, 48%, and 71%, respectively (Fig. 5.3). Modelling results showed significant inter-annual variability of atmospheric deposition caused by the changes of meteorological conditions (precipitation amount, atmospheric transport patterns) from year to year. Decline of calculated deposition varied among the different sub-basins of the Baltic Sea. Particularly, the highest reduction of Cd deposition was noted for the Gulf of Finland and the Sound sub-basins (around 80%). The most significant reduction of Hg deposition took place in the Sound (60%) and the Western Baltic (55%) sub-basins. In case of B(a)P the highest decline was estimated for the Western Baltic sub-basin (around 70%). The most substantial reduction of PCB-153 deposition (around 80%) was indicated for the Kattegat, Sound and Western Baltic sub-basins. In spite of general decline, atmospheric deposition to some of the sub-basins increased during the considered period (in particular, Hg deposition to the Bothnian Bay sub-basin in 2018 were higher by 23% compared to 1990).

Anthropogenic emission sources of the HELCOM countries contributed 39% (Cd), 15% (Hg), 74% (B(a)P) and 24% (PCB-153) to deposition to the Baltic Sea. Emissions of Poland and Germany were the main contributors to anthropogenic deposition of heavy metals (Cd and Hg). Main anthropogenic sources of B(a)P deposition were Poland and Russia. In case of PCB-153 the highest contribution of anthropogenic sources to atmospheric input to the Baltic Sea was made by the sources of Finland and Sweden. Significant contribution to the deposition was made by the secondary emissions (e.g. re-emission from soil and sea water compartments) and non-EMEP sources. The share of these sources was the lowest for B(a)P equalling to about 20%, while for for Cd, Hg, and PCB-153 it was about 50%, 70%, and 80%, respectively (Fig. 5.3).

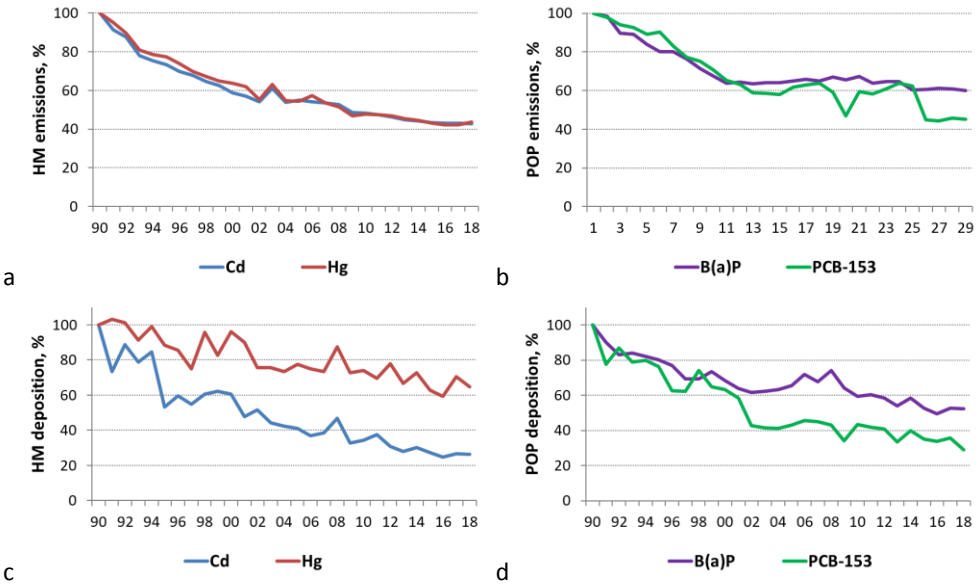

Fig. 5.3. *Relative changes of annual total emissions of HELCOM countries (a,b) and annual atmospheric Cd, Hg, B(a)P and PCB-153 deposition (c,d) to the Baltic Sea in the period 1990-2018.*

The information on airborne input of Cd, Hg, B(a)P and PCB-153 to the Baltic Sea was presented and discussed during the 12th online Meeting of the Working Group on Reduction of Pressures from the Baltic Sea Catchment Area (HELCOM PRESSURE 12-2020), in October 2020.

5.2.5. OSPAR

Convention for the Protection of the Marine Environment of the North-East Atlantic (OSPAR Convention) was adopted by 13 signatory states in 1992. In order to administer the OSPAR Convention and to develop policy and international agreement in the field of marine environment protection the OSPAR Commission was established. The work of the OSPAR Commission is focused on the following main areas:

- Protection and conservation of ecosystems and biological diversity;
- Hazardous substances;
- Radioactive substances;
- Eutrophication;
- Environmental goals and management mechanisms for offshore activities.

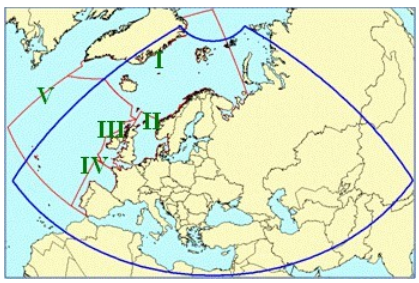

Fig. 5.4. *Location of the EMEP domain (blue line) and OSPAR regions (red line).*

This year cooperation between OSPAR and MSC-E has been resumed. It is planned to simulate deposition of Pb, Cd and Hg to the sub-regions of the OSPAR maritime area (Fig. 5.4) for the period from 1990 to 2019. Besides, source-receptor matrices will be simulated for the OSPAR regions for selected years (1995, 2005 and 2015). Since the regions I and V are not fully covered by the EMEP domain, global scale simulations will be carried out to assess long-term deposition changes and to establish source attribution.

MAIN CHALLENGES AND DIRECTIONS OF FUTURE RESEARCH

The key results of the EMEP activities related to POPs and heavy metals are summarized in the Status Report. The report includes information on emissions, monitoring and model assessment of transboundary transport of the considered pollutants. Bedsides, outcomes of the ongoing research and cooperation with the Subsidiary Bodies of the Convention and international organizations are overviewed. Main challenges of heavy metal and POP pollution assessment and proposals for directions of future research are summarized below.

- Reporting of heavy metals and POPs by countries is often inconsistent across years and sectors. Recalculations of NFR categories bigger than ±50% particularly for POPs are not rare. Also marked differences between countries with similar general conditions (economic situation, geographic location, etc.) are frequent. Thus, every year reported data of several countries has to be replaced by expert estimates. CEIP will continue the review of reported inventories also in 2022-23 and findings will be communicated to Parties and published so that the Parties can improve their emission inventories in the following submission.
- CEIP will also continue improving the dataset for modellers. It is planned to further elaborate the gap-filling procedures and the spatial distribution of the gap-filled datasets. In addition CEIP plans to check the sectoral emissions and spatial distribution of selected heavy metals and POPs by comparison of EMEP gridded emissions with other data sources (e.g. data submitted under the Minamata Convention for Hg).
- High PAH levels in the EMEP countries and slow pollution reduction are recognized as an important issue within the Convention that needs further scientific research. Detailed assessment of PAH pollution levels will be continued with focus on the analysis of population exposure to PAH and atmospheric aerosol from combustion sources. In particular, MSC-E will contribute to a multi-model study of B(a)P pollution levels as a part of the TFMM/EuroDelta-Carb intercomparison exercise.
- Pollution levels of Hg and a number of POPs in the EMEP region are caused by both the EMEP sources and sources located in other parts of the globe. Activities aimed at improvement of the modelling approaches for assessment of Hg and POP long-term trends, source-receptor relationships, and future projections on both global and regional scale will be initiated by MSC-E in collaboration with TF HTAP. The future research will include a multi-model study of Hg dispersion and cycling on a global scale with focus on air-surface exchange and secondary/natural emissions, global/regional multi-model evaluation of source-receptor relationships for combustion-related POPs, as well as contribution to the TF THAP exploratory workshops on wildfires, chemicals of emerging concern (CEC) and microplastics.
- In-depth analysis of pollution levels for individual countries in co-operation with national experts and involving variety of national data allows analysis of national emissions and monitoring data as well as improvement of the model assessment on both national and regional scales. MSC-E will continue the country-scale assessment of heavy metal and POP pollution in a form of case studies aiming at detailed analysis of pollution levels in selected countries and refinement of the EMEP operational modelling.

- Investigation of adverse effects caused by atmospheric pollution on the environment is important activity within the Convention coordinated by WGE. MSC-E plans to continue ecosystem-related analysis of heavy metal pollution and trends in cooperation with WGE. In particular, long-term trends of heavy metal deposition and measured concentrations in mosses will be examined. Besides, assessment of long-term trends of heavy metals in ecosystems (e.g. water courses) in relation to long-term and large-scale deposition trends will be carried out.
- Aquatic ecosystems and biota are vulnerable to contamination with toxic substances such as heavy metals and POPs. Therefore, information on the marine pollution is in demand in various national, regional and international regulations. Assessment of atmospheric pollution of the marine environment with heavy metals and POPs will be performed by MSC-E in co-operation with HELCOM and OSPAR and will include model evaluation of long-term trends and source apportionment of atmospheric load of heavy metals and POPs to the Baltic and North Seas.
- EMEP co-operation with other international organizations is an important activity aimed at dissemination of information and data exchange. MSC-E will continue collaboration with the Stockholm and Minamata Conventions in relation to assessment of POP and Hg long-range transport and trends. In particular, the Centre will take part in compilation of the third Global GMP Report on POPs being prepared under the Stockholm Convention.

REFERENCES

Aas W., Breivik K., Nizzetto P.B., Pfaffhuber K. A. [2021] Heavy metals and POP measurements 2019 EMEP/CCC-Report 3/2021.

Abbasi S., Keshavarzi B., Moore F., Turner A., Kelly F.J., Dominguez A.O., Jaafarzadeh N. [2019] Distribution and potential health impacts of microplastics and microrubbers in air and street dusts from Asaluyeh County, Iran. *Environ. Pollut*. 244, 153–164. https://doi.org/10.1016/j.envpol.2018.10.039.

Abdel-Shafy H.I., Mansour M.S.M. [2016]. A review on polycyclic aromatic hydrocarbons: Source, environmental impact, effect on human health and remediation. Egyptian Journal of Petroleum, 25(1), 107–123. doi:10.1016/j.ejpe.2015.03.011.

Allen S., D. Allen, V.R. Phoenix, G. Le Roux, P. Duranteza, A. Simonneau, B. Stéphane, D. Galop [2019] Atmospheric transport and deposition of microplastics in a remote mountain catchment Nat. Geosci., 12, pp. 339-344, 10.1038/s41561-019-0335-5

ALS [2013] Benzo(a)pyrene toxic equivalence quotient (TEQ) and aggregate organochlorine pesticides parameters, *EnviroMail* No. 59 Re-Release, July, 2013.

AMAP [2021] 2021 AMAP Mercury Assessment. Summary for Policy-makers. Arctic Monitoring and Assessment Programme (AMAP), Oslo, Norway. 16 pp

AMAP/UN Environment [2019] Technical Background Report for the Global Mercury Assessment 2018. Arctic Monitoring and Assessment Programme, Oslo, Norway/UN Environment Programme, Chemicals and Health Branch, Geneva, Switzerland. viii + 426 pp including E-Annexes.

AMAP/UNEP [2019] Technical Background Report for the Global Mercury Assessment 2018. Arctic Monitoring and Assessment Programme, Oslo, Norway/UN Environment Programme, Chemicals and Health Branch, Geneva, Switzerland. viii + 426 pp including E-Annexes.

Amato-Lourenço L.F., dos Santos Galvão L., de Weger L.A., Hiemstra P.S., Vijver M.G., Mauad T. [2020] An emerging class of air pollutants: Potential effects of microplastics to respiratory human health? Science of The Total Environment 749, 141676. https://doi.org/10.1016/j.scitotenv.2020.141676

Ambrosini R., Azzoni R.S., Pittino F., Diolaiuti G., Franzetti A., Parolini M. [2019] First evidence of microplastic contamination in the supraglacial debris of an alpine glacier. *Environmental Pollution* 253, 297–301. https://doi.org/10.1016/j.envpol.2019.07.005

Barber J.L., Thomas G.O., Kerstiens G., Jones K.C. [2004] Current issues and uncertainties in the measurement and modelling of air–vegetation exchange and within-plant processing of POPs. Environmental Pollution 128, 99–138. https://doi.org/10.1016/j.envpol.2003.08.024

Bash J.O. [2010] Description and initial simulation of a dynamic bidirectional air-surface exchange model for mercury in Community Multiscale Air Quality (CMAQ) model. *J. Geophys. Res*. 115, D06305. https://doi.org/10.1029/2009JD012834

Bebkiewicz K., Z. Chłopek, A. Doberska, M. Kanafa, I. Kargulewicz, A. Olecka, J. Rutkowski, J. Skośkiewicz, S. Waśniewska, D. Zasina, M. Zimakowska-Laskowska, and M. Żaczek [2020] Poland's Informative Inventory Report 2020. Submission under the UN ECE Convention on Long-range Transboundary Air Pollution and Directive (EU) 2016/2284. Air pollutant emissions in Poland 1990–2018. Warsaw 2020.

Belon E., Boisson M., Deportes I.Z., Eglin T.K., Feix I., Bispo A.O., Galsomies L., Leblond S. and Guellier C.R. [2012]. An inventory of trace elements inputs to French agricultural soils. *Science of the Total Environment*, 439 (2012) 87–95.

Bergmann, M., S. Mützel, S. Primpke, M.B. Tekman, J. Trachsel, G. Gerdts [2019] White and wonderful? Microplastics prevail in snow from the Alps to the Arctic. Sci. Adv., 5, p.eaax1157, 10.1126/sciadv.aax1157

Blunden J. and D.S. Arndt, Eds., [2020]. State of the Climate in 2019. *Bull. Amer. Meteor. Soc.*, **101** (8), Si–S429 https://doi.org/10.1175/2020BAMSStateoftheClimate.

Blunden J. and D.S. Arndt, Eds., [2019]. State of the Climate in 2018. *Bull. Amer. Meteor. Soc.*, **100** (9), Si–S305, doi:10.1175/2019BAMSStateoftheClimate.1.

Bogdal C., Müller C.E., Buser A.M., Quante M., Wang Z., Scheringer M., Gerecke A.C., Schmid P., Zennegg M., MacLeod M. and K.Hungerbühler [2014] Emissions of Polychlorinated Biphenyls, Polychlorinated Dibenzo-p-dioxins, and Polychlorinated Dibenzofurans during 2010 and 2011 in Zurich, Switzerland. *Environ. Sci. Technol.,* 48, 482−490.

Brahney J., Mahowald N., Prank M., Cornwell G., Klimont Z., Matsui H., Prather K.A. [2021] Constraining the atmospheric limb of the plastic cycle. Proc Natl Acad Sci USA 118, e2020719118. https://doi.org/10.1073/pnas.2020719118

Breivik K., Alcock R., Li Y.-F., Bailey R.E., Fiedler H. and J.M.Pacyna [2004] Primary sources of selected POPs: regional and global scale emission inventories. *Environmental Pollution,* 128, 3–16.

Breivik K., Sweetman A., Pacyna J.M. and K.C.Jones [2007] Towards a global historical emission inventory for selected PCB congeners - A mass balance approach-3. An update. *Science of the Total Environment*, 377, 296-307.

Brown T.N., Wania F. [2008] Screening chemicals for the potential to he persistent organic pollutants: A case study of Arctic contaminants. *Environ Sci Technol.,* 42: 5202-5209.

Büttner G., Kosztra B., Soukup T., Sousa A. and Langanke T. [2017] CLC2018 Technical Guidelines. Service Contract No 3436/R0-Copernicus/EEA.56665. 60p.

Cai L., J. Wang, J. Peng, Z. Tan, Z. Zhan, X. Tan, Q. Chen. [2017] Characteristic of microplastics in the atmospheric fallout from Dongguan city, China: preliminary research and first evidence. *Environ. Sci. Pollut. Res.*, 24, pp. 24928-24935, 10.1007/s11356-017-0116-x.

Carlsson P., Vrana B., Sobotka J., Borgå K., Bohlin Nizzetto P., Varpe Ø. [2018] New brominated flame retardants and dechlorane plus in the Arctic: Local sources and bioaccumulation potential in marine benthos. *Chemosphere*; 211: 1193-1202.

Catarino A.I., Macchia V., Sanderson W.G., Thompson R.C., Henry T.B. [2018] Low levels of microplastics (MP) in wild mussels indicate that MP ingestion by humans is minimal compared to exposure via household fibres fallout during a meal. *Environ. Pollut.*;237:675–684.

Chen G., Feng Q., & Wang J. [2019] Mini-review of microplastics in the atmosphere and their risks to humans. *Science of The Total Environment*, 135504. doi:10.1016/j.scitotenv.2019.135504

CLRTAP [2017]. Mapping critical loads for ecosystems, Chapter V of Manual on methodologies and criteria for modelling and mapping critical loads and levels and air pollution effects, risks and trends. UNECE Convention on Long-range Transboundary Air Pollution; accessed 10.12.2020 at www.icpmapping.org.

Colette A. et al. [2016] Air pollution trends in the EMEP region between 1990 and 2012. EMEP: CCC-Report 1/2016, Kjeller, Norway.

Crippa M., Solazzo E., Huang G., Guizzardi D., Koffi E., Muntean M., Schieberle C., Friedrich R. and Janssens-Maenhout G. [2019] High resolution temporal profiles in the Emissions Database for Global Atmospheric Research (EDGAR), *Nature Scientific Data*, 2019.

Da Costa J.P., Mouneyrac C., Costa M., Duarte A. C., & Rocha-Santos T. [2020]. The Role of Legislation, Regulatory Initiatives and Guidelines on the Control of Plastic Pollution. Frontiers in Environmental Science, 8. doi:10.3389/fenvs.2020.00104

De Vries W., Posch M., Sverdrup H.U., Larssen T., de Wet H.A., Bobbink R. and Hettelingh J-P. [2015a] Geochemical indicators for use in the computation of critical loads and dynamic risk assessment. pp 15-58. In: Critical loads and dynamic risk assessments. Nitrogen, acidity in terrestrial and aquatic ecosystems. Edited by W. de Vries, J-P. Hettelingh and M. Posch. *Envitornmental pollution* 25, Springer.

De Vries W, Groenenberg J.E. and Posch M. [2015b] Mass balance approaches to assess critical loads and target loads of metals for terrestrial and aquatic ecosystems. pp. 207-222. In: Critical loads and dynamic risk assessments. Nitrogen, acidity in terrestrial and aquatic ecosystems. Edited by W. de Vries, J-P. Hettelingh and M. Posch. *Envitornmental pollution* 25, Springer.

De Wit H.A., Hettelingh J-P., and Harmens H. [2015] Trends in ecosystem and health responses to long-range transported atmospheric pollutants. Norwegian Institute for Water Research, 92p.

Dris R., J. Gasperi, C. Mirande, C. Mandin, M. Guerrouache, V. Langlois, B. Tassin. [2017] A first overview of textile fibers, including microplastics, in indoor and outdoor environments. Environ. Pollut., 221, pp. 453-458, 10.1016/j.envpol.2016.12.013

Dris R., C.J. Gasperi, A.V. Rocher, B.M. Saad, N. Renault, B. Tassin [2015] Microplastic contamination in an urban area: a case study in Greater Paris. *Environ. Chem.*, 12, pp. 592-599

EBAS [2021] EMEP Monitoring Network Database. http://ebas.nilu.no/

ECHA [2019] Annex to the Annex XV Restriction Report. Proposal for a Restriction. https://echa.europa.eu/documents/10162/13641/rest_microplastics_axvreport_annex_en.pdf/01741d07-f06b-bf32-8d6f-d6a8de54c4d0

ECHA [2018]. Support document for identification of lead (lead powder and lead massive) as a substance of very high concern because of its toxic for reproduction properties (article 57c). 7 p.

ECHA [2013]. Support document for identification of cadmium as a substance of very high concern because of its CMR properties and because of its adverse effects nn kidney and bone tissues after prolonged exposure, which cause probable serious effects to human health which give rise to an equivalent level of concern to those of CMR and PBT/vPvB. 24 p.

ECMWF [2021] Operational archive. https://www.ecmwf.int/en/forecasts/dataset/operational-archive. Accessed 13.07.2021

EEA [2020] Air quality in Europe — 2020 report. EEA Report No 09/2020, European Environment Agency. (https://op.europa.eu/en/publication-detail/-/publication/447035cd-344e-11eb-b27b-01aa75ed71a1/language-en/format-PDF/source-211446981) accessed 31 May 2021.

EMEP [2014] EMEP Manual for Sampling and Chemical Analysis, last revision 2014. https://projects.nilu.no//ccc/manual/.

EMEP/EEA [2013] EMEP/EEA air pollutant emission inventory guidebook – 2013. EEA Technical report No 12/2013. Available at: https://www.eea.europa.eu/publications/emep-eea-guidebook-2013.

EMEP/EEA [2016] EMEP/EEA air pollutant emission inventory guidebook – 2016. EEA Technical report No 21/2016. Available at: https://www.eea.europa.eu/publications/emep-eea-guidebook-2016.

EMEP/EEA [2019] EMEP/EEA air pollutant emission inventory guidebook – 2019. EEA Technical report No 13/2019. Available at: https://www.eea.europa.eu/publications/emep-eea-guidebook-2019.

Emmons L.K., Walters S., Hess P.G., Lamarque J.-F., Pfister G.G., Fillmore D., Granier C., Guenther A., Kinnison D., Laepple T., Orlando J., Tie X., Tyndall G., Wiedinmyer C., Baughcum S.L., and Kloster S. [2010] Description and evaluation of the Model for Ozone and Related chemical Tracers, version 4 (MOZART-4), *Geosci. Model Dev.*, 3, 43–67, doi:10.5194/gmd-3-43-2010.

Enyoh C.E., Verla A.W., Verla E.N., Ibe F.C., Amaobi C.E. [2019] Airborne microplastics: a review study on method for analysis, occurrence, movement and risks. Environ Monit Assess 191, 668. https://doi.org/10.1007/s10661-019-7842-0.

European Commission [2019] Environmental and health risks of microplastic pollution. Publications Office, LU. https://ec.europa.eu/info/sites/default/files/research_and_innovation/groups/sam/ec_rtd_sam-mnp-opinion_042019.pdf.

European Parliament [2019] Directive (EU) 2019/904 of the European Parliament and of the Council of 5 June 2019 on the Reduction of the Impact Of Certain Plastic Products On The Environment, in PE/11/2019/REV/1. Brussels: European Union.

Evangeliou N., Grythe H., Klimont Z., Heyes C., Eckhardt S., Lopez-Aparicio S., Stohl A. [2020] Atmospheric transport is a major pathway of microplastics to remote regions. Nat Commun 11, 3381. https://doi.org/10.1038/s41467-020-17201-9.

Feng W., Guo Z., Xiao X., Peng C., Shi L., Ran H., Xu W. [2020]. A dynamic model to evaluate the critical loads of heavy metals in agricultural soil. *Ecotoxicology and Environmental Safety*, 197, 110607.

Fiedler H. [2007] National PCDD/PCDF release inventories under the Stockholm Convention on Persistent Organic Pollutants, *Chemosphere,* 67, 96–108.

Friedl M., Sulla-Menashe D. [2019] *MCD12Q1 MODIS/Terra+Aqua Land Cover Type Yearly L3 Global 500m SIN Grid V006* [Data set]. NASA EOSDIS Land Processes DAAC. Accessed 2021-05-14 from https://doi.org/10.5067/MODIS/MCD12Q1.006.

Friedman C.L., Selin N.E. [2012] Long-Range Atmospheric Transport of Polycyclic Aromatic Hydrocarbons: A Global 3-D Model Analysis Including Evaluation of Arctic Sources. *Environ. Sci. Technol.* 46, 9501–9510. https://doi.org/10.1021/es301904d.

Gasperi J., Wright S.L., Dris R., Collard F., Mandin C., Guerrouache M., Langlois V., Kelly F.J., and Tassin B. [2018] Microplastics in air: Are we breathing it in? Current Opinion in Environmental Science & Health. 1:1-5.

Gauss M., A. Gusev, W. Aas, A. Hjellbrekke, I. Ilyin, H. Klein, A. Nyiri, O. Rozovskaya, V. Shatalov, I. Strijkina, and O. Travnikov [2020] Atmospheric Supply of Nitrogen, Cadmium, Lead, Mercury, PCDD/Fs, PCB-153, and B(a)P to the Baltic Sea. EMEP Centres Joint Report for HELCOM, EMEP MSC-W TECHNICAL REPORT 3/2020. (Available online at: https://emep.int/publ/helcom/2020/EMEP_TechnicalReport_3_2020.pdf).

Gauss M., A. Gusev, W. Aas, H. Klein and A. Nyiri [2019] Atmospheric Supply of Nitrogen, Cadmium, Lead, Mercury, and PCDD/Fs to the Baltic Sea in 2017. EMEP Centres Joint Report for HELCOM. EMEP MSC-W Technical Report 1/2019.

The Norwegian Meteorological Institute, Oslo, Norway. (Available online at: https://emep.int/publ/helcom/2019/index.html).

Gauss M., J. Bartnicki, A. Gusev, W. Aas and H. Klein [2018] Atmospheric Supply of Nitrogen, Cadmium, Mercury, Benzo(a)pyrene and PCB-153 to the Baltic Sea in 2016. Summary Report for HELCOM. MSC-W Technical Report 1/2018. (Available online at: https://emep.int/publ/helcom/2018/index.html).

GESAMP [2015] "Sources, fate and effects of microplastics in the marine environment: a global assessment" (Kershaw, P. J., ed.). (IMO/FAO/UNESCO-IOC/UNIDO/WMO/IAEA/UN/UNEP/UNDP Joint Group of Experts on the Scientific Aspects of Marine Environmental Protection). Rep. Stud. GESAMP No. 90, 96 p.

Gusev A., N.Batrakova, V. Shatalov [2021] Assessment of PAH pollution levels, key sources and trends: Contribution to analysis of the effectiveness of the Protocol on POPs. MSC-E Technical Report on PAHs 2/2021.

Gusev A. and N. Batrakova [2020] Assessment of PAH pollution levels, key sources and trends: contribution to analysis of the effectiveness of the POPs Protocol – progress report. MSC-E Technical Report 2/2020, June 2020.

Gusev A., I. Ilyin, V. Shatalov, O. Travnikov, N. Batrakova, O. Rozovskaya, I. Strijkina, K.Brevik, Nizzetto P.B., W. Aas, K. Mareckova, S. Poupa, C. Sosa, M. Tista, R. Wankmueller, F. Couvidat [2019] Assessment of transboundary pollution by toxic substances: Heavy metals and POPs. EMEP Status Report 2/2019, July 2019.

Gusev A., O.Rozovskaya, V.Shatalov, N.Vulykh, W. Aas, K. Breivik, F. Couvidat, and M.G. Vivanco [2018] Persistent Organic Pollutants: assessment of transboundary pollution on global, regional, and national scales. EMEP Status Report 3/2018.

Gusev A., O.Rozovskaya, V.Shatalov, N.Vulykh, P. Nizzetto, K. Breivik, and W.Aas [2017] Transboundary transport of Persistent Organic Pollutants with emphasis on PAHs: regional and national scale assessment and transition to the new EMEP grid. EMEP Status Report 3/2017.

Gusev A., Shatalov V. and O.Rozovskaya [2014] Pilot Modelling of PCDD/F Transport and Fate on Global Scale and within the European Region. *Organohalogen Compounds*. Vol. 76, 958-961.

Gusev A., O.Rozovskaya, V. Shatalov [2007] Modelling POP long-range transport and contamination levels by MSCE-POP model. EMEP/MSC-E Technical Report 1/2007 .

Gusev A., Ilyin I., Mantseva L., Rozovskaya O., Shatalov V. and Travnikov O. [2006]. Progress in further development of MSCE-HM and MSCE-POP models (implementation of the model review recommendations). EMEP/MSC-E Technical Report 4/2006.

Halse A.K., Schlabach M., Eckhardt S., Sweetman A., Jones K.C., Breivik K. [2011] Spatial variability of POPs in European background air. *Atmospheric Chemistry and Physics*, 11, 1549-1564.

Halvorsen H.L., Bohlin-Nizzetto P., Eckhardt S., Gusev A., Krogseth I.S., Moeckel C., Shatalov V., Skogeng L.P., Breivik K. [2021] Main sources controlling atmospheric burdens of persistent organic pollutants on a national scale. *Ecotoxicology and Environmental Safety*, 217.

Hartl M.G.J., Gubbins E., Gutierrez T. and Fernandes T.F. [2015] Review of existing knowledge – Emerging contaminants: Focus on nanomaterials and microplastics. https://www.crew.ac.uk/sites/www.crew.ac.uk/files/sites/default/files/publication/CREW_Emerging%20Contaminants.pdf

HMCR [2020]. Hydrometeorological Centre of Russia. The main peculiarities of atmospheric circulation and weather in the northern hemisphere. https://meteoinfo.ru/circulation-review. Accessed on November 25, 2020.

Howard P.H., Muir D.C.G. [2010] Identifying New Persistent and Bioaccumulative Organics Among Chemicals in Commerce. *Environ Sci Technol* 44: 2277-2285.

Ilyin I., O. Travnikov, G. Schütze, S. Feigenspan and K. Uhse [2020] Country-scale assessment of heavy metal pollution: A case study for Germany. Joint Report of MSC-E and German Environment Agency. MSC-E Technical Report 1/2020.

Ilyin I., Rozovskaya O., Travnikov O., Aas W. and K.A.Pfaffhuber [2018] Assessment of heavy metal transboundary pollution on global, regional and national scales. EMEP Status Report 2/2018.

Jaward F.M., Farrar N.J., Harner T., Sweetman A.J., Jones K.C. [2004] Passive air sampling of PCBs, PBDEs, and organochlorine pesticides across Europe. *Environ. Sci. Technol*. 2004, 38, 34-41.

Jiang X., Li M. [2020] Interaction of Microplastics and Heavy Metals: Toxicity, Mechanisms, and Environmental Implications. In: He D., Luo Y. (eds) Microplastics in Terrestrial Environments. The Handbook of Environmental Chemistry, vol 95. Springer, Cham. https://doi.org/10.1007/698_2020_460.

JRC [2019] European Commission, Joint Research Centre (JRC) - Emission Database for Global Atmospheric Research, Global Air Pollutant Emissions (EDGARv5.0), https://edgar.jrc.ec.europa.eu/index.php/dataset_ap50

Kalina J., White K.B., Scheringer M., Pribylova P., Kukucka P., Audy O., Klanova J. [2019] Comparability of long-term temporal trends of POPs from co-located active and passive air monitoring networks in Europe. *Environmental Science-Processes & Impacts*, 21, 1132-1142.

Kalina J., Scheringer M., Boruvkova J., Kukucka P., Pribylova P., Sanka O., Melymuk L., Vana M., Klanova J. [2018] Characterizing Spatial Diversity of Passive Sampling Sites for Measuring Levels and Trends of Semivolatile Organic Chemicals. *Environ. Sci. Technol.*, 52, 10599-10608.

Klein A., F. Ravetta, J.L. Thomas, G. Ancellet, P. Augustin, R. Wilson, E. Dieudonné, M. Fourmentin, H. Delbarre, J. Pelon [2019] Influence of vertical mixing and nighttime transport on surface ozone variability in the morning in Paris and the surrounding region. *Atmos. Environ.,* 197, pp. 92-102, 10.1016/j.atmosenv.2018.10.009.

Klein M., E.K. Fischer [2019] Microplastic abundance in atmospheric deposition within the Metropolitan area of Hamburg, Germany *Sci. Total Environ*., 685, pp. 96-103, 10.1016/j.scitotenv.2019.05.405.

Krogseth I.S., Kierkegaard A., McLachlan M.S., Breivik K., Hansen K.M., Schlabach M. [2013] Occurrence and seasonality of cyclic volatile methyl siloxanes in Arctic air. *Environ. Sci. Technol.,* 47, 502-509.

Lammel G., Sehili A.M., Bond T.C., Feichter J., Grassl H. [2009] Gas/particle partitioning and global distribution of polycyclic aromatic hydrocarbons – A modelling approach. Chemosphere 76, 98–106. https://doi.org/10.1016/j.chemosphere.2009.02.017

Liu K., Wang X., Wei N., Song Z., Li D. [2019] Accurate quantification and transport estimation of suspended atmospheric microplastics in megacities: Implications for human health. Environment International 132, 105127. https://doi.org/10.1016/j.envint.2019.105127.

McLachlan M.S. [1999] Framework for the Interpretation of Measurements of SOCs in Plants. *Environ. Sci. Technol*. 33, 1799–1804. https://doi.org/10.1021/es980831t.

McLachlan M.S., Horstmann M. [1998] Forests as Filters of Airborne Organic Pollutants: A Model. *Environ. Sci. Technol*. 32, 413–420. https://doi.org/10.1021/es970592u.

Möller A., Xie Z., Sturm R., Ebinghaus R. [2010] Large-scale distribution of Dechlorane Plus in Air and seawater from the Arctic to Antarctica. *Environ. Sci. Technol*., 44 (23), 8977-8982.

Munoz-Amanz J., Roscales J.L., Ros M., Vicente A.; Jimenez B. [2016] Towards the implementation of the Stockholm Convention in Spain: Five-year monitoring (2008-2013) of POPs in air based on passive sampling. *Environ. Pollut*., 217, 107-113.

NADP/AMNet [2021] National Atmospheric Deposition Program. Atmospheric Mercury Network. http://nadp.slh.wisc.edu/AMNet/.

Nicholson F.A., Smith S.R., Alloway B.J., Carlton-Smith C. and Chambers B.J. [2003]. An inventory of heavy metals inputs to agricultural soils in England and Wales. The Science of the Total Environment 311 (2003) 205–219.

Pinterits M., K. Mareckova, B. Ullrich, R. Wankmueller [2021] Inventory Review 2021. Review of emission data reported under the LRTAP Convention and NEC Directive, Stage 1 and 2 and review, Status of gridded and LPS data. Technical Report CEIP 4/2021.

Plastics Europe (2018) Plastics – The Facts 2018: An Analysis of European Plastics Production, Demand and Waste Data https://www.plasticseurope.org/application/files/6315/4510/9658/Plastics_the_facts_2018_AF_web.pdf.

Poupa S. and R.Wankmueller [2020] Methodologies applied to the CEIP GNFR gap-filling 2020. Part II: Heavy Metals (Pb, Cd, Hg). Technical report CEIP 2/2020.

Poupa S., Tista M. and R.Wankmueller [2020] Methodologies applied to the CEIP GNFR gap-filling 2020. Part III: Persistent organic pollutants (Benzo(a)pyrene, Benzo(b)fluoranthene, Benzo(k)fluoranthene, Indeno(1,2,3-cd)pyrene, Total polycyclic aromatic hydrocarbons, Dioxin and Furan, Hexachlorobenzene, Polychlorinated biphenyls). Technical Report CEIP 3/2020.

Pozo K., Harner T., Wania F., Muir D.C.G., Jones K.C., Barrie L.A. [2006] Toward a global network for persistent organic pollutants in air: Results from the GAPS study. *Environ. Sci. Technol.*, 40, 4867-4873.

Prata J.C. [2018] Airborne microplastics: consequences to human health? *Environ. Pollut*. 234, 115–126. https://doi.org/10.1016/j.envpol.2017.11.043.

Pulles T., Kok H. and U.Quass [2006] Application of the emission inventory model TEAM: Uncertainties in dioxin emission estimates for central Europe. *Atmospheric Environment,* 40, 2321–2332.

Pulles T., Kok H., Quass U., Juery C. and J.Matejovicova [2005] Dioxin emissions in candidate countries. TNO Report R&I-A R 2005/054. Available at:http://ec.europa.eu/environment/archives/dioxin/pdf/rapport_2005.pdf.

Rice K.M, Walker E.M., Miaozong J. Wu, Gillette C. and Blough E.R. [2014]. Environmental Mercury and Its Toxic Effects. J Prev Med Public Health 2014;47:74-83.

Röhler L., Schlabach M., Haglund P., Breivik K., Kallenborn R., Bohlin-Nizzetto P. [2020] Non-target and suspect characterization of organic contaminants in Arctic air – Part 2: Application of a new tool for identification and prioritization of chemicals of emerging Arctic concern in air. *Atmospheric Chemistry and Physics*; 20 (14): 9031-9049.

Saiz-Lopez A., Travnikov O., Sonke J.E., Thackray C.P., Jacob D.J., Carmona-García J., Francés-Monerris A., Roca-Sanjuán D., Acuña A.U., Dávalos J.Z., Cuevas C.A., Jiskra M., Wang F., Bieser J., Plane J.M.C., and Francisco J.S. [2020] Photochemistry of oxidized Hg(I) and Hg(II) species suggests missing mercury oxidation in the troposphere. PNAS Latest Articles, 1-8. www.pnas.org/cgi/doi/10.1073/pnas.1922486117.

Schindlbacher S., Matthews B. and Ullrich B. [2021]. Uncertainties and recalculations of emission inventories submitted under CLRTAP, Technical Report CEIP 1/2021. Available at: https://www.ceip.at/fileadmin/inhalte/ceip/00_pdf_other/2021/uncertainties_and_recalculations_of_emission_inventories_submitted_under_clrtap.pdf.

Schuster J.K., Gioia R., Breivik K., Steinnes E., Scheringer M., Jones K.C. [2011] Trends in European Background Air Reflect Reductions in Primary Emissions of PCBs and PBDEs. *Environ. Sci. Technol.*, 44, 6760-6766.

Sehili A.M., Lammel G. [2007] Global fate and distribution of polycyclic aromatic hydrocarbons emitted from Europe and Russia. *Atmospheric Environment* 41, 8301–8315. https://doi.org/10.1016/j.atmosenv.2007.06.050

Setälä O., Fleming-Lehtinen V., Lehtiniemi M. [2014] Ingestion and transfer of microplastics in the planktonic food web. *Environ. Pollut.* 185, 77–83. https://doi.org/10. 1016/j.envpol.2013.10.013.

Shatalov V., Ilyin I., Gusev A., Travnikov O. [2015] Heavy Metals and Persistent Organic Pollutants: Multi-scale modelling and trend analysis methodology. MSC-E Technical Report 1/2015.

Shatalov V., Ilyin I., Gusev A., Rozovskaya O. and O.Travnikov [2014] Heavy Metals and Persistent Organic Pollutants: Model Assessment of Pollution and Research Activities. EMEP/MSC-E Technical report 4/2014.

Shatalov V., Gusev A., Dutchak S., Rozovskaya O., Sokovykh V. and N.Vulykh [2010] Persistent Organic Pollutants in the Environment. EMEP Status Report 3/2010.

Shen H, Huang Y, Wang R, Zhu D, Li W, Shen G, Wang B, Zhang Y, Chen Y, Lu Y, Chen H, Li T, Sun K, Li B, Liu W, Liu J, Tao S. [2013] Global atmospheric emissions of polycyclic aromatic hydrocarbons from 1960 to 2008 and future predictions. *Environ Sci Technol*. 2013 Jun 18;47(12):6415-24. doi: 10.1021/es400857z. Epub 2013 May 31. PMID: 23659377; PMCID: PMC3753807.

Six L. and Smolders E. [2014] Future trends in soil cadmium concentration under current cadmium fluxes to European agricultural soils. *Science of the Total Environment* 485–486 (2014) 319–328.

Skamarock W.C., Klemp J.B., Dudhia J., Gill D.O., Barker D.M., Duda M.G., Huang X-Y., Wang W. and Powers J.G. [2008]. A Description of the Advanced Research WRF Version 3. NCAR/TN–475+STRNCAR TECHNICAL NOTE.

Starek-Świechowicz, B., Budziszewska, B., & Starek, A. [2017] Hexachlorobenzene as a persistent organic pollutant: Toxicity and molecular mechanism of action. Pharmacological Reports, 69(6), 1232–1239. doi:10.1016/j.pharep.2017.06.013

Strahler A., Muchoney D., Borak J., Friedl, M., Gopal S., Lambin E. and Moody A. [1999]. MODIS Land Cover Product. Algorithm Theoretical Basis Document (ATBD) Version 5.0. MODIS Land Cover and Land-Cover Change. Center for Remote Sensing, Department of Geography, Boston University, Boston, MA, 66 p.

Streets D.G., Horowitz H.M., Lu Z., Levin L., Thackray C.P., Sunderland E.M. [2019a] Five hundred years of anthropogenic mercury: spatial and temporal release profiles. Environ. Res. Lett. 14, 084004. https://doi.org/10.1088/1748-9326/ab281f.

Street D.G., Horowitz H.M., Lu Z., Levin L., Thackray C.P., Sunderland E.M. [2019b] Global and regional trends in mercury emissions and concentrations, 2010–2015. *Atmospheric Environment* 201, 417–427. https://doi.org/10.1016/j.atmosenv.2018.12.031.

Strizhkina I., Gusev A., O.Rozovskaya, Shatalov V., [2021a] Heavy metals and POPs: Pollution assessment of toxic substances on regional and global scales Part I. Supplementary materials for POPs. MSC-E Data Report 2/2021.

Strizhkina I., Ilyin I., Rozovskaya O., O.Travnikov, [2021b] Heavy metals and POPs: Pollution assessment of toxic substances on regional and global scales. Part II. Supplementary materials for heavy metals. MSC-E Data Report 1/2021.

Sutton M.A., Nemitz E., Erisman J.W., Beier C., Bahl K.B., Cellier P., de Vries W., Cotrufo F., Skiba U., Di Marco C., Jones S., Laville P., Soussana J.F., Loubet B., Twigg M., Famulari D., Whitehead J., Gallagher M.W., Neftel A., Flechard C.R., Herrmann B., Calanca P.L., Schjoerring J.K., Daemmgen U., Horvath L., Tang Y.S., Emmett B.A., Tietema A., Peñuelas J., Kesik M., Brueggemann N., Pilegaard K., Vesala T., Campbell C.L., Olesen J.E., Dragosits U., Theobald M.R., Levy P., Mobbs D.C., Milne R., Viovy N., Vuichard N., Smith J.U., Smith P., Bergamaschi P., Fowler D., Reis S. [2007] Challenges in quantifying biosphere–atmosphere exchange of nitrogen species. *Environmental Pollution* 150, 125–139. https://doi.org/10.1016/j.envpol.2007.04.014.

Sutton M.A., Burkhardt J.K., Guerin D., Nemitz E., Fowler D. [1998] Development of resistance models to describe measurements of bi-directional ammonia surface–atmosphere exchange. *Atmospheric Environment* 32, 473–480. https://doi.org/10.1016/S1352-2310(97)00164-7.

The International GEOS-Chem User Community: geoschem/geos-chem: GEOS-Chem 12.8.2 (Version 12.8.2), Zenodo, https://doi.org/10.5281/zenodo.3860693, 2020.

Trainic M., Flores J.M., Pinkas I., Pedrotti M.L., Lombard F., Bourdin G., Gorsky G., Boss E., Rudich Y., Vardi A., Koren I. [2020] Airborne microplastic particles detected in the remote marine atmosphere. Commun Earth Environ 1, 64.https://doi.org/10.1038/s43247-020-00061-y

Travnikov O., Gusev A., Ilyin I., Kleimenov M [2021] Co-operative activities on Hg and POP pollution assessment within TF HTAP. Progress report.. MSC-E Technical Report 1/2021.

Travnikov O., Batrakova N., Gusev A., Ilyin I., Kleimenov M., Rozovskaya O., Shatalov V., Strijkina I., Aas W., Breivik K., Nizzetto P.B., Pfaffhuber K.A., Mareckova K., Poupa S., Wankmueller R., Seussall K. [2020] Assessment of transboundary pollution by toxic substances: Heavy metals and POPs. EMEP Status Report 2/2020.

Travnikov O. and Ilyin I. [2005]. Regional Model MSCE-HM of Heavy Metal Transboundary Air Pollution in Europe. EMEP/MSC-E Technical Report 6/2005., 68 p.

UNECE [2019] Monitoring strategy for the Cooperative Programme for Monitoring and Evaluation of the Long-range Transmission of Air Pollutants in Europe for the period 2020–2029. EB Decision 2019/1, ECE/EB.AIR/144/Add.1. URL: http://www.unece.org/fileadmin/DAM/env/documents/2019/AIR/EB_Decisions/Decision_2019_1.pdf.

UNECE [2014] *Guidelines for reporting emission data under the Convention on Long-range Transboundary Air Pollution (ECE/EB.AIR/130). Available at:* http://www.ceip.at/fileadmin/inhalte/emep/2014_Guidelines/ece.eb.air.125_ADVANCE_VERSION_reporting_guidelines_2013.pdf

UNECE [1979] *The 1979 Geneva Convention on Long-range Transboundary Air Pollution.* United Nations Economic Commission for Europe. http://www.unece.org/env/lrtap/welcome.html.

UNEP [2017] Global Monitoring Plan for POPs under the Stockholm Convention. UN Environment. Available at http://chm.pops.int/Portals/0/download.aspx?d=UNEP-POPS-COP.8-INF-38.English.pdf.

UNEP [2016] United Nations Environment Programme; Nairobi: United Nations Environment Programme. Marine Plastic Debris and Microplastics – Global Lessons and Research to Inspire Action and Guide Policy Change.

Wagner S., Reemtsma T. [2019] Things we know and don't know about nanoplastic in the environment. *Nat. Nanotechnol.* 14, 300–301. https://doi.org/10.1038/s41565-019-0424-z.

Wang T., Wang L., Chen Q., Kalogerakis N., Ji R., & Ma Y. [2020]. Interactions between microplastics and organic pollutants: Effects on toxicity, bioaccumulation, degradation, and transport. *Science of The Total Environment*, 142427. doi:10.1016/j.scitotenv.2020.142427.

Wang X., Lin C.-J., Feng X. [2014] Sensitivity analysis of an updated bidirectional air–surface exchange model for elemental mercury vapor. *Atmos. Chem. Phys.* 14, 6273–6287. https://doi.org/10.5194/acp-14-6273-2014.

WHO [2000] Air Quality Guidelines - Second Edition. Chapter 5.11 Polychlorinated dibenzodioxins and dibenzofurans. https://www.euro.who.int/__data/assets/pdf_file/0017/123065/AQG2ndEd_5_11PCDDPCDF.pdf?ua=1.

WHO [2003a] Concise International Chemical Assessment Document 55. Polychlorinated biphenyls: human health aspects. ISBN 92 4 153055 3; ISSN 1020-6167. https://www.who.int/ipcs/publications/cicad/en/cicad55.pdf?ua=1.

WHO [2003b]. Elemental mercury and inorganic mercury compounds: human health aspects. Concise International Chemical Assessment Document 50. WHO, Geneva, 2003, 61 p.

WHO [2003c] Health aspects of air pollution with particulate matter, ozone and nitrogen dioxide. Report on a WHO working group. EUR/03/5042688 WHO, Bonn.

WHO [2013a] Health effects of particulate matter Policy implications for countries in eastern Europe, Caucasus and central Asia. ISBN 978 92 890 0001 7 (http://www.euro.who.int/__data/assets/pdf_file/0006/189051/Health-effects-of-particulate-matter-final-Eng.pdf [1]).

WHO Technical report [2013b] Review of Evidence on Health Aspects of Air Pollution. REVIHAAP Project. (https://www.euro.who.int/__data/assets/pdf_file/0004/193108/REVIHAAP-Final-technical-report-final-version.pdf[2]).

WHO [2017] Evolution of WHO air quality guidelines: past, present and future. Copenhagen. WHO Regional Office for Europe. (http://www.euro.who.int/__data/assets/pdf_file/0019/331660/Evolution-air-quality.pdf).

WHO [2019] WHO technical report, Microplastics in drinking-water. ISBN: 978-92-4-151619-8. https://www.who.int/water_sanitation_health/publications/microplastics-in-drinking-water/en/.

Wong F., Shoeib M., Katsoyiannis A., Eckhardt S., Stohl A., Bohlin-Nizzetto P., Li H., Fellin P., Su Y., Hung H. [2018] Assessing temporal trends and source regions of per- and polyfluoroalkyl substances (PFASs) in air under the Arctic Monitoring and Assessment Programme (AMAP). *Atmospheric Environment*; 172:65-73.

Yang, X., Pyle, J. A., Cox, R. A., Theys, N., and Van Roozendael, M. [2010] Snow-sourced bromine and its implications for polar tropospheric ozone, *Atmos. Chem. Phys*., 10, 7763–7773, doi:10.5194/acp-10-7763-2010.

Yang, X., Cox, R., Warwick, N., Pyle, J., Carver, G., O'Connor,F., and Savage, N. [2005] Tropospheric bromine chemistry and its impacts on ozone: A model study, *J. Geophys. Res.,* 110, D23311, doi:10.1029/2005JD006244.

Zhang Y., Kang S., Allen S., Allen D., Gao T., & Sillanpää M. [2020]. Atmospheric microplastics: A review on current status and perspectives. Earth-Science Reviews, 103118. doi:10.1016/j.earscirev.2020.103118

Zhang Y., T. Gao, S. Kang, M. [2019] Sillanpaa Importance of atmospheric transport for microplastics deposited in remote areas. *Environ. Pollut*., 24, p. 112953, 10.1016/j.envpol.2019.07.121

Zhang L., Wright L.P., Asman W.A.H. [2010] Bi-directional air-surface exchange of atmospheric ammonia: A review of measurements and a development of a big-leaf model for applications in regional-scale air-quality models. *J. Geophys. Res*. 115, D20310. https://doi.org/10.1029/2009JD013589.

Zhang L., Wright L.P., Blanchard P. [2009] A review of current knowledge concerning dry deposition of atmospheric mercury. *Atmospheric Environment* 43, 5853–5864. https://doi.org/10.1016/j.atmosenv.2009.08.019.

Zhao S., Ward J.E., Danley M., Mincer T.J. [2018] Field-based evidence for microplastic in marine aggregates and mussels: implications for trophic transfer. *Environ. Sci. Technol*. 52 (19), 11038–11048. https://doi.org/10.1021/acs.est.8b03467.

Annex A.1. Reporting of priority heavy metals and POPs in EMEP East region

Table A1. *Reporting of main heavy metals (Pb, Cd, Hg) in EMEP-East region since 2015*

Reporting of main heavy metals (Pb, Cd, Hg)							
	2015	**2016**	**2017**	**2018**	**2019**	**2020**	**2021**
Armenia	2008 - 2013 (only Pb, only a few sectors)	2014		2016	2017		2019
Azerbaijan	1990 - 2013 (only Hg, only a few sectors)	1990-2014 (Pb, Cd: 1995-2014)	1990 - 2015 (Pb, Cd: 1995-2015)	1990 - 2016 (Pb, Cd: 1995-2016)	1995-2017 (Hg 1990-2017)		
Belarus	2013			2014-2016	2017	2018	2019
Georgia	2007 - 2013 (no Hg)	2007-2014 (Cd, Hg: 2013-2014)	2007 - 2015	2007-2016	2007-2017		1990-2019
Kazakhstan		2013-2014	1990, 2000, 2005, 2010 - 2015	1990 - 2016		1990 - 2018	1990-2019
Kyrgyzstan		2014 (only Hg)	2015 (only Hg)		2017	2018	
Republic of Moldova	2013	1990-2014 (no emissions calculated for the waste sector)	1990 - 2015			1990 - 2017	1990-2019
Russian Federation							
Ukraine	2013	2014	2015	2016		2016, 2017, 2018	2019
Turkey					1990 - 2017 *(just for very few IPPU categories)*	1990 - 2018 *(just for very few IPPU categories)*	1990-2019

Table A2. *Reporting of POPs (PCDD/Fs, PAHs, HCB, PCBs) in EMEP East region since 2015*

Reporting of POPs (PCDD/Fs, PAHs, HCB, PCBs)							
	2015	**2016**	**2017**	**2018**	**2019**	**2020**	**2021**
Armenia		2014		2016 (only PCDD/Fs)	2017 (No HCB, no PCBs)		2019
Azerbaijan	1995-2013	1995-2014 (no HCB, no PCBs)	1995-2015	1995-2016	1995 -2017 (HCB, PCBS no data for 2000)		
Belarus	2013			2014-2016	2017	2018	209
Georgia	2007-2013 (no HCB)	2007-2014 (PCDD/Fs) 2013-2014 (PAHs, HCB, PCBs)	2007-2015	2007-2016 (HCB only 2013-2016)	2007-2017		1990-2019
Kazakhstan		2013-2014	1990, 2000, 2005, 2010-2015	1990-2016		1990 -2018	1990-2019
Kyrgyzstan					2017	2018	
Republic of Moldova	2013	1990-2014 (no emissions calculated for the waste sector)	1990-2015			1990-2017	1990-2019
Russian Federation							
Ukraine	2013 (no PCDD/Fs)				2017	2017, 2018	2019
Turkey							

Annex A.2. Significant changes (over ±15 %) between national totals used in models in year 2020 and national totals used in models in 2021

Data values represent the 'total national totals'. The column 'data sources' in the table below indicates the following four cases:

- *"reported"*: both 2018 and 2019 data are reported by country.
- *"gapfilled":* both 2018 and 2019 data are gap-filled by expert estimates
- *"new gapfilled":* 2018 data was reported by country and 2019 data had to be gap-filled by expert estimates (because it was not reported by country)
- *"new reported":* 2018 data was gap-filled, 2019 data is as reported by country

The indicator *"new"* in column *"% change"* indicates that the value has been either reported or gap-filled for the first time.

Component	Country	Data sources	Unit	2019 value	2018 value	% change	Value change
Cd	AM	reported	t	0.044	0.013	245%	0.032
Cd	CH	reported	t	0.690	1.162	-41%	-0.472
Cd	EE	reported	t	0.552	0.813	-32%	-0.261
Cd	ES	reported	t	7.363	4.904	50%	2.459
Cd	GB	reported	t	5.589	4.046	38%	1.542
Cd	GE	new reported	t	0.179	0.242	-26%	-0.063
Cd	IT	reported	t	4.408	5.331	-17%	-0.922
Cd	MC	new reported	t	0.000	0.000	-74%	0.000
Cd	MD	new reported	t	0.732	0.368	99%	0.364
Cd	ME	reported	t	0.114	0.188	-39%	-0.074
Cd	MK	reported	t	0.227	0.603	-62%	-0.376
Cd	MT	reported	t	0.007	0.005	45%	0.002
Cd	RS	reported	t	3.767	2.614	44%	1.153
Cd	RU	gapfilled	t	24.721	43.434	-43%	-18.713
Cd	RUE	gapfilled	t	12.735	22.375	-43%	-9.640
Cd	SK	reported	t	0.900	1.682	-47%	-0.782
Cd	TR	gapfilled	t	3.211	19.190	-83%	-15.979
Cd	UA	new reported	t	8.434	3.527	139%	4.907
Hg	AM	reported	t	0.040	16.625	-100%	-16.584
Hg	BE	reported	t	1.025	1.370	-25%	-0.345
Hg	CY	reported	t	0.028	0.036	-22%	-0.008
Hg	CZ	reported	t	2.261	2.743	-18%	-0.482
Hg	EE	reported	t	0.327	0.599	-45%	-0.272
Hg	ES	reported	t	3.077	4.056	-24%	-0.979
Hg	GE	new reported	t	0.183	0.220	-17%	-0.037
Hg	HU	reported	t	0.776	1.025	-24%	-0.249
Hg	LU	reported	t	0.099	0.056	76%	0.043
Hg	LV	reported	t	0.081	0.096	-16%	-0.015
Hg	MC	new reported	t	0.001	0.004	-83%	-0.004
Hg	MD	new reported	t	0.127	0.102	24%	0.024
Hg	MT	reported	t	0.007	0.031	-79%	-0.025
Hg	NL	reported	t	0.591	0.512	15%	0.079
Hg	SK	reported	t	0.785	1.223	-36%	-0.438

Component	Country	Data sources	Unit	2019 value	2018 value	% change	Value change
Hg	TR	gapfilled	t	6.922	15.824	-56%	-8.902
Hg	UA	new reported	t	34.795	5.027	592%	29.768
Pb	FR	reported	t	84.774	113.523	-25%	-28.750
Pb	AM	reported	t	0.797	1.723	-54%	-0.926
Pb	DE	reported	t	160.785	207.364	-22%	-46.580
Pb	EE	reported	t	11.374	33.207	-66%	-21.833
Pb	GE	new reported	t	2.392	2.899	-17%	-0.507
Pb	GR	reported	t	7.875	10.595	-26%	-2.720
Pb	HR	reported	t	5.167	8.413	-39%	-3.245
Pb	IS	reported	t	0.556	0.769	-28%	-0.213
Pb	LU	reported	t	1.460	1.200	22%	0.260
Pb	MD	new reported	t	2.684	1.477	82%	1.207
Pb	PT	reported	t	25.297	43.019	-41%	-17.722
Pb	SE	reported	t	8.094	9.792	-17%	-1.698
Pb	SI	reported	t	4.308	7.565	-43%	-3.256
Pb	SK	reported	t	9.315	31.145	-70%	-21.830
Pb	TR	gapfilled	t	89.381	382.711	-77%	-293.330
Pb	UA	new reported	t	299.601	98.007	206%	201.594
B(a)P	FR	reported	t	9.814	4.737	107%	5.077
B(a)P	AL	new reported	t	0.021	2.130	-99%	-2.110
B(a)P	AM	reported	t	0.423	0.087	388%	0.336
B(a)P	BE	reported	t	2.125	2.577	-18%	-0.452
B(a)P	DE	reported	t	16.088	28.212	-43%	-12.124
B(a)P	DK	reported	t	1.458	2.237	-35%	-0.779
B(a)P	EE	reported	t	0.900	2.245	-60%	-1.345
B(a)P	ES	reported	t	15.953	27.824	-43%	-11.871
B(a)P	FI	new reported	t	7.311	2.921	150%	4.390
B(a)P	GE	new reported	t	1.449	1.889	-23%	-0.440
B(a)P	GR	reported	t	5.271	30.921	-83%	-25.651
B(a)P	KZT	gapfilled	t	36.754	20.350	81%	16.404
B(a)P	LU	reported	t	0.135	0.179	-25%	-0.044
B(a)P	MD	new reported	t	4.389	3.247	35%	1.142
B(a)P	ME	reported	t	0.003	0.002	48%	0.001
B(a)P	MK	reported	t	1.228	2.087	-41%	-0.859
B(a)P	MT	reported	t	0.017	0.006	160%	0.010
B(a)P	PL	reported	t	62.160	73.148	-15%	-10.989
B(b)F	FR	reported	t	11.408	5.756	98%	5.652
B(b)F	AL	new reported	t	0.033	2.787	-99%	-2.754
B(b)F	AM	reported	t	0.390	0.084	367%	0.307
B(b)F	BE	reported	t	2.366	2.834	-17%	-0.469
B(b)F	DE	reported	t	23.346	1.848	1163%	21.498
B(b)F	DK	reported	t	1.588	2.387	-33%	-0.799
B(b)F	EE	reported	t	0.893	2.640	-66%	-1.747
B(b)F	ES	reported	t	15.769	35.904	-56%	-20.135
B(b)F	FI	new reported	t	5.704	3.341	71%	2.362
B(b)F	GE	new reported	t	1.427	1.802	-21%	-0.376
B(b)F	GR	reported	t	5.861	77.371	-92%	-71.509
B(b)F	KZT	new reported	t	52.573	27.458	91%	25.115
B(b)F	MD	new reported	t	6.798	3.496	94%	3.302
B(b)F	ME	reported	t	0.021	0.008	168%	0.013

Component	Country	Data sources	Unit	2019 value	2018 value	% change	Value change
B(b)F	MT	reported	t	0.031	0.069	-55%	-0.038
B(k)F	FR	reported	t	7.024	3.541	98%	3.482
B(k)F	AL	gapfilled	t	0.010	0.930	-99%	-0.920
B(k)F	AM	reported	t	0.148	0.032	363%	0.116
B(k)F	BE	reported	t	1.026	1.261	-19%	-0.235
B(k)F	DE	reported	t	10.690	1.184	803%	9.506
B(k)F	DK	reported	t	0.979	1.433	-32%	-0.454
B(k)F	EE	reported	t	0.575	1.271	-55%	-0.696
B(k)F	ES	reported	t	6.541	49.054	-87%	-42.513
B(k)F	FI	new reported	t	4.340	1.542	181%	2.798
B(k)F	GE	new reported	t	0.554	0.714	-22%	-0.159
B(k)F	GR	reported	t	3.188	33.687	-91%	-30.499
B(k)F	HU	reported	t	2.786	3.393	-18%	-0.607
B(k)F	KZT	new reported	t	20.853	9.907	110%	10.946
B(k)F	MD	new reported	t	2.200	1.702	29%	0.497
B(k)F	MT	reported	t	0.020	0.013	48%	0.006
B(k)F	SK	reported	t	2.257	3.636	-38%	-1.380
IcdP	FR	reported	t	6.245	3.300	89%	2.945
IcdP	AL	new reported	t	0.197	1.509	-87%	-1.312
IcdP	AM	reported	t	0.246	0.048	408%	0.198
IcdP	BA	gapfilled	t	0.728	0.957	-24%	-0.229
IcdP	BE	reported	t	1.193	1.436	-17%	-0.242
IcdP	DE	reported	t	15.474	0.845	1730%	14.629
IcdP	DK	reported	t	0.958	1.425	-33%	-0.467
IcdP	EE	reported	t	0.846	1.572	-46%	-0.725
IcdP	FI	new reported	t	4.955	1.831	171%	3.124
IcdP	GE	new reported	t	0.817	1.069	-24%	-0.252
IcdP	GR	reported	t	2.325	24.218	-90%	-21.894
IcdP	KZT	new reported	t	17.654	15.181	16%	2.473
IcdP	LU	reported	t	0.086	0.114	-25%	-0.028
IcdP	MD	new reported	t	2.291	1.722	33%	0.569
IcdP	TM	gapfilled	t	3.023	0.341	786%	2.682
PAH	FR	reported	t	34.490	17.334	99%	17.156
PAH	AL	gapfilled	t	0.261	7.357	-96%	-7.096
PAH	AM	new gapfilled	t	1.208	0.249	386%	0.959
PAH	BE	reported	t	6.710	8.108	-17%	-1.398
PAH	DE	gapfilled	t	65.599	32.089	104%	33.510
PAH	DK	reported	t	4.982	7.481	-33%	-2.499
PAH	EE	reported	t	3.214	7.728	-58%	-4.513
PAH	ES	new gapfilled	t	46.912	140.859	-67%	-93.947
PAH	FI	reported	t	22.309	9.635	132%	12.674
PAH	GE	gapfilled	t	4.247	5.474	-22%	-1.227
PAH	GR	gapfilled	t	16.644	166.197	-90%	-149.553
PAH	KZT	gapfilled	t	127.834	72.897	75%	54.938
PAH	MD	new reported	t	16.867	10.168	66%	6.699
PAH	ME	reported	t	0.066	0.052	28%	0.014
PAH	MK	new reported	t	3.884	4.605	-16%	-0.721
PAH	MT	reported	t	0.076	0.101	-25%	-0.026
PAH	TM	gapfilled	t	8.244	5.220	58%	3.024
PCDD/F	FR	reported	g TEQ	124.153	97.193	28%	26.960

Component	Country	Data sources	Unit	2019 value	2018 value	% change	Value change
PCDD/F	AL	gapfilled	g TEQ	45.364	31.342	45%	14.022
PCDD/F	AM	reported	g TEQ	2.799	0.556	403%	2.242
PCDD/F	CH	reported	g TEQ	16.013	19.784	-19%	-3.771
PCDD/F	EE	reported	g TEQ	4.584	3.728	23%	0.856
PCDD/F	FI	reported	g TEQ	12.132	14.356	-15%	-2.225
PCDD/F	GE	new reported	g TEQ	9.943	13.123	-24%	-3.180
PCDD/F	GR	reported	g TEQ	24.176	29.301	-17%	-5.125
PCDD/F	IS	reported	g TEQ	0.460	0.369	25%	0.090
PCDD/F	LI	new reported	g TEQ	0.081	0.106	-23%	-0.025
PCDD/F	LU	reported	g TEQ	1.763	1.374	28%	0.389
PCDD/F	MC	new reported	g TEQ	1.255	0.005	23742%	1.250
PCDD/F	MT	reported	g TEQ	4.324	3.166	37%	1.158
PCDD/F	NL	reported	g TEQ	40.706	34.932	17%	5.774
PCDD/F	RO	reported	g TEQ	186.088	153.027	22%	33.060
PCDD/F	SK	reported	g TEQ	64.676	47.026	38%	17.650
HCB	FR	reported	kg	29.794	23.888	25%	5.906
HCB	AL	new reported	kg	0.016	0.084	-81%	-0.068
HCB	AM	reported	kg	0.017	0.003	461%	0.014
HCB	AT	reported	kg	17.219	35.625	-52%	-18.406
HCB	BE	reported	kg	3.072	4.832	-36%	-1.760
HCB	BY	reported	kg	1.112	1.347	-17%	-0.236
HCB	CY	reported	kg	0.023	0.028	-20%	-0.006
HCB	FI	reported	kg	22.637	32.024	-29%	-9.387
HCB	GE	new reported	kg	5.288	0.111	4654%	5.177
HCB	GR	reported	kg	1.707	3.324	-49%	-1.617
HCB	HU	reported	kg	3.219	2.257	43%	0.961
HCB	KZT	new reported	kg	7.934	1.453	446%	6.480
HCB	MD	new reported	kg	0.316	0.199	59%	0.117
HCB	MK	reported	kg	4.422	1.657	167%	2.765
HCB	NL	reported	kg	3.800	3.144	21%	0.656
HCB	PL	reported	kg	14.917	3.707	302%	11.210
HCB	PT	reported	kg	2.383	59.505	-96%	-57.122
HCB	RO	reported	kg	3.102	2.176	43%	0.927
HCB	UA	new reported	kg	118.083	512.086	-77%	-394.003
PCB	AL	new reported	kg	1.590	2.810	-43%	-1.220
PCB	AM	reported	kg	0.006	0.009	-31%	-0.003
PCB	BE	reported	kg	14.260	5.477	160%	8.783
PCB	DK	reported	kg	0.397	0.528	-25%	-0.131
PCB	EE	reported	kg	0.438	5.101	-91%	-4.663
PCB	GR	reported	kg	35.496	30.347	17%	5.148
PCB	HU	reported	kg	5.884	8.656	-32%	-2.772
PCB	KZT	new reported	kg	123.935	1 171.403	-89%	-1 047.469
PCB	LT	reported	kg	0.876	1.499	-42%	-0.623
PCB	LU	reported	kg	12.113	2.094	478%	10.019
PCB	MD	new reported	kg	2.171	1.604	35%	0.567
PCB	MK	reported	kg	238.443	29.024	722%	209.420
PCB	NL	reported	kg	0.183	0.233	-21%	-0.050
PCB	UA	new reported	kg	174.411	0.673	25828%	173.738

Annex A.3. Overview of heavy metals and POPs gap-filling in 2021

Gap filling of heavy metals (Cd, Hg, Pb)

	Cd	Hg	Pb
Albania	exp.	exp.	exp.
Armenia	R	R	R
Aral Lake	-	-	-
Asian Areas	exp.	exp.	exp.
Austria	R	R	R
Atlantic Ocean	-	-	-
Azerbaijan	exp.	exp.	exp.
Bosnia and Herzegovina	exp.	exp.	exp.
Baltic Sea	-	-	-
Belgium	R	R	R
Bulgaria	R	R	R
Black Sea	-	-	-
Belarus	R	R	R
Caspian Sea	-	-	-
Switzerland	R	R	R
Cyprus	R	R	R
Czechia	R	R	R
Germany	R	R	R
Denmark	R	R	R
Estonia	R	R	R
Spain	R	R	R
Finland	R	R	R
France	R	R	R
United Kingdom	R	R	R
Georgia	R	R	R
Greece	R	R	R
Croatia	R	R	R
Hungary	R	R	R
Ireland	R	R	R
Iceland	R	R	R
Italy	R	R	R
Kyrgyzstan	exp.	exp.	exp.
Kazakhstan	exp.	exp.	exp.

	Cd	Hg	Pb
Liechtenstein	R	R	R
Lithuania	R	R	R
Luxembourg	R	R	R
Latvia	R	R	R
Monaco	R	R	R
Republic of Moldova	R	R	R
Montenegro	R	R	R
Mediterranean Sea	-	-	-
North Macedonia	R	R	R
Malta	R	R	R
Netherlands	R	R	R
Norway	R	R	R
North Africa	exp.	exp.	exp.
North Sea	-	-	-
Poland	R	R	R
Portugal	R	R	R
Romania	R	R	R
Serbia	R	R	R
Russian Federation (RU)	exp.	exp.	exp.
Rest of Russian Federation in the EMEP domain (RFE)	exp.	exp.	exp.
Sweden	R	R	R
Slovenia	R	R	R
Slovakia	R	R	R
Tajikistan	exp.	exp.	exp.
Turkmenistan	exp.	exp.	exp.
Turkey	R+exp.	R+exp.	R+exp.
Ukraine	R	R	R
Uzbekistan	exp.	exp.	exp.

Gap filling of persistent organic pollutants (POPs)

	B(a)P	B(b)F	B(k)F	PCDD/F	HCB	IcdP	PAH	PCB
Albania	R	R	R+exp.	exp.	R	R	R	R
Armenia	R	R	R	R	R	R	sum	R
Aral Lake	-	-	-	-	-	-	-	-
Asian Areas	-	-	-	-	-	-	-	-
Austria	R	R	R	R	R	R	R	R
Atlantic Ocean	-	-	-	-	-	-	-	-
Azerbaijan	exp.	exp.	exp.	exp.	exp.	exp.	exp.	exp.
Bosnia and Herzegovina	exp.	exp.	exp.	exp.	exp.	exp.	exp.	-
Baltic Sea	-	-	-	-	-	-	-	-
Belgium	R	R	R	R	R	R	R	R
Bulgaria	R	R	R	R	R	R	R	R
Black Sea	-	-	-	-	-	-	-	-
Belarus	R	R	R	R	R	R	R	R
Caspian Sea	-	-	-	-	-	-	-	-
Switzerland	R	R	R	R	R	R	R	R
Cyprus	R	R	R	R	R	R	R	R
Czechia	R	R	R	R	R	R	sum	R
Germany	R	R	R	R	R	R	sum	R
Denmark	R	R	R	R	R	R	R	R
Estonia	R	R	R	R	R	R	R	R
Spain	R	R	R	R	R	R	sum	R
Finland	R	R	R	R	R	R	R	R
France	R	R	R	R	R	R	R	R
United Kingdom	R	R	R	R	R	R	R	R
Georgia	R	R	R	R	R	R	sum	R
Greece	R+exp.	R	R	R	R	R	sum	R
Croatia	R	R	R	R	R	R	sum	R
Hungary	R	R	R	R	R	R	R	R
Ireland	R	R	R	R	R	R	R	R
Iceland	R	R	R	R	R	R	sum	R
Italy	R+exp.	R+exp.	R+exp.	R	R	R+exp.	sum	R
Kyrgyzstan	exp.	exp.	exp.	exp.	exp.	exp.	exp.	exp.
Kazakhstan	exp.	exp.	exp.	exp.	exp.	exp.	exp.	exp.
Liechtenstein	R	R	R	R	R	R	R	-
Lithuania	R	R	R	R	R	R	R	R
Luxembourg	R	R	R	R	R	R	R	R
Latvia	R	R	R	R	R	R	R	R
Monaco	R	R	R	R	R	R	R	R
Republic of Moldova	R	R	R	R	R	R	R	R
Montenegro	R	R	R	R	R	R	R	R
Mediterranean Sea	-	-	-	-	-	-	-	-
North Macedonia	R	R	R	R	R	R	R	R
Malta	R	R	R	R	R	R	R	R

	B(a)P	B(b)F	B(k)F	PCDD/F	HCB	IcdP	PAH	PCB
Netherlands	R	R	R	R	R	R	R	R
Norway	R	R	R	R	R	R	R	R
North Africa	-	-	-	-	-	-	-	-
North Sea	-	-	-	-	-	-	-	-
Poland	R	R	R	R	R	R	sum	R
Portugal	R	R	R	R	R	R	sum	R
Romania	R	R	R	R	R	R	sum	R
Serbia	sum	R	R	R	R	R	sum	R
Russian Federation (RU)	exp.	exp.	exp.	exp.	exp.	exp.	exp.	-
Rest of Russian Federation in the EMEP domain (RFE)	exp.	exp.	exp.	exp.	exp.	exp.	exp.	-
Sweden	R	R	R	R	R	R	sum	R
Slovenia	R	R	R	R	R	R	sum	R
Slovakia	R	R	R	R	R	R	sum	R
Tajikistan	exp.	exp.	exp.	exp.	exp.	exp.	exp.	-
Turkmenistan	exp.	exp.	exp.	exp.	exp.	exp.	exp.	-
Turkey	exp.	exp.	exp.	exp.	exp.	exp.	exp.	-
Ukraine	exp.	exp.	exp.	exp.	R	exp.	exp.	R
Uzbekistan	exp.	exp.	exp.	exp.	exp.	exp.	exp.	-

R	*Reported/new reported*
sum	*Sum of sectors/components*
R+exp.	*Reported data plus expert estimates (e.g. PAH split)*
exp.	*Expert estimates*

Annex B.

Update of the assessment results with the new emission reporting data

Assessment of heavy metal and POP modelled pollution levels for 2019, presented in Chapter 3, is based on the gridded emissions data for the previous year 2018 and meteorological data for 2019. Modelling results based on both emissions and meteorological data for 2019 are presented in this annex. Therefore, modelled air concentrations and total deposition presented here differ from those described in Chapter 3 due to different emission data used in the calculations. Relative difference between these two modelling results is calculated as follows:

$$\Delta_{emis} = \frac{(Y_{2019} - Y_{2018})}{Y_{2018}} \cdot 100\% ,$$

where Y_{2019} and Y_{2018} are pollution levels (air concentrations or deposition) based on meteorological data for 2019 and emissions for 2019 and 2018, respectively. The difference shows the influence of both the changes of emissions from 2018 to 2019 as well as the effect of recalculation of emissions from the inventory, submitted in 2020 for 2018, to the inventory, submitted in 2021 for 2019. Major changes of the emissions in the EMEP countries between these two years are described in Annex A.

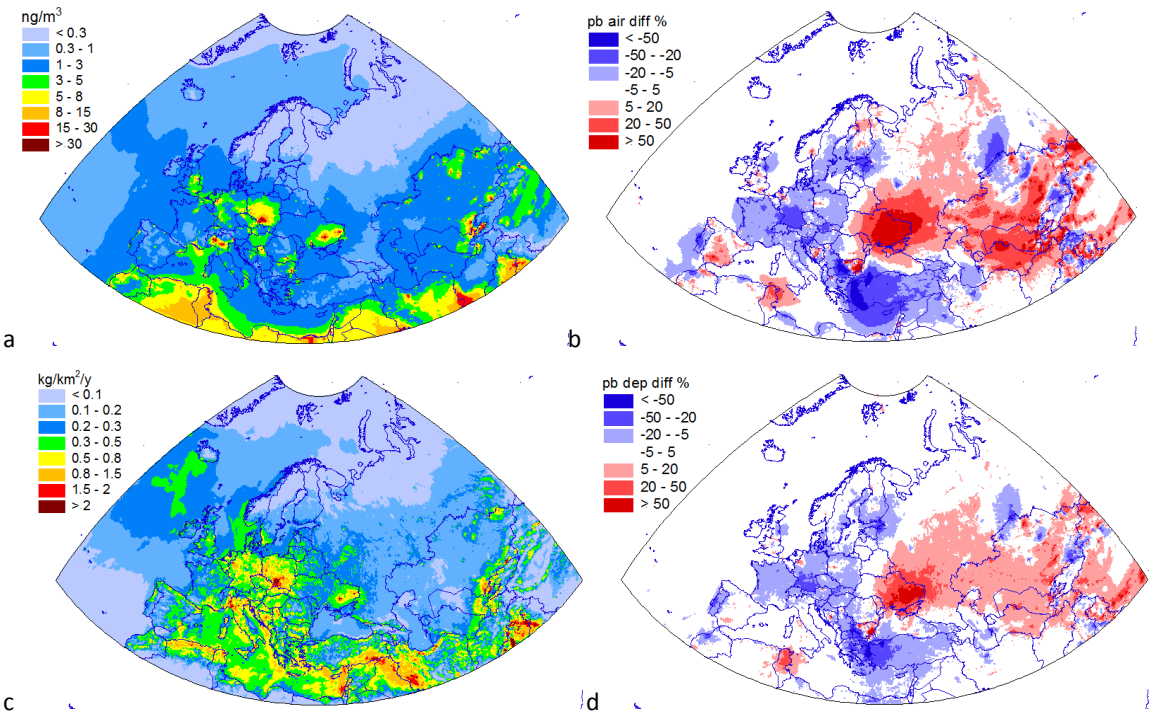

Fig. B.1. *Annual mean air concentrations (a) and total deposition fluxes (c) of Pb based on the emissions data for 2019 and their relative changes (b and d) from the results based on the emissions data for 2018.*

Air concentrations and total deposition of Pb decreased in most countries of the central and western parts of Europe, the south of Scandinavia, the Balkan region, Turkey, Portugal and some regions of Russia (Fig B.1). The highest decline is noted for the western parts of Turkey and Bulgaria (> 50%),

southern Germany, the western part of Russia, and the central part of Portugal (20-50%). The changes of emission data for Ukraine resulted in significant increase of Pb concentrations and deposition over Easter Europe and Central Asia. Besides, some increase of Pb concentrations in air is noted for Spain. Since concentrations and deposition are caused by various types of sources, i.e., EMEP anthropogenic, secondary and non-EMEP sources, the changes of concentrations and deposition are usually smaller than the changes of emissions in the EMEP countries. Besides, the changes are tended to be partly levelled off due to transboundary transport.

The most substantial increase of Cd concentrations in air and total deposition, caused by the changes of the emission data, is noted for Spain, the United Kingdom, Ukraine, Serbia, Moldova and some areas of Central Asia (Fig. B.2). The increase in these countries makes up 20-50%, and in some regions (e.g., the central part of Spain, the southern part of the UK) even exceeds 50%. The major decline (> 20%) of Cd pollution levels takes place in Turkey, Russia, countries of Caucasus, Switzerland and south of Germany. Some smaller decline is seen over most part of Central Europe, e.g., the eastern part of France, the northern parts of Germany and Italy, Poland, Austria, Slovakia etc.

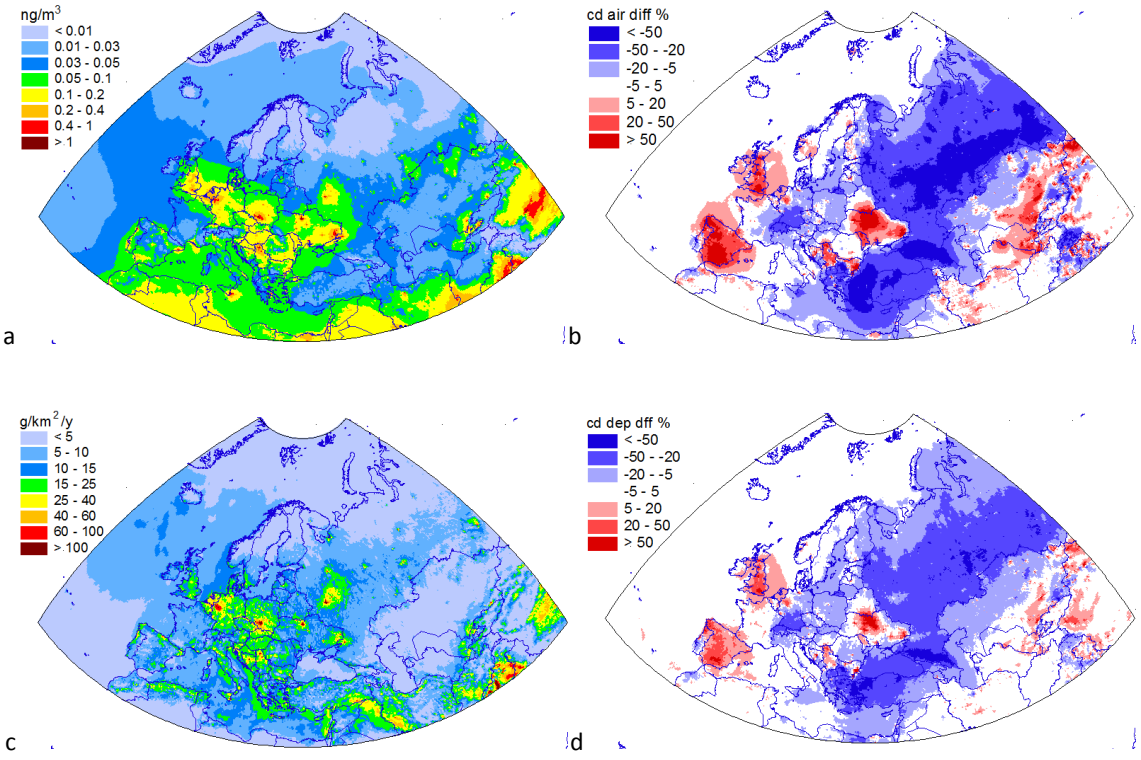

Fig. B.2. *Annual mean air concentrations (a) and total deposition fluxes (c) of Cd based on the emissions data for 2019 and their relative changes (b and d) from the results based on the emissions data for 2018.*

Relative changes of air concentrations and deposition flux of Hg caused by changes of emission data used in modelling are shown in Fig. B.3. Unlike Pb and Cd, Hg levels in the EMEP region are strongly influenced by the intercontinental atmospheric transport. Therefore, the effect of relatively small changes in the EMEP anthropogenic emissions is concealed by the significant contribution of non-

EMEP sources. Regional emissions stronger affect Hg deposition in the EMEP region than to air concentration. Therefore, the effect of the emission changes for the deposition is stronger than for the concentrations. The most significant increase of Hg concentrations (5 – 50%) and deposition (20 – 50% or even higher) occurs in the eastern part of Europe. Marked decline (around 50%) is noted for Armenia and neighbouring territories due to recalculation of national emissions in this country. Besides, decrease of Hg deposition in Turkey ranges from 5 to 20%.

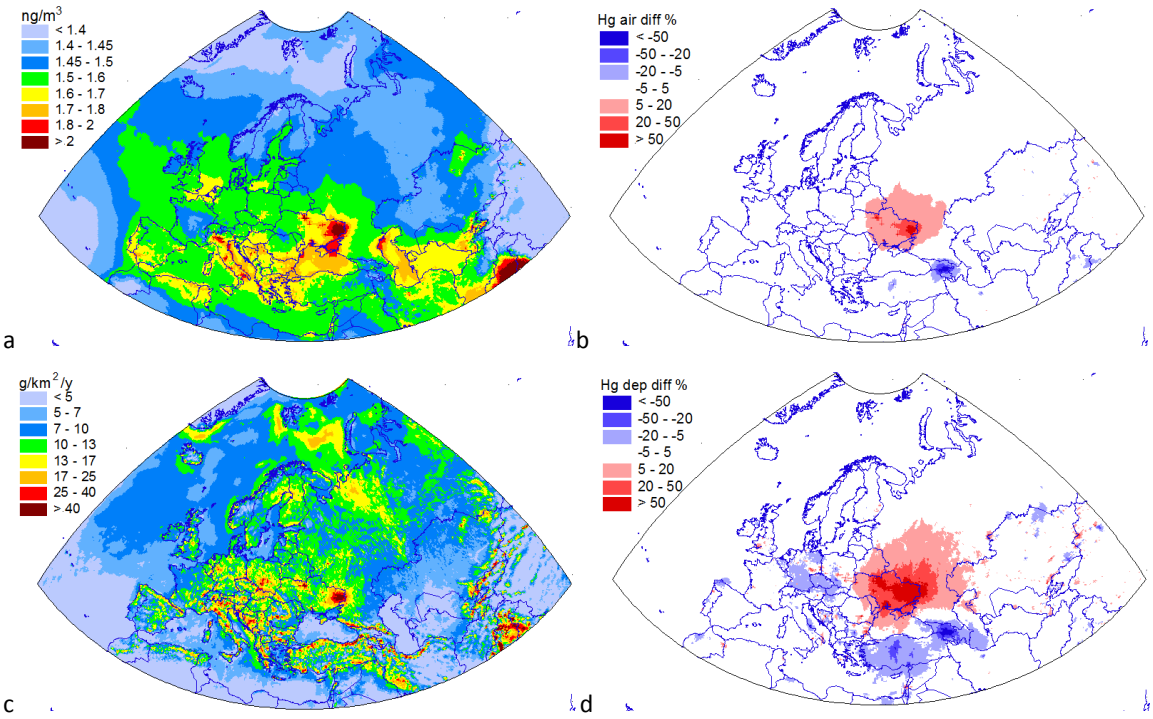

Fig. B.3. *Annual mean air concentrations (a) and total deposition fluxes (c) of Hg based on the emissions data for 2019 and their relative changes (b and d) from the results based on the emissions data for 2018.*

Comparison of model predictions of PCDD/F pollution levels for 2019, simulated on the basis of the emission inventory for 2019 (submitted in 2021) and the inventory for 2018 (submitted in 2020), is shown in Fig. B4. Model simulations were performed on the basis of emission scenarios of possible maximum level of PCDD/F emissions in the EMEP countries (see section 1.2 of the report). These scenarios were constructed taking into account range of uncertainties in the national emission estimates, provided by the countries in 2020 and 2021 in their inventory information reports. Thus, the differences obtained indicate the effect of several factors, namely, (1) of temporal changes of emissions from 2018 to 2019, (2) of recalculations of national emissions from the inventory, submitted in 2020 for 2018, to the inventory, submitted in 2021 for 2019, and (3) of recalculated estimates of emission uncertainty ranges.

Model predictions of air concentrations and total deposition fluxes of PCDD/Fs showed increase of pollution levels in Northern Europe, northern part of Russia, as well as in eastern part of Mediterranean Sea, Slovakia, Bulgaria, Black Sea, and eastern part of Kazakhstan. Increasing concentrations and deposition fluxes are attributed to higher emissions of PCDD/Fs in 2019 (e.g. in Finland, France, Slovakia, Romania) compared to 2018. Declined pollution levels can be noted for

Central, Western, and Southern Europe (e.g. Poland, Belarus, Austria, Switzerland, Spain, Greece) due to lower PCDD/F emissions in 2019. In addition to this, the updates of spatial distribution of emissions in some of the EMEP countries (e.g. Bulgaria, Russia, Kazakhstan) noticeably affects the changes of PCDD/F pollution from 2018 to 2019.

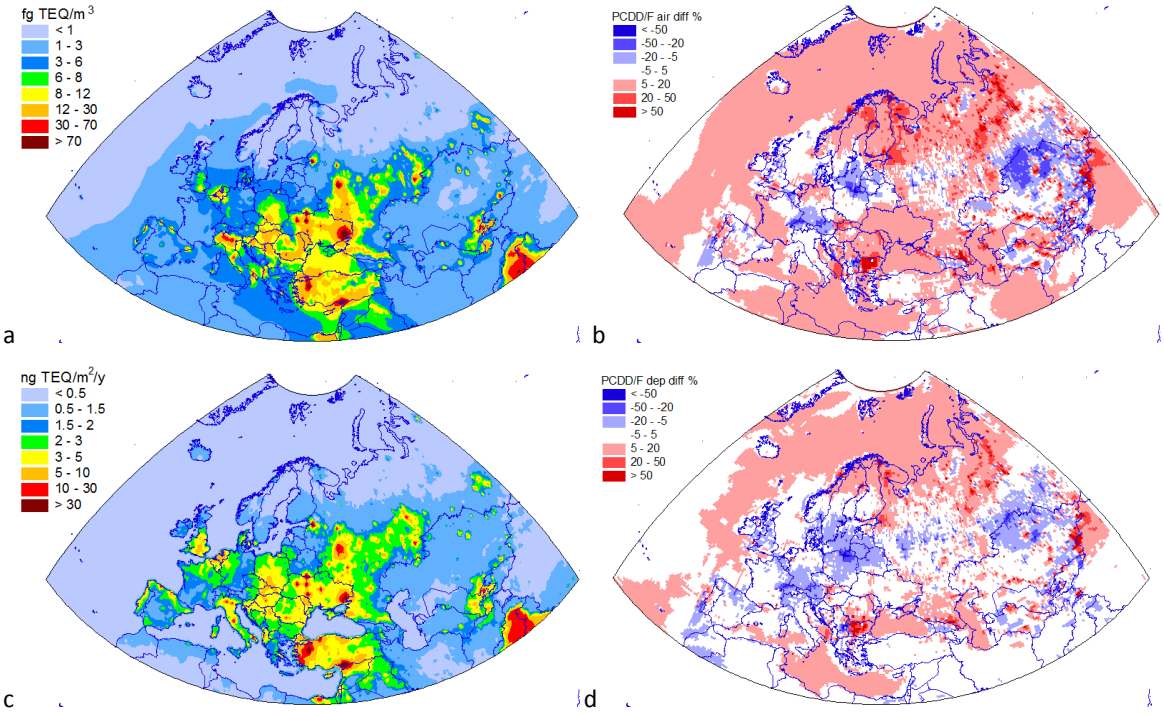

Fig. B4. *Annual mean air concentrations (a) and total deposition fluxes (c) of PCDD/Fs based on the emissions data for 2019 and their relative changes (b and d) from the results based on the emissions data for 2018.*

Modelled concentrations and deposition of HCB based on emission and meteorological data for 2019 are shown in Fig. B.5a and B.5c, respectively. The corresponding changes between the HCB levels based on emissions in 2019 and 2018 are shown in Fig. B.5b and B.5d. Concentrations and deposition of HCB in the EMEP region are strongly affected by non-EMEP and secondary sources. Therefore, the changes in the modelled pollution levels caused by the changes of emissions in the EMEP countries are smoothed. Compared to 2018, the use of emissions of 2019 led to decline of HCB concentrations and deposition in the eastern part of the EMEP region, in Portugal, Austria and some regions of the western part of Finland. Minor increase of concentrations and deposition takes place in the central part of Bosnia and Herzegovina.

Differences between the estimates of air concentrations and total deposition fluxes of PAHs are shown in Fig. B.6. Model simulations based on the 2019 emission data indicate increased levels of air concentrations and total deposition fluxes in countries in Western and Northern Europe as well as the Caucasus and Central Asia in comparison with the results based on 2018 emission data. At the same time, air concentrations of 4 PAHs in the Mediterranean region decreased from 2018 to 2019. In particular, increased PAH emissions in Germany, Finland, France, and Kazakhstan led to higher PAH pollution levels in 2019 as in these countries and in the surrounding areas comparing to 2018. On the

opposite, decreased emissions of Spain, Greece, Albania, and Poland resulted in lower PAH pollution levels in these countries in 2019.

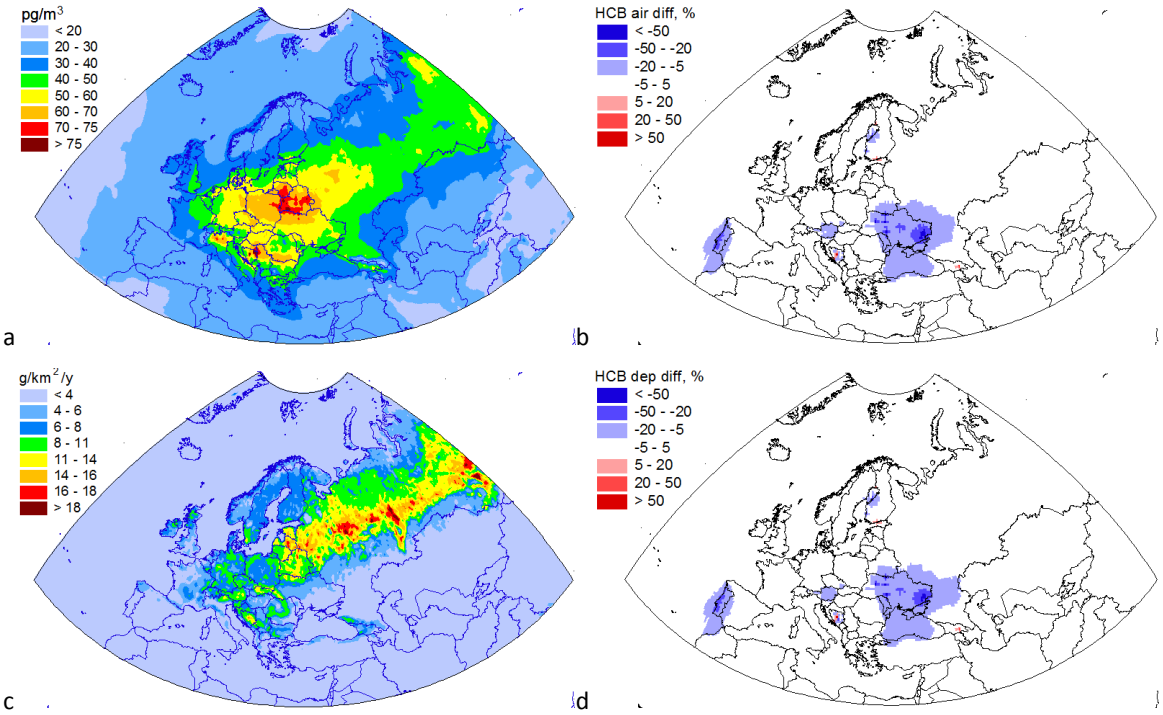

Fig. B.5. *Annual mean air concentrations (a) and total deposition fluxes (c) of HCB based on the emissions data for 2019 and their relative changes (b and d) from the results based on the emissions data for 2018.*

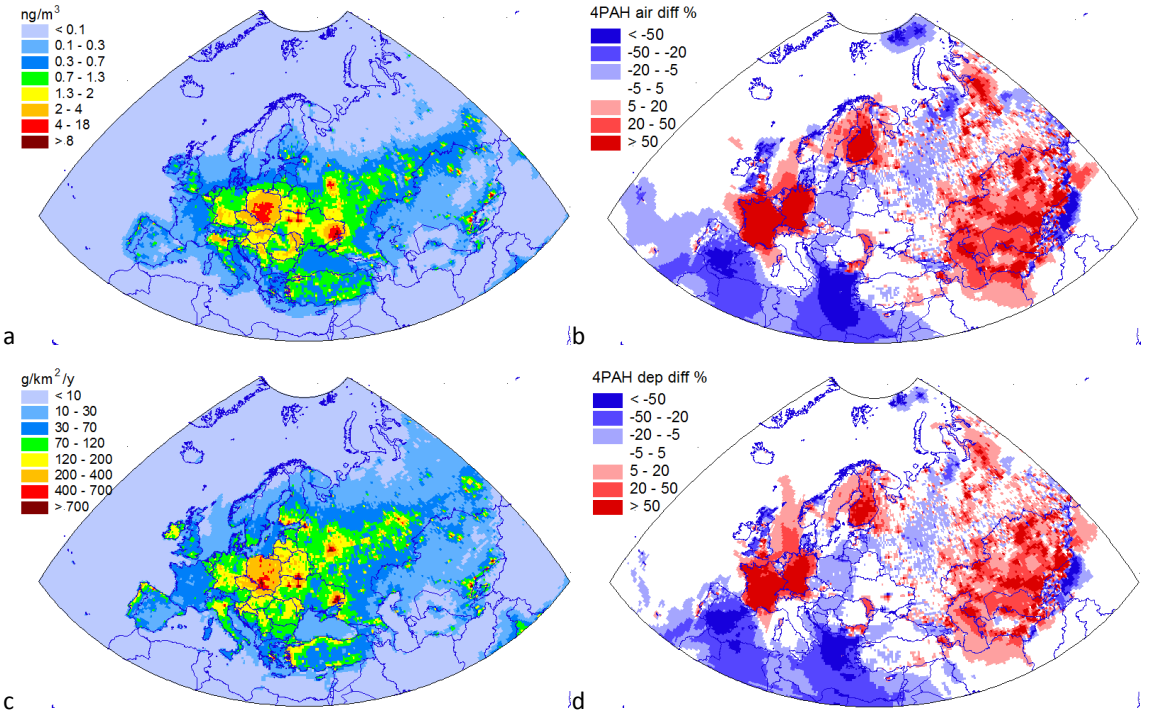

Fig. B.6. *Annual mean air concentrations (a) and total deposition fluxes (c) of the sum of 4 PAHs based on the emissions data for 2019 and their relative changes (b and d) from the results based on the emissions data for 2018.*

Annex C.
Model parameterizations for soil and vegetation compartments

Here the derivation of equation system for air, soil and vegetation concentrations for the approach considering atmosphere-soil-vegetation system as one compartment (see [*Bash*, 2010; *Zhang et al.*, 2009; 2010; *Wang et al.*, 2014] and citations therein) is given in detail. The description of exchange in such a model is based on the so-called compensation points χ_{soil}, χ_{cut} and χ_{cnp} instead of concentrations in the corresponding media. Here the indexes soil, cut (cuticle) and cnp (canopy, that is, vegetation + soil compartment) are used. These compensation points are the values of air concentrations for which the flux of the exchange between considered medium and air changes its direction. Formulas for these compensation points are given below.

Relations for fluxes for vegetation-covered soil:

$$F_{cnp\to air} = \frac{\chi_{cnp} - C_{atm}}{R_a + R_b}, \tag{C.1}$$

$$F_{soil\to cnp} = \frac{1}{R_{ac} + R_{soil}}\left(\chi_{soil} - \chi_{cnp}\right), \tag{C.2}$$

$$F_{veg\to cnp} = \frac{LAI}{R_{cut}}\left(\chi_{cut} - \chi_{cnp}\right), \tag{C.3}$$

The relations for compensation points for soil and vegetation are:

$$\chi_{cut} = \frac{S_{leaf}\cdot Q_{veg}}{LAI\cdot BCF}, \chi_{soil} = \frac{C_{soil}}{P_{soil-air}} \tag{C.4}$$

where S_{leaf} is specific surface area of vegetation, m^2/m^3, Q_{veg} is surface density of the pollutant in vegetation, ng/m^2, C_{soil} is the concentration of the pollutant in soil, ng/m^3, LAI is leaf area index, BCF is the bioconcentration factor, and $P_{soil-air}$ is soil-air partitioning coefficient. Following [*Sutton et al.*, 1998], the relation for canopy compensation point is obtained from

$$F_{cnp\to air} = F_{soi\to cnp} + F_{veg\to cnp}, \tag{C.5}$$

which leads to (here stomatal pathway of air-vegetation is not considered)

$$\chi_{cnp} = \left[\frac{C_{atm}}{R_a + R_b} + \frac{LAI\cdot\chi_{cut}}{R_{cut}} + \frac{\chi_{soil}}{R_{ac} + R_{soil}}\right] / \left[\frac{1}{R_a + R_b} + \frac{LAI}{R_{cut}} + \frac{1}{R_{ac} + R_{soil}}\right]. \tag{C.6}$$

Here C_{atm} is the atmospheric concentration, R_{soil} is soil resistance calculated in parameterization of soil processes, R_a and R_b are standard resistances of atmospheric boundary layer. The resistance R_{cut} is calculated via cuticle permeance $P_{cuticle}$ and partition coefficient $K_{Air/Water}$ [*Barber et al.*, 2004]:

$$\mathrm{R_{cut}} = \frac{\mathrm{K_{Air/Water}}}{\mathrm{P_{cuticle}}}. \tag{C.7}$$

where

$$\log \mathrm{P_{cuticle}} = 0.734 \log \mathrm{K_{cw}} - 11.26, \tag{C.8}$$

and cuticle/water partition coefficient K_{cw} is given by

$$\log \mathrm{K_{cw}} = 0.057 + 0.970 \log \mathrm{K_{ow}}, \quad \text{(C.9)}$$

K_{ow} being the octanol/water partition coefficient.

The in- canopy resistance R_{ac} (being the same for all gaseous species) can be calculated as described in [*Zhang et al.*, 2009]:

$$R_{ac} = \frac{R_{ac0} \cdot LAI^{1/4}}{u_*^2} \quad \text{(C.10)}$$

where u_* is friction velocity, and R_{ac0} can be obtained from the following table:

Surface types	Average value of R_{ac0}	Range
Deciduous forest	200	100 – 300
Coniferous forest	80	60 – 100
Grass	25	10 – 40
Shrubs	40	20 – 60
Arable lands	30	10 – 50
Bare soil	0	-
Urban	0	-
Glasier	0	-
Water	0	-

Relations for fluxes (C.1) – (C.3) can be now rewritten in the following form:

$$F_{cnp\to air} = -C_{atm} \cdot \frac{\frac{LAI}{R_{cut}} + \frac{1}{R_{ac}+R_{soil}}}{1 + \frac{(R_a+R_b)\cdot LAI}{R_{cut}} + \frac{R_a+R_b}{R_{ac}+R_{soil}}} + \frac{S_{leaf}\cdot Q_{veg}}{BCF} \cdot \frac{1/(R_a+R_b)}{\frac{R_{cut}}{R_a+R_b} + LAI + \frac{R_{cut}}{R_{ac}+R_{soil}}} + \frac{C_{soil}}{P_{soil-air}} \cdot \frac{1/(R_a+R_b)}{\frac{R_{ac}+R_{soil}}{R_a+R_b} + LAI \cdot \frac{R_{ac}+R_{soil}}{R_{cut}} + 1}, \quad \text{(C.11)}$$

$$F_{soil\to cnp} = -C_{atm} \cdot \frac{1/(R_{ac}+R_{soil})}{1 + \frac{(R_a+R_b)\cdot LAI}{R_{cut}} + \frac{R_a+R_b}{R_{ac}+R_{soil}}} - \frac{S_{leaf}\cdot Q_{veg}}{BCF} \cdot \frac{1/(R_{ac}+R_{soil})}{\frac{R_{cut}}{R_a+R_b} + LAI + \frac{R_{cut}}{R_{ac}+R_{soil}}} + \frac{C_{soil}}{P_{soil-air}} \cdot \frac{\frac{1}{R_a+R_b} + LAI \cdot \frac{1}{R_{cut}}}{\frac{R_{ac}+R_{soil}}{R_a+R_b} + LAI \cdot \frac{R_{ac}+R_{soil}}{R_{cut}} + 1}, \quad \text{(C.12)}$$

$$F_{veg\to cnp} = -C_{atm} \cdot \frac{LAI/R_{cut}}{1 + \frac{(R_a+R_b)\cdot LAI}{R_{cut}} + \frac{R_a+R_b}{R_{ac}+R_{soil}}} + \frac{S_{leaf}\cdot Q_{veg}}{BCF} \cdot \frac{\frac{1}{R_a+R_b} + \frac{1}{R_{ac}+R_{soil}}}{\frac{R_{cut}}{R_a+R_b} + LAI + \frac{R_{cut}}{R_{ac}+R_{soil}}} - \frac{C_{soil}}{P_{soil-air}} \cdot \frac{LAI/R_{cut}}{\frac{R_{ac}+R_{soil}}{R_a+R_b} + LAI \cdot \frac{R_{ac}+R_{soil}}{R_{cut}} + 1}, \quad \text{(C.13)}$$

These formulas can be represented as

$$F_{cnp\to air} = -C_{atm} \cdot A_0 + Q_{veg} \cdot B_0 + C_{soil} \cdot C_0, \quad \text{(C.14)}$$

$$F_{soil\to cnp} = -C_{atm} \cdot A_1 - Q_{veg} \cdot B_1 + C_{soil} \cdot C_1, \quad \text{(C.15)}$$

$$F_{veg\to cnp} = -C_{atm}\cdot A_2 + Q_{veg}\cdot B_2 - C_{soil}\cdot C_2, \quad \text{(C.16)}$$

where the coefficients are calculated from (for vegetation-covered soil) via conductances by

$$A_1 = \frac{g_{ab}\cdot g_{soil}}{g_{tot}}, \quad \text{(C.17)}$$

$$A_2 = \frac{g_{ab}\cdot g_{cut}}{g_{tot}}, \quad \text{(C.18)}$$

$$B_1 = \frac{S_{leaf}}{BCF}\,\frac{g_{soil}}{R_{cut}\cdot g_{tot}}, \quad \text{(C.19)}$$

$$B_2 = \frac{S_{leaf}}{BCF}\,\frac{g_{ab}+g_{soil}}{R_{cut}\cdot g_{tot}}, \quad \text{(C.20)}$$

$$C_1 = \frac{1}{P_{soil-air}}\cdot\frac{(g_{ab}+g_{cut})\cdot g_{soil}}{g_{tot}}, \quad \text{(C.21)}$$

$$C_2 = \frac{1}{P_{soil-air}}\cdot\frac{g_{cut}\cdot g_{soil}}{g_{tot}}, \quad \text{(C.22)}$$

$A_0 = A_1 + A_2$, $B_0 = B_2 - B_1$, $C_0 = C_1 - C_2$, and

$$g_{ab} = \frac{1}{R_a+R_b} \quad \text{(C.23)}$$

$$g_{cut} = \frac{LAI}{R_{cut}} \quad \text{(C.24)}$$

$$g_{soil} = \frac{1}{R_{ac}+R_{soil}} \quad \text{(C.25)}$$

$$g_{tot} = g_{ab} + g_{cut} + g_{soil} \quad \text{(C.26)}$$

As a consequence of relations (C.14) – (C.16) we can obtain the system of differential equations for C_{atm}, C_{soil} and Q_{veg}, namely

$$\frac{\partial C_{atm}}{\partial t} = F_{cnp\to air}/dZ_{atm} = \left(-C_{atm}\cdot A_0 + Q_{veg}\cdot B_0 + C_{soil}\cdot C_0\right)/dZ_{atm}, \quad \text{(C.27)}$$

$$\frac{\partial C_{soil}}{\partial t} = -F_{soil\to cnp}/dZ_{soil} = \left(C_{atm}\cdot A_1 + Q_{veg}\cdot B_1 - C_{soil}\cdot C_1\right)/dZ_{soil}, \quad \text{(C.28)}$$

$$\frac{\partial Q_{veg}}{\partial t} = -F_{veg\to cnp} = C_{atm}\cdot A_2 - Q_{veg}\cdot B_2 + C_{soil}\cdot C_2, \quad \text{(C.29)}$$

Here dZ_{atm} and dZ_{soil} are thicknesses of lower atmosphere and upper soil layers. Formulas (C.27) – (C.29) should be used for the modelling of vegetation-air exchange.

Further, inter-media fluxes can be calculated in terms of A_i, B_i and C_i:

$$\text{AirSoilFlux} = C_{atm}\cdot A_1, \quad \text{(C.30)}$$

$$\text{AirVegFlux} = C_{atm}\cdot A_2, \quad \text{(C.31)}$$

$$\text{SoilAirFlux} = C_{soil} \cdot C_0, \tag{C.32}$$

$$\text{SoilVegFlux} = C_{soil} \cdot C_2, \tag{C.33}$$

$$\text{VegAirFlux} = Q_{veg} \cdot B_0, \tag{C.34}$$

$$\text{VegSoilFlux} = Q_{veg} \cdot B_1. \tag{C.35}$$

Equation system (C.27) – (C.29) can be easily solved explicitly since conservation law gives first integral for the system:

$$C_{atm} * dZ_{atm} + C_{soil} * dZ_{soil} + Q_{veg} = const. \tag{C.36}$$

So, for the construction of explicit solution it is necessary to solve quadratic equation only. However, in the case when vegetation uptake through stomata is considered (as for Hg), the equation system should be of 4x4 size, and for explicit solution characteristic equation is cubic and should be solved by Cardano formulas.

For bare soil the flux from soil to the atmosphere is given by

$$F_{soil} = \frac{1}{R_a + R_b + R_{soil}} (\chi_{soil} - C_{atm}). \tag{C.37}$$

Substituting the expression for soil compensation point from (4) we obtain

$$F_{soil-air} = \frac{1}{R_a + R_b + R_{soil}} \left(\frac{C_{soil}}{P_{soil-air}} - C_{atm} \right). \tag{C.38}$$

So, for this land use the coefficients in (C.14) – (C.16) are

$$A_0 = A_1 = \frac{1}{R_a + R_b + R_{soil}}, \tag{C.39}$$

and

$$C_0 = C_1 = \frac{1}{(R_a + R_b + R_{soil}) \cdot P_{soil-air}}. \tag{C.40}$$

The rest coefficients should be put to zero (if used).